Oil recovery by low salinity waterflooding

Jamoowantee Ballah

THESE

pour obtenir le grade de Docteur

de l'Université Pierre et Marie Curie, Sorbonne Universités

Ecole doctorale ED388: Chimie Physique et Chimie Analytique de Paris-Centre

Récupération du pétrole par injection d'eau douce

Présentée et soutenue publiquement par

Jamoowantee BALLAH

Soutenue le 13 Mars 2017

Membres du Jury

Prof. Jocelyne BRENDLE	ENSCMu	Rapporteur
Dr. Jean Eric POIRIER	COLAS-CST	Rapporteur
Prof. Maguy JABER	UPMC	Examinateur
Dr. Lydie LE FORESTIER	Université Orléans	Examinateur
Dr. Manuel CHAMEROIS	TOTAL	Co-encadrant
Dr. Pierre LEVITZ	UPMC	Co-encadrant
Dr. Laurent MICHOT	UPMC	Directeur

DEDICACES

Je dédie ce travail à :

Mes chers Parents, Mantee et Bissoon

Ma chère tante, Pou

Mes Sœurs, Pritee et Arti

Ainsi qu'à tous ceux qui tient à cœur ma réussite.

REMERCIEMENTS

Cette thèse, résultat d'un travail de recherche de trois ans est loin d'être un travail solitaire. C'est pour cela que je tiens à remercier les personnes qui ont contribué à sa réalisation.

Pour commencer, je voudrais remercier les membres du Jury d'avoir accepté d'évaluer mes travaux. Les rapporteurs : Mme Jocelyne Brendle et M. Jean Eric Poirier ; l'examinatrice Mme Lydie le Forestier et la présidente du Jury Mme Maguy Jaber.

Les travaux présentés dans cette thèse ont bénéficié d'un financement TOTAL et ont été réalisés au laboratoire PHysicochimie des Electrolytes et Nanosystèmes InterfaciauX (PHENIX). Je tiens donc à remercier Manuel Chamerois, sans qui cette thèse n'aurait pas vue le jour. Je tiens également à lui dire un grand merci pour les discussions scientifiques ainsi que tous ses conseils avisés pendant ces trois années. Et même après la soutenance. Je suis ravie d'avoir travaillé avec lui.

Mes remerciements vont ensuite naturellement à mon directeur de thèse, Laurent Michot, pour la confiance qu'il m'a accordé en me donnant l'opportunité de réaliser ce travail doctoral. J'aimerais lui faire part de ma gratitude pour ses divers conseils et le temps qu'il a consacré à diriger cette thèse. Je suis ravie d'avoir travaillé avec lui, il m'a fait confiance et m'a laissé une grande liberté dans mes recherches. J'espère avoir été à la hauteur de ses attentes.

Je tiens à exprimer mes plus vifs remerciements à mon co-directeur, Pierre Levitz. Il fut pour moi, outre une référence scientifique, un mentor disponible malgré ses nombreuses charges de travail. Ses connaissances multiples ont répondu à plusieurs de mes préoccupations et m'ont ainsi permis de progresser. Je garderai à jamais dans mes souvenirs tous les petits moments que j'ai passé avec lui à l'écouter me parler de science, de l'histoire de France et pleins d'autres choses encore. Je voudrais lui dire merci pour ses qualités humaines que j'ai apprises à connaitre petit à petit.

J'adresse ma gratitude à Natalie Malikova qui a été présente pendant ces années de thèse en m'apportant un soutien scientifique, une aide inestimable pour la réalisation de mes expériences. Elle a également été disponible à chacune de mes sollicitations.

Mes sincères remerciements et ma profonde gratitude vont naturellement à Serge Durand-Vidal, qui m'a aidé avec les mesures de l'AFM. Au-delà de son soutien scientifique, Il s'est toujours intéressé sur l'avancée de mes travaux, qui plus est de manière bénévole. Je voudrais le remercier pour sa disponibilité, sa réactivité (même les week-ends), d'avoir toujours été à l'écoute, d'avoir participé à la lecture et correction de mon manuscrit. Je ne pourrais citer toutes ses contributions mais je tenais à lui dire un énorme merci, surtout pour ses qualités humaines. Pour ma part, j'ai été ravie d'avoir pu partager un peu de mes connaissances avec ses filles.

Je ne saurais oublier les permanents, Jérôme, Ali, Sophie, Sébastien, Delphine, Frédéric, Véronique, Juliette, Anne-Laure, Laurent, Cécile, Olivier, Jean-Pierre, Amandine, Richard et Marie. Une mention spéciale pour Agnès avec qui j'ai partagé des moments inoubliables dans les transports. Les doctorants que j'ai côtoyés depuis mon arrivée au PHENIX : Clément, Layali, Veronica, Clarisse, Blandine, Sophia, Caterina, Wilfried, Ourania et Stéphane.

Enfin, dans la simplicité j'aimerais adresser ma forte reconnaissance à Nebelula, GG, Yas et Nadia. C'est sûr que je ne pourrais pas mentionner tout ce que j'ai partagé avec vous pendant ces 3 années mais sachez qu'ils resteront à jamais gravé dans ma tête et dans mon cœur. Vous allez me manquer les 'zoreilles' mais les nombreuses photos et vidéos resteront les preuves et les souvenirs de ces belles années qui ont commencées au bâtiment F. Et puis comment dire le plus important, j'aimerais remercier la princesse qui est passée par notre chemin pour nous rapprocher à jamais !

Ces remerciements seraient incomplets sans citer mes proches et mes amis. Maman, Papa merci à vous car c'est grâce à vous que je suis la aujourd'hui. Mes sœurs Arti et Pritee, mon beau-frère Nadaraj, ma nièce Yutika, mon neveu Yovin, même si vous êtes loin vous avez été ma source d'énergie. Mon mari Rakesh qui m'a aidé et soutenue pendant toutes ces années. Ma tante Ved, mes amis Heshika, Didier, Ritesh, JuJu, Christelle, Isabelle, Navisha, Siddick, Tasleema et Thibaut. Eric et Marie, je voudrais vous dire merci pour tous vos aides et encouragements, il n'y a pas d'autres mots c'est la maison porte-bonheur.

J'ai oublié certainement plusieurs personnes et je m'en excuse. Je tiens encore une fois à vous dire un grand merci. Ces années de thèse sont les meilleures années de tout mon cursus et le jour de la soutenance sera à jamais un des plus mémorable.

Jamoowantee Ballah

Table of contents

II. Main materials

III. Wettability of clay minerals

IV. Liquid-Liquid interactions

V. Triple phase interaction

Symbols and Abbreviations

Abbreviations

API	American Petroleum Institute
COBR	Crude Oil Brine Rock
EOR	Enhanced Oil Recovery
HLB	Hydrophilic Lipophilic Balance
IFT	Interfacial tension
LSW	Low Salinity Waterflooding
MIE	Multicomponent Ionic Exchange
MS	Model System
OOIP	Original Oil In Place
RH	Relative Humidity
SARA	Saturates, Aromatics, Resins, Asphaltenes
TAN	Total Acid Number
TBN	Total Base Number

Introduction

Introduction and context

Oil exploitation is carried out through different processes, namely: primary, secondary and tertiary modes. In the primary process, oil is displaced from reservoirs to production wells by naturally occurring build-up of water and gas pressure inside the reservoir. As production proceeds, the differential pressure between the reservoir and the earth surface tumbles down and artificial lift methods like pump rods are used. The secondary process includes water or gas flooding to maintain pressure and consequently expel more oil out of the reservoir. However, the oil still remaining in the reservoirs after the primary and secondary processes is estimated to be approximately 60-70 % of the Original Oil In Place (OOIP). The tertiary mode, collectively labelled Enhanced Oil Recovery (EOR) thus aims at mobilising the trapped oil which remains unrecovered by the conventional primary and secondary processes. The techniques employed during this phase involve:

- thermal and CO_2 injections which aim at reducing the viscosity of resident oil;
- chemical such as polymer and surfactant injections to bring the viscosity of the injected water close that of the oil and reduction of oil/water interfacial tension respectively;
- low salinity waterflooding (LSW), where brines of lower salt concentration compared to formation water are injected into reservoirs.

Regarding this latter technique, in the 1990's, Morrow and his co-workers noticed that the composition of injected brine influenced the amount of oil recovered [1], [2]. Since then, many studies focussed in that direction and have postulated different pore scale mechanisms to account for benefits in oil recovery during LSW. For instance, the presence of clays [3]–[5], the particle release theory [3], the pH increase theory [6], multicomponent ion exchange [7], [8] and wettability modifications [9]–[11] have been put forward. However, to date these theories are still prone to debate and the LSW mechanism is not clear.

Based on the displacement of residual oil (after the primary and secondary processes) by injected brines, this technique is governed by the efficiency of both macroscopic and microscopic displacements [12]. Macroscopic displacement quantifies the ability of the injected brine to come in contact with the oil-containing part of the reservoir and its efficiency is affected by parameters such as the heterogeneities and anisotropy of oil reservoir (porosity, permeability), the relative mobility of the displacing and displaced fluids, and the rock matrix [12]. Microscopic displacement in its turn determines the ability of the brine, once in contact

with the oil, to displace it. The parameters governing the efficiency of microscopic displacement are the interfacial and surface tensions of the coexisting fluids and solids, wettability of the reservoir, capillary pressure in the pores and relative permeability [7]. Improving oil recovery efficiency by LSW is challenging since it requires to overcome both viscous and capillary forces [13]–[15]. In addition to that, the complex nature of oils thwarts the process of oil recovery. However, with respect to the well understood EOR techniques (polymer, surfactant, gas and steam injection), LSW presents the advantage of operating in a similar way to conventional waterflooding, uses relatively cheap and available materials and is a low-CO_2 footprint technology [16].

Objectives

This thesis aims at understanding LSW in sandstone reservoirs. As such, the reservoir is a porous medium where several solid and fluid phases coexist and the success of oil extraction lies in the understanding of the complex crude oil/brine/rock (COBR) interactions (Figure 1 [17]). Taking into consideration a drop of oil on a mineral surface, the equilibrium is a result of solid/brine interaction (γ_{SB}), solid/oil interaction (γ_{SO}) and oil/brine interaction (γ_{OB}). Firstly, each contribution is studied individually and then, the three phases are confronted.

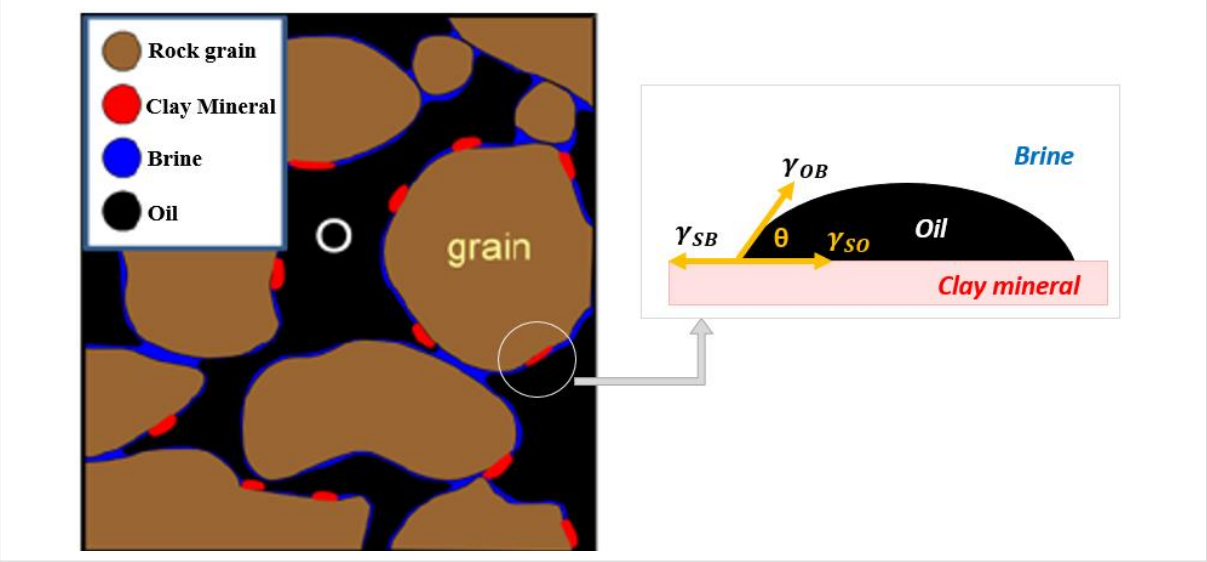

Figure 1 : Schematic representation of oil in a clay containing reservoir

The work in this thesis is presented as follows:

- Chapter 1 is the state of the art section. Firstly we provide a literature review of the different mechanisms put forward in relation to LSW. Since our study deals with LSW

in sandstone reservoirs, the second part of the chapter provides the scientific background of clay minerals and the associated wettability review. A third part is dedicated to the description of crude oils and the basic concepts of oil/brine interactions. In addition we also report the literature advances of crude oil/brine interactions.

- In chapter 2, we chose to report the different clay minerals and crude oils used in this thesis. Indeed, these materials have been used in the experiments of the different chapters. However, detailed experimental procedures and set-ups are provided at the beginning of each of the following chapters (3, 4 and 5).
- In chapter 3 we investigated solid/liquid interactions by studying the wettability of clay minerals in an extensive way (effect of surface ions, relative humidity, particle size and surface roughness on contact angles). We show that the water wettability of clay minerals are highly dependent on the nature of surface ions.
- Chapter 4 is dedicated to the investigation of crude oil/aqueous phase interfacial tension. Due to the complex nature of crude oils, we designed a simplified model system and carried out identical experiments on both systems. We show that interfacial tension of the organic phase (containing surface active molecules) is dependent on the nature and concentration of ions in the aqueous phase. In the second part of the chapter, oil/brine interactions are studied by analysing the stability of emulsions.
- Finally, in chapter 5, we confront oil, brine and clay minerals. Interactions between these phases are firstly studied via contact angle measurements. We show that exchangeable ions at the surface of mica drive its wettability. In the second part of the chapter, triple phase interactions are probed by the study of the stability of emulsions in the presence of different clay minerals.

Bibliography

[1] P. P. Jadhunandan and N. R. Morrow, “Spontaneous imbibition of water by crude oil/brine/rock systems,” *Situ U. S.*, vol. 15:4, Jan. 1991.

[2] P. P. Jadhunandan and N. R. Morrow, “Effect of Wettability on Waterflood Recovery for Crude-Oil/Brine/Rock Systems,” *SPE-22597-PA*, Feb. 1995.

[3] G.-Q. Tang and N. R. Morrow, “Influence of brine composition and fines migration on crude oil/brine/rock interactions and oil recovery,” *J. Pet. Sci. Eng.*, vol. 24, no. 2–4, pp. 99–111, Dec. 1999.

[4] A. Lager, K. Webb, and C. Black, “Impact of brine chemistry on oil recovery,” presented at the IOR 2007-14th European Symposium on Improved Oil Recovery, 2007.

[5] J. C. Seccombe, A. Lager, K. J. Webb, G. Jerauld, and E. Fueg, “Improving Wateflood Recovery: LoSalTM EOR Field Evaluation,” in *SPE-113480-MS*, SPE, 2008.

[6] P. L. McGuire, J. R. Chatham, F. K. Paskvan, D. M. Sommer, and F. H. Carini, “Low Salinity Oil Recovery: An Exciting New EOR Opportunity for Alaska’s North Slope,” in *SPE-93903-MS*, SPE, 2005.

[7] A. Lager, K. Webb, C. Black, M. Singleton, and K. Sorbie, “Low Salinity Oil Recovery-An Experimental Investigation1,” *Petrophysics*, vol. 49, no. 1, 2008.

[8] K. S. Sorbie and I. Collins, “A Proposed Pore-Scale Mechanism for How Low Salinity Waterflooding Works,” in *SPE-129833-MS*, SPE, 2010.

[9] J. S. Buckley, Y. Liu, and S. Monsterleet, “Mechanisms of Wetting Alteration by Crude Oils,” *SPE-37230-PA*, Mar. 1998.

[10] S. Berg, A. W. Cense, E. Jansen, and K. Bakker, “Direct Experimental Evidence of Wettability Modification By Low Salinity,” *SPWLA-2010-V51n5a3*, Oct. 2010.

[11] R. A. Nasralla, M. A. Bataweel, and H. A. Nasr-El-Din, “Investigation of Wettability Alteration by Low Salinity Water,” in *SPE-146322-MS*, SPE, 2011.

[12] R. E. Terry, “Enhanced oil recovery,” *Encycl. Phys. Sci. Technol.*, vol. 18, pp. 503–518, 2001.

[13] T. Sheorey, K. Muralidhar, and P. P. Mukherjee, “Numerical experiments in the simulation of enhanced oil recovery from a porous formation,” *Int. J. Therm. Sci.*, vol. 40, no. 11, pp. 981–997, Nov. 2001.

[14] M. K. Sharma and D. O. Shah, “Use of Surfactants in Oil Recovery,” in *Developments in Petroleum Science*, vol. Volume 17, Part B, G. V. C. and T. F. Y. Erle C. Donaldson, Ed. Elsevier, 1989, pp. 255–315.

[15] D. Yang and Y. Gu, “Interfacial Interactions Between Crude Oil and CO2 Under Reservoir Conditions,” *Pet. Sci. Technol.*, vol. 23, no. 9–10, pp. 1099–1112, Sep. 2005.

[16] H. Mahani *et al.*, “Analysis of field responses to low-salinity waterflooding in secondary and tertiary mode in Syria,” presented at the SPE EUROPEC/EAGE Annual Conference and Exhibition, 2011.

[17] H. Mahani, S. Berg, D. Ilic, W.-B. Bartels, and V. Joekar-Niasar, “Kinetics of the Low Salinity Waterflooding Effect Studied in a Model System,” in *SPE-165255-MS*, SPE, 2013.

I: State of the art

Table of contents

List of Tables

List of Figures

Introduction

This chapter, divided into four subparts, aims at (1) summarising the literature results dealing with low salinity waterflooding; (2) describing the prerequisites of the wettability of clays; (3) providing an insight into oil/aqueous phase interactions; and (4) providing our analysis of the literature in order to correlate the objectives of the present work.

1. Low salinity waterflooding (LSW) and literature mechanisms

Low salinity waterflooding experiments under both laboratory and field conditions have revealed increased oil recovery in most cases (but not always). As stated in the introduction, it all started with the pioneer work of Morrow and his co-workers in the early 1990's, where they noticed that brine composition influenced the amount of oil recovered [1], [2]. Since then, many studies have focussed in that direction and reported the necessary conditions for observing low salinity effect as: (i) the presence of clays (even if the type and amount of clay has not been clearly identified yet); (ii) the presence of polar components in oils; (iii) the presence of connate water (water trapped into the pores of the rock); (iv) the presence of divalent cations in the connate water; (v) a significant difference between the salinity of injected brine and in place water (injected brine concentration being much lower than that of the connate water) [3]–[5]. However, working under these conditions have not always ensured benefits in oil recovery. In line with the benefits provided by this technique, a number of theories have then been postulated in order to explain the possible associated mechanisms. These main theories are described herein:

1.1 The presence of clay minerals

The presence of clay minerals has been considered as a key parameter in order to obtain increased oil recovery during LSW. Formerly, Tang and Morrow [6], performed numerous experiments on kaolinite containing sandstones and observed positive low salinity responses. They observed that the presence of potentially mobile fines played a key aspect in oil recovery. For instance, this phenomenon has been linked to permeability reduction (described in *section 1.2*) causing injected water to take alternate pathways and hence increase sweep efficiency. Furthermore, Tang and Morrow [6] reported that if a core containing kaolinite was fired and acidified to destroy its structure, low salinity effect was no longer observed. In line with the work of Tang and Morrow, it became obvious, and a general assumption that the presence of

clays was an essential condition for positive low salinity effect. Furthermore, Lager et al. [7] and Seccombe et al. [8] performed their experiments in the presence of clay minerals, with special emphasis on kaolinite content. They concluded that low salinity response was in fact linked to the amount of kaolinite present. Following these observations, another step was made in relation to clay and low salinity effect, where this time, attention was paid to the type of clay [9]. It followed that highly charged clay minerals were likely to respond more positively to low salinity brines. Indeed, injected brine cause cation exchanges with the rock surface. It is worth mentioning that most clay minerals possess a cation exchange capacity (CEC, *cf section 2.1.4.*). However, it is must be pointed out that many other studies have observed increased oil recovery in clay-free sandstones [10]–[13].

1.2 Particle release theory

Particle release (clays mainly) has been evoked for explaining benefits in oil recovery. According to such interpretation, when the salinity of injected brine is less than the critical salt concentration needed for the flocculation of clays, in agreement with the DLVO theory, the electrical double layer (Figure 1. [14]) between the clay particles is expanded.

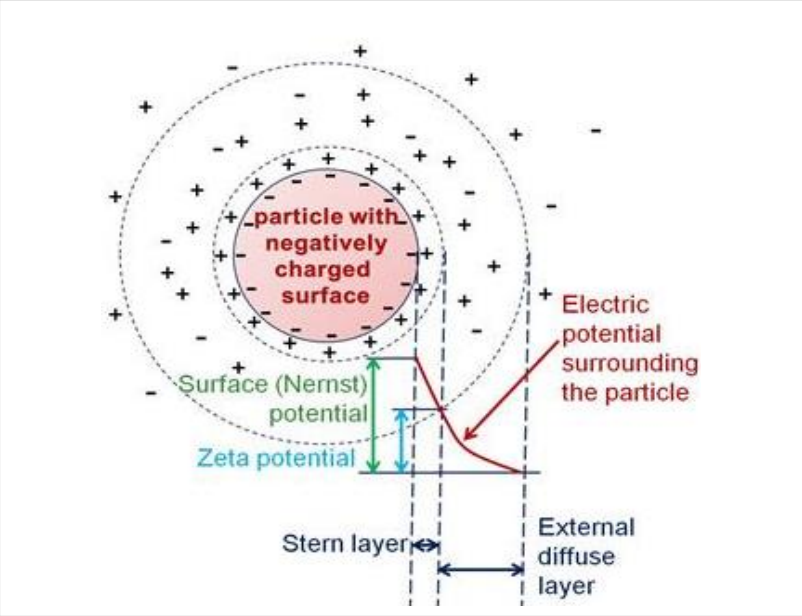

Figure 1: Double electrical layer

As a consequence, particles may get detached from the walls and during their flow, get blocked at pore constrictions which results in permeability reduction of the reservoir (*cf section 2*). This phenomenon of permeability reduction in reservoirs [15], termed *formation damage*, has been

reported to be linked to three different processes (Figure 2), namely: (i) Migration (in the presence of non-swelling clays); (ii) swelling (in the presence of the swelling clays); and (iii) swelling induced migration (swelling clays destabilise non-swelling clays and cause them to detach from the walls).

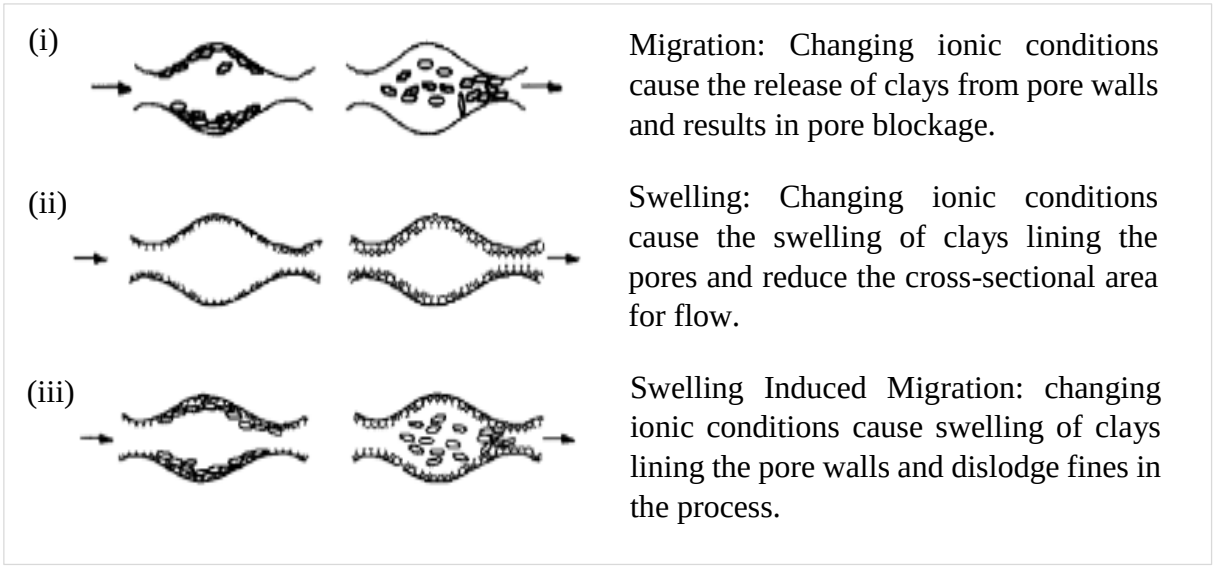

Figure 2: Mechanisms of damage in sandstones containing swelling and non-swelling clays due to changes in aqueous composition.

Particle release, permeability reduction and increase in differential pressure have been associated to increased oil recovery by Tang and Morrow [6]. As we described earlier, the blockage of fine particles at pore constrictions, the associated permeability reduction and increase in differential pressure have been reported to force injected fluid into different flow paths and hence increase sweep efficiency. However, in the studies of Zang and Morrow [9] and Lager et al. [16] without any permeability reduction, they recorded increased oil recovery. Literature thus reports that fine release and migration and the related permeability reduction cannot be the prime mechanism driving oil recovery during LSW. Indeed, increases in differential pressure have been observed without the detection of clay particles in effluent brine. Moreover, when similar experiments were performed by using mineral instead of crude oils, no net increase in differential pressure was recorded. It is clear that the interactions of crude oil/brine/rock are complex.

1.3 pH increase theory

During low salinity waterflooding, pH increases have been reported to occur as a result of cation exchange between Na^+ cations at the rock surface and H^+ from water in injected brine [15]. The resulting brine was then reported to act in a similar way as the alkaline flooding method. As such, during alkaline flooding, injected water contains chemicals such as sodium hydroxide or sodium carbonate, which react with carboxylic acids present in oils and generate surfactants [17] . As a result, the oil and water interfacial tension is reduced, eventually promoting the formation of emulsions (oil/water or water/oil) and hence increases oil recovery by capillary desorption.

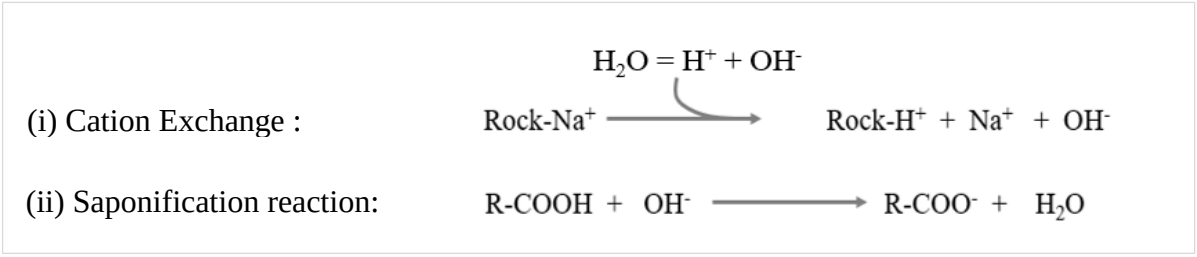

Figure 3: schematic representation of low salinity brine acting in a similar way as alkaline flooding to promote saponification.

Elsewhere, changes in solution pH have been reported to influence the zeta potential of rock particles and eventually lead to desorption of organic components from the surface [18]. However, the theory of pH increases to account for LSW has been contradicted by many studies where the authors observed either very slight pH increases or even pH decreases [10], [11], [16].

1.4 Multicomponent ion exchange (MIE) theory

The multicomponent ionic exchange is another theory postulated to explain low salinity effect. In reservoirs, the crude oil/brine/rock interactions result from a thermodynamic equilibrium and upon injection of brines different from in place connate water, the equilibrium is disturbed. Considering the adsorption of molecules from crude oils onto clay minerals, it has been reported that this process is likely to take place according to the mechanisms described in Table 1 [11], [19], [20]. However, only the mechanisms of cation exchange processes, cation bridging, ligand bridging, or water bridging (shown in Figure 4 [5], [8]) have been considered relevant to the field of LSW [5], [19].

Mechanism	Organic functional group
Cation exchange	Amino, ring NH, heterocyclic N (aromatic ring)
Cation bridging	Carboxylate, amines, carbonyl, alcoholic OH
Ligand exchange	Carboxylate
Water bridging	Amino, carboxylate, carbonyl, alcoholic OH
Anion exchange	Carboxylate
Hydrogen bonding	Amino, carbonyl, carboxyl, phenolic OH
Protonation	Amino, heterocyclic N, carbonyl, carboxylate
Van der Waals interaction	Uncharged organic units

Table 1: Mechanisms for multicomponent ionic exchange.

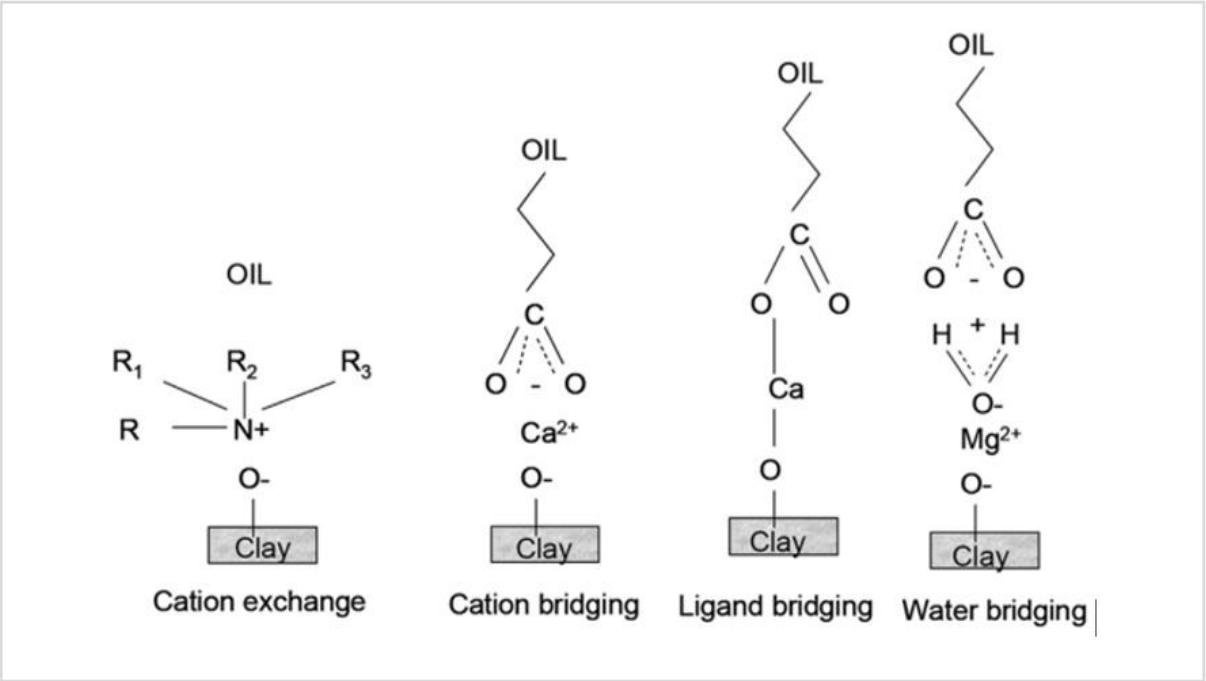

Figure 4: Different adsorption mechanisms of crude oil components on clay mineral surface.

Multivalent cations such as Ca^{2+} and Mg^{2+} strongly bind to rock surfaces. On their side, polar components from crude oils (such as naphtenic acids, asphaltene and resin, *cf section 3.1*) are bonded either via the cations or directly onto the mineral surface and hence tune the wetness of reservoirs to oil-wet state. During their studies, Lager et al. [16], observed that the presence of divalent cations in connate water was a necessary condition in order to obtain additional oil recovery during LSW in the tertiary phase. Moreover, they postulated that the molecules from

crude oils which were directly adsorbed on the mineral surface (without any bridge) could be easily displaced by uncomplexed divalent ions in the injected brines (rock affinity for Ca^{2+} > polar component from crude oil). Indeed, in another study they observed that the adsorption of Mg^{2+} ions led to increased oil production (the concentration of Mg^{2+} in injected brine > than that measured in effluent brine) [8].

However, in their studies, Boussour et al. [11] showed that the presence of divalent ions was neither compulsory nor did systematically increase oil production. The same authors concluded that MIE mechanism could not be generalised, but could however not be completely discarded to explain the impact of brine composition on the efficiency of LSW.

1.5 Wettability modifications in the presence of low salinity brine

Wettability modification has a dominant influence on oil recovery. In this context, Rao [21] observed that highest oil recoveries were obtained when the rock was in an intermediate and mixed-wet states. As such an intermediately wet surface implies that it has no strong wetting preferences towards the fluids while mixed-wet state refers to different wetting affinities towards different fluids. Indeed, in relation to LSW, wettability modification is desirable for cores to evolve from intermediate or mixed-wet to more water-wet states upon flooding with low salinity brine (Figure 5 [5]). On a more fundamental basis, the phenomenon of wettability will be detailed in *section 2.2*.

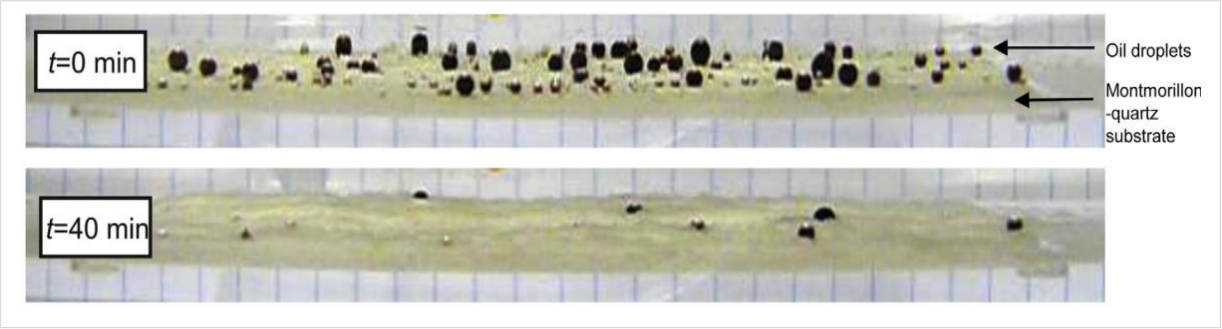

Figure 5: Mobilization of oil droplets to leave a water-wet state when low salinity brine flows past a model montmorillonite-quartz substrate.

The wettability of a sandstone by crude oils in the presence of brines was probed by contact angle measurements that revealed variations according to brines salinity [22]. Indeed, the system was shown to evolve towards more water-wet state in the presence of low salinity brines

compared to high salinity ones. Analysis of zeta potential under changing ionic conditions, revealed modifications of the charges at the rock/oil interface and hence impacted the adsorption/desorption of organic molecules from the crude oils. Elsewhere, studies performed in carbonates have also shown some evolution towards more water-wet states in the presence of low salinity brines [23].

In line with wettability modifications as a function of brine salinity, impact of the pH of solutions was formerly studied by Drummond and Israelachvili [24]. They observed evolution from water-wet to intermediate wet system at pH<9 and from oil-wet to water-wet state at pH>9, as shown in Figure 6 [24].

Wettability modifications (ideally from mixed-wet to water-wet) during LSW is a key parameter and impacts the amount of oil recovered. However, the efficiency of this process is governed by many parameters such as the properties of the crude oils (polar components), that of the mineral surfaces and that of connate water (salinity and pH). In a general way, the previously described mechanisms (1.1 to 1.4) have been described to be linked to this theory.

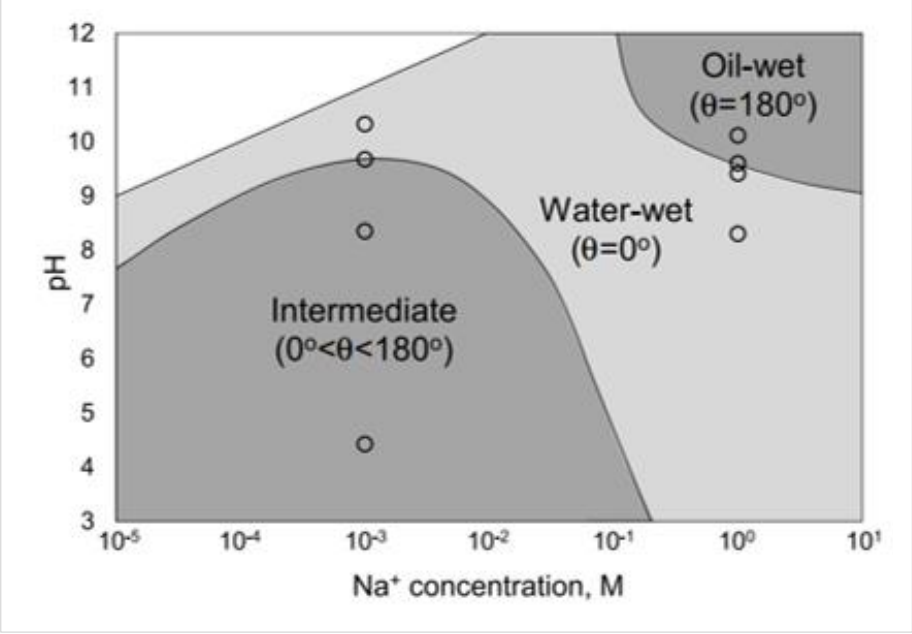

Figure 6: Wettability as a function of pH and salinity.

1.6 Simulations of low salinity waterflooding

Despite the growing interest for LSW as an alternative EOR technique, only few papers have shown interest in the modelling of low salinity waterflooding. Mostly the studies have simulated the potential of LSW by using data from coreflood experiments [25]–[27].

Even if the mechanisms at the origin of LSW remain debatable, the most agreed theory is wettability alteration driven by the MIE mechanism. In line with these theories, Underwood et al. performed molecular dynamic simulations of the interactions of a smectite clay (montmorillonite) with neutral decane, polar decanoic acid and charged sodium decanoate under varying salinity conditions [20]. Firstly, the authors observed that salinity did not impact the expansion of the electrical double layer. Secondly, the MIE mechanisms (described *section 1.4*) were independent of salt concentration. For instance, they neither observed an interaction between the non-polar decane and clay's surface nor between the uncharged polar decanoic acid and the clay's surface. However, the charged sodium decanoate was able to interact with the basal plane of the clay in the presence of Mg^{2+} cations. On the other hand, the authors observed that for the clay in both an oil- and water- wet state, dehydrated Ca^{2+} cations were present in the Stern layer and that the amount of the cations was not impacted by salt concentration. The authors thus concluded that cation and ligand bridging between the organic molecules and the clay surface were not driven by salt concentration.

Recently, a core-scale numerical model was used to examine whether MIE is the dominant mechanism which drives the low salinity effect [28] . Since the divalent cations have been mentioned various times to play a key role on the adsorption of organic molecules, the authors modelled the desorption of divalent Ca^{2+} by monovalent Na^{+} ions on clay minerals. For instance, they substituted adsorbed Ca^{2+} with Na^{+} by using NaCl of salinity of 50000, 10000 and 2000 ppm. They observed that 100% of adsorbed Ca^{2+} were removed in the presence of NaCl at 50000 and 10000 ppm but 10% of the sites were still occupied by Ca^{2+} when NaCl of 2000 ppm was used. These results were not in agreement with experimental data, since more oil (hence desorption of organic molecules), was recovered with low salinity brine of NaCl at 2000 ppm. The authors thus concluded that MIE is not the prevailing mechanism and if the detachment of molecules from the surface is on one hand governed by cation exchange phenomenon, on the other hand, it also lies on the breakage of the chemical bond (through repulsive forces). In short, this phenomenon should be directly linked to the electrical double layer which upon exhibiting sufficient repulsive forces should drive the detachment of oil droplet from the pore walls.

2. Sandstones and wettability of clays

Oil reservoirs are principally consisted of either sandstones or carbonates. These two types of rocks have a remarkable porosity and hence act as a "sponge" in order to retain oil. Our work aims at studying the recovery of oil in sandstone reservoirs (the most abundant type) and hence we are focussing our description on sandstones. Basically, they are sedimentary rocks composed of sand grains (siliceous minerals like quartz, feldspaths and sometimes phyllosilicate minerals like mica) of sizes ranging between 60 µm – 2 mm and are held together by cements of silica, carbonate or clays. In the interstitial pore space, fine materials of sedimentary origin called *matrix* may also be present.

Regarding the pores of sandstones, they are either able to communicate between themselves (with at least one pore), be of cul-de-sac morphology (only one opening) or without any connection with the neighbouring pores. Whichever the type of pores, they all together define the *porosity* of a rock as:

$$\emptyset = V_P/V_T \ = (V_T - \ V_G)/V_T \qquad \text{Equation 2}$$

With $\emptyset$: being the porosity; V_P: volume of pores; V_T: total volume and V_G: volume occupied by rock grains and other particles

If on one hand stands the *porosity* of the reservoir, on the other hand its *permeability* is a major concern for the petroleum industry. It defines the ability of fluids to pass through the porous medium and is only possible in the presence of pores which are able to communicate with each other. In the reservoir, different phases such as water, oil and gases coexist each having an effective permeability designated by k_w , k_o and k_g respectively. Indeed a highly porous rock with a low permeability would not be of great interest. As described in the LSW mechanisms associated to the particle release theory (*section 1.2*), a reduction of permeability has been used to account for increases in oil recovery.

In sandstone reservoirs, clay minerals are often present at the surface of pores or in the cement in between the grains of the rocks. The most common minerals found in sandstones are kaolinite, illite, chlorite and smectites. However, from one sandstone reservoir to another, the amount of clay minerals vary. As stipulated in the LSW mechanisms, the presence of clays has been considered as one of the working conditions in order to observe benefits in oil recovery by this particular technique. Also, in order for the MIE mechanism to take place, the crude oil components have to be adsorbed on surfaces with a capacity to exchange ions (for instance clays). Taking into consideration these mentioned features, the following subsections are

dedicated to the description of the structures of clay minerals, followed by their influence in the wettability of reservoirs.

2.1 Clay minerals

Clay minerals are fine grained particles of sizes < 2 µm in diameter and consist of crystal sheets having a repetitive atomic structure. They belong to the phyllosilicate family, distinguishable by their layered structure of silica tetrahedra (SiO_4) and of alumina, magnesium or iron octahedra $(Al, Mg, Fe)(O,OH)_6$.

2.1.1. Tetrahedral sheet

The tetrahedral sheet consists of tetrahedra with Si^{4+} as central cation (sometimes substituted by Al^{3+} and Fe^{3+}) and four oxygen anions (O^{2-}) at the corners (Figure 7a) [29]). The tetrahedra are linked in such a way that the three basal oxygen delimit a two dimensional hexagonal pattern (Figure 7b) [30]). The fourth oxygen anion, called the apical oxygen, is free compared to the basal anions and act as connection between the tetrahedral the octahedral sheet.

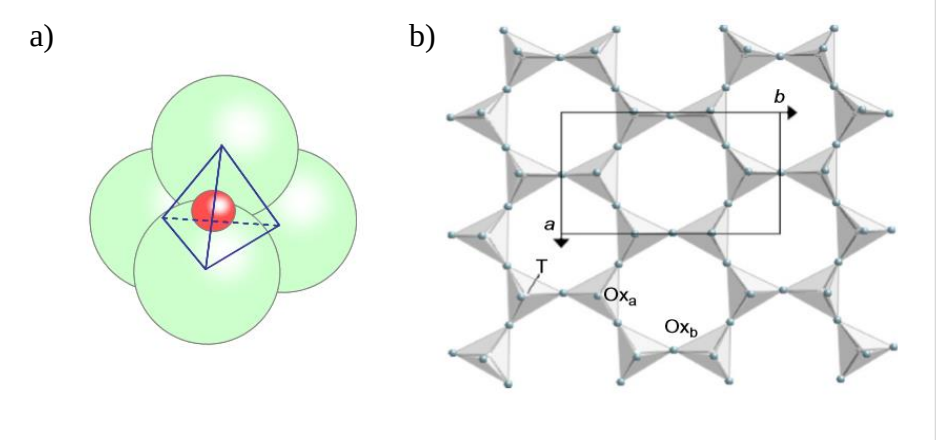

Figure 7: a) Tetrahedron of silicium $(SiO_4)^{4-}$; b) The tetrahedral sheet. T, tetrahedral cations; Ox_a, apical oxygen atoms; Ox_b, basal oxygen atoms. **A** and **b** refer to unit cell parameters.

2.1.2. Octahedral sheet

The octahedral sheet is composed of octahedra with a central trivalent (Al^{3+} or Fe^{3+}) or divalent (Fe^{2+}, Mg^{2+}) cation coordinated by six anions (O^{2-}, OH^-), the neighbouring octahedra being linked by sharing of their edges. In the presence of divalent cations, each anion is shared between 3 neighbouring octahedra and the layer is termed *trioctahedral* (Figure 8b) [31]). In the presence of trivalent cations, each anion is shared between 2 neighbouring octahedra and

hence only $2/3$ of the cationic sites are occupied. In this configuration the sheet is termed *dioctahedral* (Figure 8c) [31]).

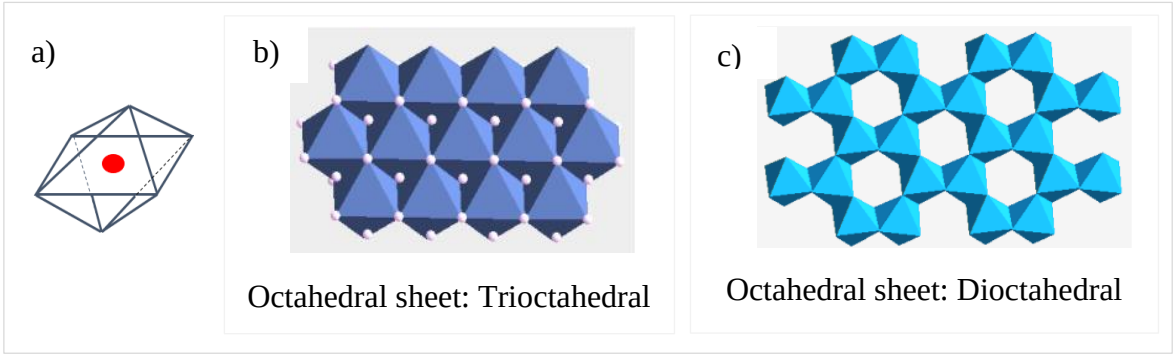

Figure 8: a) Octahedron with central cation coordinated to six anions; b) and c) octahedral sheet in trioctahedral and dioctahedral configurations respectively.

The basic building block of clay minerals is made up of stacked sheets of tetrahedra (T) and octahedra (O), which defines the *clay platelet*.

2.1.3. Classification of clay minerals

The AIPEA (Association Internationale Pour l'Etude des Argiles) has classified clay minerals according to the structuring of their building blocks (stacking of sheets of tetrahedra and octahedra). It is the most widely adopted classification of clay minerals and describe them as follows [30]:

- 1:1 or TO clay minerals: The layer is composed of a tetrahedral sheet (T) and an octahedral sheet (O). The thickness of such a layer (base of the tetrahedral sheet in one layer to the base of the tetrahedral sheet in the next layer) is about 7A°.
- 2:1 or TOT clay minerals: The layer is characterised by two tetrahedral sheets sandwiching an octahedral sheet. The thickness of such a layer (TOT + interlayer spacing) is 9A°.
- 2:1:1 or TOTO clay minerals: The layer is composed of a TOT structure and contain an octahedral sheet in the interfoliar spacing. The thickness of such a layer (TOT+ interlayer spacing containing the octahedral sheet) is 14A°.
- Regular mixed-layer clay minerals: This type of layer is constituted by the stacking of layers of different types (TO, TOT, TOTO) and hence have variable thicknesses.

After the gross classification according to the layered structure, the clay minerals are further separated into subgroups which differ from each other with respect to their net surface charges as shown in Table 2 [30].

Layer Type	Mineral group	Charge/ unit formula	Dioctahedral minerals	Trioctahedral minerals
1:1	**Non-expanding**			
	Serpentine-Kaolin	~ 0	Kaolinite	Serpentine
2:1	**Non-expanding**			
	Talc-pyrophyllite	~ 0	Pyrophyllite	Talc
	Expanding			
	Smectites	0.2 – 0.6	Montmorillonite beidellite	Nontronite Hectorite Saponite
	Vermiculite	0.6 – 0.9	Vermiculite	Vermiculte
	Mica	0.9 – 1.0 ~1.0	Muscovite	Phlogopite Biotite
2:1:1	**Non-expanding**		i. Trioctahedral: interlayer and 2:1 octahedral sheets are trioctahedral	
	Chlorite	variable	ii. Dioctahedral: interlayer and 2:1 octahedral sheets are dioctahedral	
			iii. Di-trioctahedral: 2:1 octahedral sheet is dioctahedral and interlayer sheet is trioctahedral	
			iv. Tri-dioctahedral: 2:1 octahedral sheet is trioctahedral and interlayer sheet is dioctahedral	

Table 2: Properties of clay mineral group.

As observed in Table 2, some are neutral clay minerals while others possess surface charges. When the tetrahedral and octahedral sheets assemble to form the layers, the net resulting charge (neutral or negative) constitute the permanent structural charges as follows:

- *Electrically neutral layers* occur with the combination of:

(i) Tetrahedral sheets made up of tetrahedra, all containing Si^{4+} as the central cation and,

(ii) Trioctahedral sheets containing Mg^{2+}, Fe^{2+} or other divalent cations as central cation of all the octahedra constituting the octahedral sheet or,

(iii) Dioctahedral sheets containing Al^{3+} or Fe^{3+} as central cation of all the octahedra constituting the octahedral sheet.

- *Negatively charged layers* occur in the presence of:

(i) Isomorphic substitutions of Si^{4+} by Al^{3+} in the tetrahedral sheet;

(ii) A vacancy of cation in the trioctahedral sheet;

(iii) Isomorphic substitutions of Al^{3+} by divalent (or lower charge) cations in the octahedra of the dioctahedral configuration.

The different layered minerals used in our study are described herein:

- **1:1**

Kaolinite is the most common mineral from the kaolin subgroup belonging to the 1:1 structured clay minerals (Figure 9 [32]). It contains Si^{4+} as the central cation of the tetrahedra and Al^{3+} in the centre of octahedra in dioctahedral configuration. Due to the absence of isomorphic substitution, kaolinite minerals are known to possess negligible internal CEC (cation exchange capacity, *section 2.1.4.*) and hence do not contain interlayer cations. The charges occurring are primarily pH dependent charges (at the edges and on basal (OH) surfaces) [33].

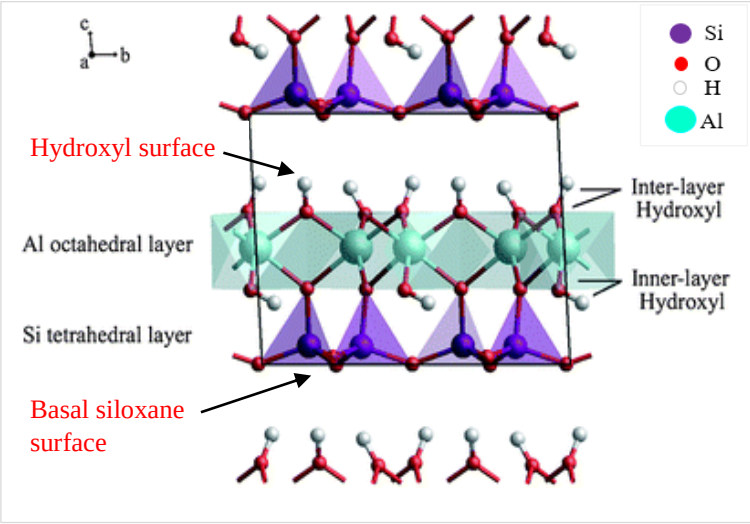

Figure 9: Kaolinite structure

When the tetrahedral and octahedral sheets stack into a layer, the apical hydroxyls of the octahedral sheets face the basal oxygen of the tetrahedral sheets. A strong hydrogen bonding is thus exerted between these entities causing limited expansion and no room for water molecules to fit into the interlayer spacing.

- **2:1**

Smectites: are characterised by the 2:1 layer structure (Figure 10 [34]).

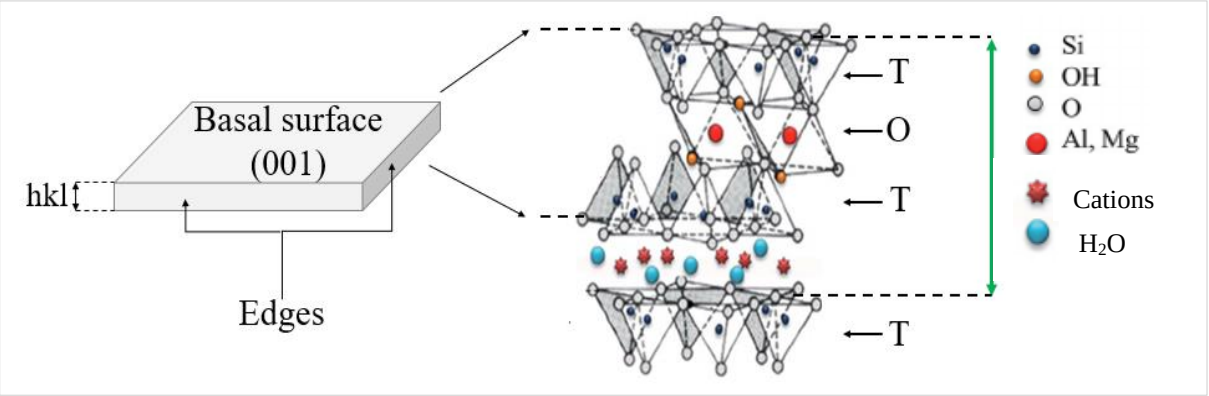

Figure 10: a) A clay platelet with the basal surface and the edges shown; structure of clay platelet resulting from stacking of TOT layers.

Well known smectite clay minerals are dioctahedral montmorillonite and beidelite and trioctahedral nontronite. The permanent charges at the surface of these clays are a result of isomorphic substitutions as follows [35]:

- Montmorillonite: in the octahedral layer, Al^{3+} by Mg^{2+}
- Beidelite: in the tetrahedral layer, Si^{4+} by Al^{3+}
- Nontronite: in the tetrahedral layer, Si^{4+} by Fe^{3+}.

Unlike kaolinite, due to the permanent charges of the smectites, the interlayer spacing contain exchangeable cations in order to equilibrate the negative charges of the platelets. Most commonly encountered cations in order of relative abundance are Ca^{2+}, Mg^{2+}, H^{+}, K^{+} and Na^{+} [36]. With respect to the nature of the cations (their hydration energies) and the relative humidity conditions, water molecules are also likely to be found in the interfoliar space and cause swelling of the clays. As such, the layers are held together by van de Waals forces between interlayer cations and the adjoining negatively charged layers. Some authors reported that the hydration energy of interlayer cations can overcome the attractive forces between the cations and the charged layers in such a way that the interlayer spacing is increased (swelling occurs) [37]. In the presence of Na^{+} as exchangeable ions, one, two or three hydrate layers are likely to be found in the interlayer space according to the relative humidity. Indeed under high humidities, swelling of smectites occur in such a way that clay particles delaminate (i.e basal spacing tending to ∞) and hence easily disperse in water as individual platelets. In comparison, in the presence of Ca^{2+} as interlayer cation, a maximum of three layer hydrate occurs.

Mica also forms part of the 2:1 structured clay minerals (Figure 11 [38]). Two tetrahedral sheets sandwiching an octahedral sheet (either a di- or tri-octahedral sheet) are made up of a repetition of 3 tetrahedra of Si^{4+} and a fourth tetrahedron containing Al^{3+} as central cation. This substitution gives rise to an excess of negative charge, which is compensated by an interlayer cation, usually K^+ (e.g. muscovite -dioctahedral configuration with Al^{3+} in the octahedral sites or biotite –trioctahedral configuration with Mg^{2+} and Fe^{2+} in octahedral sites).

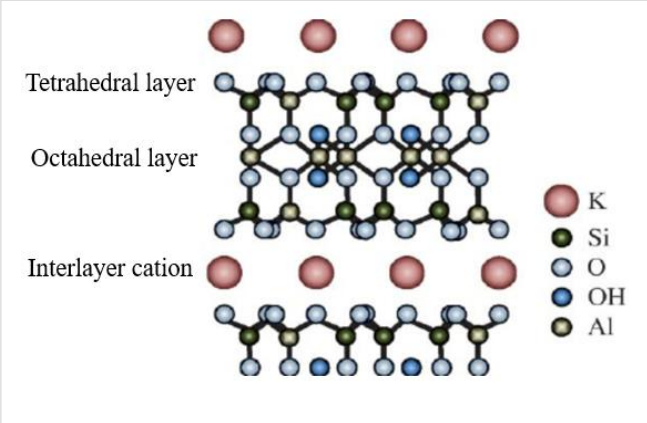

Figure 11: Mica structure

When several TOT layers are stacked, the interlayer cations form a strong bond between the basal oxygens of the adjoining tetrahedral sheets. As such K^+ ions can exactly fit into the hexagonal cavities of the tetrahedral sheets. Expansion of the interlayer spacing of mica is very limited and the mineral is known as a non-expanding clay.

Similar to the basic building unit of muscovite mica (2 tetrahedral sheets sandwiching a dioctahedral sheet), **Illite** clay minerals are also known as “hydrous” or “weathered” mica. As mica, the interlayer spacing contains K^+ as exchangeable cation, in a sufficient amount to limit its expansion when in contact with water (indeed K^+ ions are known to be poorly hrdrated) , but not enough amount to neutralise surface charges arising from isomorphic substitutions. As a consequence, unlike muscovite, some water molecules are able to enter into the interlayer spacing.

In addition to the permanent structural charges, the clay minerals also possess pH dependent charges. As suggested by the name, these charges are not permanent and depend on the pH of solutions. Amphoteric OH present at the apex of octahedra are subject to protonation or dissociation according to pH of the surrounding environment and hence, play an important role in the development of surface charges. In addition, at the edges, in order to saturate the valencies of silicium and oxygen in the tetrahedral sheet and that of aluminium and oxygen in the octahedral sheets, water molecules are hydrolysed and give rise to silanols and aluminols respectively. According to the pH of the surroundings, the silanols and aluminols dissociate and protonate as follows:

- In the tetrahedral sheet: dissociation of silanol

$$\equiv Si\text{-}OH + OH^- \leftrightarrow \equiv Si\text{-}O^- + H_2O \qquad \text{Equation 3}$$

Due to the low pKa of silanols, they do not get protonated under normal pH range and are unlikely to contribute to the edge positive charges [39].

- In the octahedral sheet: dissociation of aluminol

$$\equiv Al\text{-}OH + OH^- \leftrightarrow \equiv Al\text{-}O^- + H_2O \qquad \text{Equation 4}$$

- In the octahedral sheet: protonation of aluminol

$$\equiv Al\text{-}OH + H^+ \leftrightarrow \equiv Al\text{-}OH_2^+ + H_2O \qquad \text{Equation 5}$$

2.1.4. Cation exchange capacity of clay minerals

In relation to the permanent and pH dependent charges, clay minerals retain cations to maintain electrical neutrality. This property of clay minerals is referred as the Cation Exchange Capacity (CEC) and is defined for each mineral at a given pH. As such, the CEC (expressed in milliequivalents per 100g of clay mineral) refers to the total number of negative charges which are likely to attract exchangeable cations by van der Waal forces. As described above, the charges of clay minerals are either of permanent or non-permanent origin and hence define two types of CEC respectively:

- Internal CEC: is linked to the amount of cations in the interfoliar spacing required to compensate permanent layer charges
- External CEC (at the edges): is linked to pH dependent charges.

2.2 Wettability of oil reservoirs

This section aims at reviewing the wettability of oil bearing sandstone reservoirs, with special emphasis on the wettability of clay minerals. Briefly, the phenomenon of wettability characterises the affinity of one fluid to spread on a solid surface in the presence of other immiscible fluids (Figure 12 [40]). The reservoir (fluid/rock system) can grossly be classified either as *oil-wet* or *water-wet* depending on the fluid that coats the rock surface. In the former case, the majority of the rock surface as well as the small pores within the rock are respectively in contact and occupied by oil. In the latter case, water is in contact with the rock surface and occupies the small pores. As seen above, systems of *mixed wettabilities* are defined when both oil and water tend to adhere to rock surfaces. In such cases, the large pores are oil-wet and small pores water-wet, with oil and water wet regions continuously connected. In some reservoirs, the rocks are of irregular mineral composition and surface chemistry, thus giving rise to wettability termed *fractional* as it varies depending on the part of the core investigated.

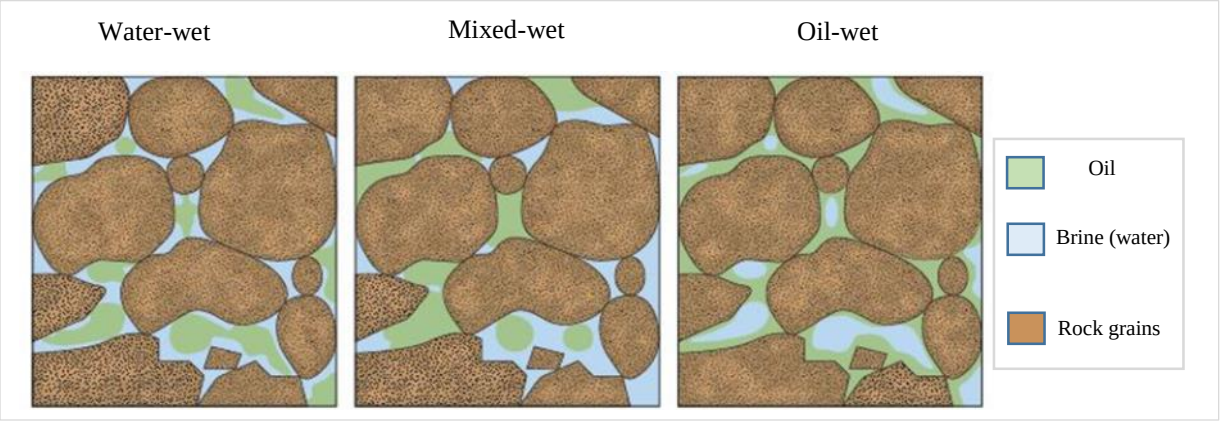

Figure 12: Wetting in pores. In a water-wet case (left), oil remains in the center of the pores. The reverse conditions holds if all the surfaces are oil-wet (right). In the mixed-wet case, oil has displaced water from some of the surfaces, but is still in the centers of the water-wet pores (middle). The three conditions shown have similar saturations of water and oil.

In the oil industry, determination of reservoir core wettability is either achieved on a quantitative or qualitative basis. The Amott wettability measurements, USBM (U.S. Bureau of mines) method, electrical resistivity method and contact angle measurement method are generally used techniques to quantify wettability of reservoir cores [41]. Qualitative methods for the determination of the wettability of reservoir cores include imbibition rates, microscope examination, flotation of particles in fluids, glass slide method, relative permeability curves,

capillary pressure curves, capillarimetric method, displacement capillary pressure, permeability/saturation relationships, reservoir logs, nuclear magnetic resonance and dye adsorption methods [41].

Our study focusses on the wettability of clay minerals found at the surface of rocks and to reach such a goal, the contact angle measurement method was appropriate to determine the wettability of pure minerals.

2.2.1 Contact angle method

When a small drop of liquid is deposited on a solid surface, the three phases (solid *S*, liquid *L* and the vapour *V*) are in contact. As a result of intermolecular interactions between them, the liquid either spreads or shapes up on that particular surface. For instance, when adhesive forces (the attractive forces between the molecules of the liquid and those of the solid) are stronger than the cohesive forces (the attractive forces between the molecules within the liquid), the liquid spreads on the solid surface. On the other hand, if the cohesive forces outweigh the adhesive forces, the liquid shapes up spherically in order to minimise contact with the surface. The extent to which a liquid is actually in contact with the solid gives rise to two different wetting regimes: partial (with a finite contact angle θ) or complete (contact angle θ = 0°) wetting as illustrated by Figure 13 below:

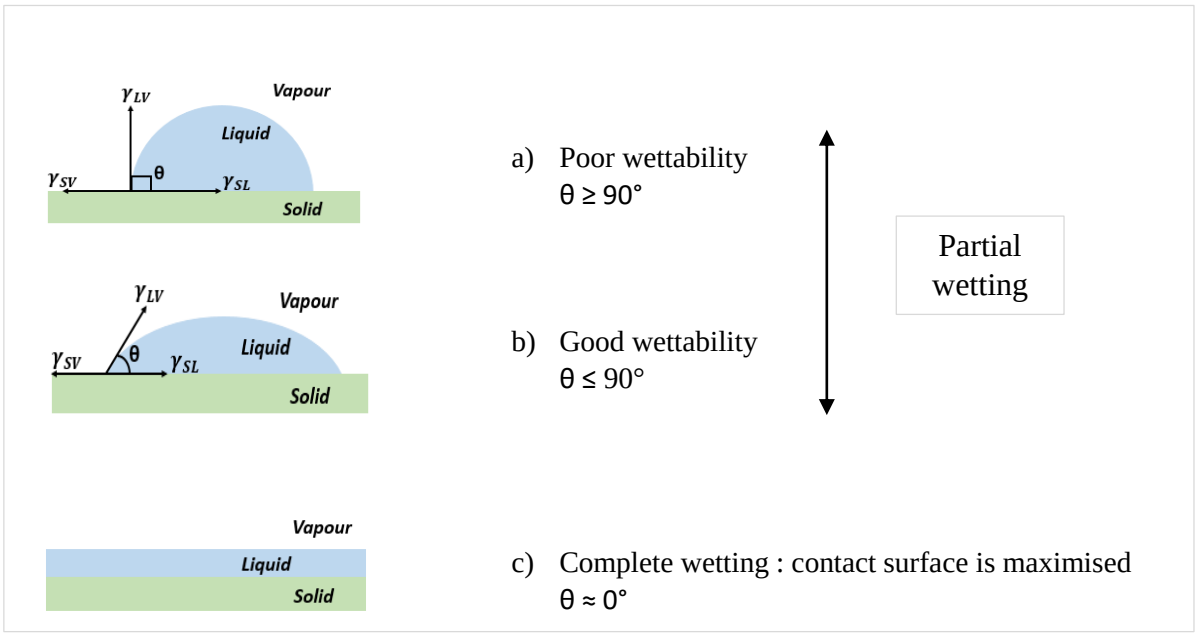

Figure 13: Schematic representation of different wetting regimes when a liquid is deposited on a flat solid surface. The geometry of the sessile droplet is characterised by the contact angle θ.

The global equilibrium configuration of a sessile droplet on a smooth and chemically homogeneous solid surface is driven by the minimisation of surface energies. In the case of finite contact angles, the wetted portion is delimited by the triple phases contact line *L* and characterised by the contact angle θ as described the Young-Dupré equation:

$$cos\,\theta = \frac{\gamma_{SV} - \gamma_{SL}}{\gamma_{LV}} \qquad \text{Equation 6}$$

Where, γ_{SV}, γ_{LV} and γ_{SL} are the surface tensions at the solid-vapour, liquid-vapour and the interfacial tension at the solid-liquid interfaces respectively.

It is worth outlining that in the context of oil reservoirs, in the presence of a solid surface (rock), water and crude oil the most widely accepted classification of wetting is that of Anderson [41]:

Contact angle of water , θ (°)	**State of wetness**
0 ~ 75	**Water-wet**
- 55 ~ 75	- Weakly water-wet
75 ~ 115	**Intermediate-wet**
115 ~ 180	**Oil-wet**
- 115 ~ 135	- Weakly oil-wet

Table 3: Classification of wetness according to Anderson.

- **Surface tension and Interfacial tension (IFT)**

The tension present at the surface (for e.g liquid-vapour: γ_{LV}), arises from the fact that molecules which are located within the bulk are subjected to equal forces of attraction in all directions, while those located at the interface experience unbalanced attractive forces. Consequently, the cohesive forces between molecules at the surface are stronger than those in the bulk and result in a surface "film" with a high energy. This enhancement of cohesive forces is referred as the *surface tension*. In a similar way, interfacial tension exists at interfaces. Distinction between surface and interfacial tension is made when considering the tension at solid/vapour and liquid/vapour in the former case and solid/liquid and liquid/liquid interfaces for the latter case.

Generally, surface/interfacial tensions are the free energy per unit area (expressed in joules per square meter: J m^{-2}) or the force per unit length (expressed in newtons per meter: Nm^{-1}) [42].

2.2.2. Parameters influencing contact angle measurements

When possible, i.e. for smooth and non-porous surfaces, the Static Sessile Drop (SSD) method is well adapted and relatively easy to use. In this technique, a drop of the probed liquid is deposited on the substrate and the contact angle is defined as an equilibrium of the triple phase contact line. However, for clay minerals, this method is more prone to difficulties and the results can strongly vary depending on various parameters such as nature of the surface ions [43], [44], relative humidity [44], [45]**,** particle size [46], [47] and surface roughness [48]–[53].

a) Surface Ions

As far as the effect of cations nature is concerned, a few studies investigated their influence on wettability. In the case of kaolinite, a non-swelling clay mineral with exchangeable ions (H^+, Na^+, K^+, Ca^{2+}, Mg^{2+}, Ba^{2+} and Al^{3+}), Biaeopiotrowicz et al. [43] measured the contact angles of water and diiodomethane. In terms of surface free energy of the different kaolinite samples, their results revealed no major differences of the dispersive components (Van der Waals type force). In contrast, the non-dispersive components (dipole-dipole, dipole-induced dipole, hydrogen bonding type forces) increased linearly on clays exchanged with H^+, Na^+, Ca^{2+}, Mg^{2+} and Al^{3+}. A linear correlation was thus found between the non-dispersive forces and the respective entropy of hydration of the ions. Both the K^+ and Ba^{2+} samples did not follow the obtained linear relationship. The authors assigned the latter results to the large size of these two ions (K^+ and Ba^{2+}) compared to the other ones. In contrast to these results, Shang et al. [44] observed negligible effect of the nature of surface ions (Na^+, K^+, Mg^{2+} and Ca^{2+}) on water contact angles measured on samples of smectites, kaolinite and illite.

b) Relative Humidity, RH

Relative humidity, RH, is an important parameter to be taken into consideration during contact angle measurements. Indeed, as described in the previous sections, clay minerals are likely to contain water molecules in the interlamellar space. The interaction mechanisms of water molecules with swelling clays can be described according to two main processes [54]–[56]. At high water content osmotic swelling occurs for smectites with monovalent cations such as Li^+ or Na^+ leading to a complete exfoliation of the structure [37], [55], [56]. At lower RH, the hydration capacity of smectites mainly depends on the nature of the interlayer cation [45], [57], [58]. Cases et al. [45] and Michot et al. [57] analysed montmorillonite swelling for various

interlayer cations and observed an increase in basal spacing with hydration energy according to the following series: $Cs^+ < Rb^+ < K^+ < Na^+ < Li^+ < Ba^{2+} < Sr^{2+} < Ca^{2+} < Mg^{2+}$. Consequently the most hydrated clays (hence with the proper exchangeable cations) are expected to give the lowest water contact angles. During their studies, Shang et al. [44] investigated the effect of relative humidities of 19, 33, 75 and 100% on smectite, kaolinite and illite with Ca^{2+} as exchangeable cation. Overall, they did not observe any general trend of the contact angles of water and diiodomethane as a function of RH at 33 and 75% but at 100% RH they recorded a decrease of the contact angles of water and an increase of that of diiodomethane.

c) Particle Size

The effect of particle size on wettability has to our knowledge not been investigated in the case of clay minerals. Data on the effect of particle size are available for other materials. For instance, Synystka et al. [46] measured dynamic contact angles on hexagonally packed silicon particles of different sizes (containing grafted polymers) and observed that increasing vertical roughness did not modify the advancing angles for particles sizes ranging from 0.2 to 10 µm. However, the receding contact angles increased until the particles size reached 5 µm and then decreased. In their investigations, Yang et al. [47] determined contact angles of molybdenite powders of various sizes by Washburn's method and found that smaller particles exhibited smaller contact angles.

d) Surface Roughness

Surface roughness is a key parameter influencing contact angle measurements. In opposition to chemically homogeneous and smooth surfaces, when a liquid is dropped on a rugged surface, the triple phase contact line is unable to stabilise to a minimum energy [59]. Wenzel, Cassie and Baxter have described models relating contact angles to the roughness of surfaces [60], [61]. Wenzel on his side described the homogeneous wetting regime and stated that upon addition of roughness on a surface, its wettability is enhanced and driven by the chemistry of the surface. For instance, a chemically hydrophobic surface becomes even more hydrophobic provided that the liquid penetrates into the grooves and that the size of the droplet is two to three times larger in magnitude than the roughness. On their side, Cassie and Baxter described the heterogeneous wetting regime where drops bridge across surface protrusions and do not penetrate into the grooves.

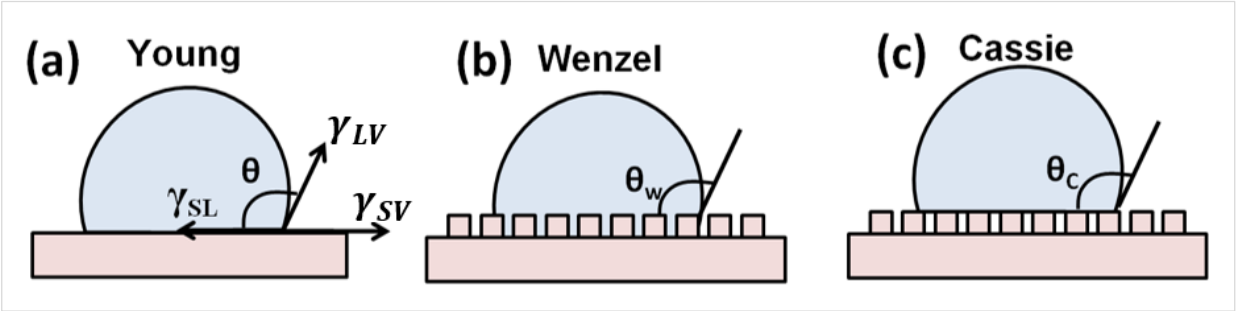

Figure 14: Different wetting regimes; a) Young model; b) Wenzel model; c) Cassie-Baxter model.

Whether drops penetrate in grooves (homogeneous wetting regime: Wenzel model) or not (heterogeneous wetting regime with air trapped in between the grooves under the liquid: Cassie-Baxter model), surface roughness plays a key role in the determination of contact angles (Figure 14 [62]). As far as clay films roughness is concerned, Zabat et al. [53] reported that the nature of the interlayer ions defines the profile of the surface. They studied the roughness of montmorillonite films with various interlayer ions Li^+, Na^+, Cs^+, Mg^{2+}, Ba^{2+}, Al^{3+} and La^{3+} by fractal analysis. The results showed that *H*, the Hurst exponent of fractal Brownian motion (*cf chapter 3, section 1.4.3.*), decreased in the order of clays exchanged with monovalent cations to divalent cations and finally to trivalent cations. In short, this indicated that clay films exchanged with monovalent ions are smoother while those with trivalent ions are the roughest ones.

3. Oil/aqueous phase interactions

3.1 Crude oil

Otherwise known as petroleum, **crude oil**, primarily consists of a mixture of hydrocarbons of different molecular weights naturally occurring in sedimentary rocks (porous and permeable lithological structures such as sandstones and carbonates). In addition to hydrocarbons, complex molecules containing elements like sulphur, nitrogen, oxygen and trace of metals (Na, Ca, Mg Al, Fe, Ni and V) are commonly found [63]–[65].

Crude oils are classified according to physical parameters such *viscosity* and the *API* (American Petroleum Institute) gravity. Viscosity (resistance to flow of liquids), qualifies oils from low viscosity liquids up to tar-like (nearly under the solid form). It is determined at different temperatures (for example at 25°C and 100°C) by measuring the time for a volume of a liquid to flow under gravity. On its side, the API gravity, determines how heavy the crude oil is with respect to water (whether it floats on or sink into water). Light crude oils have low densities and high API values while heavy crude oils have high densities and low API values. Typical API values and examples of oils ranging from light to heavy are reported in Table 4 [63].

$$API\ gravity\ (°) = \frac{141.5}{specific\ gravity} - 131.5 \qquad \text{Equation 7}$$

With the $specific\ gravity$ being the ratio between the density of the crude oil and the density of a reference liquid, usually water at 60°F (15.6°C).

Classification	API range (° API)	Examples Crude Name, API (° API)
Light	> 33	Saudi super light, 39.5 Nigerian light, 36 North Sea Brent, 37
Medium	28 – 33	Kuwait, 31 Venezuela light, 30
Heavy	< 28	Saudi heavy, 28 Venezuela heavy, 24

Table 4: classification of Petroleum crude.

The chemical composition of crude oils varies from one source to another. However, the elemental constituents have been reported to vary over a quite narrow range as [66], [67]:

C	83.0 - 87.0	wt. %	O	0.05 -1.5	wt. %
H	10.0 - 14.0	wt. %	S	0.06 – 6.0	wt. %
N	0.1 - 2.0	wt. %	Metals	< 0.01	wt. %

In order to valorise crude oils, they are separated into fractions by distillation under atmospheric pressure (for components of boiling points ≤ 360°C and produce light gases C1-C4, gasoline, naphtha, kerosene, fuel oil etc.) and under vacuum conditions (where constituents boil and evaporate at lower temperatures under reduced pressure to produce light and heavy vacuum gas oils). The fraction remaining after vacuum distillation is termed *bitumen* or *asphalt*.

It is of greater interest for the petroleum industry to separate the constituents into hydrocarbon groups rather than into elemental constituents. Indeed, separation into different hydrocarbon groups provide handier information for example, during reservoir evaluation (such as estimation of potential flow rates), determination of petroleum origin, studies of degradation processes and environmental effects [68].

The separation and isolation of the constituents of crude oils is generally achieved by a process known as the *SARA* fractionation (Figure 15 [67]). Based on the difference of solubility and polarity of the components, this method separates dead oil (oil that has lost its gaseous components) into four classes, namely the ***S**aturates*, ***A**romatics*, ***R**esins* and ***A**sphaltenes*. The asphaltenes are first precipitated and the *SAR* class (also known as maltenes) separation is usually achieved by high-performance liquid chromatography (HPLC).

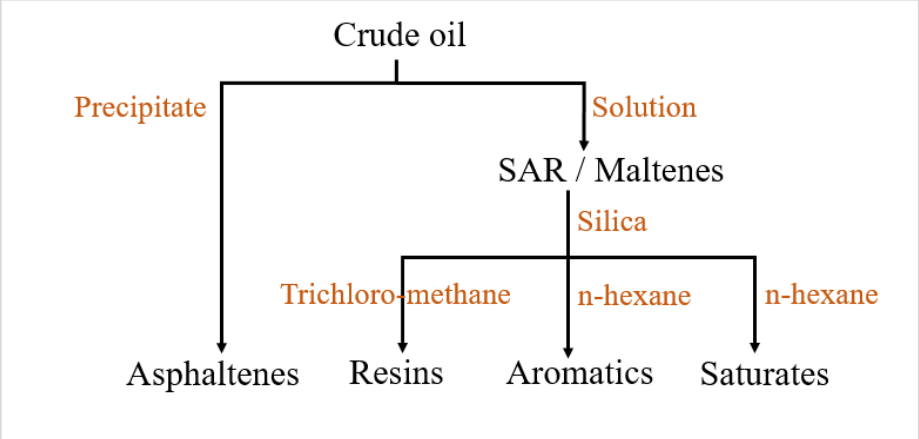

Figure 15: Scheme for SARA Fractionation.

- **Saturates** include the *paraffins* (linear or branched alkanes), *naphthenes* (cycloparaffins) and a subclass of saturates named *waxes* (straight-chain alkanes of C_{20} to C_{30}).

- The **Aromatic** class consists of benzene based molecules (unsaturated single or multiple closed rings) which contain alkyl and cycloalkanes as substitutions. Polar molecules on aromatics of high molecular weights are assimilated to the resin or asphaltene classes.
- The **resin** and **asphaltene** classes are usually defined as solubility classes. For instance, resins are soluble in n-alkanes such as n-pentane and n-heptane but insoluble in propane [64], [69], [70] while asphaltenes are soluble in aromatic solvents like benzene and toluene but insoluble in the n-alkanes [71]. Both resins and asphaltenes are compounds of high molecular masses (500 -1000 g/mol [72]) and contain heteroatoms like sulphur, nitrogen and oxygen. Structurally similar, resins differ from asphaltenes by their lower molecular weights and higher H/C ratios (1.2-1.7 for resins and 0.9-1.2 for asphaltenes) [70], [71]. Resins (Figure 16 [73]) have been reported to play an important role in the stabilisation of asphaltenes in petroleum and hence prevent their precipitation.

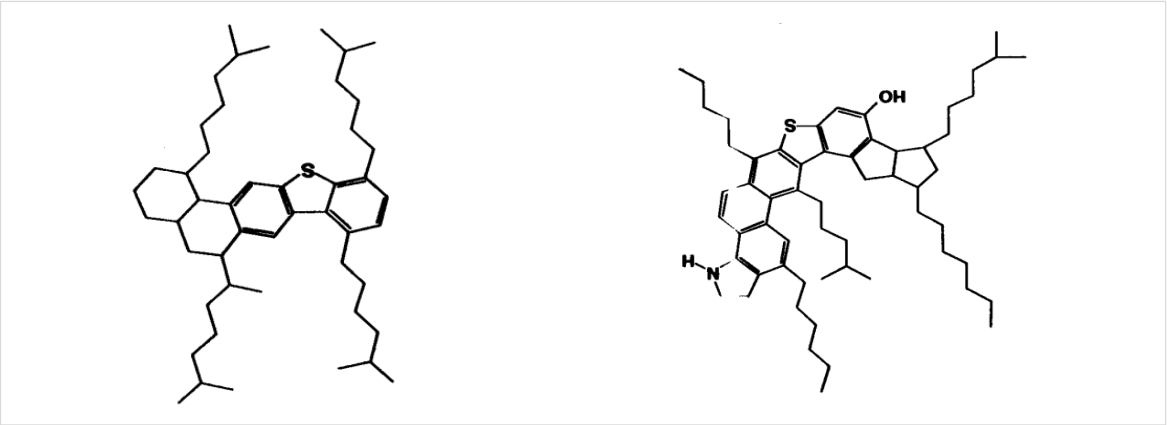

Figure 16: Structures of resin molecules.

As such, it is generally accepted that asphaltenes are polycyclic aromatic hydrocarbons but due to the complexity of the molecules, the exact number and arrangement of the aromatic cycles are not precise. Consequently, the molecular structure of asphaltene is still debatable [74]. Two different possible structures of asphaltene molecules are shown in Figure 17 underneath. The molecule 17.a), consists of a number of polyaromatic rings linked by alkyl chains and the molecule 17.b) on its side shows a central block of polyaromatic rings with peripheral alkyl chains [75], [76]. The average gyration radius of asphaltenes have been reported to be 15A° [72].

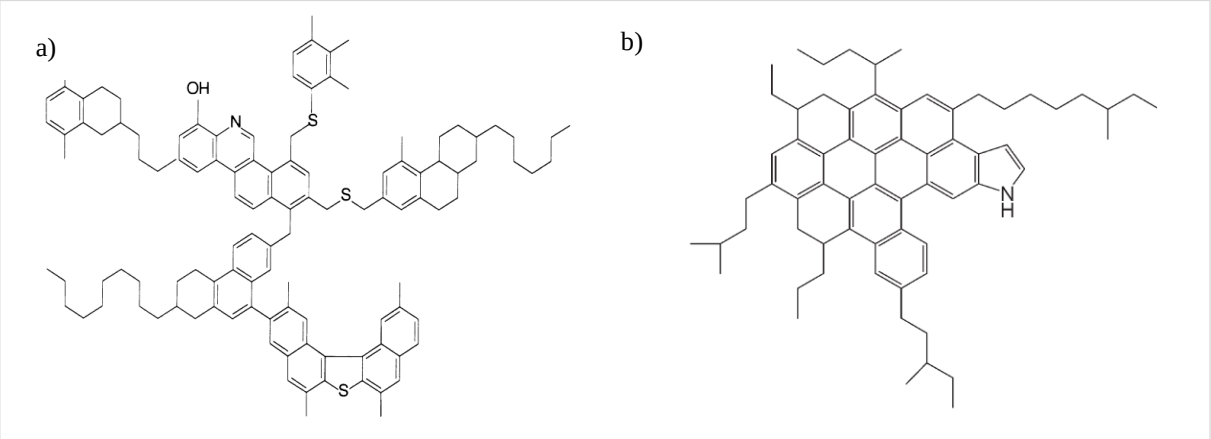

Figure 17: Hypothetical structures of asphaltene molecules.

Due to the presence of various polar atoms and the large hydrocarbon skeleton, asphaltenes and resins have been reported to be interfacial active (*surfactants*) molecules [77], [78].

3.1.1. Surfactants

In this section, definition of surfactants is being given on the basis of the classical and commonly known ones. As such ***surfactants*** or *surface active agents*, are amphiphilic organic molecules possessing a polar headgroup (hydrophilic) and a nonpolar (hydrophobic or lipophilic) end [79]. Accordingly to the polar headgroup, surfactants are classified as follows:

- Anionic: the head possessing a negative charge;
- Cationic: the head possessing a positive charge;
- Non-ionic: no charged moiety on the head;
- Zwitterionic: the head possessing both negative and positive charges.

Surfactants possess the property of adsorbing at oil/water interfaces and alter their interfacial free energies [80]. When the concentration of surfactants in a solution reaches a critical value known as the critical micelle concentration, CMC, the molecules assemble into micelles (direct or inverse, Figure 18). On the other side, the formation of micelles is also affected by temperature. Below a certain temperature known as the *Kraft temperature*, the surfactant molecules are crystallised and it is only above this temperature that they solubilise to liberate individual molecules which eventually associate into micelles.

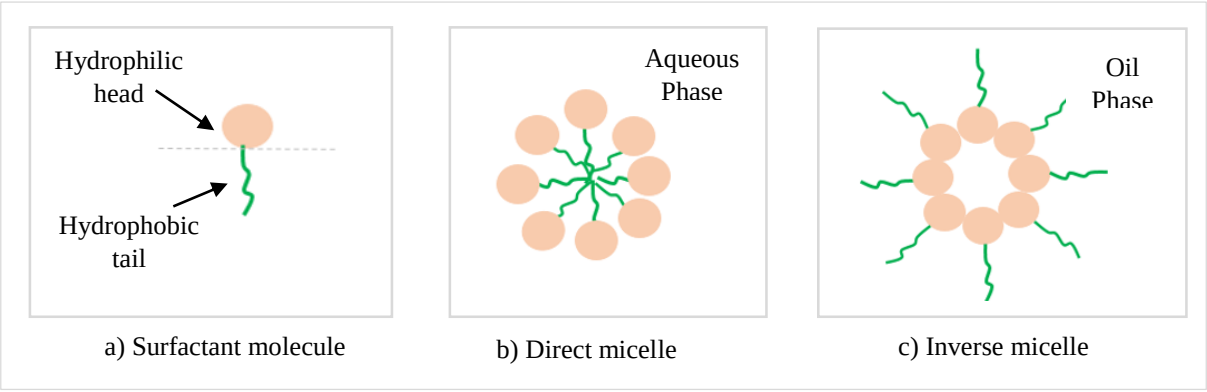

Figure 18: Schematic representation of a) a surfactant molecule; b) a direct micelle; c) an inverse micelle.

The proportion of the hydrophilic to lipophilic parts of surfactant molecules is described by the *Hydrophile Lipophile Balance* (HLB) i.e. the balance of the size and strength of the polar and the non-polar groups. HLB thus characterises the solubility of surfactants in water and ranges from 0 for a completely hydrophobic molecule to 20 for a completely hydrophilic molecule (i.e. the limits being non-surfactants and the higher the HLB the more soluble the surfactant in water). The HLB is an important parameter which is actually helpful in determining the type of emulsion formed (O/W: oil in water or W/O: water in oil) when surfactants act as emulsifiers.

HLB range	Application
3-6	**W/O emulsifier**
7-9	Wetting agent
8 – 20	**O/W emulsifier**
13-16	Detergent
15-18	Solubiliser

Table 5: HLB range of surfactant relative to different applications.

Bancroft's rule (and accordingly to table 5), states that the phase in which the surfactant is more soluble tends to be the continuous phase.

3.1.2. Emulsions

Two immiscible phases lead to thermodynamically unstable emulsions. Due to their amphiphilic nature, surfactants can act as linkers between organic and aqueous phases by decreasing surface tension. An emulsion is made when a shearing force is applied to two immiscible liquids (e.g. oil and water) in the presence of a linker such as a surfactant/ an emulsifier. It consists of one liquid dispersed (the dispersed phase) into the other liquid (the continuous phase). According to the dispersed and continuous phases, two main types of emulsions can be distinguished: O/W (oil droplets in water as the continuous phase) also known as direct emulsion and W/O (droplets of water dispersed in oil as the continuous phase) also known as inversed emulsion.

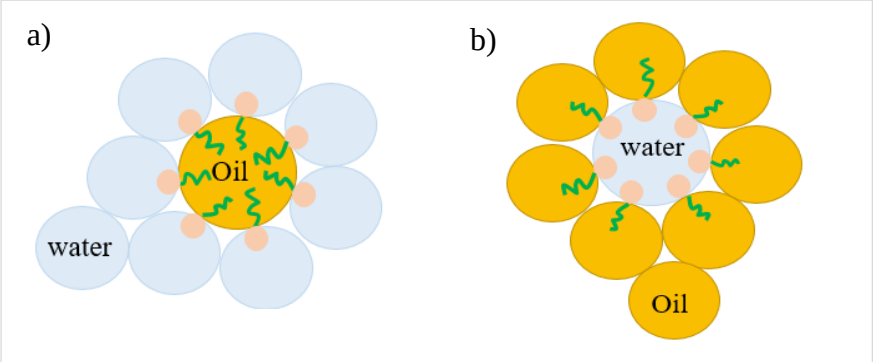

Figure 19: Representation of simple emulsions a) O/W emulsion and b) W/O emulsion.

Accordingly to the IUPAC definition, emulsions are subdivided into different categories depending on the size of the droplets which constitute the dispersed phase:

- Macroemulsion: droplet size > 400 nm
- Minioemulsion also called nanoemulsion: droplet size 100 - 400 nm
- Microemulsion: droplet size < 100 nm.

Macroemulsions

Even if macroemulsions can be kinetically stable, they are known to be thermodynamically unstable. Depending on the nature of the emulsifier, macroemulsions can be of both W/O or O/W type. Indeed, as seen above, in the presence of an emulsifier of low HLB, the emulsion formed would rather be of W/O type and vice-versa. Moreover, a W/O or O/W macroemulsion can be tuned by controlling the order of mixing of the different phases. For instance, adding oil into water is likely to form an O/W emulsion.

Miniemulsions / Nanoemulsions

As macroemulsions, miniemulsions can be W/O or O/W types which are thermodynamically unstable. They consist of finely dispersed droplets (much finer than macroemulsions) and can be regarded as colloidal dispersions. To reach the droplet size characteristic of a nanoemulsion, the amount of surfactant present should represent about 1 – 3% of the oil fraction.

Microemulsions

Like macroemulsions and miniemulsions, microemulsions can be both of W/O or O/W types. However unlike the latter emulsions, microemulsions are thermodynamically stable. Actually, this stability is driven by the free energy of the colloidal dispersion. For instance, the free energy of the emulsion is lower than the free energy when the phases are separated.

Microemulsions are formed to favour a lowering of interfacial tension between the oil and aqueous phase. In order to reach the droplet size characteristic to microemulsions, about 15 – 30 % of surfactant is necessary.

Apart from the simple emulsions described above, complex emulsions, also called multiple emulsions can also be encountered. For example:

- **O/W/O**: resulting from the dispersion of an oil in water emulsion into a continuous oil phase; the dispersed oil droplets containing smaller water droplets.
- **W/O/W**: resulting from the dispersion of a water in oil emulsion into a continuous phase of water; the dispersed water droplets containing smaller oil droplets.

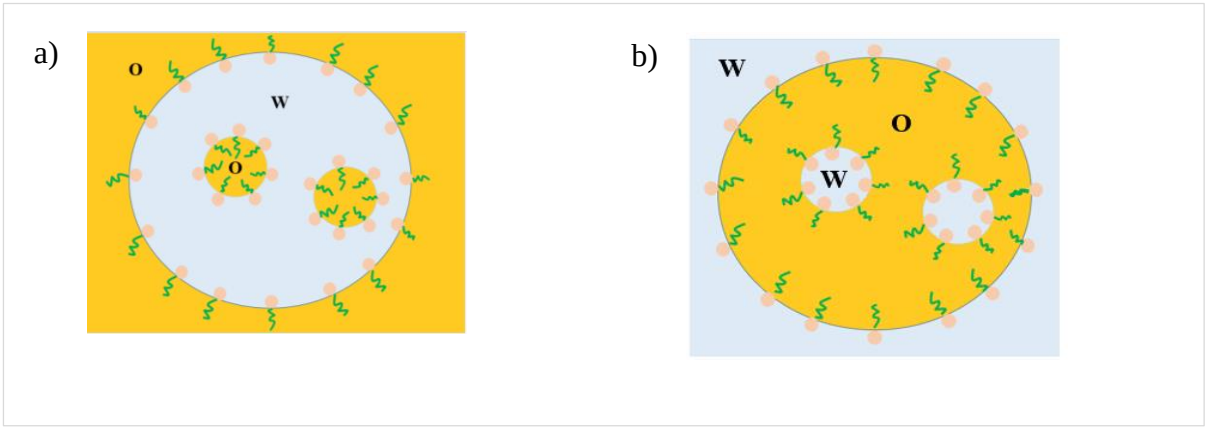

Figure 20: Schematic representation of a) O/W/O emulsion; b) W/O/W emulsion.

Pickering emulsions

Pickering emulsions are particles-stabilised emulsions. Unlike the stabilisation of emulsions due to lowering of interfacial tension by surfactants, particle-stabilised emulsions depend on the size of the particles. Indeed, the particles need to be smaller than the droplets in order to be located around them. Similarly as the surfactant-stabilised emulsions, particles can stabilise both W/O and O/W emulsions. However, the effectiveness of the stabilisation is dependent on various factors such as: particle shape and size, particle's wettability and particle-particle interactions.

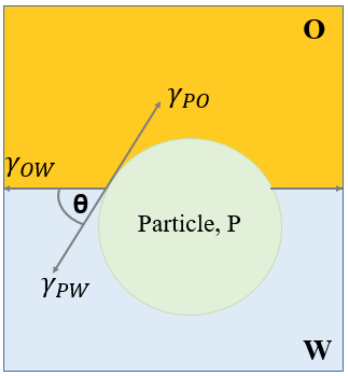

A contact angle, θ < 90°, hydrophilic particle and mostly in continuous phase, i.e. resulting in O/W emulsion.

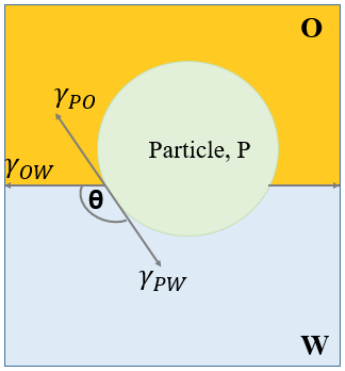

A contact angle, θ > 90°, hydrophobic particle and mostly in continuous phase, i.e. resulting in W/O emulsion.

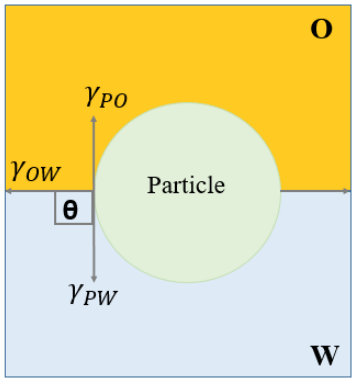

Contact angle, θ = 90°, particle equally wet by oil and water phases and hence provide maximum stability to emulsion.

Figure 21: Wettability of a particle in a pickering emulsion.

3.1.3. Crude oil surfactants and surrounding aqueous phase

During the process of LSW, crude oils containing surfactant molecules are in contact with the injected brines and depending on the conditions of the surrounding environment, the surfactants either adsorb at or move away from the oil/water interfaces. These processes have respectively been termed the **salting-in** and **salting-out effects** and play a key role in the oil/brine interfacial tension. Initially, these terms were used to characterise the solubility of proteins in electrolytes and led to a classification of ions according to their effectiveness to salt-in/out proteins. This series is commonly known as the *Hofmeister series* (Figure 22 [81]). Ions in the series are referred as kosmotropes and chaotropes according to their ability to modify hydrogen bonding in a network of water [82]. For instance, kosmotropic ions, structure water molecules since interactions between ion-H_2O > H_2O-H_2O. Kosmotropic ions thus stabilise and have a salting-out effect on proteins. On the other hand, chaotropic ions are "structure breakers". Indeed, these ions lose their hydration shell and interact with proteins causing them to solubilise.

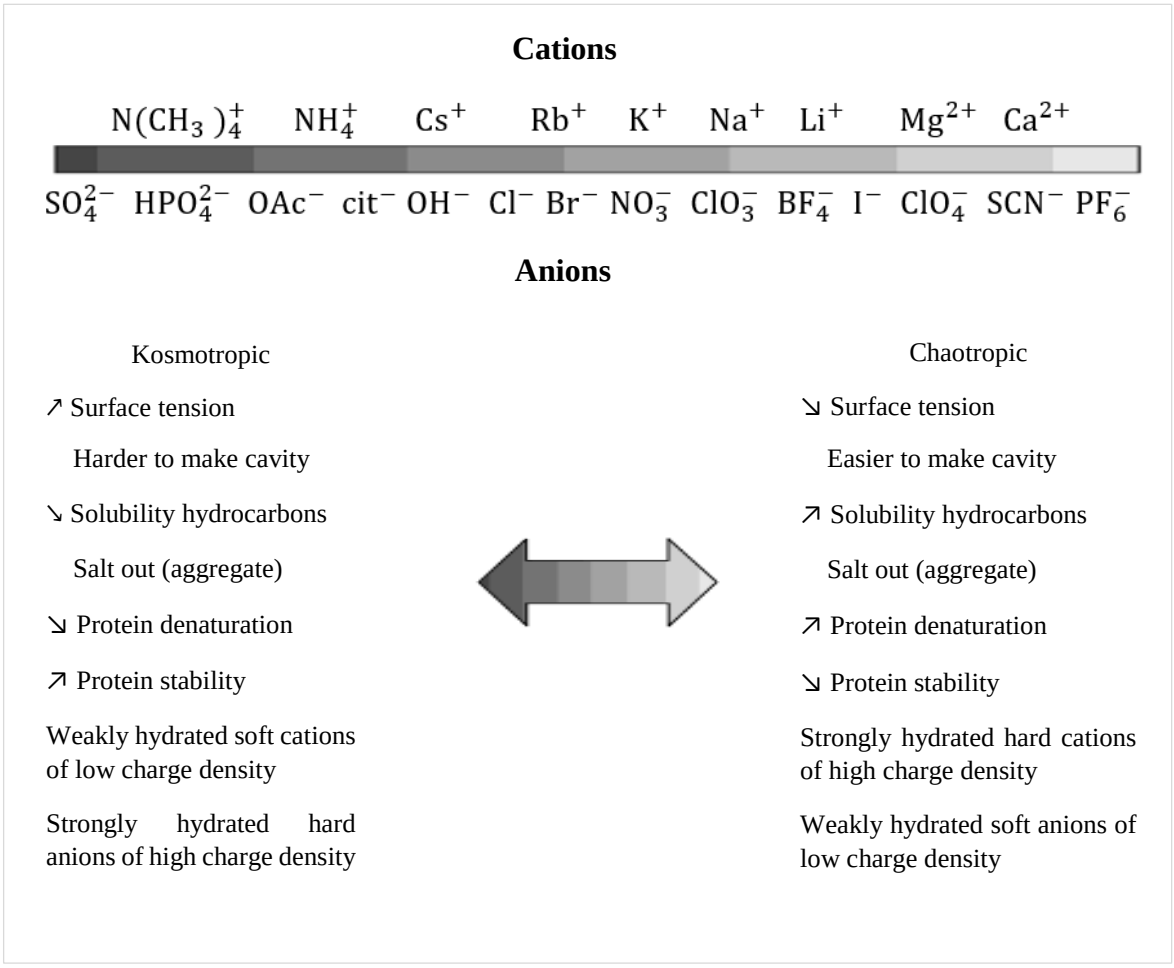

Figure 22: Hofmeister Series: typical ordering of cations and anions.

In order to provide the necessary conditions for the displacement of adsorbed oil by the injected brines, it is necessary to have an insight of the IFT between the aqueous phases (connate water and injected brines) versus the oil present in the reservoirs. The measurement of interfacial tension between two liquids can be achieved by several methods. For instance, the drop-weight [83], the Du Noöy ring [84], spinning drop [85] and the pendant drop [86] methods are widely used techniques. In our study, the interfacial tension measurements have been made by the *pendant drop* method.

3.1.3.1. The pendant Drop method

The pendant drop method used for measuring interfacial tension between two fluids consist of suspending, for example, a drop of a liquid at the tip of a needle into another liquid and analysing its shape. The interfacial tension between the inner and outer phase results in a difference in pressure (ΔP) across the curved interface as described by the classical Yong-Laplace equation as follows:

$$\Delta P = P_{IN} - P_{OUT} = \gamma \left[\frac{1}{R_1} + \frac{1}{R_2}\right] \qquad \text{Equation 8}$$

Where, P_{IN} *and* P_{OUT} are respectively the pressure inside and outside the drop; γ is the interfacial tension; R_1 and R_2 are the two principal radii of curvature of the surface.

The increase in volume results in an elongation of the drop (spherical to 'pear-shape': Figure 23 [86]) as a result of an equilibrium between the surface tension and gravity.

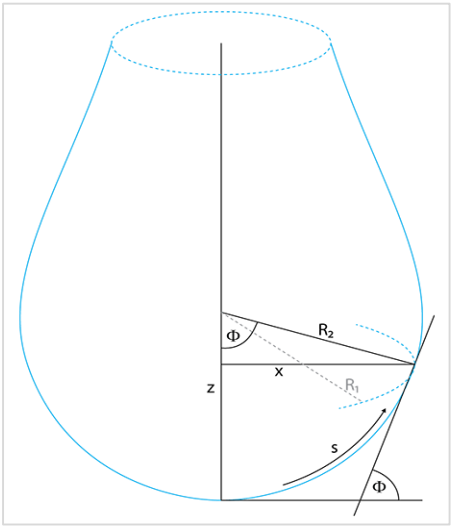

Figure 23: Schematic representation for the derivation of the Young-Laplace fit on a pendant drop.

3.1.3.2. Gibbs treatment and surface excess concentration

When two liquids A and B are in contact, an interfacial layer separates them. This interfacial layer is a "transition zone" of non-negligible thickness in which physical parameters such as concentration vary continuously from their values in the bulk phases A and B ("real situation") [87]. Gibbs treatment considers a geometrical surface of negligible thickness, which is parallel to the interface and within the interfacial zone. This surface is known as the *Gibbs dividing surface* (Figure 24: "Gibbs method") and is located at the surface of physical discontinuity. It is a hypothetical surface used to define the volumes of the bulk phases and is used in the calculation of the extent of adsorption and of other surface excess properties [88], [89].

At an interface, the adsorption or *surface excess* of a given component is defined as the difference between the amount of component actually present in the system, and that which would be present (in a reference system) if the bulk concentration in the adjoining phases were maintained up to the Gibbs dividing surface [88]–[90].

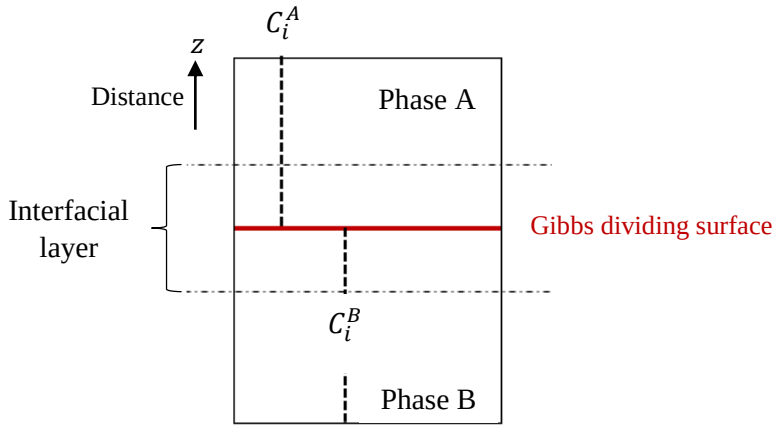

Figure 24: Schematic representation of two bulk phases A and B in contact via the interfacial layer. The Interfacial layer is treated by Gibbs as a surface parallel to the interface and termed the Gibbs dividing surface. C_i^A and C_i^B represent the concentration of component i in phases A and B respectively.

Gibbs thus defined, at constant temperature, the change in energy of the interfacial region by, $d\gamma$, according to following adsorption equation:

$$d\gamma = -\sum_i \frac{n_i}{A}\, d\mu_i = -\sum_i \Gamma_i\, d\mu_i \qquad \text{Equation 9}$$

$$\text{And } d\mu_i = RT\, d\ln a_i \qquad \text{Equation 10}$$

where: $\frac{n_i}{A} = \Gamma_i$ is the number of moles of component "i" adsorbed per unit area (surface concentration); $d\mu_i$ is the change in chemical potential of "i"; R is the gas constant; T is the absolute temperature and a_i is the activity of "i" in the bulk phase.

Depending on the nature of components in the bulk, they are either likely to adsorb at or move away from the interface. Accordingly, when a component moves towards the interface, *positive adsorption* is said to have occurred. In contrast, movement of a component away from the interface is termed *negative adsorption*. It thus follows that:

$\Gamma_i < 0$: negative adsorption $\rightarrow \Delta\gamma > 0$: IFT ↗
$\Gamma_i > 0$: positive adsorption $\rightarrow \Delta\gamma < 0$: IFT ↘

3.2 Effect of salts on oil/brine interfacial tension

During the process of low salinity waterflooding, injected brines are in contact with adsorbed oils. Depending on the nature of the oil, interfacial tension between the two liquids can be favoured by injection of brines of monitored composition. It is thus important to have an insight of the variation of IFT with varying brines composition. In this view, a chronological review of some main advances on firstly, pure hydrocarbon/brine system and secondly, crude oil/brine systems is presented.

3.2.1. Effect of salinity on pure hydrocarbon systems

In 1976, Aveyard and Saleem investigated the interfacial tension of dodecane against aqueous electrolytes of NaCl, NaBr, Na_2SO_4 KCl, KBr and LiCl. They reported their results as increments of interfacial tension as $\Delta\gamma = \gamma_{\text{dodecane-electrolyte}} - \gamma_{\text{dodecane-water}}$. Their results showed that for all salts, apart from KI, increasing the molalities of the electrolytes were accompanied by positive increments which were linear functions of the molalities. Due to the positive values of the increments and hence increase in interfacial tension, they concluded that the salts were negatively adsorbed at the interface. In the case of KI electrolyte, the increments were negative and no clear tendency was observed as a function of increasing molality. The authors hence reported that the iodide ion acted as a surfactant and hence decreased the interfacial tension between dedocane and the aqueous phase [91].

In 1996, Cai et al. focused their study on the effect of carbon number on the interfacial tension of different hydrocarbons against water/brine system. Firstly, for C6, C8, C10, C12, C14 and C16 alkanes, they observed a slight increase of the interfacial tension with the molecular masses of the hydrocarbons against water. As far as the effect of salinity is concerned, they measured the interfacial tension of octane against brines of different concentration of NaCl to investigate the effect of salt concentration and brine of $MgCl_2$ and that of $CaCl_2$ in order to investigate the effect of salt species. In a general way, they observed that the interfacial tension of octane increased with increasing salt concentration but salt species had no effect on the interfacial tension [92].

In 2004, Serrano-Saldana et al. [93] measured the interfacial tension of n-dodecane in NaCl brines with concentrations ranging from 0 to 1.5M. In a general way, they fitted an exponential decay to their results and concluded that as NaCl concentration was increased, the oil/brine interfacial tension decreased. However, for brine concentration from 0.5 to 0.9 M, irregular increasing-decreasing behaviours were observed and the authors could not provide any plausible explanation with respect to this phenomenon. Taking into consideration the general tendency of decreasing IFT with increasing salt concentration, these results were in contradiction with those obtained in the previous studies [91], [92]. The authors thus tentatively tried to explain this behaviour by arguing that there are ionic strengths that preferentially cause the ions to be located in the vicinity of the interface and hence lower interfacial tension.

In 2012, Lima et al. [94] studied specific ion effects on the interfacial tension of hydrocarbon/brine systems. They measured the interfacial tensions of cyclohexane and n-heptane and as Aveyard et al. reported their results as the difference between the hydrocarbon/electrolyte system and hydrocarbon/water system. Results on cyclohexane/electrolytes ($CuSO_4$, $MgSO_4$ and Na_2SO_4) and n-heptane/electrolytes ($CuSO_4$, K_2SO_4 and Na_2SO_4) showed that the larger cations were able to increase interfacial tension the most. Moreover, they concluded that the conformation of the hydrocarbon played an important role since the increase in interfacial tension was less significant for the linear saturated n-heptane compared to cyclohexane. Furthermore, they analysed the effect of anions by measuring the interfacial tension of n-heptane against electrolytes of $NaSO_4$, NaCl, $NaNO_3$, NaI and NaAc. Due to its large size and high charge, SO_4^{2-}, increased IFT the most, followed

by Cl^- and NO_3^- which increased to the same extent. On the other hand, AC^- and I^- behaved as surfactant and decreased interfacial tension in the order of IFT AC^- < IFT I^-. Finally, comparison between $CaAc_2$ and $NaAc_2$ revealed that calcium ions enhanced the effect of decreasing interfacial tension of n-heptane. They concluded that Ac^- acted as a surfactant, moved towards that interface and conferred a negative charge to it. Ca^{2+} ions were thus attracted to the negatively charged interface.

3.2.2. Effect of salinity on crude oil systems

In 1995, Abdel-Wali et al. [95] added oleic acid and octadecylamine of different concentrations into crude oil from Saudi Oil field (API gravity of 33) as acid and basic polar compounds respectively. They then investigated the effect of salinity on the interfacial tension of organic/aqueous phase by using NaCl with concentration ranging from 0 to 200,000 ppm. In the absence of any additives, the crude oil/water interfacial tension measured was 28 mPa/cm. Increasing NaCl concentration lead to a gradual decrease of IFT that reached 10 mPa/cm at 200,000 ppm. In the presence of oleic acid of concentration ranging from 0.0035 to 0.042 gm-mole/lit, interfacial tension decreased to reach minima (between 2 and 3 mPa/cm) at 40,000 ppm and then increased slightly (up to 5mPa/cm except for 0.0035 gm-mole/lit which increased to 10 mPa/cm) with increasing salinity. The authors explained that when brine concentration is increased from 0 to 40000 ppm, IFT decreased since oleic acid acted as an anionic surfactant. Beyond 40,000 ppm, they postulated that the positive charge of sodium was attracted to the negative charge and hence decreased the solubility of oleic acid in water. Similar behaviour was observed in the presence of octadecylamine (0.007 to 0.045 gm-mole/lit) and for all concentrations of the additive, the minima of interfacial tension (from 10 mPa/cm for 0.007 gm-mole/lit to 5 mPa/cm for 0.045 gm-mole/lit at 4000 and 100,000ppm respectively) and then increased slightly.

In 2004, Moeini et al. [96] analysed the effect of salinity to understand heavy crude oil (API gravity of 20.2)/brine interaction. Basically, they studied the effect of NaCl and $CaCl_2$ concentration on the interfacial tension of the crude oil. They observed that for both salts in a concentration range of 0 to 200,000 ppm, interfacial tension decreased to a minimum at an optimum concentration and then increased with increasing salinities. They observed for all salt concentrations, the interfacial tension was higher with $CaCl_2$ compared to NaCl. The authors

also reported that their oil phase composed of high amounts of surface active molecules such as resins, waxes and asphaltenes had much lower interfacial tension compared to pure hydrocarbon systems and since the effect of salt was recorded on the interfacial tension of their system, they assimilated asphaltenes to ionic surfactants. They argued that before the optimum salinity, it is the surfactant effect which plays the most important role in IFT reduction. Beyond, the optimum salinity, they observed an increase in interfacial tension with increasing salt concentration due to salting-out effects, the surfactants become more oil soluble and moved away from the interface. However, their arguments were based mostly on asphaltenes acting as the only surfactant. Moreover, based on the two salt species, NaCl and $CaCl_2$, they proposed that interfacial tension should increase according to the following trend: $Cs^+ < Rb^+ < NH_4^+ < K^+ < Na^+ < Li^+ < Ca^{2+} < Mg^{2+}$. However, no study has up to now been proposed in the literature as per the respective contribution of monovalent and divalent cations that could back up their arguments.

Later in 2014, Lashkarbolooki et al. [78] studied the effect of salinity on interfacial tension of a crude oil (API gravity of 21.49) by analysing the respective contribution of resins and asphaltenes. The effect of salt species on the crude oil was studied by using electrolytes of NaCl, $MgCl_2$ and $CaCl_2$ in the range of 0 to 45,000 ppm. Their experiments on the crude oil showed that with the three salts, interfacial tension decreased to a minimum and then stayed constant, the interfacial tensions being in the order of $NaCl > CaCl_2 > MgCl_2$ at all concentrations. Further investigation on the respective contribution of extracted resin and asphaltene in toluene showed that NaCl had little influence on their IFTs. Comparing the effect of $MgCl_2$ and $CaCl_2$ concentration on resins, it was observed that low salt concentrations had little effect on their interfacial tension and it was at high salinities that the IFT dropped significantly. Moreover, the interfacial tension recorded with $MgCl_2$ was lower than that of $CaCl_2$ and the authors attributed this effect to the high affinity of Mg^{2+} ions towards the oxygen present in the resin molecules. As far as asphaltene is concerned, at low concentrations of $MgCl_2$ and $CaCl_2$, the IFT dropped significantly to a minimum and then increased slightly beyond this optimum salinity with increasing salt concentration. Here, interfacial tension was lower with $CaCl_2$ compared to $MgCl_2$. This reverse trend with the salts was attributed to the fact that asphaltenes are bigger than resins and Ca^{2+} being slightly bigger than Mg^{2+}, could complex the big asphaltenes easier [78].

4. Analysis of literature review

This first chapter, dedicated to the state of the art, had for main objectives to outline the progresses in relation to the technique of low salinity waterflooding. To date, even if no consensus on the mechanism seems to have been found, the most frequently encountered postulate is that of wettability modification through multi ionic exchanges. As such, in oil reservoirs, the different phases (crude oil, brine, rock and also gases) coexist as a result of thermodynamic equilibrium. Even if the injection of brines should theoretically disturb the in-place equilibrium and increase oil production, this has not been always observed.

In our opinion, to appreciate (or criticize) the advances in the field, it seems crucial to understand each and every interaction giving rise to the stability of the triple phases COBR (crude oil, brine, rock). Consequently, this thesis aims at understanding the implementation of LSW in sandstone-based reservoirs. Different aspects are overviewed on a fundamental basis. For instance, the phenomenon of wettability of clay minerals, surface and interfacial tension and different emulsions which could influence the amount and quality of oil recovered. With respect to emulsions, it is worth noting here, that the oils recovered in production wells are mixtures of hydrocarbons, water (fresh or saline) and solids for example particles of rocks and sand.

The first part of the work thus aims at providing a better understanding of the wettability of different clay minerals in an extensive way (exchangeable cation, relative humidity, particle size and surface roughness).

The second part focusses on liquid-liquid interactions. Indeed, many authors described crude oil/brine interactions but their studies were restricted to brines which are commonly tested for LSW (NaCl for salts of monovalent cations, $CaCl_2$ and $MgCl_2$ for salts of divalent cations). Moreover, it is only recently that some authors reported the effect of brine concentration on the individual interfacial tension of the polar components (asphaltenes and resins) of crude oils. As a complement in this direction, this work aims to provide a more complete analysis of the crude oil/brine interactions by scanning the effects of cations as well as that of anions. On the other side, it is true that large molecules such as asphaltenes and resins play a significant role in the interfacial tension of crude oils. It is however also known that crudes contain naphtenic acids which are also likely to influence oil / brine interfacial tensions. We, thus designed a model system, containing a naphtenic acid and analysed the effects of a wide span of brines.

After analysis of solid-liquid and liquid-liquid interactions, the third part of this work aims at studying triple phase (clay/brine/rock) interactions. Firstly, contact angle of oil drops have been performed on mica mineral in the presence of water and brines. Secondly, triple phase interactions have been investigated by analysing the stability of crude oil/brine emulsions in the presence of different clay minerals. Indeed, it well known that inorganic solids like clay minerals are able to stabilise emulsions (pickering emulsions) more than surfactants (like asphaltenes) on their own [97]. We thus analysed the effect of different clay minerals in 1 to 1 ratio of oil/aqueous phases which led to stable emulsions on their own.

5. Bibliography

[1] P. P. Jadhunandan and N. R. Morrow, “Spontaneous imbibition of water by crude oil/brine/rock systems,” *Situ U. S.*, vol. 15:4, Jan. 1991.

[2] P. P. Jadhunandan and N. R. Morrow, “Effect of Wettability on Waterflood Recovery for Crude-Oil/Brine/Rock Systems,” *SPE-22597-PA*, Feb. 1995.

[3] N. Morrow and J. Buckley, “Improved Oil Recovery by Low-Salinity Waterflooding,” *SPE-129421-JPT*, May 2011.

[4] J. J. Sheng, “Critical review of low-salinity waterflooding,” *J. Pet. Sci. Eng.*, vol. 120, pp. 216–224, Aug. 2014.

[5] M. D. Jackson, J. Vinogradov, G. Hamon, and M. Chamerois, “Evidence, mechanisms and improved understanding of controlled salinity waterflooding part 1: Sandstones,” *Fuel*, vol. 185, pp. 772–793, Dec. 2016.

[6] G.-Q. Tang and N. R. Morrow, “Influence of brine composition and fines migration on crude oil/brine/rock interactions and oil recovery,” *J. Pet. Sci. Eng.*, vol. 24, no. 2–4, pp. 99–111, Dec. 1999.

[7] A. Lager, K. Webb, and C. Black, “Impact of brine chemistry on oil recovery,” presented at the IOR 2007-14th European Symposium on Improved Oil Recovery, 2007.

[8] J. C. Seccombe, A. Lager, K. J. Webb, G. Jerauld, and E. Fueg, “Improving Wateflood Recovery: LoSalTM EOR Field Evaluation,” in *SPE-113480-MS*, SPE, 2008.

[9] Y. Zhang and N. R. Morrow, “Comparison of Secondary and Tertiary Recovery With Change in Injection Brine Composition for Crude-Oil/Sandstone Combinations,” in *SPE-99757-MS*, SPE, 2006.

[10] H. Pu, X. Xie, P. Yin, and N. R. Morrow, “Application of Coalbed Methane Water to Oil Recovery from Tensleep Sandstone by Low Salinity Waterflooding,” in *SPE-113410-MS*, SPE, 2008.

[11] B. Soraya, C. Malick, C. Philippe, H. J. Bertin, and G. Hamon, “Oil Recovery by Low-Salinity Brine Injection: Laboratory Results on Outcrop and Reservoir Cores,” in *SPE-124277-MS*, SPE, 2009.

[12] T. Hassenkam, A. C. Mitchell, C. S. Pedersen, L. L. Skovbjerg, N. Bovet, and S. L. S. Stipp, “The low salinity effect observed on sandstone model surfaces,” *Colloids Surf. Physicochem. Eng. Asp.*, vol. 403, pp. 79–86, Jun. 2012.

[13] Y. K. Suman, “EVALUATION OF LOW SALINE ‘SMART WATER’ ENHANCED OIL RECOVERY IN LIGHT OIL RESERVOIRS.” [Online]. Available:

http://ourspace.uregina.ca:8080/xmlui/bitstream/handle/10294/5459/Suman_Yogesh_20 0312036_MASC_PSE_Spring2014.pdf?sequence=1. [Accessed: 04-Dec-2016].

[14] "The Theory and Practice of Pharmaceutical Technology|Digital Textbook Library." [Online]. Available: http://www.tankonyvtar.hu/en/tartalom/tamop412A/2011-0016_01_the_theory_and_practise_of_pharmaceutical_technology/ch12.html. [Accessed: 04-Dec-2016].

[15] K. K. Mohan, R. N. Vaidya, M. G. Reed, and H. S. Fogler, "Water sensitivity of sandstones containing swelling and non-swelling clays," *Collect. Pap. Present. Int. Symp. Colloids Aquat. Environ. Organ. SCI Surf. Chem. Group*, vol. 73, pp. 237–254, Jun. 1993.

[16] A. Lager, K. Webb, C. Black, M. Singleton, and K. Sorbie, "Low Salinity Oil Recovery-An Experimental Investigation1," *Petrophysics*, vol. 49, no. 1, 2008.

[17] P. L. McGuire, J. R. Chatham, F. K. Paskvan, D. M. Sommer, and F. H. Carini, "Low Salinity Oil Recovery: An Exciting New EOR Opportunity for Alaska's North Slope," in *SPE-93903-MS*, SPE, 2005.

[18] T. Austad, "Water-based EOR in carbonates and sandstones: new chemical understanding of the EOR potential using smart water," *Enhanc. Oil Recovery Field Case Stud.*, pp. 301–335, 2013.

[19] T. S. Arnarson and R. G. Keil, "Mechanisms of pore water organic matter adsorption to montmorillonite," *Mar. Chem.*, vol. 71, no. 3–4, pp. 309–320, Aug. 2000.

[20] T. Underwood, V. Erastova, P. Cubillas, and H. C. Greenwell, "Molecular Dynamic Simulations of Montmorillonite–Organic Interactions under Varying Salinity: An Insight into Enhanced Oil Recovery," *J. Phys. Chem. C*, vol. 119, no. 13, pp. 7282–7294, Apr. 2015.

[21] D. N. Rao, "Wettability Effects in Thermal Recovery Operations," *SPE-57897-PA*, Oct. 1999.

[22] R. A. Nasralla, M. A. Bataweel, and H. A. Nasr-El-Din, "Investigation of Wettability Alteration and Oil-Recovery Improvement by Low-Salinity Water in Sandstone Rock," *SPE-146322-PA*, Mar. 2013.

[23] A. Y. Zekri, M. S. Nasr, and Z. I. Al-Arabai, "Effect of LoSal on Wettability and Oil Recovery of Carbonate and Sandstone Formation," in *IPTC-14131-MS*, IPTC, 2011.

[24] C. Drummond and J. Israelachvili, "Fundamental studies of crude oil–surface water interactions and its relationship to reservoir wettability," *J. Pet. Sci. Eng.*, vol. 45, no. 1–2, pp. 61–81, Nov. 2004.

[25] I. Fjelde, S. M. Asen, and A. V. Omekeh, “Low Salinity Water Flooding Experiments and Interpretation by Simulations,” in *SPE-154142-MS*, SPE, 2012.

[26] H. Mahani *et al.*, “Analysis of field responses to low-salinity waterflooding in secondary and tertiary mode in Syria,” presented at the SPE EUROPEC/EAGE Annual Conference and Exhibition, 2011.

[27] C. Dang, L. Nghiem, N. Nguyen, Z. Chen, and Q. Nguyen, “Mechanistic modeling of low salinity water flooding,” *J. Pet. Sci. Eng.*, vol. 146, pp. 191–209, Oct. 2016.

[28] E. Pouryousefy, Q. Xie, and A. Saeedi, “Effect of multi-component ions exchange on low salinity EOR: Coupled geochemical simulation study,” *Petroleum*, vol. 2, no. 3, pp. 215–224, Sep. 2016.

[29] L. Caner, “PHYLLOSILICATES DES SOLS: DE L’IDENTIFICATION A LA QUANTIFICATION.” [Online]. Available: https://tel.archives-ouvertes.fr/tel-00605819/document. [Accessed: 04-Dec-2016].

[30] C. Bergaya and G. Lagaly, “Handbook of Clay Science. Second Edition.,” vol. 5A, 2013.

[31] “Minéralogie des roches mères.” [Online]. Available: http://www.cnrs.fr/mi/IMG/pdf/mineralogie_roches_meres.pdf. [Accessed: 04-Dec-2016].

[32] S. Sperinck, P. Raiteri, N. Marks, and K. Wright, “Dehydroxylation of kaolinite to metakaolin-a molecular dynamics study,” *J. Mater. Chem.*, vol. 21, no. 7, pp. 2118–2125, 2011.

[33] C. Ma and R. A. Eggleton, “Cation exchange capacity of kaolinite,” *Clays Clay Miner.*, vol. 47, no. 2, p. 174, Apr. 1999.

[34] M. Ghadiri, W. Chrzanowski, and R. Rohanizadeh, “Biomedical applications of cationic clay minerals,” *RSC Adv.*, vol. 5, no. 37, pp. 29467–29481, 2015.

[35] C. S. Ross and S. B. Hendricks, “Minerals of the montmorillonite group, their origin and relation to soils and clays,” 2330–7102, 1945.

[36] X. Liu, J. Cheng, X. Lu, and R. Wang, “Surface acidity of quartz: understanding the crystallographic control,” *Phys. Chem. Chem. Phys.*, vol. 16, no. 48, pp. 26909–26916, 2014.

[37] G. Brown and P. Nadeau, “Crystal Structures of Clay Minerals and Related Phyllosilicates [and Discussion],” *Philos. Trans. R. Soc. Lond. Math. Phys. Eng. Sci.*, vol. 311, no. 1517, pp. 221–240, 1984.

[38] A. Keller *et al.*, “Tuning the hydrophobicity of mica surfaces by hyperthermal Ar ion irradiation,” *J. Chem. Phys.*, vol. 134, no. 10, p. 104705, 2011.

[39] C. Barton, “Clay minerals,” 2002.

[40] W. Abdallah *et al.*, “Fundamentals of wettability,” *Technology*, vol. 38, no. 1125–1144, p. 268, 1986.

[41] W. Anderson, “Wettability Literature Survey- Part 2: Wettability Measurement,” *SPE-13933-PA*, Nov. 1986.

[42] A. W. Adamson and A. P. Gast, “Physical chemistry of surfaces,” *Wiley*, vol. 6th edition, 1997.

[43] T. BIAEOPIOTROWICZ and J. STAWrNSKI, “Influence of exchangeable cations on the surface free energy of kaolinite as determined from contact angles,” *Clays Clay Miner.*, vol. 37, no. 3, pp. 269–272, 1989.

[44] J. Shang, M. Flury, J. B. Harsh, and R. L. Zollars, “Contact angles of aluminosilicate clays as affected by relative humidity and exchangeable cations,” *Colloids Surf. Physicochem. Eng. Asp.*, vol. 353, no. 1, pp. 1–9, Jan. 2010.

[45] J. M. Cases, I. Berend, M. Francois, J. P. Uriot, L. J. Michot, and F. Thomas, “Mechanism of adsorption and desorption of water vapor by homoionic montmorillonite; 3, The Mg (super 2+) , Ca (super 2+) , and Ba (super 3+) exchanged forms,” *Clays Clay Miner.*, vol. 45, no. 1, p. 8, Feb. 1997.

[46] A. Synytska *et al.*, “Tuning wettability by controlled roughness and surface modification using core-shell particles,” *Polym Mater Sci Eng*, vol. 90, pp. 624–625, 2004.

[47] B. Yang, S. Song, and A. Lopez-Valdivieso, “Effect of particle size on the contact angle of molybdenite powders,” *Miner. Process. Extr. Metall. Rev.*, vol. 35, no. 3, pp. 208–215, 2014.

[48] J. P. Oliver, C. Huh, and S. G. Mason, “An experimental study of some effects of solid surface roughness on wetting,” *Colloids Surf.*, vol. 1, no. 1, pp. 79–104, Jan. 1980.

[49] J. Drelich, J. D. Miller, and R. J. Good, “The Effect of Drop (Bubble) Size on Advancing and Receding Contact Angles for Heterogeneous and Rough Solid Surfaces as Observed with Sessile-Drop and Captive-Bubble Techniques,” *J. Colloid Interface Sci.*, vol. 179, no. 1, pp. 37–50, Apr. 1996.

[50] S. Shibuichi, T. Yamamoto, T. Onda, and K. Tsujii, “Super Water- and Oil-Repellent Surfaces Resulting from Fractal Structure,” *J. Colloid Interface Sci.*, vol. 208, no. 1, pp. 287–294, Dec. 1998.

[51] W. Chen, A. Y. Fadeev, M. C. Hsieh, D. Öner, J. Youngblood, and T. J. McCarthy, “Ultrahydrophobic and Ultralyophobic Surfaces: Some Comments and Examples,” *Langmuir*, vol. 15, no. 10, pp. 3395–3399, May 1999.

[52] M. Miwa, A. Nakajima, A. Fujishima, K. Hashimoto, and T. Watanabe, “Effects of the Surface Roughness on Sliding Angles of Water Droplets on Superhydrophobic Surfaces,” *Langmuir*, vol. 16, no. 13, pp. 5754–5760, Jun. 2000.

[53] M. Zabat, R. Harba, and H. V. Damme, “Fractal analysis of surface roughness of montmorillonite clay self-supported films: Effects of exchanged cations and of mechanical tensile stress,” *Colloids Surf. Physicochem. Eng. Asp.*, vol. 486, pp. 38–44, Dec. 2015.

[54] K. Norrish, “The swelling of montmorillonite,” *Discuss. Faraday Soc.*, vol. 18, no. 0, pp. 120–134, 1954.

[55] L. J. Michot, I. Bihannic, S. Maddi, C. Baravian, P. Levitz, and P. Davidson, “Sol/Gel and Isotropic/Nematic Transitions in Aqueous Suspensions of Natural Nontronite Clay. Influence of Particle Anisotropy. 1. Features of the I/N Transition,” *Langmuir*, vol. 24, no. 7, pp. 3127–3139, Apr. 2008.

[56] L. J. Michot *et al.*, “Sol−Gel and Isotropic/Nematic Transitions in Aqueous Suspensions of Natural Nontronite Clay. Influence of Particle Anisotropy. 2. Gel Structure and Mechanical Properties,” *Langmuir*, vol. 25, no. 1, pp. 127–139, Jan. 2009.

[57] I. Berend *et al.*, “Mechanism of adsorption and desorption of water vapor by homoionic montmorillonites: 2. The li § na § k § rb § and cs+-exchanged forms,” *Clays Clay Min.*, vol. 43, pp. 324–336, 1995.

[58] W. Xu, C. T. Johnston, P. Parker, and S. F. Agnew, “Infrared study of water sorption on Na-, Li-, Ca-, and Mg-exchanged (SWy-1 and SAz-1) montmorillonite,” *Clays Clay Miner.*, vol. 48, no. 1, p. 120, Feb. 2000.

[59] C. D. Volpe, D. Maniglio, M. Morra, and S. Siboni, “The determination of a ‘stable-equilibrium’ contact angle on heterogeneous and rough surfaces,” *Colloids Surf. Physicochem. Eng. Asp.*, vol. 206, no. 1–3, pp. 47–67, Jul. 2002.

[60] R. N. Wenzel, “RESISTANCE OF SOLID SURFACES TO WETTING BY WATER,” *Ind. Eng. Chem.*, vol. 28, no. 8, pp. 988–994, Aug. 1936.

[61] A. B. D. Cassie and S. Baxter, “Wettability of porous surfaces,” *Trans. Faraday Soc.*, vol. 40, no. 0, pp. 546–551, 1944.

[62] Y. Yoon, D. Kim, and J.-B. Lee, “Hierarchical micro/nano structures for super-hydrophobic surfaces and super-lyophobic surface against liquid metal,” *Micro Nano Syst. Lett.*, vol. 2, no. 1, p. 1, 2014.

[63] H. K. Abdel-Aal and M. A. Alsahlawi, *Petroleum economics and engineering*. CRC Press, 2013.

[64] J. G. Speight, *The chemistry and technology of petroleum*. CRC press, 2014.

[65] “Reservoir rock properties - SPE Connect.” [Online]. Available: http://connect.spe.org/blogs/donatien-ishimwe/2014/09/29/reservoir-rock-properties. [Accessed: 01-Dec-2016].

[66] A. Silset, “Emulsions (w/o and o/w) of Heavy Crude Oils. Characterization, Stabilization, Destabilization and Produced Water Quality,” *PhD NTNU*, 2008.

[67] N. Aske, “Characterisation of crude oil components, asphaltene aggregation and emulsion stability by means of near infrared spectroscopy and multivariate analysis,” 2002.

[68] H. P. Roenningsen and I. Skjevrak, “Characterization of North Sea petroleum fractions: aromatic ring class distribution,” *Energy Fuels*, vol. 4, no. 5, pp. 608–626, Sep. 1990.

[69] J. A. Koots and J. G. Speight, “Relation of petroleum resins to asphaltenes,” *Fuel*, vol. 54, no. 3, pp. 179–184, Jul. 1975.

[70] S. I. Andersen and J. G. Speight, “PETROLEUM RESINS: SEPARATION, CHARACTER, AND ROLE IN PETROLEUM,” *Pet. Sci. Technol.*, vol. 19, no. 1–2, pp. 1–34, Mar. 2001.

[71] J. G. Speight, “Petroleum Asphaltenes - Part 1: Asphaltenes, Resins and the Structure of Petroleum,” *Oil Gas Sci. Technol. - Rev IFP*, vol. 59, no. 5, pp. 467–477, 2004.

[72] A. R. Hortal, P. Hurtado, B. Martínez-Haya, and O. C. Mullins, “Molecular-Weight Distributions of Coal and Petroleum Asphaltenes from Laser Desorption/Ionization Experiments,” *Energy Fuels*, vol. 21, no. 5, pp. 2863–2868, Sep. 2007.

[73] J. Murgich, Rodríguez, and Y. Aray, “Molecular Recognition and Molecular Mechanics of Micelles of Some Model Asphaltenes and Resins,” *Energy Fuels*, vol. 10, no. 1, pp. 68–76, Jan. 1996.

[74] O. C. Mullins, E. Y. Sheu, A. Hammami, and A. G. Marshall, *Asphaltenes, heavy oils, and petroleomics*. Springer Science & Business Media, 2007.

[75] R. Cimino, S. Correra, A. Del Bianco, and T. P. Lockhart, “Solubility and Phase Behavior of Asphaltenes in Hydrocarbon Media,” in *Asphaltenes: Fundamentals and Applications*, E. Y. Sheu and O. C. Mullins, Eds. Boston, MA: Springer US, 1995, pp. 97–130.

[76] O. C. Mullins, “The Modified Yen Model,” *Energy Fuels*, vol. 24, no. 4, pp. 2179–2207, Apr. 2010.

[77] T. E. Havre, J. Sjöblom, and J. E. Vindstad, “Oil/Water-Partitioning and Interfacial Behavior of Naphthenic Acids,” *J. Dispers. Sci. Technol.*, vol. 24, no. 6, pp. 789–801, Jan. 2003.

[78] M. Lashkarbolooki, S. Ayatollahi, and M. Riazi, “Effect of Salinity, Resin, and Asphaltene on the Surface Properties of Acidic Crude Oil/Smart Water/Rock System,” *Energy Fuels*, vol. 28, no. 11, pp. 6820–6829, Nov. 2014.

[79] L. L. Schramm, *Surfactants: fundamentals and applications in the petroleum industry*. Cambridge University Press, 2000.

[80] M. J. Rosen and J. T. Kunjappu, *Surfactants and interfacial phenomena*. John Wiley & Sons, 2012.

[81] W. Kunz, “Specific ion effects in colloidal and biological systems,” *Curr. Opin. Colloid Interface Sci.*, vol. 15, no. 1–2, pp. 34–39, Apr. 2010.

[82] Y. Zhang and P. S. Cremer, “Interactions between macromolecules and ions: the Hofmeister series,” *Model Syst. Biopolym.*, vol. 10, no. 6, pp. 658–663, Dec. 2006.

[83] W. D. Harkins and F. Brown, “The determination of surface tension (free surface energy), and the weight of falling drops: The surface tension of water and benzene by the capillary height method.,” *J. Am. Chem. Soc.*, vol. 41, no. 4, pp. 499–524, 1919.

[84] P. L. du Noüy, “An interfacial tensiometer for universal use,” *J. Gen. Physiol.*, vol. 7, no. 5, pp. 625–631, 1925.

[85] B. Vonnegut, “Rotating bubble method for the determination of surface and interfacial tensions,” *Rev. Sci. Instrum.*, vol. 13, no. 1, pp. 6–9, 1942.

[86] “DataPhysics - Pendant drop method.” [Online]. Available: http://www.dataphysics.de/2/start/understanding-interfaces/drop-shape-analysis/pendant-drop-method/. [Accessed: 12-Dec-2016].

[87] B. Jean, “Un polymère thermosensible à l’interface eau-air: interaction avec les tensioactifs et stabilisation de films minces,” 2000.

[88] A. C. Mitropoulos, “What is a surface excess,” *J Eng Sci Technol Rev*, vol. 1, no. 1, pp. 1–3, 2008.

[89] M. Nič, J. Jirát, B. Košata, A. Jenkins, and A. McNaught, Eds., “Gibbs surface,” in *IUPAC Compendium of Chemical Terminology*, 2.1.0., Research Triagle Park, NC: IUPAC, 2009.

[90] M. Nič, J. Jirát, B. Košata, A. Jenkins, and A. McNaught, Eds., “surface excess, nσ,” in *IUPAC Compendium of Chemical Terminology*, 2.1.0., Research Triagle Park, NC: IUPAC, 2009.

[91] R. Aveyard and S. M. Saleem, “Interfacial tensions at alkane-aqueous electrolyte interfaces,” *J. Chem. Soc. Faraday Trans. 1 Phys. Chem. Condens. Phases*, vol. 72, no. 0, pp. 1609–1617, 1976.

[92] B.-Y. Cai, J.-T. Yang, and T.-M. Guo, “Interfacial Tension of Hydrocarbon + Water/Brine Systems under High Pressure,” *J. Chem. Eng. Data*, vol. 41, no. 3, pp. 493–496, Jan. 1996.

[93] E. Serrano-Saldaña, A. Domínguez-Ortiz, H. Pérez-Aguilar, I. Kornhauser-Strauss, and F. Rojas-González, “Wettability of solid/brine/n-dodecane systems: experimental study of the effects of ionic strength and surfactant concentration,” *Proc. Third Int. TRIPrinceton Workshop Charact. Porous Mater. Angstroms Millim.*, vol. 241, no. 1–3, pp. 343–349, Jul. 2004.

[94] E. Lima, B. De Melo, L. Baptista, and M. Paredes, “Specific ion effects on the interfacial tension of water/hydrocarbon systems,” *Braz. J. Chem. Eng.*, vol. 30, no. 1, pp. 55–62, 2013.

[95] A. Abdel-Wali, “Effect of simple polar compounds and salinity on interfacial tension and wettability of rock/oil/brine system,” *J. King Saud Univ.*, 1996.

[96] F. Moeini, A. Hemmati-Sarapardeh, M.-H. Ghazanfari, M. Masihi, and S. Ayatollahi, “Toward mechanistic understanding of heavy crude oil/brine interfacial tension: The roles of salinity, temperature and pressure,” *Fluid Phase Equilibria*, vol. 375, pp. 191–200, Aug. 2014.

[97] D. M. Sztukowski and H. W. Yarranton, “Oilfield solids and water-in-oil emulsion stability,” *J. Colloid Interface Sci.*, vol. 285, no. 2, pp. 821–833, May 2005.

II. Main materials

Table of contents

List of Tables

List of Figures

1. Clay minerals

In this thesis, both swelling and non-swelling clays have been used and are described herein. The first part of this section describes the swelling clay minerals whereas the second part is dedicated to the non-swelling clays.

1.1 Swelling clays

The aluminosilicate swelling clay colloids used are four dioctahedral smectites, namely: Beidellite (Beid), Australia Nontronite (NAu1), Wyoming and Arizona Montmorillonites (SWy and SAz respectively). Initially, they were purchased during the previous works of my supervisor, Laurent Michot, and his co-workers from the Source Clay Minerals Repository at Purdue University, West Lafayette, Indiana, USA. The smectites used during this thesis were thus available as purified samples, size selected and exchanged by the authors in [1], [2]. Underneath, Table 1 reports the various smectites used, their main morphological features and the different exchangeable cations.

Clay	**Origin**	**Exchanged Ions**	**Particles shapes and sizes**
Beidellite (Beid)	Idaho, USA	Li^+, Na^+, Ca^{2+}	Discs of irregular contour, 400 nm in diameter
Nontronite 1 (NAu1)	Southern Australia	Li^+, Na^+, K^+, Ca^{2+}	Laths of 200-700 nm
Montmorillonite Wyoming (SWy)	Wyoming, USA	Li^+, Na^+, Ca^{2+}	Discs of irregular contour, 250 nm in diameter
Montmorillonite Arizona (SAz)	Arizona, USA	Na^+	Discs of irregular contour of sizes : - S1: 300 nm - S2: 150 nm - S3: 95 nm - S4: 40 nm

Table 1: Characteristics of swelling clays used during the study

E. Paineau [3] characterised the different minerals. As an indication of the morphology of the different smectites, his transmission electron micrographs are shown in Figure 1. As far as particle size measurements are concerned, due to the irregular contours of beidellite and

montmorillonite, he reported the diameter as the average of the longest diagonal of the platelets. He also reported that the average size polydispersity for all the samples were around 30 to 40%.

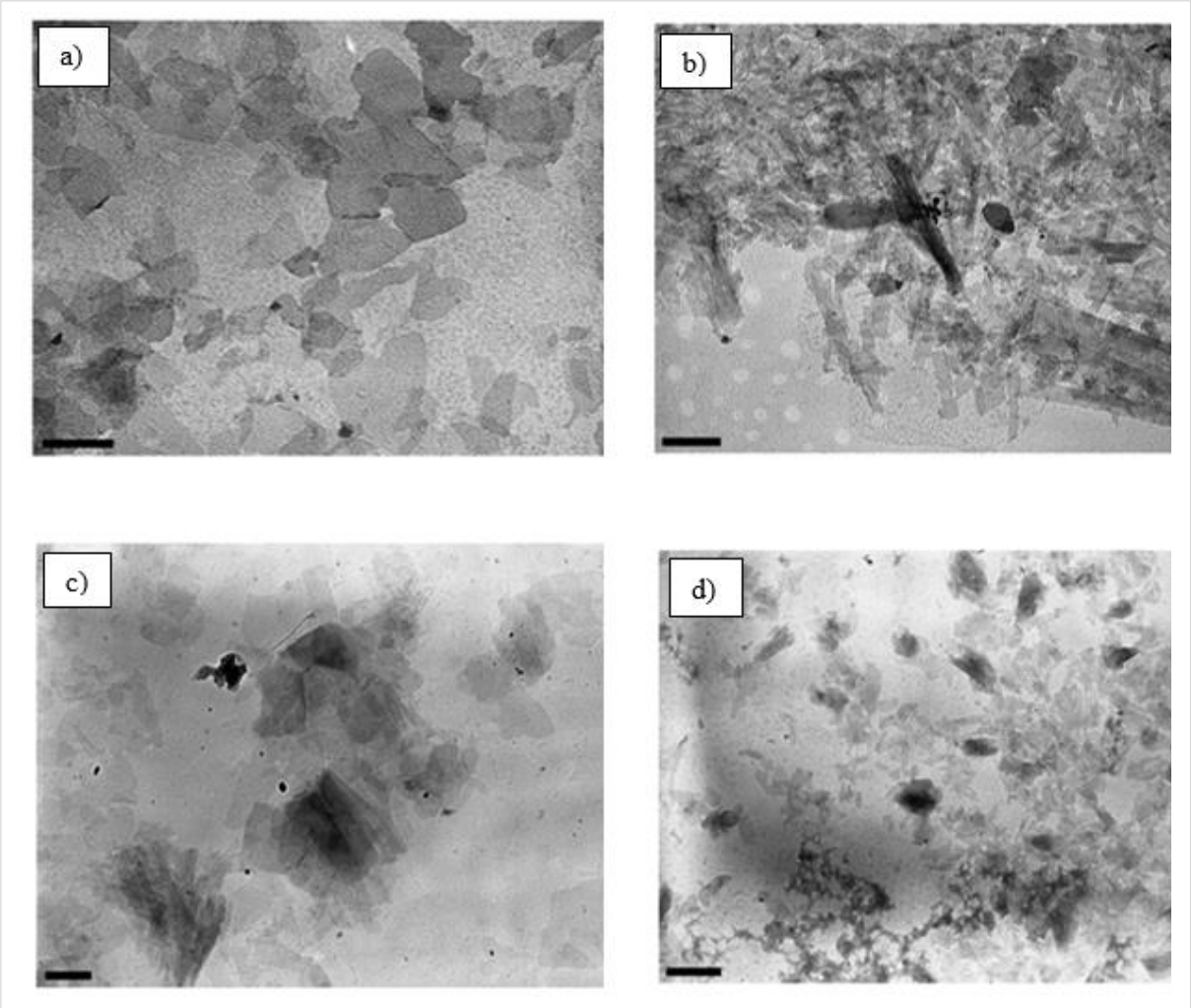

Figure 1: Transmission Electron micrographs of sodium exchanged smectite particles: a) Beid; b) NAu1; c) SWy and d) SAz; Scale bars on each micrographs correspond to 0.3 µm

1.2 Non-swelling clays

Two non-swelling clay minerals purchased from the Source Clay Minerals Repository at Purdue University were used during this thesis and reported in Table 2. During this work, we followed similar procedures as described in [1], [2] in order to purify the non-swelling clays. The procedure is described in Figure 2.

Clays	Origin
Kaolinite (K4)	Oneal Pit, Macon, Georgia, USA
Illite (Imt2)	Silver Hills, Montana, USA.

Table 2: Different non-swelling clays used and their origin

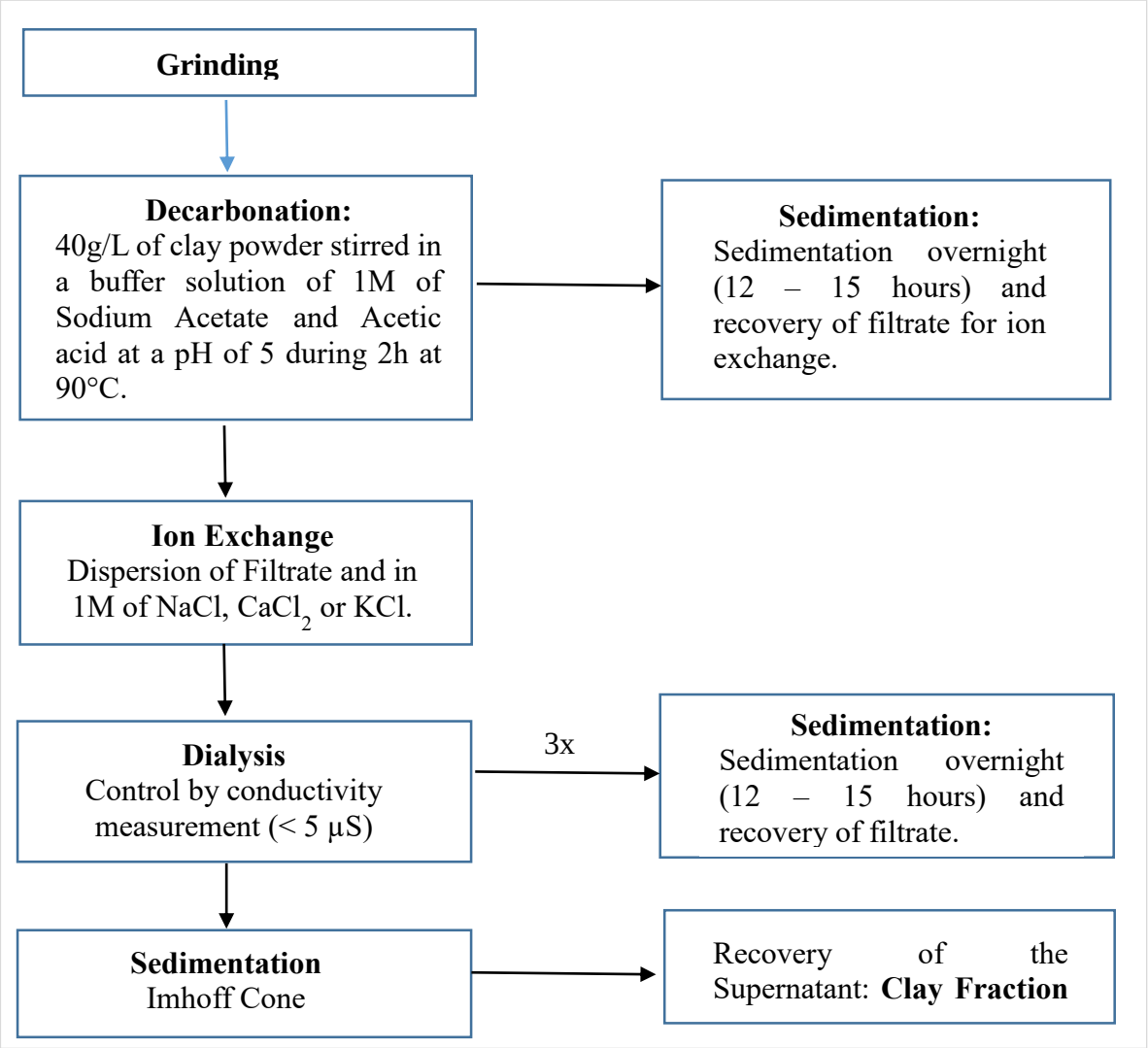

Figure 2: Protocol for the purification of non-swelling clays

After the purification process, both K4 and Imt2 exchanged with the different cations available for our experiments are as follows:

- K4: Na^+, K^+ and Ca^{2+}
- Imt2: Na^+, K^+ and Ca^{2+}

1.2.1 Characterisation of non-swelling clays

- **Transmission Electron Microscopy, TEM**

Transmission electron microscopy images of clay suspensions were obtained with a 1011 microscope from JEOL with an acceleration voltage of 100 kV. Figure 3 displays a typical micrograph of kaolinite platelets with well-defined hexagonal shape. The corresponding particle size distribution (200 nm to 1.8 µm) has been calculated on a total of 450 platelets and shows that about 80% of them are of sizes ranging between 200 and 600 nm. As far as the larger platelets are concerned (600 nm – 1.8 µm), they comprise of about 20% of the measured sample. The absence of any shape other than the hexagonal ones was also an indication of the purity of our kaolinite sample.

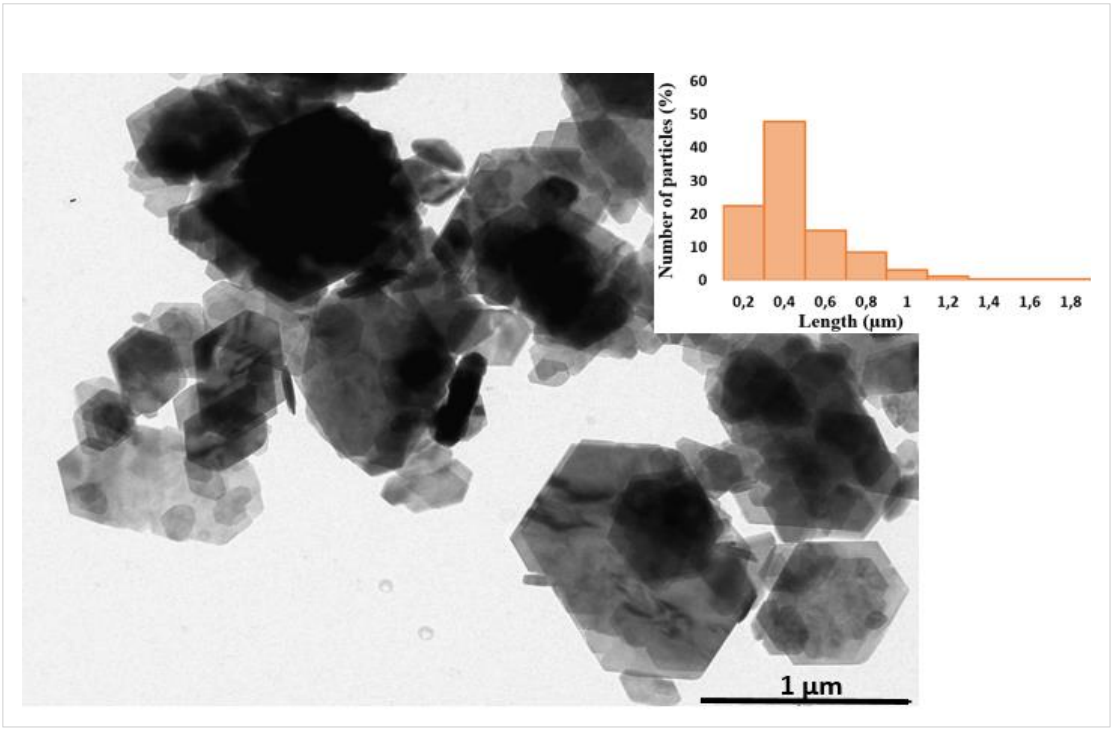

Figure 3: TEM image of kaolinite exchanged with Na^+

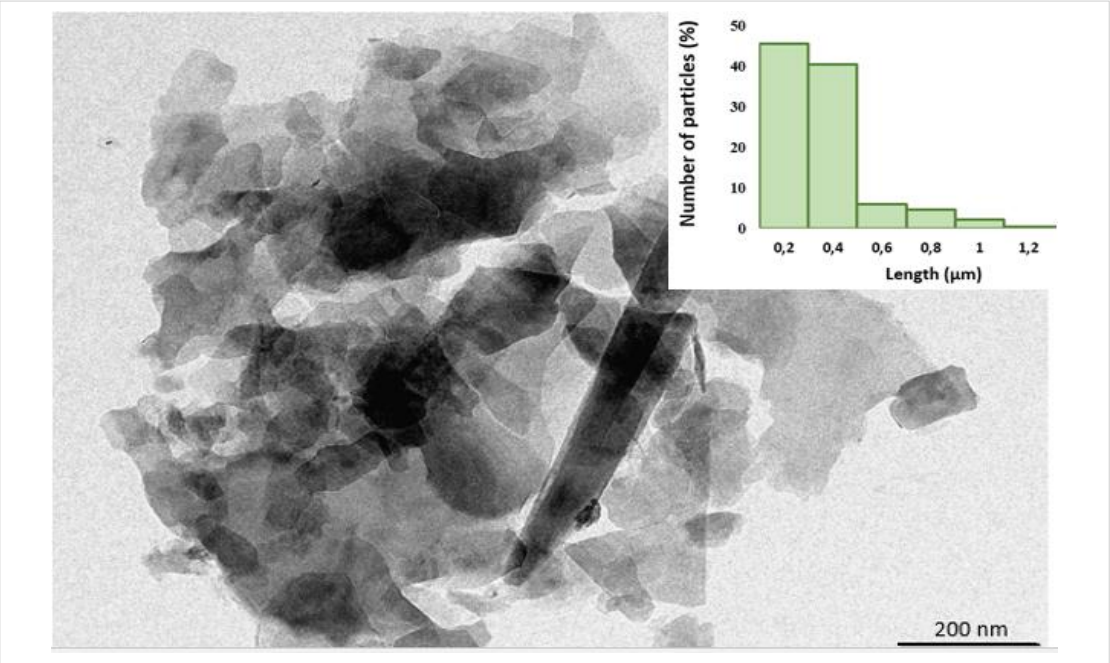

Figure 4: TEM image of illite exchanged with Na^+

Figure 4 shows the particles of illite. Different to the uniform hexagonal shape observed for kaolinite, illite platelets can be observed with a rather undefined morphology. The size distribution, measured along the longest diagonal of a total of 300 platelets, ranged from 200 nm up to 1.2 µm. Though in very small numbers, rod-like particles can also be observed on the TEM image.

- **X-ray Powder Diffraction, XRD of kaolinite and illite**

In addition to morphological characterisation by the transmission electron microscopy, in order to ensure the purity of our samples, we performed x-ray diffraction. Supernatants of non-swelling clays obtained after the process of purification were dried at 80°C to obtain the corresponding solids. X ray powder diffraction was then carried out using a D8 ADVANCE diffractometer from Bruker of Cu Kα radiation (λ=154.05 pm). Figures 5 and 6 show the diffraction patterns of kaolinite and illite (identifiable by peaks characteristic of the minerals) respectively. The illite sample however, show very fine peaks at at d=4.27A° and d=3.34 A° which are caracteristic of quartz most probably remaining after the process of purification.

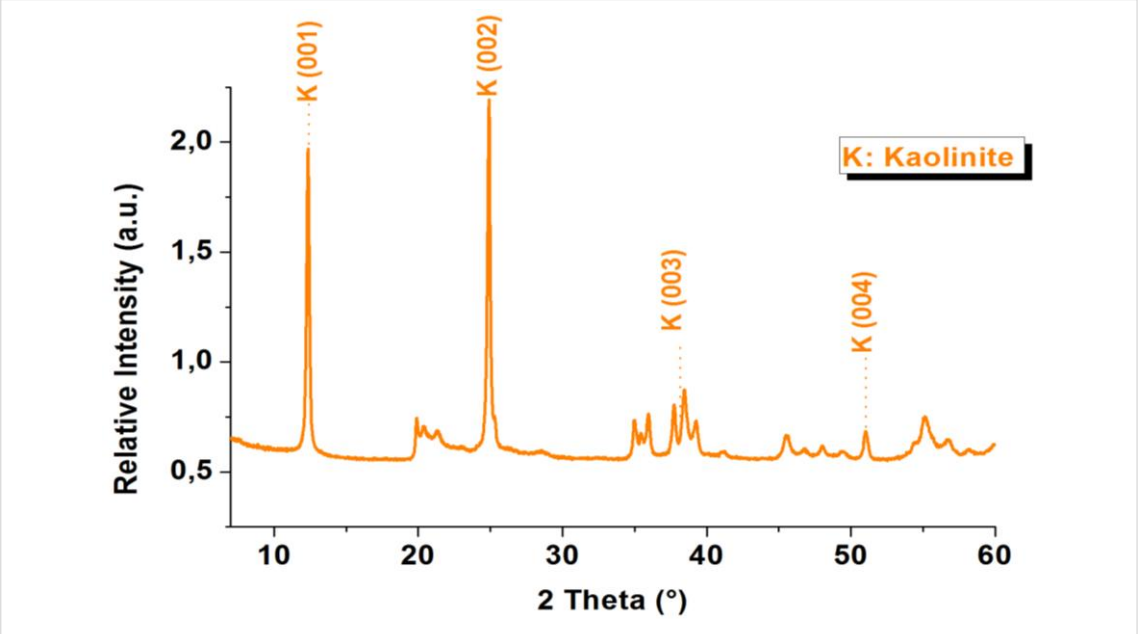

Figure 5: Diffraction pattern of kaolinite after purification

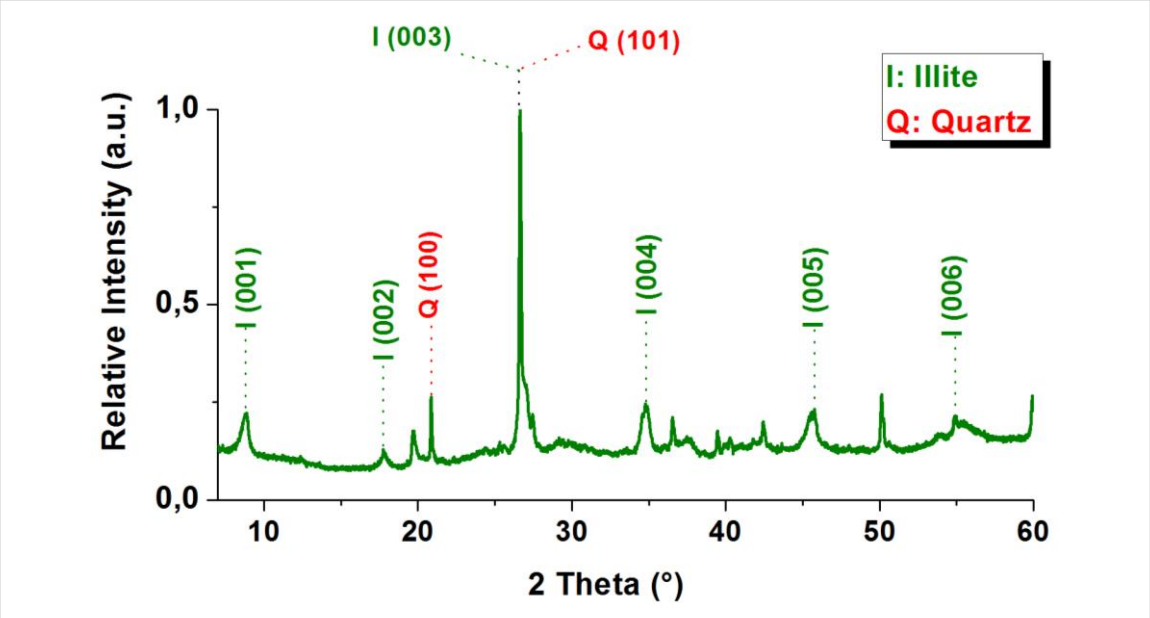

Figure 6: Diffraction pattern of illite after purification.

- **Fourier Transformed Infrared spectroscopy , FTIR**

Identification of clay minerals are often provided by their different absorption frequencies. For this purpose, the Fourier Transformed Infrared spectra of kaolinite and illite samples are provided by Figures 7 and 8. The spectra have been measured in absorption mode with a Bruker Vertex 70 spectrometer (resolution 2 cm^{-1}, 128 scans) respectively. The characteristic vibrational regions are:

i. Si-O-M vibrations (M= Al, Mg etc)
ii. Stretching and bending of Si-O groups } 1200 – 400 cm^{-1}
iii. Al-Al-OH vibrations

iv. Stretching vibrations of surface hydroxyls
v. Stretching vibrations of inner hydroxyl groups } 3600 – 3700 cm^{-1}

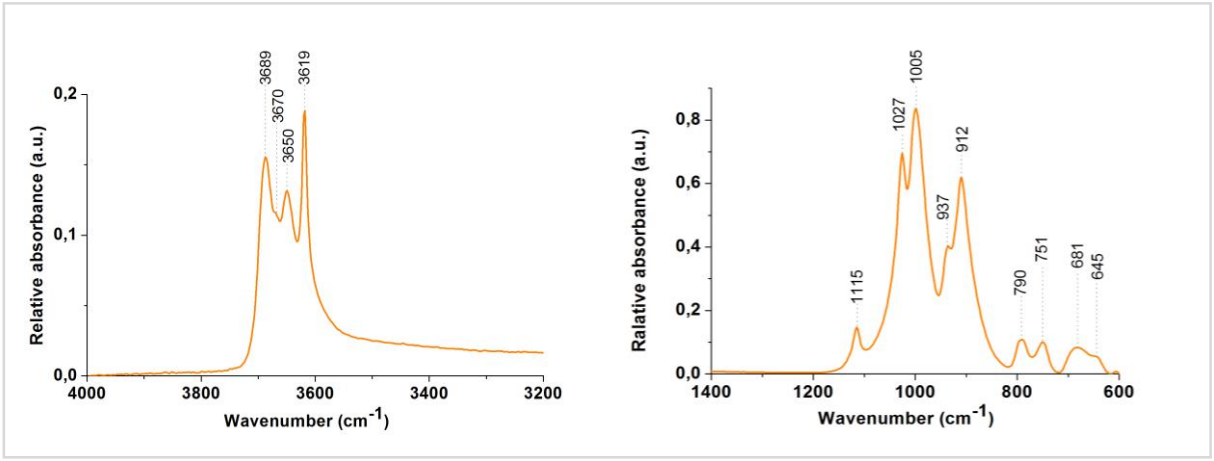

Figure 7: Absorption spectra of kaolinite exchanged with Na^+.

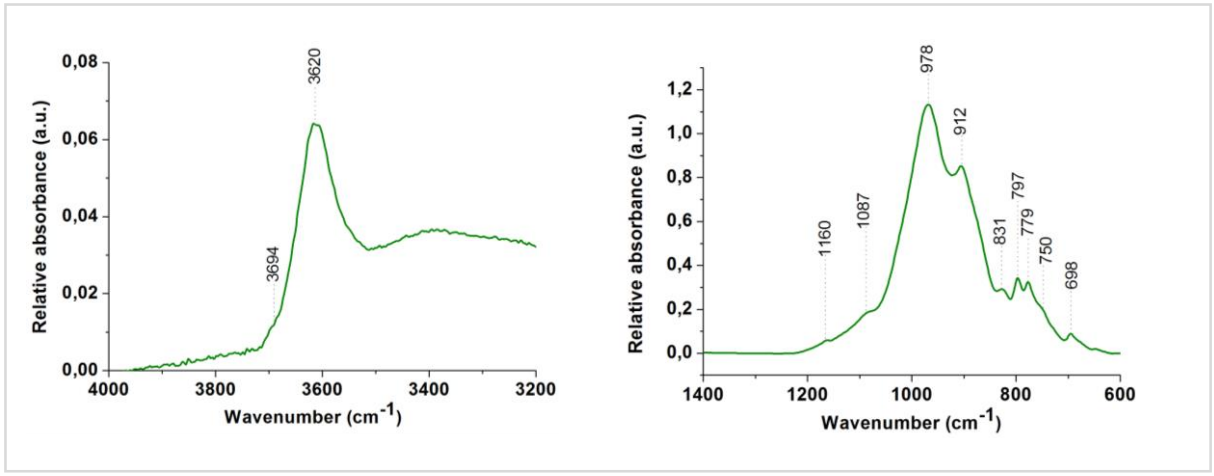

Figure 8: Absorption spectra of illite exchanged with Na^+.

As far the sample of illite is concerned, as observed on the XRD pattern, absorption peaks at ν (779 and 797 cm^{-1}) are characteristic to Si-O stretching in quartz.

2. Crude Oils

During this thesis, two dead crude oils have been used for the experiments: (i) a light and good quality (low sulphur content, 0.28 weight percentage) crude oil and, (ii) a medium gravity sour crude oil. It is worth noting that the term *dead* is used to refer to crude oils that have lost their gaseous components. On the other hand, *live crude oils* refer to crude oils containing dissolved gases [4]. For the purpose of this work, these oils are respectively referred under generic names of ***light viscous crude***, LVC(C) and ***medium fluid crude***, MFC(B).

2.1 Characteristics of the crude oils

2.1.1. Oil LVC(C)

Characteristics (API gravity, density, molecular weight, viscosity, TAN and TBN) and the SARA analysis of the crude oil are reported in Tables 3 to 4 respectively.

Crude oil LVC(C)	
API gravity (°)	38.6
Density (kg/m^3)	
- At 15 °C	832.1
- At 30 °C	822.4
Viscosity (cPo)	
- At 15 °C	7.26
- At 30 °C	4.14
TAN[1] (mg/g KOH)	0.2
TBN[2] (mg/g KOH)	1.77

Table 3: Characteristics of oil LVC(C)

[1]: TAN (Total Acid Number) is a measurement of the acidic components of oil. It refers to the amount of KOH (in milligrams) that is needed to neutralise the acidic components in one gram of oil.

[2]: TBN (Total Base Number) is a measurement of the amount of basic components of crude oil. Expressed in milligrams of KOH per gram of oil, it is the equivalent of bases present in crude oil.

Constituents	**weight %**
Saturates	38.6
Aromatics	30
Resins	5.3
Asphaltenes	2.9

Table 4: SARA analysis of LVC(C)

2.1.2. Oil MFC(B)

Crude oil MFC(B)	
API gravity (°)	32.5
Density (kg/m^3)	
- At 15 °C	868
- At 30 °C	858
Viscosity (cPo)	
- At 15 °C	13.9
- At 30 °C	8.40
TAN (mg/g KOH)	0.12
TBN (mg/g KOH)	0

Table 5: Characteristics of oil LVC(C)

Constituents	**weight %**
Saturates	38.9
Aromatics	45.5
Resins	10.4
Asphaltenes	5.3

Table 6: SARA analysis of MFC(B)

According to the data provided by Tables 3 to 4, it is clearly that the crudes undeniably contain polar molecules ranging from acidic components (revealed by the TAN), basic components (revealed by the TBN), resins and asphaltenes, all disposed interact as surface active molecules.

2.2 Fourier Transformed Infrared spectrum of the crude oils

The absorption spectra of oils LVC(C) and MFC(B) are shown in Figure 9 below. Being complex mixtures of hydrocarbons, they showed identical absorption peaks.

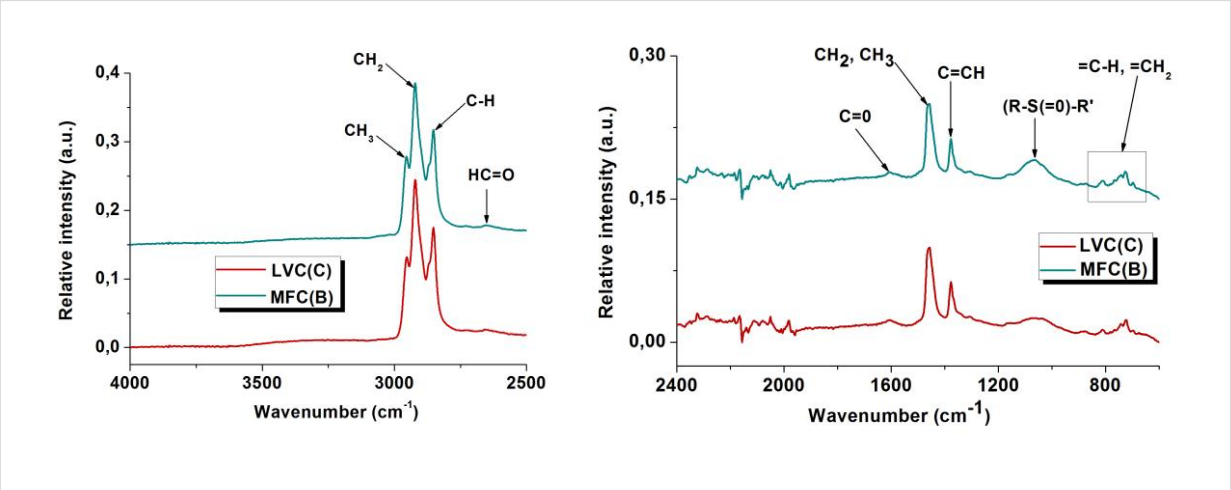

Figure 9: Absorption spectra of oils LVC(C) and MFC(B)

However, finer characterisation of the crude oils could be provided by mass-spectrometry coupled with chromatography techniques.

3. Bibliography

[1] E. Paineau *et al.*, "Aqueous Suspensions of Natural Swelling Clay Minerals. 1. Structure and Electrostatic Interactions," *Langmuir*, vol. 27, no. 9, pp. 5562–5573, May 2011.

[2] L. J. Michot *et al.*, "Phase Diagrams of Wyoming Na-Montmorillonite Clay. Influence of Particle Anisotropy," *Langmuir*, vol. 20, no. 25, pp. 10829–10837, Dec. 2004.

[3] E.-N. Paineau, "Transitions de phases dans les argiles : influence de la minéralogie et de la morphologie : comportement sous écoulement et sous champs," 2011.

[4] "live oil - Schlumberger Oilfield Glossary." [Online]. Available: http://www.glossary.oilfield.slb.com/Terms/l/live_oil.aspx. [Accessed: 07-Dec-2016].

III. Wettability of clay minerals

Table of contents

List of Tables

List of Figures

1. Experimental methods and set-up for contact angle measurements

In this thesis, characterisation of the wettability of clay minerals has been performed by the method of contact angle measurements. Precisely, the measurements have been performed by the static sessile drop (SSD) method, where probed liquids (water, brines and crude oils) have been deposited on clay mineral films predeposited on glass slides. To get to our targets, first, microscope glass slides have successively been cleaned with distilled water and acetone to remove any impurities. The different clay suspensions were then homogenised in an ultrasonic bath during five minutes and then deposited on the pre-cleaned glass slides (Tables 1 and 2).

1.1 Preparation of clay films

1.1.1 Clay films of different exchangeable ions

Type of clays	Clay minerals	Concentration clay suspension (g/L)	Volume of clay suspension	
			µL	mL
Swelling	• Beid (Li^+, Na^+, Ca^{2+})	3		1.5
	• NAu1 (Li^+, Na^+, K^+, Ca^{2+}) • SWy (Li^+, Na^+, Ca^{2+})	3	200	1.5
Non-swelling	• K4 (Na^+, Ca^{2+}) • Imt2 (Na^+, Ca^{2+})	3	200	1.5
		20		1.5 4

Table 1: Type of clays, different clay minerals, concentration and volume of suspension used for clay film preparation.

1.1.2 Clay films of different platelet size

Clay minerals	Average platelet size (nm)	Concentration clay suspension (g/L)	Volume of clay suspension deposited	
			µL	mL
Az (Na^+)	S1: 300 S2: 150 S3: 95 S4: 40	3	200	1.5

Table 2: Platelet sizes, concentration and volume of clay suspension of Arizona montmorillonite deposited on glass slides.

Different concentrations and volume of clay suspensions have been used so as prepared films of different thicknesses. After deposition of the clay suspensions on the glass slides, they were let to dry under ambient conditions.

1.2 Relative humidity (RH) control set-up

The effect of humidity on water contact angles has been investigated on swelling clays (Beid, NAu1 and Wy). After the clays films were dried in air during several hours, they were placed in air tight transparent plastic boxes (750 ml in volume) in which the relative humidity was kept at 84 and 100% by using potassium chloride saturated solution and deionised water respectively. The reached RH was permanently monitored using a pen-style digital thermo-hygrometer from VWR and the films were equilibrated during 48 hours before contact angle measurements. Figure 1 shows the set-up which has been used for monitoring humidity and measurement of contact angle under the controlled conditions.

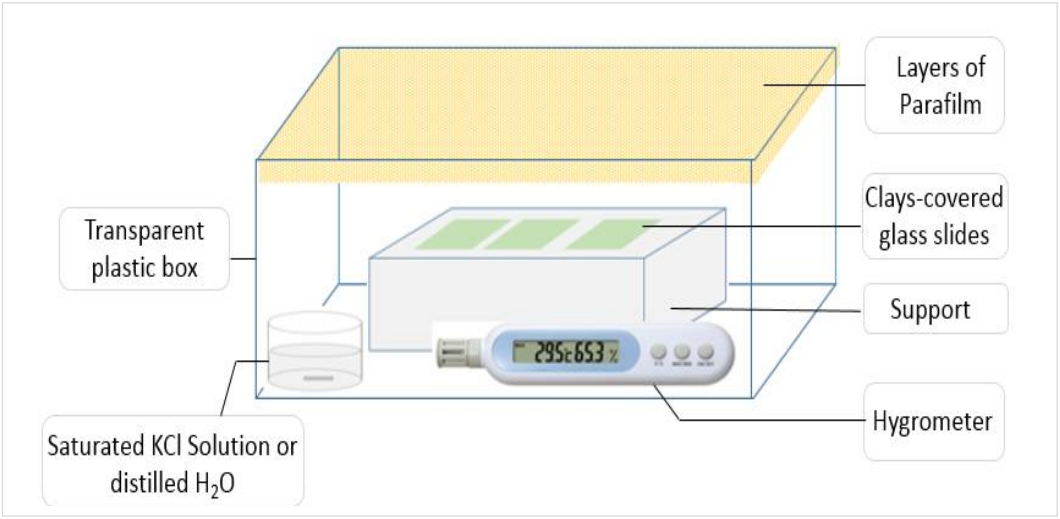

Figure 1: Set-up for humidity control experiment.

1.3 Contact angle measurements

As stated above, contact angle measurements on the different films have been carried out by using the static sessile drop method (SSD). For this purpose, a goniometer, the DSA100 from Krüss GmbH, Hamburg, Germany has been used. Contact angles on clay films have been measured by depositing 2 and 5µl of water, brine and crude oil LVC(C) and crude oil MFC(B) as probe liquids. The liquids were dispensed by a 1ml syringe fitted with steel needle 0.5mm in diameter.

- Probed liquids : - Milli-Q water (resistivity 18 MΩ.cm)
  - Brines of NaCl (1M), KCl (1M) and $CaCl_2$ (0.5M)
  - Crude oils LVC(C) and MFC(B)

The temperature recorded at the time of measurement was between 23 and 25°C and contact angle (Young equation) between the sessile drop and the clay film was measured by lining a cross hair with the tangent where the drop was in contact with solid (Figure 2 below). The angle at the left (θ_L) and that at the right (θ_R) were averaged to give the contact angle of a drop.

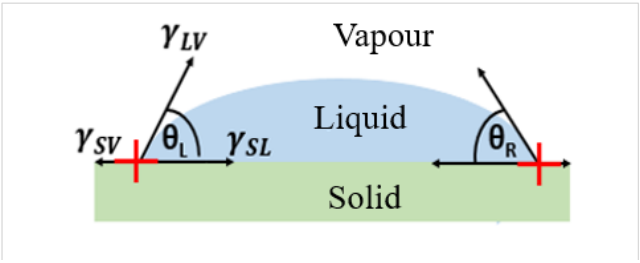

Young Equation:

$$\cos\theta = \frac{\gamma_{SV} - \gamma_{SL}}{\gamma_{LV}}$$

Figure 2: measurement of contact angle of a drop on a clay film.

For a given sample, the final contact angle was given by the mean of the contact angles of at least 5 drops.

1.4 Atomic force microscopy, AFM.

The atomic force microscope has been used to probe the surface of clay films for the purpose of surface roughness measurements. As such, the AFM forms part of the scanning probe microscopes (SPM) where very fine probes are used to scan a surface. Actually, it all started with the work of Gerd Binning and Heinrich Röhrer in 1981 [1] where, with a STM (scanning tunnelling microscope), they imaged atoms on a conducting surface. For instance, they measured the tunnelling current between the probe and the surface when a potential difference was applied between them. Since then, different specific physical parameters such as magnetic fields, resistivity and atomic interaction forces have been exploited to design STM derived microscopes. For instance, the AFM is based on the measurement of atomic interaction forces between a tip and a surface. Contrary to STM which can image only conducting surfaces, the AFM is able to analyse both conducting and non-conducting surfaces. In addition, the AFM has a lateral resolution of $<10^{-9}$ m and an axial resolution of 10^{-10} m allowing the imaging of samples in three dimensions up to (120 x 120 x 4) µm respectively in the (x, y , z) directions with our "scanner J" [2].

1.4.1. Principle of AFM

As stated above, the AFM is used to access to the topography of surfaces by probing atomic interaction forces by a tip located close to the sample, (0.1 - 100) nm. The main parts of the AFM shown in figures 3a and 3b consist of:

- A very fine tip (of atomic resolution and often made up of silicium) supported by a flexible cantilever (Figure 3a); the tip senses the surface properties and causes the cantilever to deflect; the cantilever can be of different materials and lengths to tune its resonant frequency.
- A source of red laser (1mW and wavelength 670nm used during our experiments);
- A position sensitive photodiode detector consisting of four segments on which the laser spot is reflected after incidence on the back of the cantilever. The differences between the segments indicate the position of the laser spot and hence indicate the deflection of the cantilever.
- A piezo-electric system, which expands or contracts in the presence of a potential gradient. The system, also called the scanner, support the sample and positions it in (x, y, z) with angstrom accuracy.
- A feedback loop connecting the photodiode and the scanner so as to monitor the motion of the piezo as the sample is being scanned.

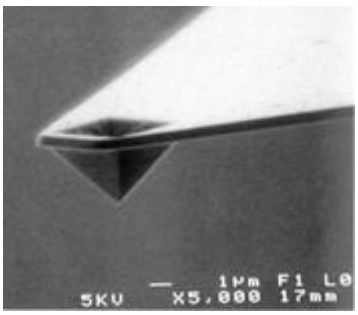

3a): Scanning electron microscope image of a tip

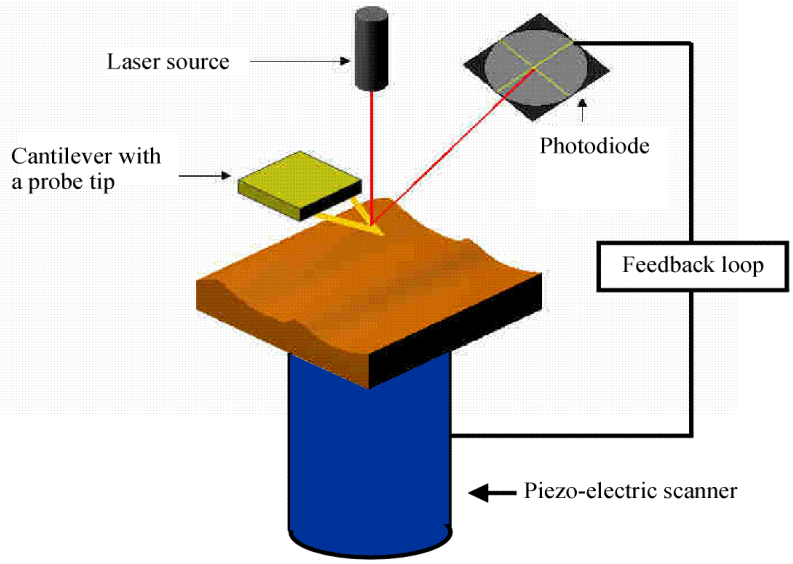

3b)

Figure 3: a) SEM of a tip; b) Different part of the AFM.

As the sample is scanned, the forces of interaction between the tip and the sample vary causing the cantilever to be deflected. The deflection, by an angle of θ, of the cantilever is so small that it can be assimilated to the linear extension (Δd) of a spring of constant K when a force F is applied to it according to Hooke's law:

$$F = -K\,\Delta d \qquad \text{Equation 1}$$

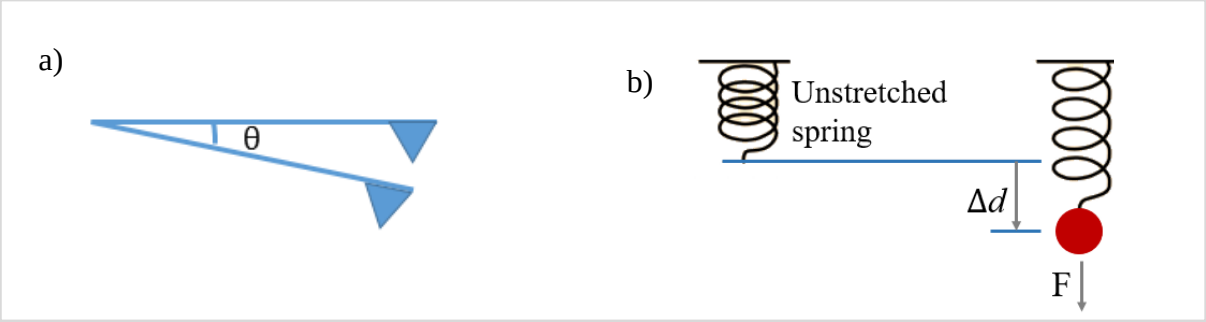

Figure 4: a) Deflection of cantilever supporting tip by θ; b) extension of a spring by a force F.

Most common AFMs make use of the feedback loop to generate the topography of the surface. For instance, this mode of measurement is termed the "constant force" mode. The initial deflection of the cantilever is recorded as an input (the setpoint). As the sample is scanned (moved in the x and y direction by the piezo), upon reaching a height or a valley, the cantilever respectively bends upwards or downwards. This deflection sensed by the photodiode, a retro-control mechanism operates via the feedback loop and the piezo is made to adjust the z position of the sample so as to restore the cantilever deflection back to its original value. The different adjustments of the piezo, caused by the deflections of the cantilever, are used to generate the topography of the surface.

Our measurements have been performed in the constant force mode and the interaction (accordingly to the heights and depths) corresponding to each scanned point is given in a matrix, (512 x 512). Each of the z displacement (to maintain the force constant) thus recorded is represented according to a grid of colours in order to construct the topography of the imaged surface.

1.4.2. Forces of attraction and mode of functioning of the AFM

The forces measured between the tip of the AFM and the samples can be grouped as short/long range attractive/repulsive forces and can be modelled by the Lennard-Jones potential as:

$$U(r) = \frac{\alpha}{r^{12}} - \frac{\beta}{r^{6}} \qquad \text{Equation 2}$$

With r being the distance between the tip and the sample; α and β are respectively the repulsive and attractive interaction constants.

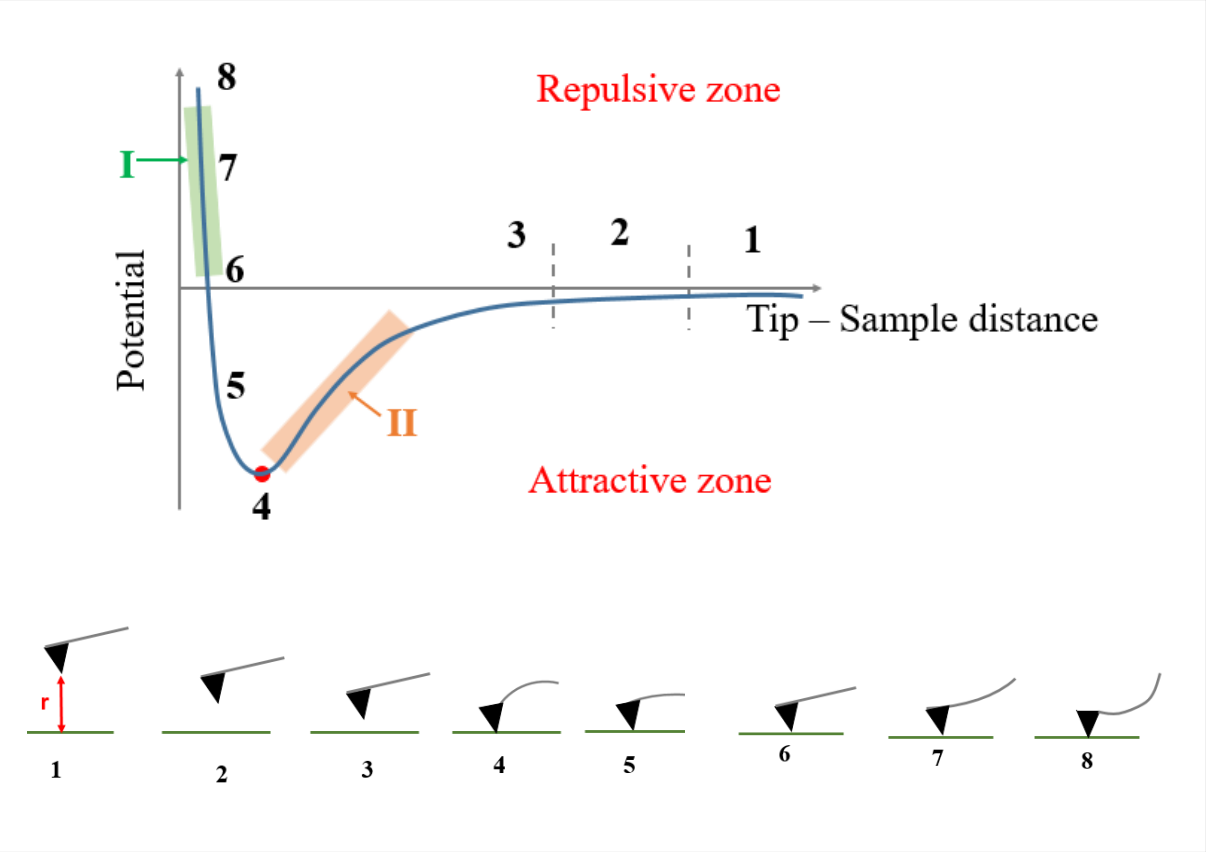

Figure 5: Lennard-Jones potential; evolution of cantilever deflection as tip approaches the surface, with r being the tip-surface distance.

In Figure 5, the different positions denoted by 1 to 8, represents the cantilever deflection as the tip is brought close to the surface of the sample during measurements:

1. The tip is located far from the surface (for instance during the process of alignment of the laser beam, the tip is about some millimetres to few micrometres away from the surface) and hence no interaction exists between them;
2. The distance between the tip and the surface is reduced (r > 100 nm), yet no interaction is felt at such distances; the cantilever does not deflects;
3. At r < 100 nm, the forces start acting on the tip and the cantilever starts to bend. The cantilever is sensible to the forces operating at such distances (low spring constant);
4. At this point, the forces of attraction are such that cantilever bends in a way that the tip comes into contact with the surface;
5. The tip is in contact with the surface and any further approach is followed by a decrease of the net attractive forces. As a consequence, the cantilever is less bended compared to the previous position;
6. At this very position, the net deflection of the cantilever is equal to zero since the attractive component of forces is balanced by the repulsive component;
7. In this position, the repulsive forces take over attractive forces and hence the cantilever bends in the other direction;
8. The repulsive forces are such that the tip "detaches" from the surface.

Accordingly to the interactions defined above, surface topography measurements by the AFM are performed according to three different modes:

- **Contact mode**

In the contact mode, the measurements are performed with the tip in contact with the surface but in the repulsive forces zone (shaded zone I in figure 5). As the tip scans the surface, the cantilever is accordingly deflected upon reaching a change in the topography.

- **Non-contact mode**

In the non-contact mode, the cantilever oscillates over the surface without the tip touching the surface. The operating zone corresponds to the attractive zone, shaded zone II in figure 5. Upon reaching a height, crashing onto the surface is prevented by the feedback loop. The surface topography is thus generated by the record of changes of the piezo system.

- **Tapping mode**

In the tapping (or oscillating) mode, the cantilever is set to oscillate at a resonant frequency with a "free amplitude" A_r over the sample. As, it approaches the surface, the forces of interaction with the sample causes a modification of the amplitude of vibration. During measurements, when the tip senses a height, the amplitude of oscillation decreases. Conversely, when the tip senses a valley, the amplitude of oscillation increases. The feedback loop thus adjusts the sample position downwards and upwards respectively so as to restore the oscillating amplitude and force. The different z displacements of the piezo are used to generate the topography of the sample.

The roughness parameters provided by the AFM and investigated during the study are:

- 2D and 3D image surface areas;

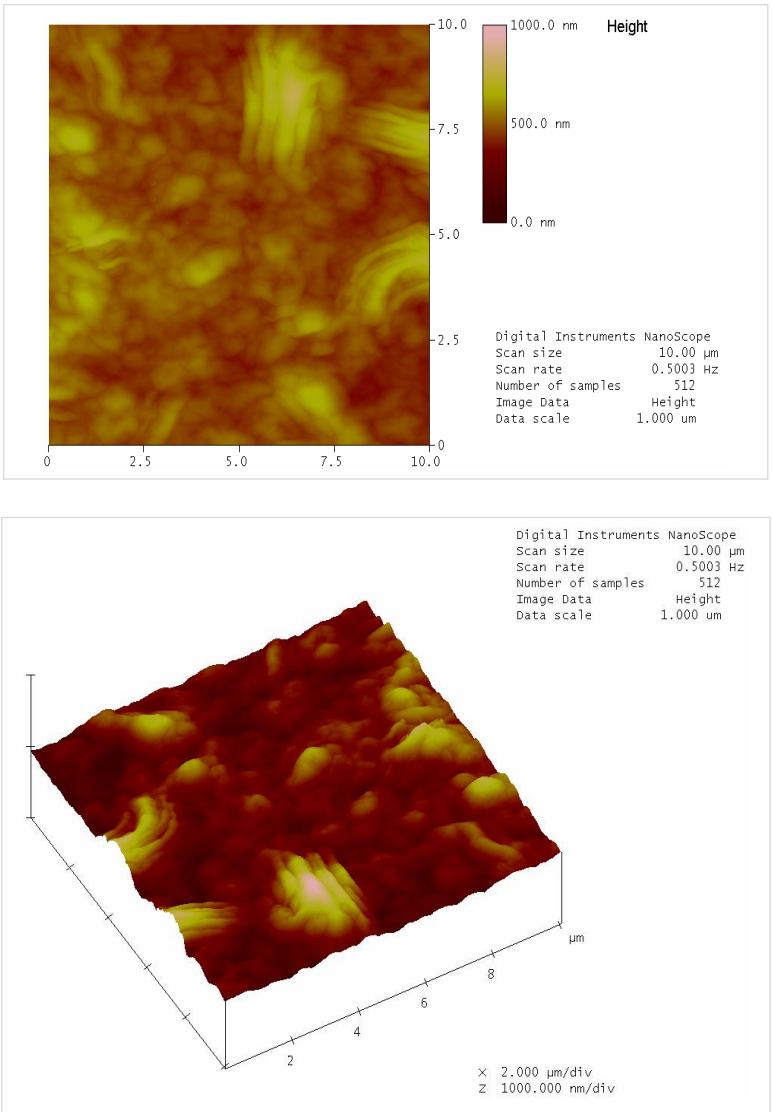

Figure 6: a) (10x10) µm 2D image of Wy-Ca^{2+}; b) (10x10) µm 3D image of Wy-Ca^{2+}.

- The difference in image surface area, corresponding to the difference between the image's three-dimensional surface area and its two-dimensional footprint;
- The root mean square (RMS) of heights and R_{max}. The RMS is the root mean square average of the height deviations (h) taken from the mean data plane ($RMS = \sqrt{\frac{\sum h_i^2}{n}}$). R_{max} corresponds to the maximum vertical distance between the highest and the lowest data points in the image.

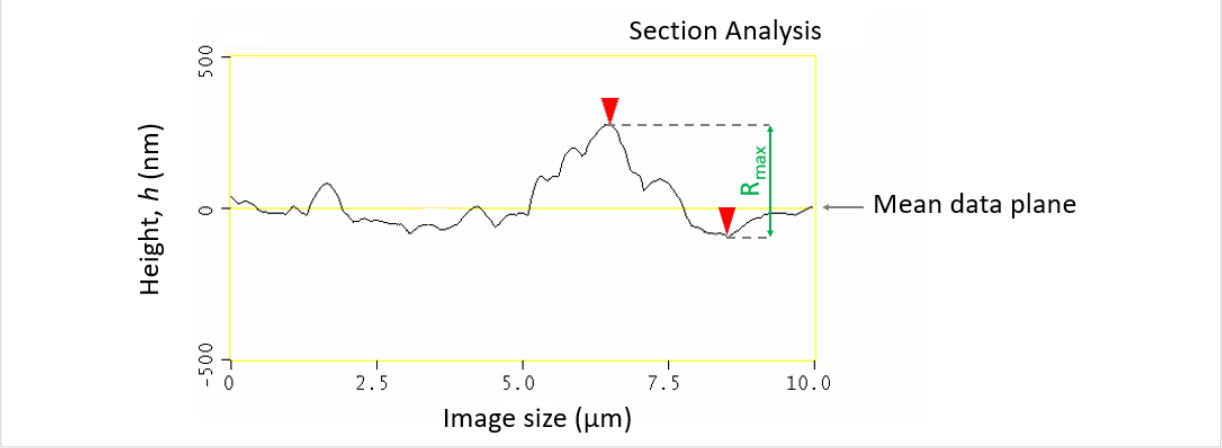

Figure 7: Measurement of surface roughness parameters, RMS of heights and R_{max} from the profile of the Wy-Ca^{2+} surface.

1.4.3. Fractal analysis

As such the roughness parameters provided by the AFM should provide a global indication of the state of roughness of our clay films. However, even if these information could be handy at first sight, they are debatable. For instance, let us consider the RMS and R_{max} as indicated in the previous section, having a look at Figure 8 below, it is clear that relying on these parameters would be over-estimating the roughness of a such globally "smooth" surface.

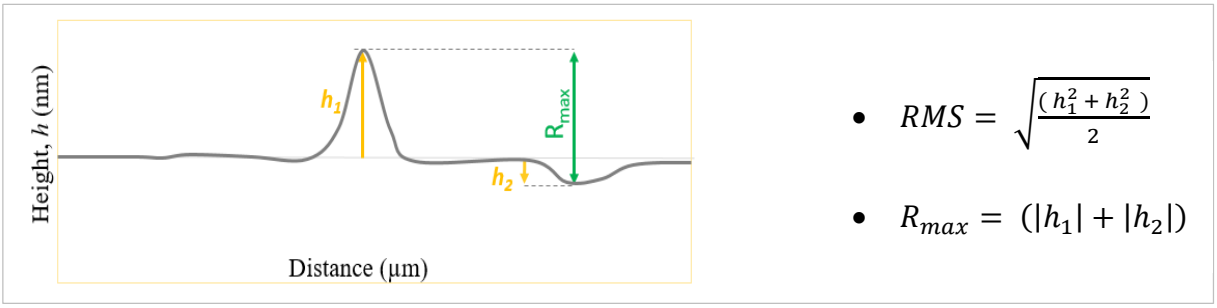

Figure 8: showing an over estimation of the roughness of a surface which can be regarded as "smooth" depending on the location.

It thus appeared necessary to characterise the roughness of the clay films via some other parameters. For instance, the imaged height structures of the clay films have been regarded as fractals and characterised by fractal dimensions. It follows that a change in the fractal dimension with the correlation length indicates a change in the topography of the surface.

To reach such a goal, correlation of heights has been performed in such a way that local information is conserved as the distance is increased from a statistical origin. Precisely, this has been achieved as follows:

1. Estimation of the variogram, V ($\vec{r}_{2D}$), of the heights *h*, between 2 points, let's say situated at r'_{2D} and r_{2D} (Figure 9b) :

$$V[h(\vec{r}_{2D})] = [h(\vec{r}'_{2D} + \vec{r}_{2D}) - h(\overrightarrow{r'}_{2D})]^2 \qquad \text{Equation 3}$$

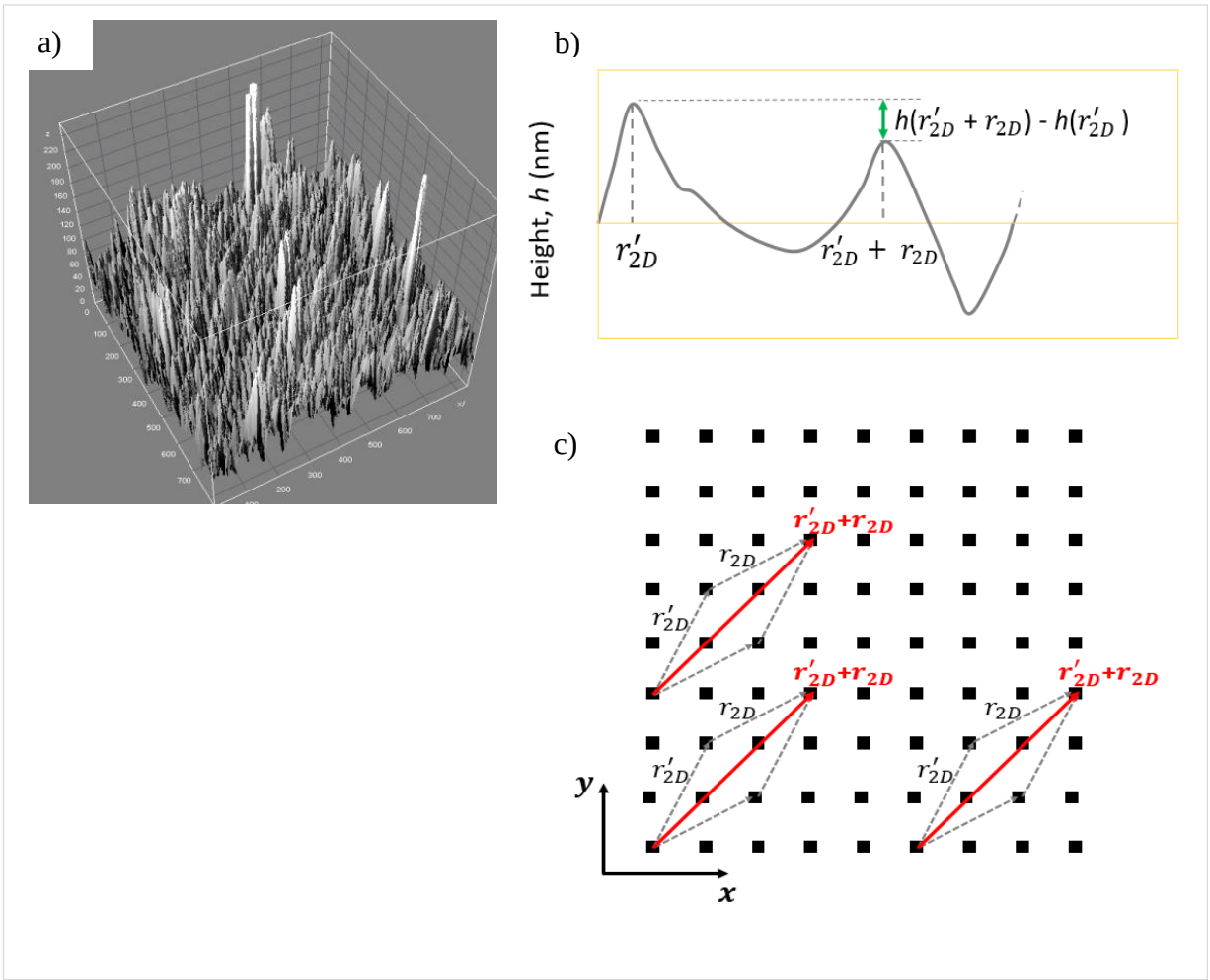

Figure 9: a) 3D image of sample; b) difference of height between 2 points situated at r'_{2D} and $r'_{2D} + r_{2D}$ *separated* by a distance r_{2D} ; c) variance calculated over the whole image between r'_{2D} , and a point at $r'_{2D} + r_{2D}$ by moving the statistical origin.

2. The origins have then been changed over the whole image in such a way so as to conserve the distance between the points r'_{2D} and $r'_{2D} + r_{2D}$ fixed (Figure 9c) and an average of the variogram has been calculated:

$$V[h(\vec{r}_{2D})] = \langle [h(\vec{r}'_{2D} + \vec{r}_{2D}) - h(\overrightarrow{r'}_{2D})]^2 \rangle_{\overrightarrow{r}_{2D}} \quad \text{Equation 4}$$

3. The distance r_{2D} has then been gradually increased and the the variance calculated in a similar way as indicated by equation 4.

4. For isotropic images, the morphology is statistically invariant along the axes (x,y) and the variance is an angular average calculated as **[variance isotropic images]**:

$$V[h(r)] = \langle V[h(\vec{r}_{2D})] \rangle_{2\pi} \quad \text{Equation 5}$$

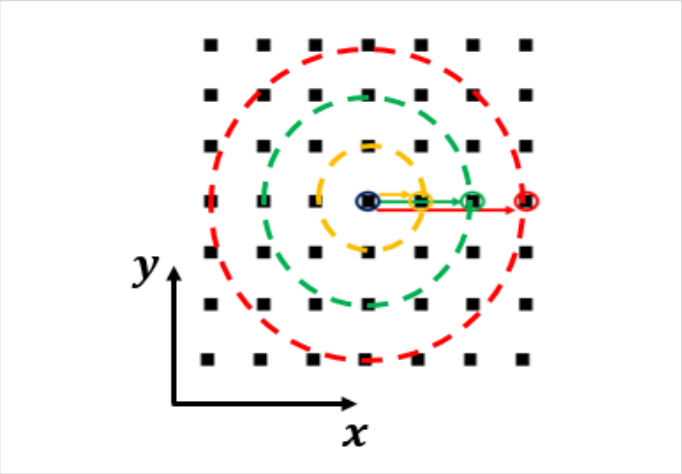

Figure 10: Averaging of the variogram on 2π, for a given statistical origin, as r_{2D} is increased.

5. Probing surface roughness is dealing with heights (in the z direction), which are perpendicular and non-equivalent to the mean data plane (xy). Mandelbrot [3] thus introduced the concept of self (or auto)-affinity, a concept which has particularly used for the study of roughness of fault surfaces by Schmittbuhl et al. [4]. As such, self-affinity describes independenly the magnification of z and (xy) such that the profil is statistically unchanged upon magnification. It follows that, the variogram of heights follows a power-law written as [5]:

$$V[h(r)] \propto r^{2H} \quad \text{Equation 6}$$

With *r*, the correlation length; *H* is the Hurst exponent that varies between 0 for rough surfaces and 1 for smooth surfaces. The fractal dimension, $\bar{d} = 3 - H$, indicating an evolution of surface roughness accordingly with $2 < \bar{d} < 3$ ($\bar{d}$=2 for *H*=1 and $\bar{d}$=3 for H=0).

1.4.4. Experiments

A Nanoscope III multimode scanning probe microscope (Digital Instrument) (TM-AFM) was used in tapping mode to probe the surface of clay films and make images of (10µm x10µm) at a scanning rate of 0.5-0.8 Hz and a resolution of 512x512. A Phosphorus (n) doped Silicium tip from Veeco used during AFM measurements had a cantilever of resonance frequency of 250 KHz and spring constant 20-80 N/m. In order to analyse the effect of particle size (SAz-Na+ of four different sizes) and exchangeable ions (NAu1 exchanged with $Li^{+,}$ Na^{+}, K^{+} and Ca^{2+}) on the roughness of films, 200µl of clay suspensions (corresponding to similar clay content per cm^2 as films composed of 1.5 ml of clay suspensions used for contact angle measurements) were deposited on 1cm^2 of pre-cleaned glass slides and left to dry in air before analysis. 5 images of the size of (10 x10) µm with a resolution of 512 x 512 were then carried out and the roughness parameters were averaged for each sample.

2. Effect of exchangeable ions

The SSD method was chosen for the measurement of contact angles. When a liquid is dropped on a surface, the contact angle is defined as the stabilisation of the three phase line. Consequently, we found it necessary to investigate the variation of contact angle with time and to define the time of measurements. For instance, these measurements have been performed on a swelling clay (SWy).

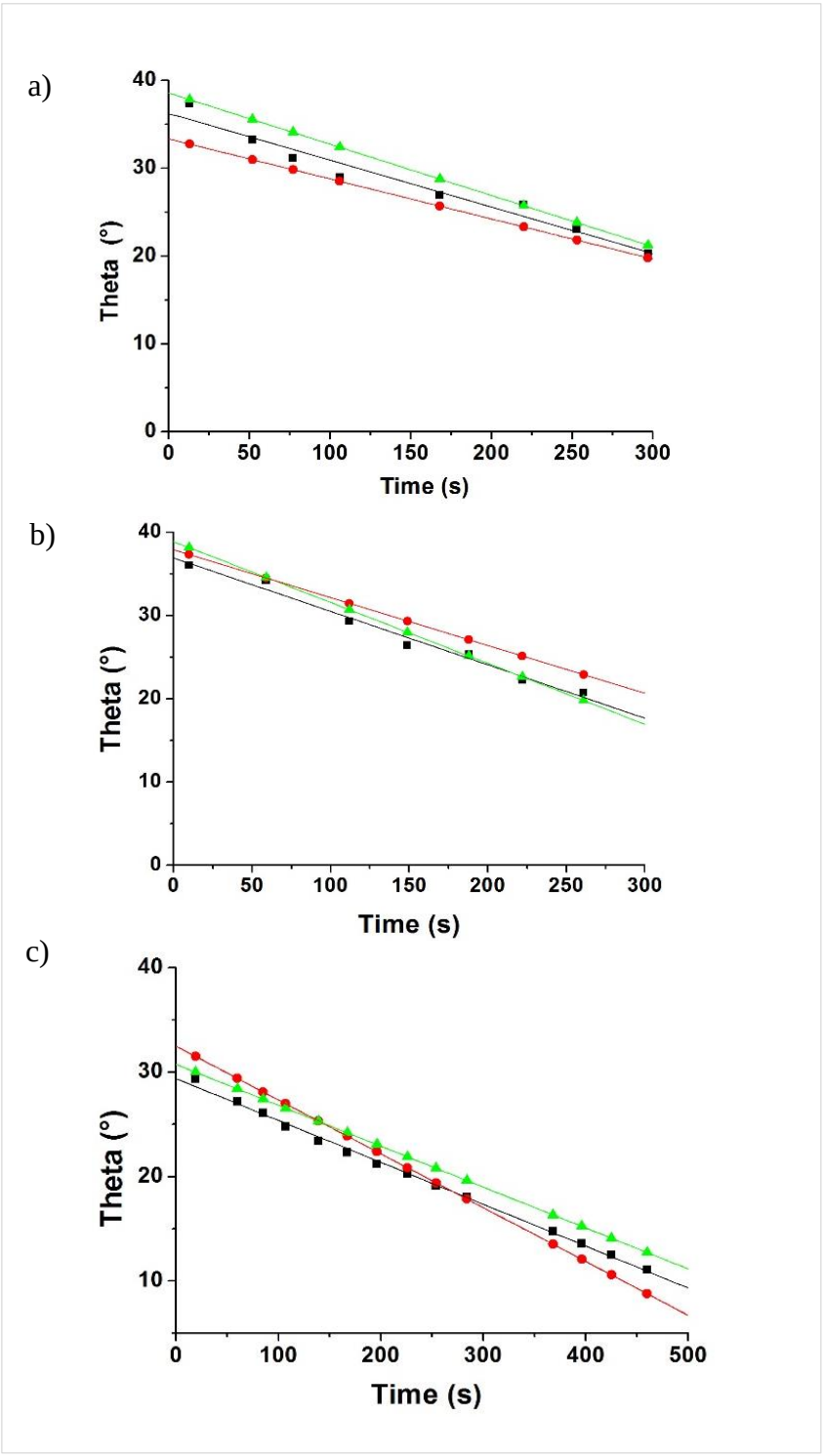

Figure 11: a), b), and c) respectively show the contact angles (°) of drops of 5µL on each sample as a function of time of: SWy-Li^{+}, SWy-Na^{+} and SWy-Ca^{2+} at RH=45%.

Figures 11a to 11c display the time evolution of water contact angles measured for films of Wyoming montmorillonites exchanged with various cations under ambient conditions (RH = 45%). Whatever the cation, the measured contact angles significantly decrease with time, which may be assigned to evaporation phenomena that were recently studied in detail [6]. It was decided in the following to focus on the contact angles measured for the shortest times (at 10s after drop deposit for all the samples).

2.1 Swelling clays

2.1.1. Water contact angles

The mean water contact angles measured at ambient humidity (RH=45%) on films of beidelite, nontronite and Wyoming montmorillonite exchanged with different ions are reported in Tables 3 -5.

Exchangeable ion	**Contact angles of drops of 5µl of water on film composed of 1.5mL of clay suspension (°)**
Li^+	29
Na^+	17
Ca^{2+}	26

Table 3: Water contact angles (±3-5°) at 45% RH obtained on films of beidelite at 3g/L.

- **NAu1**

Exchangeable ion	**Contact angles of film composed of 200µL of clay suspension (°)**	**Contact angles of film composed of 1.5mL of clay suspension (°)**
Li^+	13	40
Na^+	17	30
K^+	45	50
Ca^{2+}	23	26

Table 4: Water contact angles (±3-5°) at 45% RH obtained on films of nontronite at 3g/L.

- **SWy**

Exchangeable ion	**Contact angles of film composed of 200µL of clay suspension (°)**	**Contact angles of film composed of 1.5mL of clay suspension (°)**
Li^+	26	37
Na^+	33	38
Ca^{2+}	20	31

Table 5: Water contact angles (±3-5°) at 45% RH obtained on films of montmorillonite at 3g/L.

At first sight, for the different clays and exchangeable cations, the contact angles measured on films resulting from 200µL of suspension are lower than those of 1.5mL. This observation can a priori be attributed to the presence of more clay particles and hence more surface roughness on films made up of 1.5 mL of suspension.

Regarding the effect of exchangeable cations on the wettability of the swelling clay minerals, let us consider the films resulting from 1.5mL of clay suspension. The smallest contact angle on beidellite was obtained with Na^+ whereas for both nontronite and montmorillonite, the smallest contact angles was obtained with Ca^{2+}. Even if the case of K^+ was only analysed for nontronite, it displayed the highest values of all the tested materials. In the series of analysed monovalent ions, K^+ is the least hydrated (the standard ion hydration enthalpies $\Delta_{hyd}H$ of Li^+, Na^+ and K^+ are -520, -405 and -321 kJ/mole respectively [35]). These hydration energies are linked to the charge densities (charge/ionic radius ratio) of the ions that decrease in the order of Li^+, Na^+ and K^+ and, naturally, are followed by a decrease of the affinity for water molecules. This is partly revealed by the contact angle on the K^+ sample which is the highest among the three. However, the results obtained with Na^+ and Li^+ are not always consistent with that sequence, a feature that will be discussed later on. As far as Ca^{2+} is concerned, having the highest charge density and the most favourable hydration energy ($\Delta_{hyd}H$ of Ca^{2+} = -1650 kJ/mole [7]), the corresponding exchanged clays are expected to have the smallest contact angles.

In order to investigate if, as indicated by these first measurements, K^+, due to its low hydration enthalpy actually leads to higher contact angles, additional experiments with concentrated chloride solutions, instead of water, were performed.

Probed Liquid and concentration	**Interlayer ion**			
	Li^+	Na^+	K^+	Ca^{2+}
H_2O	26	26	**35**	29
NaCl (1M)	26	21	**29**	28
KCl (1M)	**35**	**36**	**38**	**42**
$CaCl_2$ (0.5M)	25	22	**29**	27

Table 6: Contact angles (±3-5°) at 45% RH with drops of 2µL in volume on nontronite films (200µL of suspension).

Probed Liquid and concentration	**Interlayer ion**		
	Li^+	Na^+	Ca^{2+}
H_2O	34	38	24
NaCl (1M)	37	36	31
KCl (1M)	**50**	**49**	**36**
$CaCl_2$ (0.5M)	34	35	29

Table 7: Contact angles (±3-5°) at 45% RH with drops of 2µL in volume on Wyoming montmorillonite films (200µL of suspension).

As shown in Tables 6 and 7, the results clearly reveal that the presence of K^+ ions generates higher contact angles than any of the other ions used in the present study.

On the basis of surface tension, γ_{LV}, of the brines are higher compared to water [8]. Precisely, these authors reported that the surface tension (γ_{LV}) of brines-(NaCl and KCl)/air was greater than that of water/air. With the samples of NAu1 and SWy exchanged with Li^+, Na^+ and Ca^{2+}, the contact angles recorded with the brines (NaCl and $CaCl_2$) are more or less similar to those recorded with water. The constant contact angle, θ, is for sure driven by the increase in γ_{LV} and consequently an equivalent increase of ($\gamma_{SV-}\gamma_{SL}$) since ($\cos\theta = \frac{\gamma_{SV}-\gamma_{SL}}{\gamma_{LV}}$). The increase of ($\gamma_{SV-}\gamma_{SL}$) being partly possible by a decrease of γ_{SL}, implying that the surface is more wet in the presence of brines of NaCl and $CaCl_2$ compared to water.

However, with KCl as the probed liquid, the contact angles on Li^+, Na^+ and Ca^{2+} of both NAu1 and SWy, the contact angles increased considerably compared to water. In line with the previous observations, it is thus appropriate to conclude that the increase of γ_{LV} (of KCl

compared to water) as well as either a constant value or a decrease of ($\gamma_{SV-}\gamma_{SL}$) would be in line with the increase of contact angle. In this case, a decreased solid-liquid interaction (increase of γ_{SL}) could partly explain the observed results.

On the other hand, despite that these results are available only for the NAu1 samples, it is also important to note that contact angle with brines of NaCl and $CaCl_2$ were lower compared to water on the K^+ exchanged clay. As described above, the clay minerals are more wet in the presence of brines of NaCl and $CaCl_2$. All together, these results clearly show the specific behaviour of K^+ ions.

2.1.2. Oil contact angles

Both crude oils LVC(C) and MFC(B) have been used to measure contact angles on films of the swelling clays. However, no measurable contact angles could be recorded as both of the oils spread instantaneously on the surfaces.

2.2 Non-swelling clays

2.2.1. Water contact angles

The effect of ions has been analysed on films of kaolinite and illite both exchanged with Na^+ and Ca^{2+}. Measurements have tentatively been made on films of different thicknesses (200µL, 1.5mL and 4mL of clay suspension at concentrations of 3g/L and 20g/L) but in almost all cases, the drops of water disappeared almost immediately after deposit by a sort of “blotting effect”. Indeed, the non-swelling clays films were porous (compared to non-swelling ones) and no net conclusion could be drawn.

2.2.2. Oil contact angles

Both crude oils LVC(C) and MFC(B) have been used to measure contact angles on films of kaolinite and illite. However, as with the swelling clays no measurable contact angles could be recorded as both of the oils spread instantaneously on the surfaces/ penetrated into the pores.

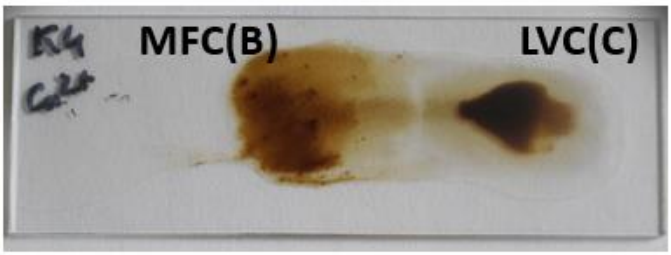

Drops of oils MFC(B) and AC on film of kaolinite-Ca^{2+} made from 200µL of suspension at 3g/L.

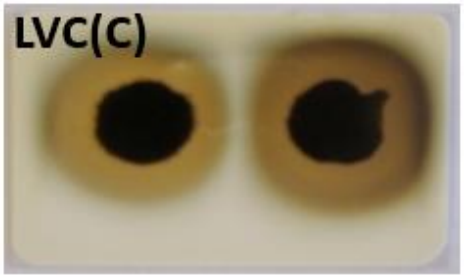

Drops of oils LVC(C) on film of kaolinite-Ca^{2+} made from 1.5mL of suspension at 20g/L.

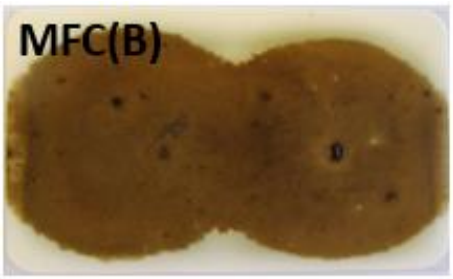

Drops of oils MFC(B) on film of kaolinite-Ca^{2+} made from 1.5mL of suspension at 20g/L.

Figure 12: Drops of crude oil which spread on films of kaolinite, MFC(B) being less viscous than LVC(C), spread more on the films.

It is to be noted that contact angle measurements with the crude oils as probed liquids have been challenging and fastidious on the swelling as well as the non-swelling clays. For instance, a contact angle of ~ 0° was recorded for all the clay minerals. If on one hand, this could be attributed to the porosity of the non-swelling clays, on the other hand, it also seems to be linked to the wetness of the clay minerals with respect to the oils. Indeed, contact angles being an equilibrium at the three phase interface, it seems that adsorption of crude oil components onto the minerals surfaces are in favour of solid/oil surface tensions. Regarding these results, modification of surface/ interfacial tensions have been applied to record measureable contact angles (*cf chapter V section 2*).

Consequently, for the analysis of the other parameters (relative humidity, particle size and surface roughness) were emphasised on the swelling clays by using water as probed liquid.

3. Effect of relative humidity

While considering the evaporation phenomena mentioned earlier, the role of relative humidity (RH) may be particularly important in view of the specific interactions between water and clay minerals. Furthermore, the way according to which clay hydrates strongly depend on the nature of the interlayer cations, RH is then likely to modify the different results obtained for different cations at ambient humidity. The first effect of increased RH can be seen from the curves displayed in Figures 13a to 13c (Wyoming Montmorillonite exchanged with Li^+, Na^+ and Ca^{2+}) that exhibit the time evolution of contact angles. Indeed, compared to the curves obtained in Figures 11a to 11c, high RH leads to a stabilisation of the contact angle at long times, which was not the case at 45%RH where a linear decrease was observed. This can be attributed to a strong decrease in evaporation. Still, if one considers the values obtained at short times, RH marginally modifies the contact angles measured for samples exchanged with Na^+ and Li^+ that display a slight decrease, in agreement with previous results, whereas it does not seem to have any effect for the Ca^{2+}-exchanged system. This can tentatively be assigned to the difference in hydration between these cations. Indeed, for Na^+ and Li^+, upon an increase in RH from 46% to 84%, the samples evolve from a situation where the dominant hydration state is a one-layer to a situation where the two-layer hydrates dominates [9], [10]. This is not the case for Ca^{2+} where at 45%RH, most layers are already in a two-layer hydrate state [10].

Finally, at high RH, the fact that a plateau is observed at long times may indicate that some equilibrium can be reached in such conditions, whereas this is not the case for lower RH. It is then relevant to compare the values obtained at the plateau that can be referred to as stabilised values (Table 8). This table reveals once more the specific role of K^+ as clays exchanged with this cation display significantly higher contact angles.

Clay mineral	Relative Humidity, RH, (%)	Interlayer ion			
		Li^+	Na^+	K^+	Ca^{2+}
Beid	84	17	13	-	21
	100	15	15	-	20
NAu1	84	23	20	45	21
	100	23	20	43	21
SWy	84	20	23	-	25
	100	23	23	-	23

Table 8: Mean stabilised water contact angles (± 3-5°) recorded on beidellite, nontronite and montmorillonite films at relative humidities of 84 and 100%.

a)

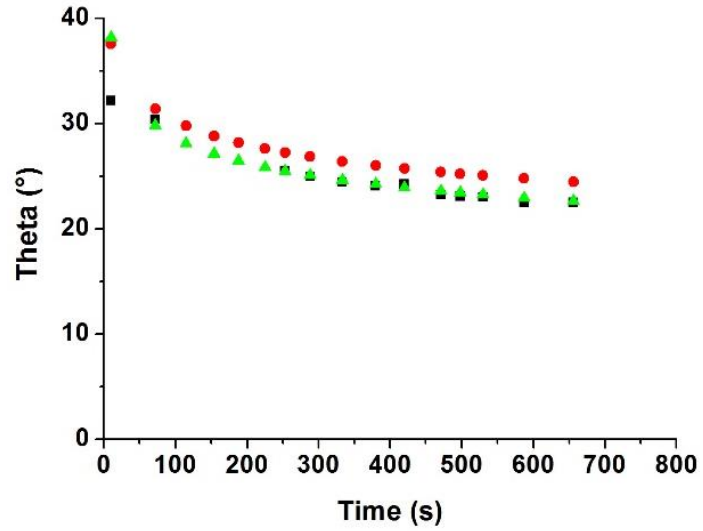

b)

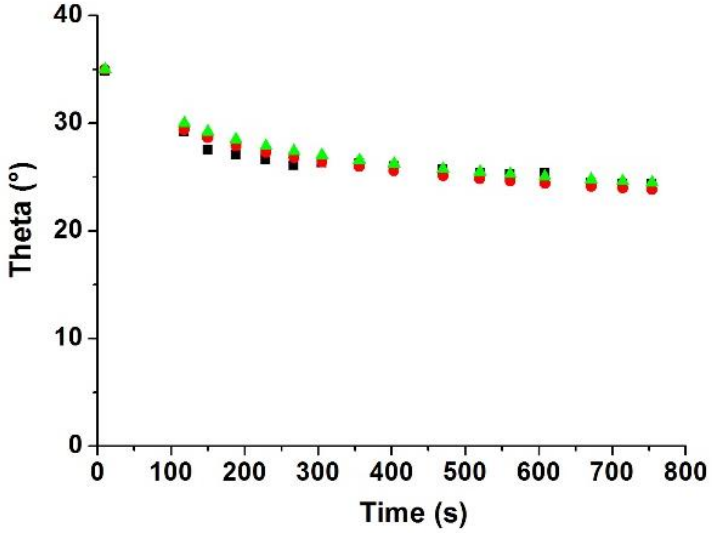

c)

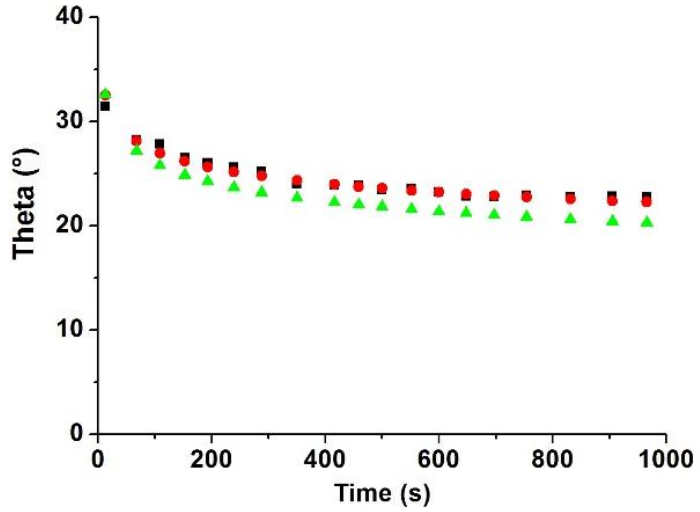

Figure 13: a), b) and c) respectively show the contact angles (°) of different drops as a function of time on samples of: SWy-Li^+, SWy-Na^+ and SWy-Ca^{2+} at RH=100%.

4. Effect of surface roughness

The effect of surface roughness on the wettability of clay films has been investigated as a function of exchangeable ions and of clay platelet size. The main objectives of this part of the work is to find the respective contribution of the physico-chemical aspects on contact angles. Indeed, both the chemistry (hydration energies) and the topography (roughness) of the surface are likely to drive contact angles. For instance, the influence of exchangeable ions on the roughness of clay films has been analysed on films of:

- SWy platelets of 250 nm exchanged with Li^+, Na^+ and Ca^{2+} and NAu1 of platelets of (200 x 700) nm exchanged with Na^+, Li^+, K^+ and Ca^{2+}.

Moreover, the effect of platelet sizes on the roughness of clay films has been investigated on:

- Na^+-exchanged Arizona montmorillonites.

4.1 Surface roughness as a function of exchangeable ions

- **SWy exchanged with Li^+, Na^+ and Ca^{2+}**

Table 9 shows the contact angles and corresponding roughness parameters of the different exchanged films of SWy. All the roughness indicators point towards the following order of increasing surface roughness $Li^+ < Na^+ << Ca^{2+}$. It is to be noted that, despite the Ca^{2+} sample exhibiting the highest 3D-2D surface difference, R_{max} and RMS, it shows the lowest water contact angle.

Exchangeable ion	**Li^+**	**Na^+**	**Ca^{2+}**
Contact Angle at 45% RH / °	26	33	20
Image surface area difference (3D-2D) / %	1.82	2.11	3.38
RMS / nm	13.3	25.4	55.6
R_{max} / nm	31.0	115	394

Table 9: Contact angles and mean roughness parameters on SWy film exchanged with Li^+, Na^+ and Ca^{2+}.

- **NAu1 exchanged with Li^+, Na^+, K^+ and Ca^{2+}**

The results obtained on films of nontronite possessing different surface ions are shown in Table 10. In the order of increasing surface roughness are the films of $Na^+ < Li^+ < K^+ << Ca^{2+}$. Though

the trend for Li^+ and Na^+ are not constant with that observed with SWy, the results can be classified into three main groups: the Li^+/Na^+, K^+ and Ca^{2+}. As an illustration, the 2D images of the different samples are show in Figures 14a to 14d.

Exchangeable ion	**Na^+**	**Li^+**	**K^+**	**Ca^{2+}**
Contact Angle at 45% RH / °	30	40	50	21
Image surface area difference (3D-2D) / %	2.71	2.71	4.24	7.50
RMS / nm	57.0	76.0	105	261
R_{max} / nm	370	412	534	1263

Table 10: Contact angles and mean roughness parameters calculated on 5 images of each NAU1 film exchanged with Li^+, Na^+, K^+ and Ca^{2+}.

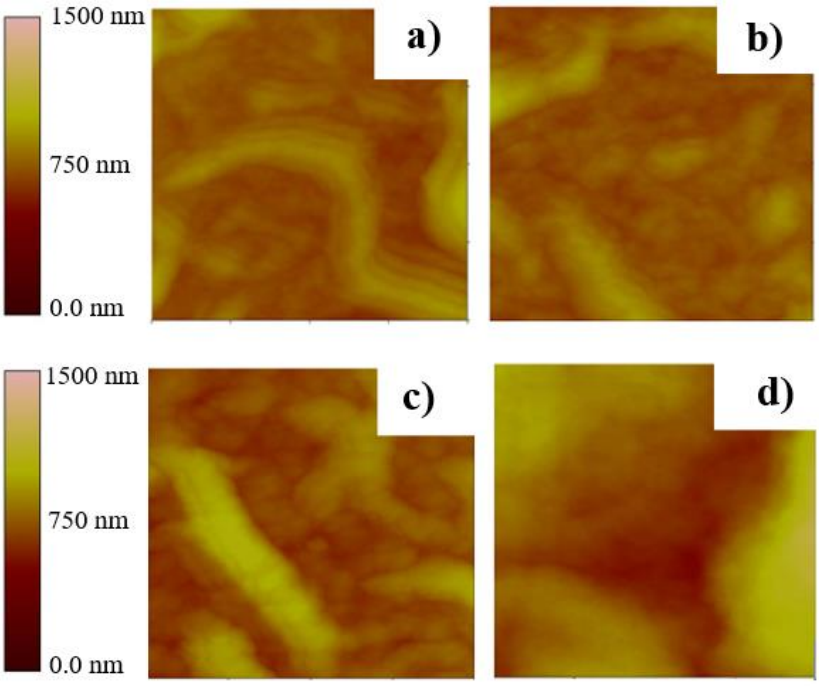

Figure 14: (10x10) µm AFM of NAu1 films. a) Li^+ film; b) Na^+ film; c) K^+ film and d) Ca^{2+} film. Contrasts linked to the topography of the films appear as bright zones corresponding to higher altitudes while those situated in depth appear as dark zones

Further analysis of the spatial correlation of roughness was applied to nontronite films data. Figure 15 below shows the variance of heights with respect to *r*, the correlation length between two points. The fractal analysis parameters deduced from the graph are given in Table 11. For instance, *H*, the Hurst exponent has been deduced in the linear part of each curve; r_{CO}, the correlation length at which the variance reaches a plateau; the variance at plateau, indicating the maximum variance recorded between two heights and beyond which the sample can be regarded as "smooth".

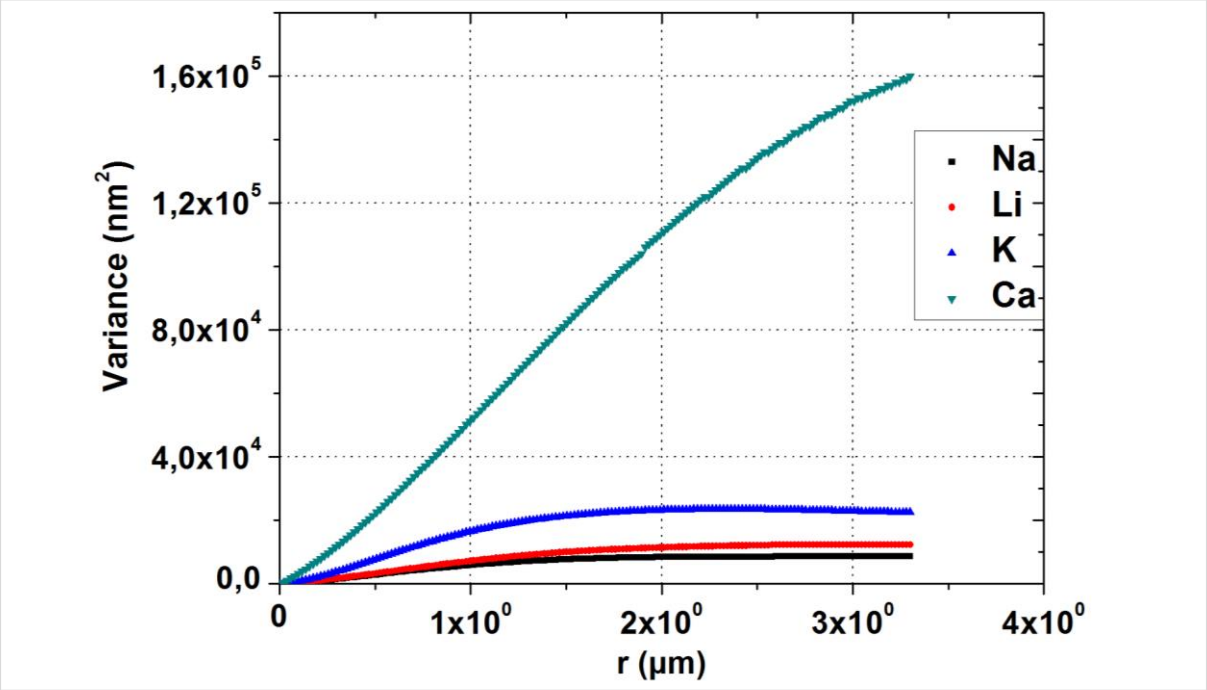

Figure 15: Variance of heights on films of nontronite exchanged with Na^+, Li^+, K^+ and Ca^{2+} with respect to the correlation lengths.

Exchangeable ion	**Na^+**	**Li^+**	**K^+**	**Ca^{2+}**
H, Hurst exponent	0.69	0.69	0.71	0.60
Fractal dimension, $\bar{d}$ = 3-H	2.31	2.31	2.29	2.4
r_{co} (µm)	1.5	1.6	2.0	4.0
Variance at plateau (nm^2)	9000	11500	23000	170000[a]

Table 11: Fractal analysis parameters on films of nontronite exchanged with Na^+, Li^+, K^+ and Ca^{2+}; [a] has been estimated by extrapolation.

The Hurst exponents recorded on the samples of Na^+, Li^+, K^+ are the same, around 0.7, while that recorded on the sample of Ca^{2+} is significantly lower, H=0.6. Furthermore, from the maximum variances of the heights, it can be observed that the plateau recorded on the Ca^{2+} sample is 18 times that recorded on Na^+ (the smoothest) and about 7 times that of the K^+ sample. It follows that, the correlation length, r_{CO}, is much longer for the Ca^{2+} sample compared to the other three.

Undeniably, these results (AFM roughness as well as fractal analysis) point towards an increase in surface roughness in the order of $Na^+ < Li^+ < K^+ << Ca^{2+}$. The difference between monovalent

and divalent cations can be tentatively assigned to the nature of the particles in the suspension where ion specific effects (or so called Hofmeister series of cations, Figure 16 [11]) drive the quality of the clay suspensions. For all monovalent cations, delaminated suspensions are obtained whereas in the Ca^{2+} case, particles formed with a few platelets are present [12], [13]. Indeed, these authors observed for montmorillonite clay mineral, that the number of platelets per tactoid increased in the order of $Li^+ < Na^+ < K^+ < Mg^{2+} < Ca^{2+}$. In the series of monovalent cations, highly hydrated monovalent Li^+ and Na^+ counterions are only weakly or not at all adsorbed on clay surfaces. They thus maintain a stable and evenly dispersed clay platelet suspension. The K^+ counterions, less hydrated than the previous cations, show a higher affinity for the negatively charged clay platelets than the previous cations.

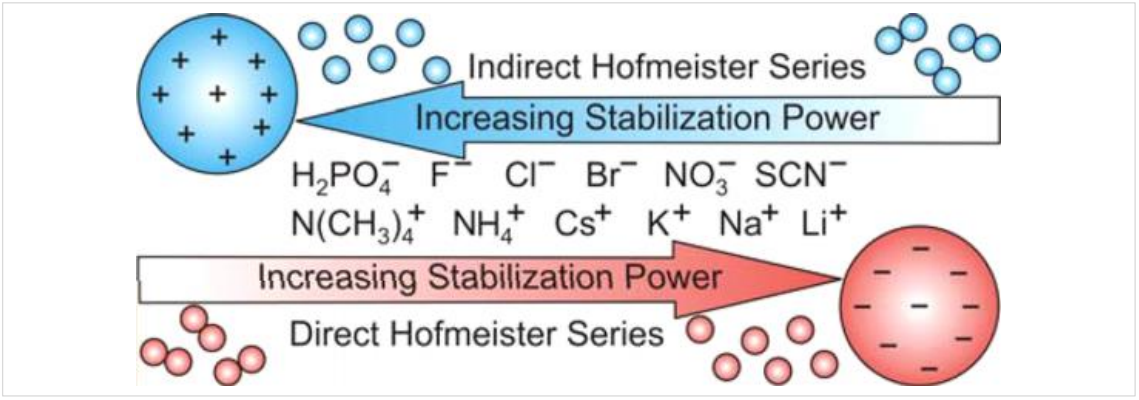

Figure 16: Particle aggregation induced by monovalent salts within the Hofmeister series.

As far as the divalent Ca^{2+} ions are concerned, despite their high hydration energies, they primarily follow the Schulze-Hardy rule and result in particle aggregation and hence very rough surfaces [11], [14], [15]. As such this rule states that the aggregation of charged particles in the presence of highly charged ions occurs at lower salt concentration compared to low charged ones.

As a conclusion to the wettability of clay minerals with respect to different exchangeable ions, it clear that the nature of surface ions primarily influences the suspension, which upon deposit form more or less rough films. However, the contact angles recorded seems to be rather in agreement with the model of Wenzel [16], where, the chemistry of the surface governs the measured contact angle. For instance, Ca^{2+} ions possess the most favourable hydration enthalpy and surface roughness of NAu1-Ca^{2+} film being the highest, the hydrophilic character is enhanced and hence resulted in the lowest contact angle. On the other hand, the NAu1-K^+ film

possess intermediate roughness among the analysed series and possess the highest contact angle essentially driven by the chemistry of the surface (low free hydration energy).

4.2 Surface roughness as a function of particle size

The effect of particle size and hence surface roughness on the wettability of Arizona montmorillonite are shown in Table 12 (with sizes S1>S2>S3>S4). The results indicate that the film composed of particles with the largest size (S1) has the largest contact angle while that composed of particles of the smallest size (S4) displays the smallest contact angle. The average individual particle size in the films therefore appears to affect contact angles. As observed by Paineau [17], the physico-chemical characteristics of the platelets are independent of their sizes. Indeed, they possess identical CEC and equidistant charges equilibrated by Na^+ so that the contact angles are undeniably linked to the difference in roughness of the different films investigated. The given AFM parameters (3D-2D image difference, RMS and R_{max}) all point towards increasing film roughness in the order of S4 < S3 ≈ S2 < S1.

Particle Size	**S1**	**S2**	**S3**	**S4**
Contact Angle at 45% RH / °	38	31	28	20
Image surface area difference (3D-2D) / %	15.5	4.70	4,66	2.90
RMS / nm	118.3	85.3	82.26	43.5
R_{max} / nm	764.7	467.6	454.17	251.9
H, Hurst exponent	0.68	0.65	0.65	0.66
r_{co} (µm)	3.0	2.3	2.3	1.3
Variance at plateau (nm^2)	30000	15800	15000	4000

Table 12: Contact angles and mean AFM roughness parameters and fractal analysis parameters calculated on 5 images of each film of Arizona montmorillonite-Na^+ composed of particles of sizes S1, S2, S3 and S4.

In terms of fractal analysis (derived from Figure 17), at small correlation lengths, the *H* exponent is similar for the 4 particle sizes. In contrast, both the r_{co} value and the variance at the plateau evolve with particle size in similar ways as that observed for the non spatialized parameters (3D-2D image difference, RMS and R_{max}), i.e. S4 < S3 ≈ S2 < S1. These results clearly indicate that the film formed with the largest particles (S1) exhibits higher peaks and

requires a longer dimension in the horizontal (x, y) plane to be regarded as smooth. Upon decreasing particle size, r_{co} decreases.

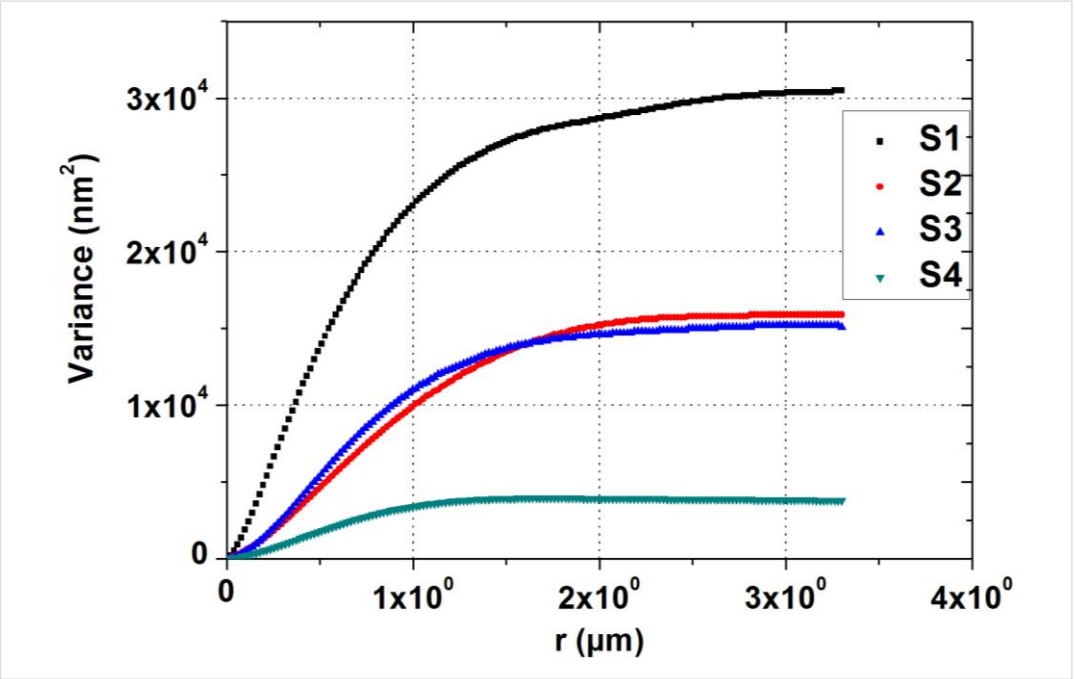

Figure 17: Variance of heights on films of nontronite exchanged with Na^+, Li^+, K^+ and Ca^{2+} with respect to the correlation lengths.

In terms of surface roughness, it is particularly interesting to note that in the presence of a given cation, the platelet size influences the wettability of the clay mineral. By using Na^+-exchanged montmorillonite clay, delaminated platelets have been deposited during the films preparation. Indeed, as seen in the last section, the nature of exchangeable cation indirectly influences the state of roughness of a clay mineral and hence it seemed important to us to eliminate any additional source of roughness apart from that induced by the platelet size. The results have clearly indicated that large platelet sizes result in higher surface roughness and hence higher contact angles while smaller platelets result in low surface roughness and correspondingly low contact angles.

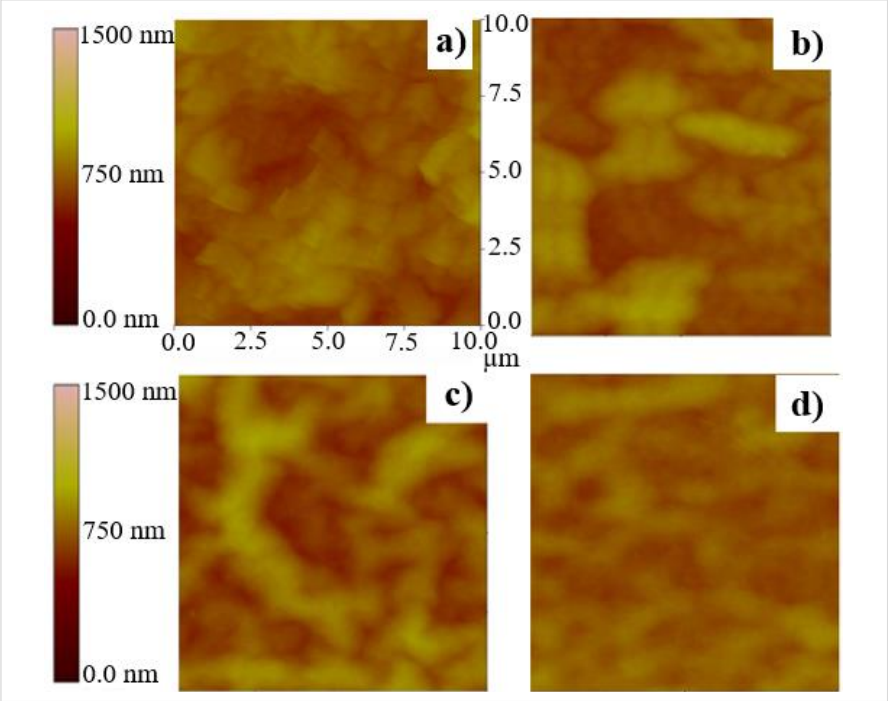

Figure 18: (10x10) µm AFM of SAz. a) S1 film; b) S2 film; c) S3 film and d) S4 film. Contrasts linked to the topography of the films appear as bright zones corresponding to higher altitudes while those situated in depth appear as dark zones.

5. Conclusion

In this chapter, solid-liquid interactions have been studied via the wettability of clay minerals in an extensive way. Contact angle measurements have been used to investigate the wettability of swelling (beidellite, nontronite and montmorillonite) as well as non-swelling (kaolinite and illite) clay minerals. For this purpose, both water and crude oils have been used as probed liquids. However, on one hand, due to the porosity of the non-swelling clay films, none of the probed liquids revealed any concluding results and on the other hand, the crude oils spread instantaneously on the swelling clays. These results could partly reveal the high affinity of crude oils for the clay minerals, at least under the measurement conditions which have been applied. Consequently, the water-wettability and the effect of various parameters influencing contact angles (nature of exchangeable cations, relative humidity, surface roughness and particle size) have been investigated on the swelling clay minerals.

Even if these parameters have been investigated individually, the nature of cations, surface roughness and particle size are closely linked. For instance, the nature of exchangeable cation indirectly drives the state of roughness of the clay films as shown by detailed analysis of AFM images (roughness of films decreasing in the order of Ca^{2+} >>> K^+ > (Li^+, Na^+). However, it's the hydration energy which ultimately takes over, as pretty well illustrated by the case of K^+ and Ca^{2+}. Indeed, the surface roughness of nontronite-K^+ is way less compared to that of nontronite-Ca^{2+} but the contact angles followed the reverse trend. On the other hand, for a given clay mineral, exchanged with a given cation, the wettability of the film is influenced by the size of the particles. For instance, the larger the size of the clay platelets, the rougher the film and the higher the contact angle.

As far as the influence of relative humidity on contact angles is concerned, only a marginal effect has been observed. However, working at high humidity suppresses (or at least diminishes) the phenomenon of evaporation and hence has revealed more stable contact angles with the evolution of time.

On the basis of the different results obtained, the nature of exchangeable cations have shown to be a key aspect of clays wettability.

6. Bibliography

[1] G. Binnig and H. Rohrer, “Scanning tunneling microscopy-from birth to adolescence,” *Phys. 1981-1990*, vol. 2, p. 389, 1993.

[2] A. Cadene, “Etude expérimentale multiéchelle du transport ionique et aqueux en milieu poreux chargé: argiles,” 2005.

[3] Benoit B Mandelbrot, “Self-Affine Fractals and Fractal Dimension,” *Phys. Scr.*, vol. 32, no. 4, p. 257, 1985.

[4] J. Schmittbuhl, S. Gentier, and S. Roux, “Field measurements of the roughness of fault surfaces,” *Geophys. Res. Lett.*, vol. 20, no. 8, pp. 639–641, Apr. 1993.

[5] M. F. Barnsley *et al.*, *The science of fractal images*. Springer Publishing Company, Incorporated, 2011.

[6] V. Soulie *et al.*, “The evaporation behavior of sessile droplets from aqueous saline solutions,” *Phys. Chem. Chem. Phys.*, vol. 17, no. 34, pp. 22296–22303, 2015.

[7] J. Bockris and A. Reddy, *’ Modern Electrochemistry, Vol. 1*, Plenum Press, New Yolk. 1970.

[8] R. Aveyard and S. M. Saleem, “Interfacial tensions at alkane-aqueous electrolyte interfaces,” *J. Chem. Soc. Faraday Trans. 1 Phys. Chem. Condens. Phases*, vol. 72, no. 0, pp. 1609–1617, 1976.

[9] I. Berend *et al.*, “Mechanism of adsorption and desorption of water vapor by homoionic montmorillonites: 2. The li § na § k § rb § and cs+-exchanged forms,” *Clays Clay Min.*, vol. 43, pp. 324–336, 1995.

[10] E. Ferrage, B. Lanson, B. A. Sakharov, and V. A. Drits, “Investigation of smectite hydration properties by modeling experimental X-ray diffraction patterns: Part I. Montmorillonite hydration properties,” *Am. Mineral.*, vol. 90, no. 8–9, pp. 1358–1374, 2005.

[11] T. Oncsik, G. Trefalt, M. Borkovec, and I. Szilagyi, “Specific Ion Effects on Particle Aggregation Induced by Monovalent Salts within the Hofmeister Series,” *Langmuir*, vol. 31, no. 13, pp. 3799–3807, Apr. 2015.

[12] M. Segad, S. Hanski, U. Olsson, J. Ruokolainen, T. Åkesson, and B. Jönsson, “Microstructural and Swelling Properties of Ca and Na Montmorillonite: (In Situ) Observations with Cryo-TEM and SAXS,” *J. Phys. Chem. C*, vol. 116, no. 13, pp. 7596–7601, Apr. 2012.

[13] L. L. Schramm and J. C. Kwak, “Influence of exchangeable cation composition on the size and shape of montmorillonite particles in dilute suspension,” *CLAYS CLAY Min. Clays Clay Min.*, vol. 30, no. 1, p. 40, 1982.

[14] N. Schwierz, D. Horinek, and R. R. Netz, “Reversed Anionic Hofmeister Series: The Interplay of Surface Charge and Surface Polarity,” *Langmuir*, vol. 26, no. 10, pp. 7370–7379, May 2010.

[15] M. Pavlovic, R. Huber, M. Adok-Sipiczki, C. Nardin, and I. Szilagyi, “Ion specific effects on the stability of layered double hydroxide colloids,” *Soft Matter*, vol. 12, no. 17, pp. 4024–4033, 2016.

[16] Y. Yoon, D. Kim, and J.-B. Lee, “Hierarchical micro/nano structures for super-hydrophobic surfaces and super-lyophobic surface against liquid metal,” *Micro Nano Syst. Lett.*, vol. 2, no. 1, p. 3, Sep. 2014.

[17] E. Paineau *et al.*, “Aqueous Suspensions of Natural Swelling Clay Minerals. 1. Structure and Electrostatic Interactions,” *Langmuir*, vol. 27, no. 9, pp. 5562–5573, May 2011.

IV: Liquid-liquid interactions

Table of contents

List of tables

List of Figures

Introduction

Low salinity waterflooding aims at recovering oils trapped into pores of reservoirs by both capillary and viscous forces [1], [2]. As such, the capillary forces are governed by both adhesive forces (between the oils and the surface of the rock) and interfacial/surface tensions (of oils against connate water/gases respectively). Having studied the wettability of clay minerals (balance of surface and interfacial forces), this chapter aims at investigating interfacial tension of crude oils against a wide span of brines (both in terms of composition and concentration). During LSW, injected water is brought into contact with in-place oils. Accordingly to the nature of ions in the aqueous phase, oil/brine interfacial tension is modified and likely to mobilise the trapped oils [3]–[6] through salting-in [7] of surface active molecules. If the conditions favour salting-out of the surfactants, the molecules either become more oil soluble or promote the adhesion of oils onto the rock surface (the system becoming more oil-wet) [8]. Consequently, to disturb in-place equilibrium in reservoir and tend the system towards more water-wetness, the ionic composition and concentration of injected brines during LSW need to be optimised.

As detailed in the state of the art section, crude oils are mixtures of hundreds of hydrocarbons, polar components, gases and components of heavy metals. The oils under investigation during this thesis (chapter II, section 2), are dead crude oils each containing polar acidic, basic molecules and components like resins and asphaltenes, all of them being interfacially active. In the aim of providing a better insight of crude oil/brine interactions, it appeared important to decompose the complex crude oil system into a simplified system made up of an organic phase and a unique surface active molecule. Consequently, a model system, MS, has been designed with an alkane (dodecane) and a carboxylic acid bearing linear hydrocarbon (oleic acid, HLB =1.0) and in terms of interfacial tension measurements, identical experiments have been performed on the **MS** and the **crude oils**.

In the last part of this chapter, we aimed at studying the stability of emulsions when the crude oils were mixed with brines at concentration leading to the lowest IFT. Different salts leading to different minimum IFTs [9], [10], we found it particularly interesting to compare the stability of the different emulsions.

1. Experiments and set-up for interfacial tension measurements

1.1 Model system, MS.

Dodecane a saturated linear alkane of anhydrous grade and purity of ≥ 99% was purchased from Sigma-Aldrich. Oleic acid of purity 99% was bought from Alfa-Aesar. The model system was prepared by adding 30mg of oleic acid per litre of dodecane (a concentration of $1x10^{-4}$ M).

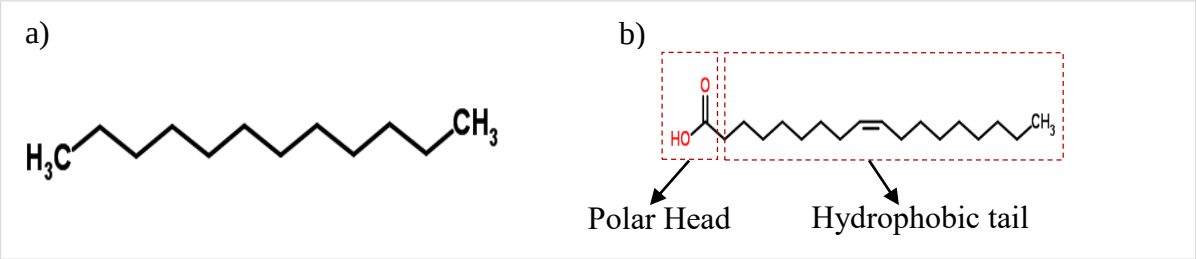

Figure 1: a) molecule of dodecane; b) molecule of oleic acid

1.2 Brines for interfacial tension measurements

1.2.1 Effect of salt species and concentration

The effect of salt concentration has first of all been investigated on the interfacial tension of pure dodecane by using a salt of monovalent cation (NaCl) and a salt of divalent cation ($MgCl_2$). Afterwards, the effect of the concentration of NaCl, $CaCl_2$ and $MgCl_2$ has been investigated on the interfacial tension of the model system, crude oils LVC(C) and MFC(B).

Salt	Purity (%)	Purchased from:
NaCl	99.9	Sigma-Aldrich
$CaCl_2$	99.9	Sigma-Aldrich
$MgCl_2$	99.9	Alfa-Aesar

Table 1: salts used to investigate the effect of salt species and concentration

As such, during LSW tests, some studies have pointed out the importance of the presence of divalent cations in order to increase oil recovery [11], [12]. Accordingly, low salinity effects have been tested by using brines of salt of divalent cations as well as brines composed of mixtures of monovalent/divalent salts [13]. It thus appeared important to compare the evolution of the interfacial tension of the crude oils as a function of brines composed of mixture of salts.

For instance, the effect of brines of NaCl/$CaCl_2$ and that of NaCl/$MgCl_2$ have been investigated. For this purpose, NaCl at a concentration of 1M and the salts of divalent cations at a concentration of 0.5M have been mixed into different proportions as shown in Table 2.

NaCl at 1M (%)	**Salt of divalent cation at 0.5M (%)**
100	0.00
97.5	2.50
95.0	5.00
92.5	7.50
90.0	10.0
85.0	15.0
75.0	25.0
50.0	50.0
25.0	75.0
0.00	100

Table 2: Proportion of NaCl and salt of divalent cation to prepare brines

1.2.2 Effect of the nature of ions

The effect of the nature of ions constituting the salts has been analysed by investigating the effect of their polarisability. As such, the polarisability of an ion is the ability of its electron cloud to be distorted by an external electric field. For instance, large and low valence ions are highly polarisable. On the contrary, small and high valence ions are highly polarising. For the purpose of this work, polarisability of ions has been defined as follows:

$$Polarisability \propto \frac{1}{\left({}^{|Z|}/_{r^2}\right)} \qquad \text{Equation 1}$$

With $|Z|$ being the absolute charge of the ion and r its crystallographic radius.

Table 3 shows the different salts which have been used to investigate the effect of cations and anions. As far as the cations are concerned, chloride salts of monovalent as well as that of the divalent cations have been tested. Regarding the effect of anions, sodium halides have been used.

Effect tested	Salt	Purchased from	Concentration (M)
Monovalent cations	LiCl, NaCl, KCl, RbCl, CsCl	Sigma-Aldrich	1
Divalent cations	$MgCl_2$	Alfa-Aesar	0.5
	$CaCl_2$, $SrCl_2$, $BaCl_2$	Sigma-Aldrich	0.5
Anions	NaF, NaBr, NaI	Alfa-Aesar	1
	NaCl	Sigma-Aldrich	1

Table 3: Different salts to test the effect cations and anions; all salts used were of purity of >99% or 99.9%.

1.3 Set-up for interfacial tension measurements

The densities of the organic phases under investigation being lower than that of water and brines, interfacial tension was measured by the rising drop method using a Drop Shape Analyser, DSA100, from Krüss, Hamburg, Germany. The lighter phase (oil) was placed in a glass syringe and the volume of drops were increased at a rate of 100µl/min via a hook-shape needle of 2.0mm in diameter into the heavier phase (water or brines). Analysis of the shape of the oil drops was made according to the Laplace equation:

$$\Delta p = \gamma \left[\frac{1}{R_1} + \frac{1}{R_2}\right] \qquad \text{Equation 2}$$

Where Δp is the difference in pressure between the inner and outer phase as the drop size is increased; γ is the interfacial tension between the oil and the aqueous phase; $R_1$and R_2 are the main radii of curvature as the pendant drop is deformed under the effect of gravity.

During our measurements, the deformation of the drop size (from spherical to a “pear shape”) was given by the *B* parameter, which characterises the deformation of the drop as the volume was gradually increased.

It is worth mentioning that each IFT measurement is a mean of at least three independent drops.

a)

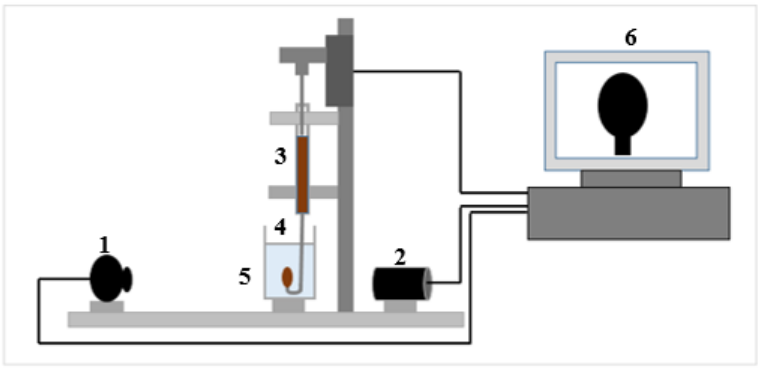

1: CCD Camera
2: Source of light
3: Glass syringe
4: Hook-shape needle
5: Cell for analysis
6: Computer with control and image analysis software

b)

Figure 2: a) Set-up of Drop shape Analysis experiment; b) an oil drop into water.

1.4 Oil / aqueous phase emulsion: bottle test

1.4.1. Proportion of crude oil/water to form stable emulsion

Crude oil/aqueous phase interactions have also been assessed via the stability of emulsions formed. However, to determine the respective volumes of each phase, primary tests have been performed to determine the stability of oil/water emulsion (Table 4). As such, during all the experiments the total volume of the liquids (oil + aqueous phase) was fixed to 5ml. For instance, different volumes of oil were added to water previously present into a container and the whole was mixed by using a vortex from VWR international during 30 seconds at 2500 rpm. The resulting emulsions were left to stand and analysed afterwards.

Crude oil (%)	Aqueous phase (%)
10	90
20	80
25	75
40	60
50	50

Table 4: Proportion of crude oil and water to test the stability of emulsions.

1.4.2. Proportions of crude oils/brines to form stable emulsion

The effect of salts commonly tested for LSW (Table 5) namely, NaCl, $CaCl_2$ and $MgCl_2$, has also been tested on the stability of emulsions. Similar experiments and proportion of the different phases (as reported in Table 4) have been carried out to determine the proportion of oils/brines leading to stable emulsions. Here, it is worth noting that the concentration of these salts corresponded to those leading to the crude oils/brine minimum interfacial tension measured in section 1.2.1).

Brines	Concentration of the brines (M) with oils	
	LVC(C)	MFC(B)
NaCl	0.50	0.25
$CaCl_2$	0.25	0.075
$MgCl_2$	0.20	0.25

Table 5: Brines composition and concentration used to determine oil/brine to form stable emulsions with the two crude oils.

1.5 Analysis of emulsions

The different crude oil/aqueous phase emulsions have been analysed under an optical microscope with a sufficient depth of field for observing the whole diameter of the drops. Size distribution of the drops have then been characterised by using image analysis software (ImageJ).

2. Interfacial tension (IFT) of the Model system

2.1 Interfacial tension (IFT) of pure dodecane/water

Prior to all experiments, dodecane/water interfacial tension was measured and resulted in 52.75±0.05 mN/m. This value corresponds closely to those reported in the literature [14]–[17]. The effect of salt concentration was then tested by using electrolytes of a monovalent salt (NaCl) and a divalent salt ($MgCl_2$) and shown in Figure 1a). Further analysis of the effect of anions on the IFT of dodecane is shown in Figure 1b).

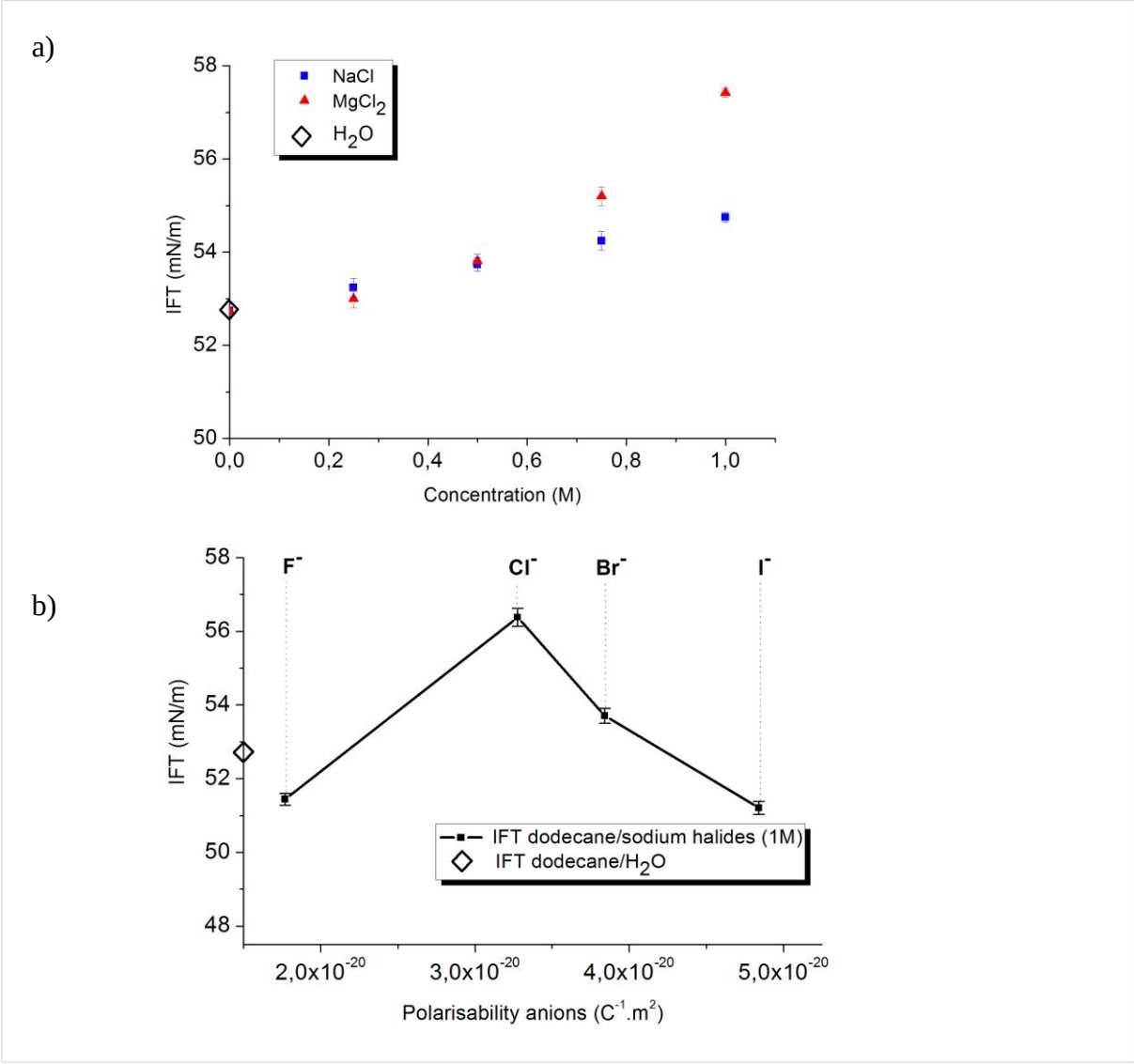

Figure 3: a) IFT of dodecane with respect to increasing concentration of salts; b) IFT dodecane as a function of salts of sodium halides at a concentration of 1M.

From Figure 3a), it can be observed that for dodecane/brine system, IFT increased with increasing concentration of the salts. These results indicate that at the pure alkane/aqueous phase interface, negative adsorption of ions took place ($\Gamma_i < 0$, Γ_i being the concentration of ions at the interface and corresponds to the number of moles of component "i" adsorbed per unit area). As the concentration of the salts increased, IFT increased accordingly to the equation described by Gibbs:

$$d\gamma = -RT \sum \Gamma_i \, dln \, a_i \qquad \text{Gibbs equation}$$

Where, $d\gamma$ is the increment in IFT; R is the universal gas constant; T is the absolute temperature; and a_i is the chemical activity of the ith component in the solution.

In addition to the general tendency of increasing IFT recorded with both NaCl and $MgCl_2$, it can be observed that in the presence of divalent Mg^{2+}, the increments in IFT at salinities ≥ 0.8M are more significant compared to Na^+. As far as the results with NaCl are concerned, they are in good agreement with those obtained by Aveyard et al. [18] . However, for $MgCl_2$, the results are slightly different from those observed by Cai et al. [14], where they observed negligible effect of salt species on octane/aqueous phase IFT. Nevertheless, our results do not seem to be surprising and can be attributed to a dual effect of the cations kosmotropic character and the concentration of the counterions. Let's consider a concentration of salt of 1M in water (NaCl $\rightarrow Na^+$, Cl^-; $MgCl_2 \rightarrow Mg^{2+}$, $2Cl^-$), the number of moles of dissociated components in the bulk is greater in the presence of $MgCl_2$ compared to NaCl. Regarding the polarising capacity of the cations, the small and highly charged Mg^{2+} is more polarising than larger and singly charged Na^+. In a pure organic/aqueous phase system, Mg^{2+} is able to disrupt the hydrogen bonding of the bulk phase and structure the water molecules to a greater extent. This latter phenomenon is linked to the kosmotropic character of the ions (the kosmotropic character of $Mg^{2+} > Na^+$) [19]**.** According to Gibbs equation, the concentration of ions in the bulk being greater in the case of $MgCl_2$, an increase of IFT was recorded.

It is now interesting to seek out the behaviour of anions at the oil/water interface. Figure 3b) shows the interfacial tension of dodecane against brines of sodium halides at a concentration of 1M. In the presence of Cl^- and Br^-, the IFT increased compared to that recorded against pure water. However, in the presence of F^- and I^-, the IFT decreased. Accordingly to Gibbs equation, F^- and I^- were thus positively adsorbed ($\Gamma_i > 0$) and hence located in the interfacial layer. This behaviour is typical of surfactants as already observed for I^- by Aveyard et al. [18] and Lima et al. [20]. On their side, Santos and Levine [12] postulated that large anions such as I^- accumulate

at the oil/water interface due to their chaotropic nature, (large polarisability, low hydration and cavitational hydrophobic energy). In opposition to kosmotropes, the chaotropic ions move towards the interface and decrease IFT. However, as far as F^- is concerned, it is the smallest of all the investigated anions and was expected to induce the largest increase of IFT compared to Cl^-, Br^- and I^-. Though a slight decrease (51.44±0.16 mN/m for dodecane/NaF compared to 52.75±0.05 for dodecane/water) has been recorded, it is nevertheless clear that F^- exhibits a specific behaviour.

2.2 Interfacial tension of Model system: dodecane + oleic acid

Due to its long hydrocarbon chain and the presence of a polar carboxylic group at one end, oleic acid acts as a surface active molecule. According to the pH of the surrounding medium, it is either able to act as a non-ionic or an anionic surfactant as shown in Figure 4 below. For instance, at a pH equivalent to its pKa, 50% of the carboxylic acid is under the anionic form. At pH= pKa+3, 99.9% of the carboxylic acid is ionized. Table 6 shows the pH of the different brines with respect to the pKa of carboxylic acid.

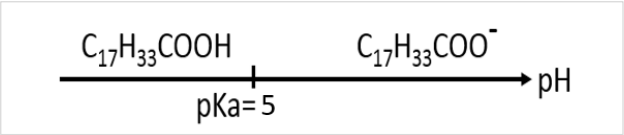

Figure 4: Ionization of oleic acid according to the pH of the surrounding medium.

pH = pKa	**pH = pKa+1**	**pH ≈ pKa+2**	**pH ≥ pKa+3**
	H_2O		LiCl
RbCl	NaCl		
	KCl	$SrCl_2$	$MgCl_2$
$BaCl_2$	CsCl		$CaCl_2$
	NaBr	NaI	NaF

Table 6: pH of the different brines with respect to the pKa of carboxylic group of oleic acid.

The addition of 30mg/L of oleic acid into dodecane reduced its interfacial tension against water from 52.75±0.05 mN/m to 44.06±0.07 mN/M. This is primarily due to the partitioning of surface active molecules at the oil/water interface where their free energy is minimum. This first effect here is being referred as the ***surfactant effect***. It is then interesting to investigate the effect of ionic species and concentration on the IFT of the MS. Indeed, the presence of salts is likely to modify the solubility of the surfactants and hence the IFT.

2.2.1. Effect of concentration of NaCl, $CaCl_2$ and $MgCl_2$ on IFT of MS

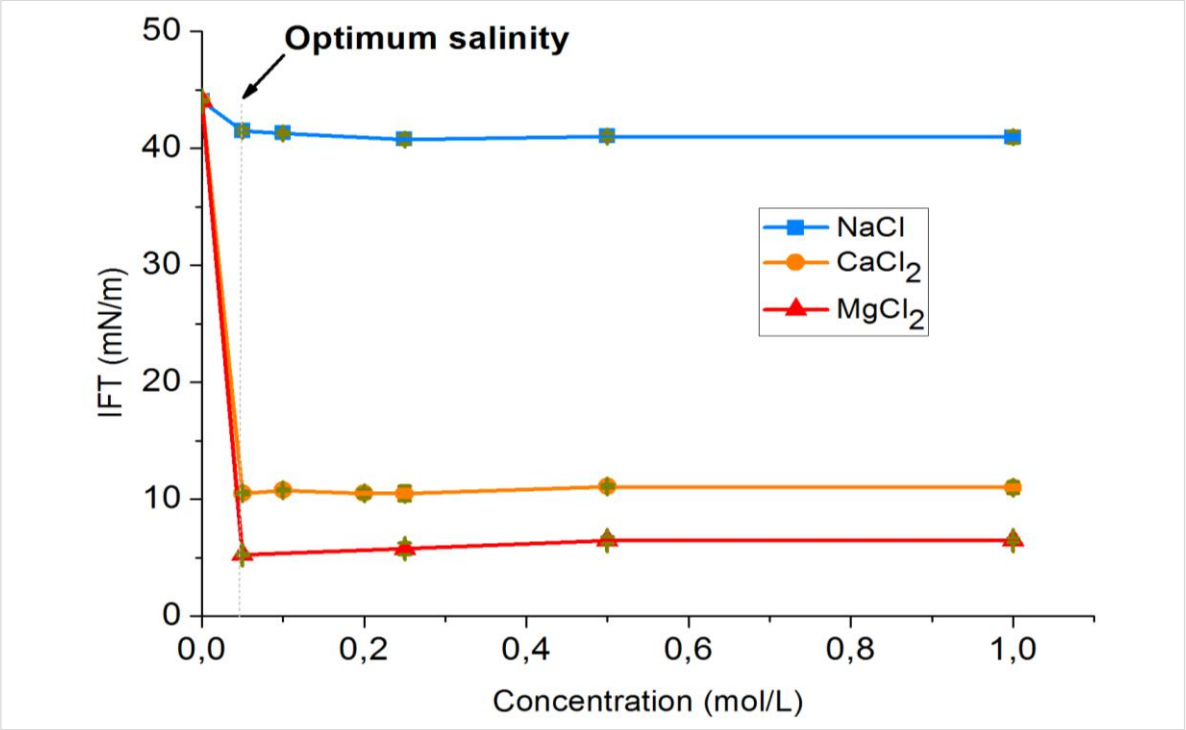

Figure 5: Effect of salt species and concentration on the IFT of the model system.

From Figure 5 it is primarily interesting to note that the trend of IFT compared to pure dodecane/brines is reversed, i.e. in the presence of oleic acid, the three salts lead to a decrease in IFT (certainly to different extents with the different salts) while for pure dodecane/brines, an increase of IFT was observed.

Moreover, for the model system, the following observations can be made from Figure 5:

i. Increasing salt concentration is firstly accompanied by either a slight drop (NaCl) or marked drops ($CaCl_2$ and $MgCl_2$) of IFT to reach a minimum;
ii. Different minimum IFTs observed with the three brines;
iii. In the range of studied salt concentrations, an "optimum salinity" has been recorded with the three salts. The optimum salinity here, is being used to identify the salt concentration where the IFT is first minimum;
iv. IFTs against the three salts stayed constant beyond the "optimum salinity".

The difference concerning the trend of IFT against the different brines observed with the model system compared to pure dodecane can be attributed to electrostatic attraction between cations

from the bulk towards the negatively charged oil interface in the presence of surfactants ($\Gamma_i > 0$ and $d\gamma < 0$) . It is now appropriate to seek out for the differences of the minimum IFTs and similarity of the optimum salinity with respect to the different brines.

- **Concerning the different minimum IFTs:**

As revealed by Table 6, in the presence of NaCl identical ionisation of surfactant as in the presence of water can be considered (~ 50% -COOH and ~50% COO^-). According to Gibbs equation, electrostatic attraction of Na^+ ions towards the interface leads to decrease in IFT compared to water. In the presence of $MgCl_2$ and $CaCl_2$ (pH of the brines ≥ pKa+3), 100% of the polar headgroup of the surfactants present at the interface, are under the carboxylate form. Like with Na^+, as a result of electrostatic attraction, a decrease of IFT is recorded. In addition, the drastic IFT reduction with the divalent ions compared to Na^+ can primarily be attributed to specific ion effects. In the order of increasing hardness are $Na^+ <<< Ca^{2+} < Mg^{2+}$ and accordingly, these ions are attracted towards to the hard carboxylate headgroup and lead to IFT in the order of $Mg^{2+} < Ca^{2+} <<< Na^+$. Taking into consideration these interactions, it follows that in the presence of the divalent cations salting-in of the surfactants is favoured, the phenomenon of salting-in being more marked in the presence of Mg^{2+}.

- **Concerning the optimum salinity:**

From the above results, the concentration of salt leading to the minimum IFTs recorded with the three salts "seems" to be identical. It is however most probable that in the presence of such a low concentration of surface active molecule ($1x10^{-4}$M), the subtle difference of minimum salinity is most probably lying below the investigated salinity range (< 0.05M).

All the above results show that IFT of the system is indeed a function of salt concentration and species. However, for this particular system, once the salinity leading to the minimum IFT has been achieved, salt concentration has no further impact on the IFT. Tentative explanations to this phenomenon could either be that all of the surfactants are already present at the interface or that a maximum of them have already occupied the interface (taking into consideration electrostatic repulsion between the heads). Further analysis of the effect of salt species was thus carried out at identical ionic strength of brines but after the optimum salinity had been reached, for instance 1M for salts of monovalent cations and 0.5M for salts of divalent cations.

2.2.2. Effect of the polarisability of cations on the IFT of the MS

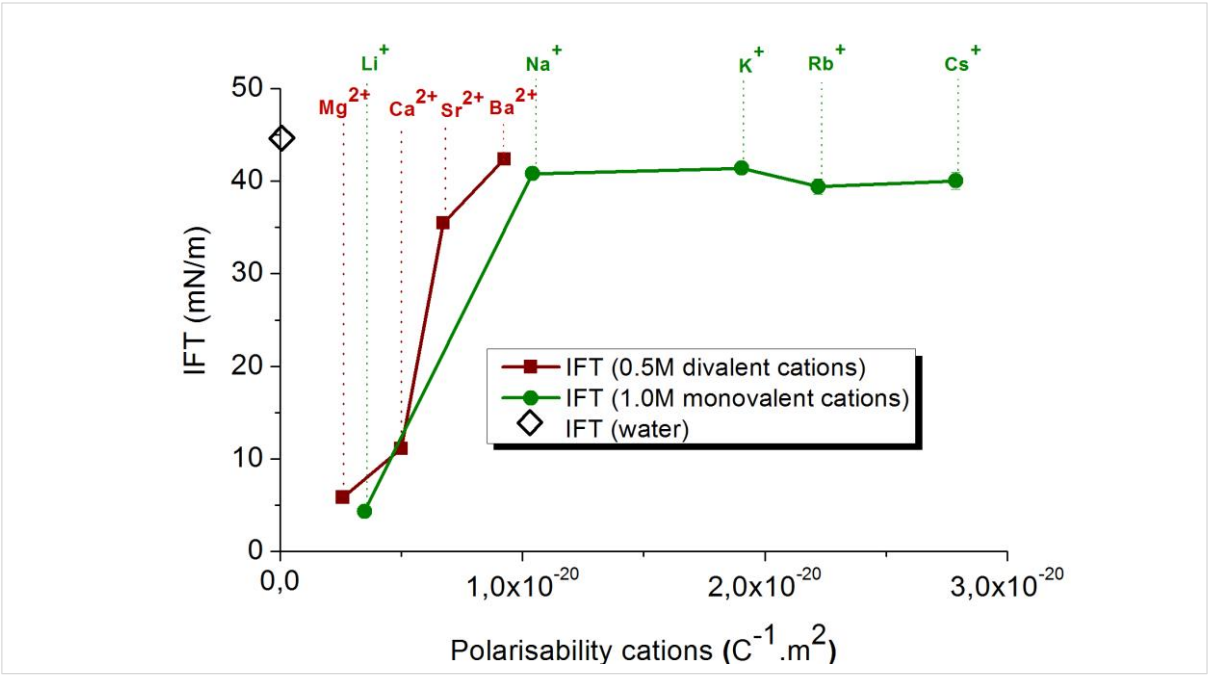

Figure 6: Effect of cation polarisability on the interfacial tension of the model system.

Figure 6 shows the interfacial tension of the model system as a function of the polarisability of cations present. In the presence of brines of LiCl, $MgCl_2$ and $CaCl_2$, the surfactants at the interface are under similar state of ionisation (totally anionic, pH of solution ≥ pKa+3 of carboxylic group) and hence, can be used to analyse the effect of cations. As observed previously, electrostatic attraction caused the cations to move towards the oil/water interface and decreased IFT ($\Gamma_i > 0$ and $d\gamma < 0$). These three cations as well as the carboxylic group are kosmotropes [21], [22]. Firstly, According to the "law of matching water affinities" [23], [24], ion-paring occurs between these cations and the carboxylic headgroup. Indeed, in aqueous salt solutions, this law characterises the strength of interactions in decreasing order as: kosmotrope-kosmotrope > kosmotrope-H_2O > H_2O-H_2O > chaotrope-H_2O > chaotrope-chaotrope. The subtle differences of IFT between these cations can then be attributed in terms of their respective hardness. For instance, in decreasing order of hardness are $Li^+ > Mg^{2+} > Ca^{2+}$; the interfacial tensions revealed the favoured hard cation-hard carboxylate headgroup interaction in the order of $Li^+ < Mg^{2+} < Ca^{2+}$. This effect being directly linked to their respective sizes (Table 7, ionic radius from [25]) , the smallest cation, Li^+, promote salting-in of the

surfactants at the oil/water interface to the greatest extent (by reducing electrostatic repulsion between the carboxylate headgroups surface coverage by surfactants is increased).

Cation	Ionic radius (nm)	IFT (mN/m)
Li^+	0.059	4.33 ± 0.19
Mg^{2+}	0.072	5.83 ± 0.19
Ca^{2+}	0.100	11.1 ± 0.12
Sr^{2+}	0.116	35.45 ± 0.41
Ba^{2+}	0.136	42.39 ± 0.23

Table 7: IFT of MS against brines composed of different cations.

Increasing polarisability compared to the latter cations, Sr^{2+} resulted in higher IFT. Its larger crystallographic size ($r_{Sr^{2+}} > r_{Ca^{2+}} > r_{Mg^{2+}} > r_{Li^+}$), hence less hardness and lower pH of its solution compared to the previous cations could altogether account for the decrease in electrostatic attraction and increase in interfacial tension recorded.

As far as Ba^{2+} is concerned, its size ($r_{Ba^{2+}} > r_{Sr^{2+}} > r_{Ca^{2+}} > r_{Mg^{2+}} > r_{Li^+}$), softness tendency and low pH were all subject to less favourable interaction with the carboxylate head. Moreover, from Ba^{2+} to Cs^+, the pH of the solutions oscillated around the pKa of the surfactant which in turn governed the state of ionisation of the carboxylate headgroup (only 50% ionised). In addition, the size of the cations getting larger ($r_{Na^+} < r_{Ba^{2+}} < r_{K^+} < r_{Rb^+} < r_{Cs^+}$,Table 8, ionic radius [25]) compared to the high charge densities (inverse of the polarisability) of Li^+, Mg^{2+} and Ca^{2+}, electrostatic attraction was hampered.

Cation	Ionic radius (nm)	IFT (mN/m)
Na^+	0.102	40.81 ± 0.18
K^+	0.138	41.42 ± 0.20
Rb^+	0.149	39.91 ± 0.85
Cs^+	0.167	40.33 ± 0.91

Table 8: IFT of MS against brines of monovalent cations.

2.2.3. Effect of the polarisability of anions on the interfacial tension of the MS

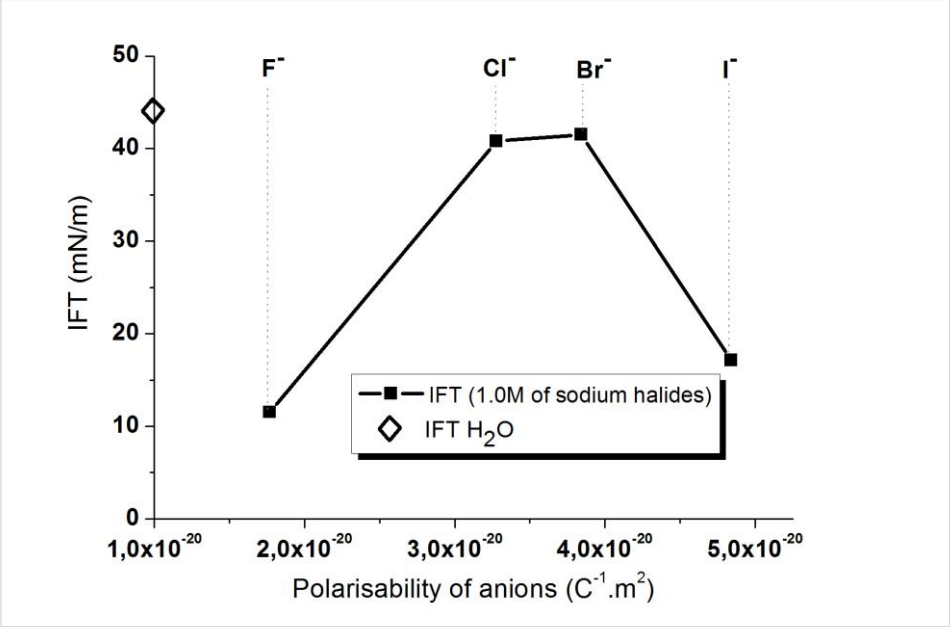

Figure 7: Effect of anion polarisability on the interfacial tension of the model system.

For ions of same charge densities, the anions are far more polarisable than the cations [26]. It has been pointed out that ions of higher polarisability move towards macromolecule/water interface and destabilise them. Figure 7 shows the variation of the interfacial tension as a function of the polarisability of the anions composing the salts of sodium halides. In the presence of brines of NaCl and NaBr, very slight decreases of IFT have been recorded. Cl^- and Br^- act as "spectator ions" and do not specifically alter IFT. As far as the I^- is concerned, it moved to the interface due to its chaotropic character, high polarisability, low hydration and cavitational energy. As such, we already observed this behaviour of I^- at the pure dodecane/water interface (Figure 3b) and has been reported in the literature [18], [27]. Moreover, it is to be noted that in the presence of surfactants, the effect is more pronounced. Regarding F^-, the only data found in the literature are the simulation results of Levin et al. [27], where they compared IFT as a function of increasing concentration of potassium halide salts. They found that I^- increased IFT the most when comparing all the anions going down the halogen column. Our results are in agreement with their simulations except for F^-. At first, we recorded a tendency to lowering IFT at pure organic/aqueous phases and an even more drastic reduction in the presence of surfactants. A specific behaviour other than high polarisability, low hydration is likely to cause F^- ions to move towards the interface ($\Gamma_i > 0$ and $d\gamma < 0$). Going back to the previously cited "law of matching water affinities" of Collins [23], [24], the relative affinity of ions in solution depends on the matching of cation and anion sizes. As such small-

small and large-large ionic species tend to associate in water, while small-large ions dissociate. These tendency have also been shown in the simulation studies of Fennell [28], where they observed the small-small ions associate as a result of strong electrostatic attractions between them. Consequently, NaF is thought to act as an entity as a whole and it's this particular ion pair which moved to the interface and lowered IFT. Table 9 recapitulates the sizes [25] and IFT in the presence of the anions.

In addition it is worth noting that in the presence of anionic surfactant in our system, IFT reduction has been more pronounced with the highly polarising cations.

Anion	**Ionic radius (nm)**	**IFT (mN/m)**
F^-	0.133	11.51 ± 0.36
Cl^-	0.181	40.81 ± 0.18
Br^-	0.196	41.53 ± 0.05
I^-	0.220	17.14 ± 0.39

Table 9: IFT of MS against brines of sodium halides.

As a conclusion to IFT of the model system against the different brines, the following observations and conclusions can be made:

i. Salt species and concentration contribute to IFT reduction of the model system (minimum IFT at an optimum salinity);
ii. Small and highly polarising cations (Li^+, Mg^{2+} and Ca^{2+}) reduced IFT the most;
iii. In the series of anions, F^- reduced IFT, while an increase was expected;
iv. Large, highly polarisable and weakly hydrated I^- reduced IFT.

As a global conclusion in the presence of salts made up of highly polarising ions (both cations and anions) and highly polarising anions, IFT of the our MS against brines was the lowest.

3. Interfacial tension of crude oils LVC(C) and MFC(B)

IFTs of the crude oils (LVC(C) and MFC(B)) have been measured in a similar to those with the model system. The crude oils under investigation possess respectively 8.2% and 15.7% by mass of a mixture of polar molecules compared to the MS (which possessed 0.004% by mass of one surface active molecule). As a matter of comparison Table 10 reports the IFT of the three organic phases against water.

Organic phase	Total mass of polar components (%)	IFT (mN/m)
MS	0.004	44.06 ± 0.07
Crude oil LVC(C)	8.2	25.58 ± 0.05
Crude oil MFC(B)	15.7	20.23 ± 0.40

Table 10: IFT of the three investigated organic phases against water

It is clear that the presence of surface active molecules alter IFT of the systems, for instance, the higher the content of the polar components the lower the IFT. Here, it is worth noting that IFT of pure alkane phases against water are much higher (>50 mN/m) [14]–[18], [20].

3.1 Effect of concentration of brines on the IFT of oils LVC(C) and MFC(B)

Figure 8 shows the IFT of oil LVC(C) as a function of the concentration of three different brines, where the same trend of: decrease to a minimum value, followed by slight increases to reach constant IFTs were recorded. Like with the MS, IFT NaCl > $CaCl_2$ > $MgCl_2$.

As far as oil MFC(B) is concerned (Figure 9), despite that a similar trend of IFT NaCl > $CaCl_2$ > $MgCl_2$ has been recorded, as the concentration of the salts is increased, the IFTs dropped to minimum values at optimum salinities, after which, a global increasing tendency of the IFTs has been recorded. In this particular case of oil MFC(B), after the salting-in of surfactants (up to optimum salinities), the surfactants salted-out at high salt concentrations causing the IFTs to increase.

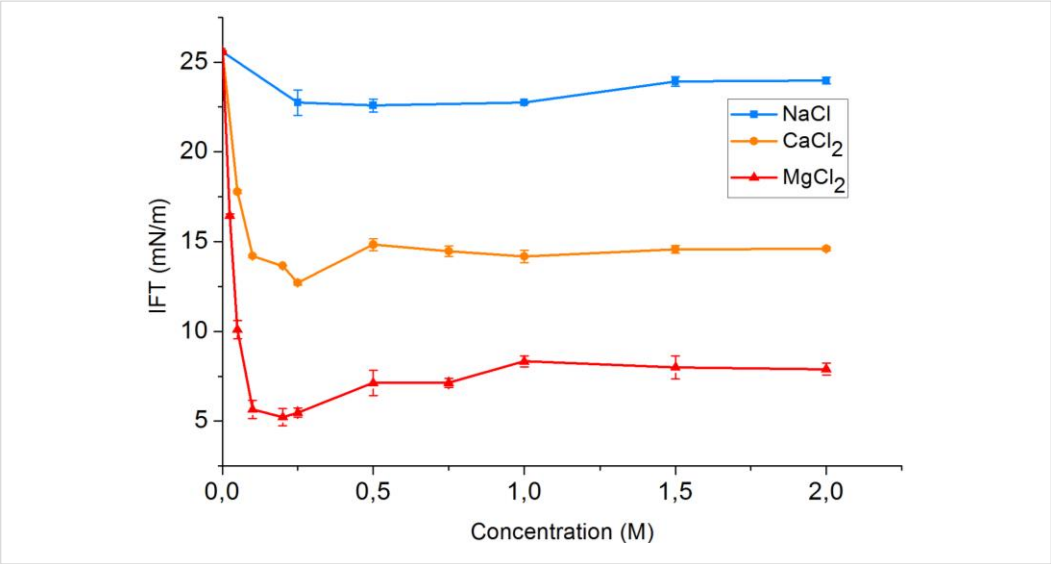

Figure 8: Interfacial tension of oil LVC(C) as a function of concentration of NaCl, $CaCl_2$ and $MgCl_2$.

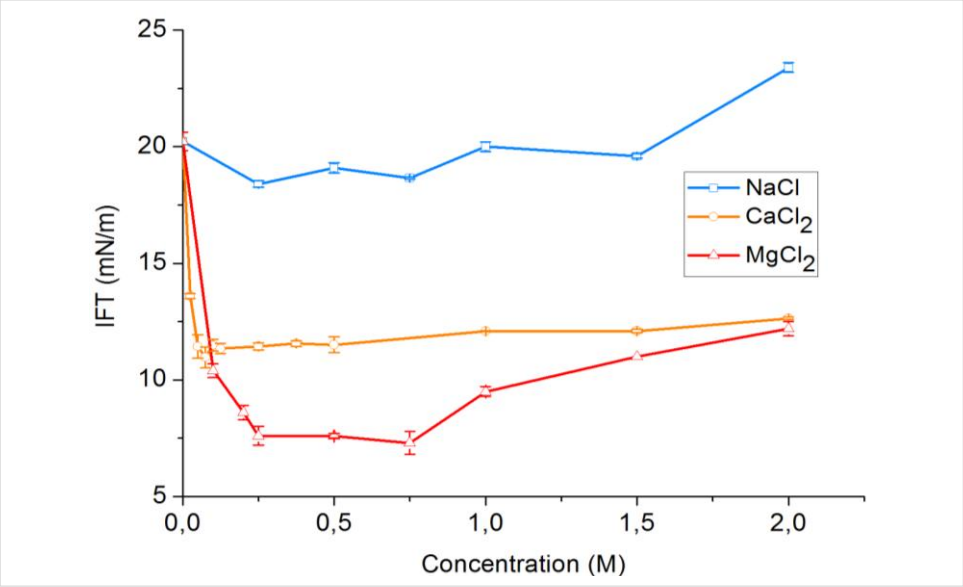

Figure 9: Interfacial tension of oil MFC(B) as a function of concentration of NaCl, $CaCl_2$ and $MgCl_2$.

The difference in behaviour between the two oils surely lies in the respective contribution of the polar components (LVC(C): 2.9% asphaltenes and 5.3% resins; MFC(B): 5.3% asphaltenes and 10.4% resins). In a recent study, Lashkarbolooki et al. [9] extracted asphaltenes and resins from an Iranian oil field and studied the influence of NaCl, $CaCl_2$ and $MgCl_2$ concentration on

the IFT the respective components (Figure 10 [9]). The asphaltenes and resins each represented 8% by weight in toluene.

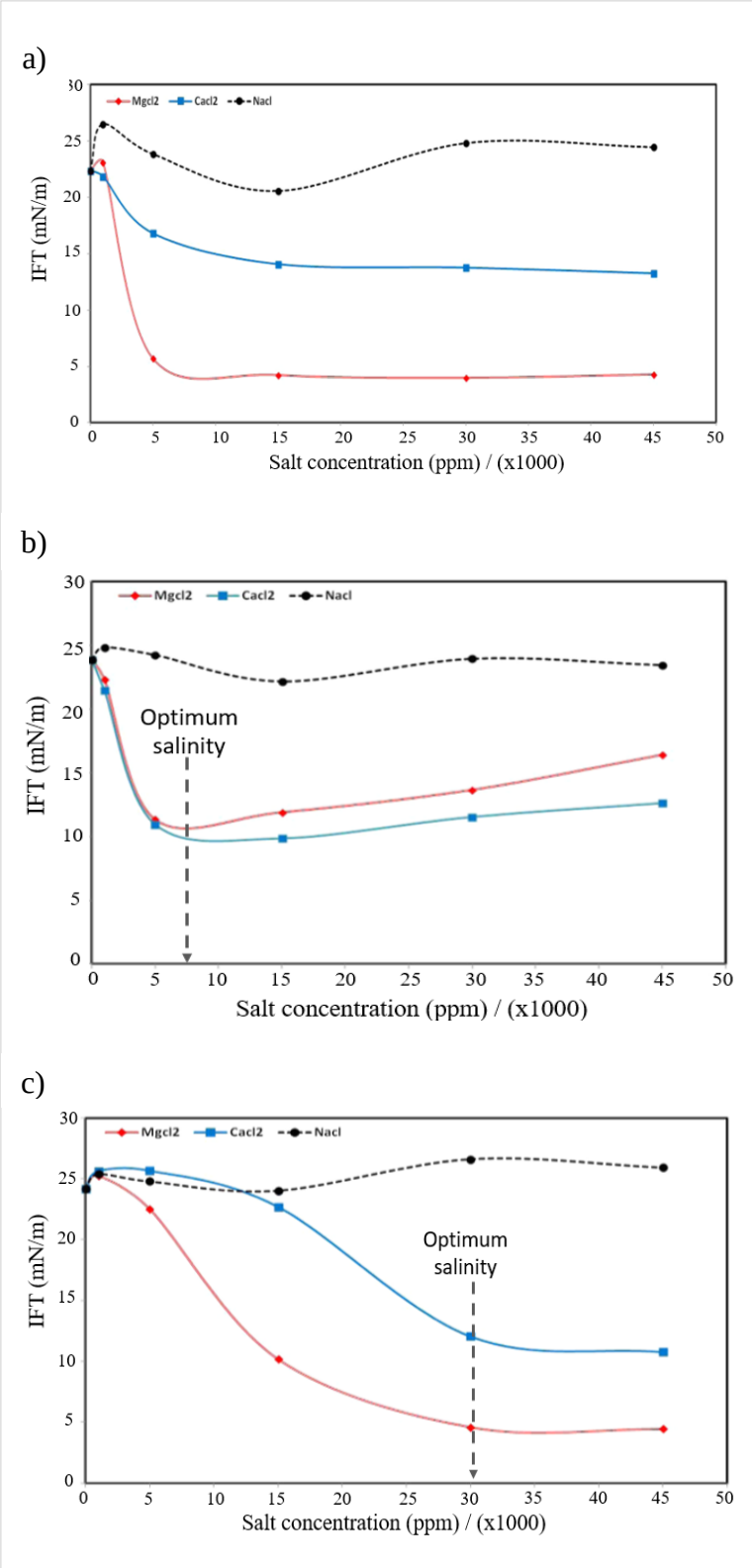

They observed that NaCl had low effect on the IFT of both asphaltenes and resins, consequently on their crude oil in general. However, $CaCl_2$ and $MgCl_2$ showed specificities towards asphaltenes and resins respectively, thus lowered IFT. They put forward the bigger size of Ca^{2+} for the complexation of the large asphaltenes and the affinity of Mg^{2+} ions for the oxygen in the resins. As such, the optimum salinity for asphaltenes occurred at lower divalent salt concentration compared to that of resin. However, beyond the optimum salinity, the IFT of asphaltenes increased while that of resin stayed constant (Figures 10: b) and c)). Moreover, they reported that when both of these polar components act together they show a synergistic effect and IFT reduction is even more pronounced.

Figure 10: a): IFT of crude oil against salinity of different brines; b) IFT of extracted asphaltene against salinity of different brines; c) IFT of extracted resin against salinity of different brines.

With both oils under investigation in our study, IFT NaCl > $CaCl_2$ > $MgCl_2$. As far as the effect of NaCl is concerned, it showed a very low effect on the IFT of oil LVC(C) in the whole range of concentration and on the IFT of oil MFC(B) up to a concentration of 1.5M. These results confirm the low synergism observed between Na^+ ions with the surfactants (in our MS with oleate and in the crude oils with the natural surfactants).

In both oils, the amount of asphaltenes is much lower than that of resins. Consequently, taking into consideration the specificity of Ca^{2+} towards asphaltenes [9], the higher IFT we recorded in the presence of Ca^{2+} compared to Mg^{2+} is most probably linked to interfacial asphaltenes. Moreover, due to their large sizes, only a limited amount is likely to be present at the interface.

Let's consider the individual effect of the divalent cations on the IFT of the oils. For instance, with both oils, in the presence of $CaCl_2$ a marked IFT reduction occurred until an optimum salinity was reached. This effect can particularly be attributed to the salting-in of asphaltenes. Beyond this salinity, salting-out of the asphaltenes increased the IFTs. It was only then that resins came into play. Indeed, they interact with the divalent salts at higher salt concentrations and resulted in more or less stabilised IFTs.

As far as the effect of $MgCl_2$ is concerned, the striking IFT reduction can essentially be attributed to the resins. With both oils, increasing concentration of $MgCl_2$ caused the IFT to decrease to a minimum value and then increased due to salting-out effects.

With the aid of the studies of Lashkarbolooki [9] we know that asphaltenes lower IFT at low salt concentration and resins at higher salt concentrations but, crude oils constitute of a mixture of surface active molecules and the variation of the IFT against the different salts is the result of the surfactants acting together.

3.2 Effect of divalent cation content on the IFT of LVC(C) and MFC(B)

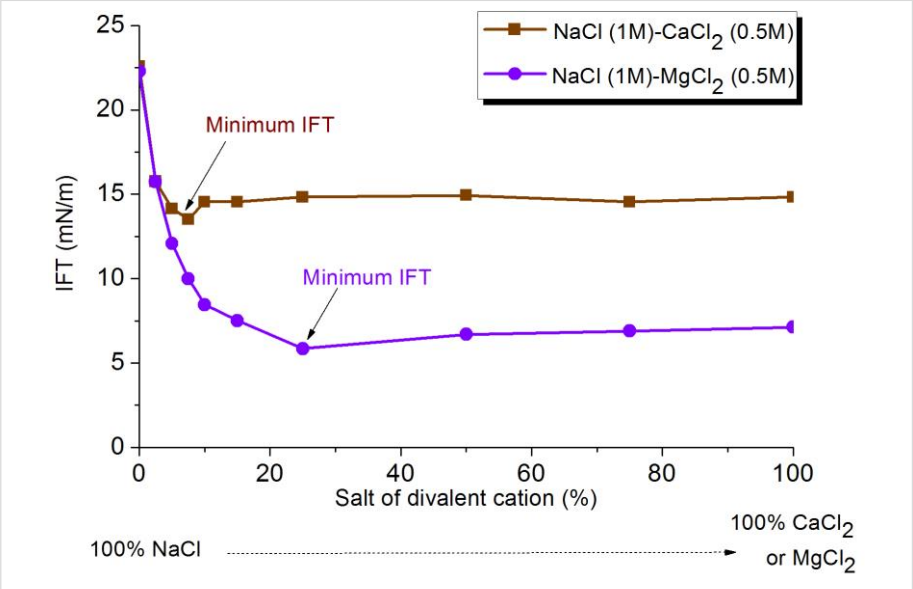

Figure 11: Interfacial tension of oil LVC(C) as a function brines of increasing concentration of divalent salts.

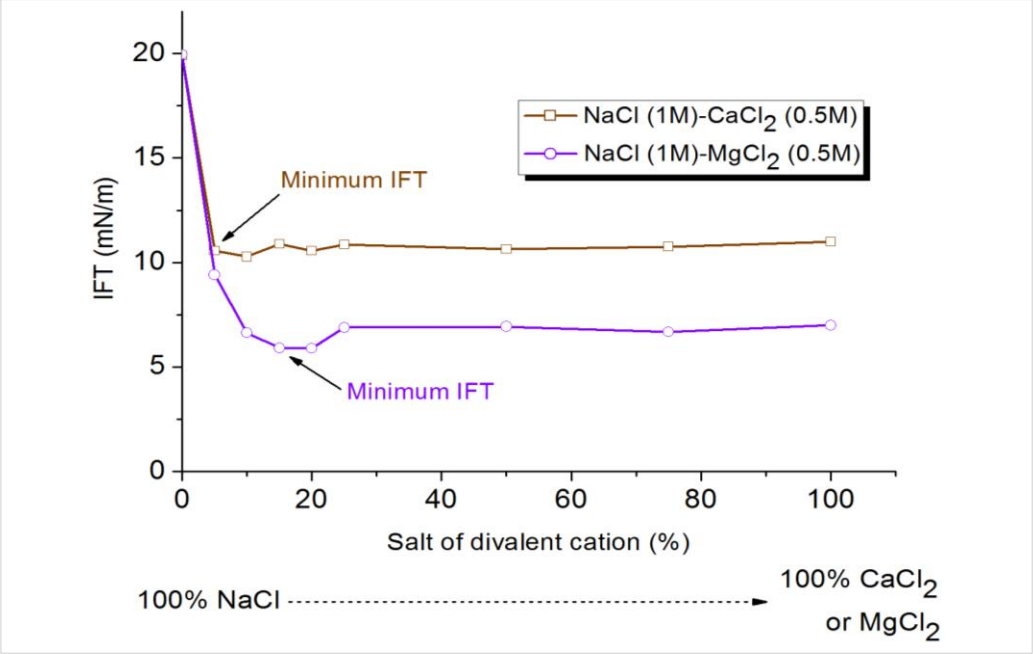

Figure 12: Interfacial tension of oil MFC(B) as a function of brines of increasing concentration of divalent salts.

Figures 11 and 12 respectively show the variation of IFT of oils LVC(C) and MFC(B) as a function of brines made up of increasing concentration of salts of divalent cations. Again with both oils, the IFT decreased to a minimum value with increasing concentration of divalent salts in the brines; the IFTs in the presence of Mg^{2+} ions being lower than Ca^{2+}. As a matter of

comparison, Figure 13 and 14 respectively show the variation of the IFT of the oil LVC(C) and MFC(B) with brines composed of divalent salts only and brines composed of the mixture of salts.

- **Oil LVC(C)**

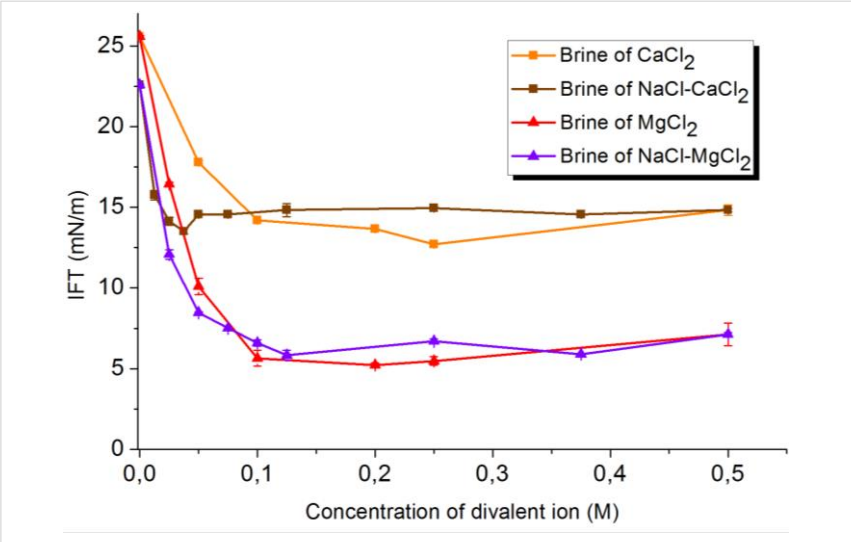

Figure 13: Comparison of the interfacial tension of oil LVC(C) with brines of single salts and brines composed of mixture of salts.

- **Oil MFC(B)**

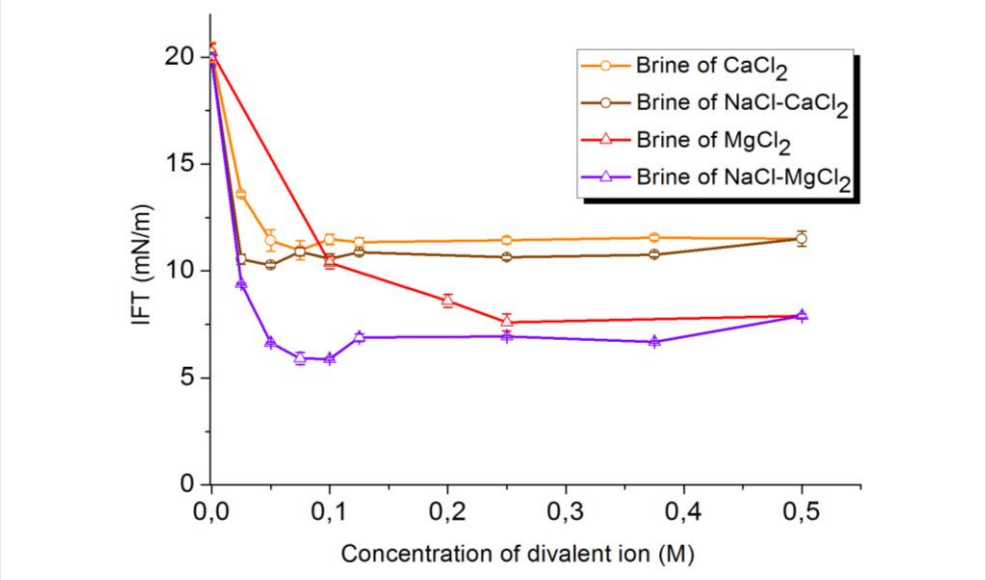

Figure 14: Comparison of the interfacial tension of oil MFC(B) with brines of single salts and brines composed of mixture of salts.

From the superposed graphs in Figures 13 and 14 (and Table 11), in a general way, it appears that the minimum IFT occurs at lower divalent salt concentrations when used in combination with NaCl. However, as far as the value of the minimum IFT is concerned not much difference is observed between these two brines. As such, when comparing the ionic strength of these solutions, we observe that in fact the minimum of interfacial tension in the presence of brines composed of mixture of salts are much higher compared to the brines of divalent salts only.

Oil	**Brine**	**Concentration of divalent salt (M)**	**Ionic strength (M)**	**Minimum IFT (mN/m)**
LVC(C)	$CaCl_2$	0.25	0.750	12.75 ± 0.14
	$NaCl+CaCl_2$	0.0375	1.038	13.51 ± 0.15
	$MgCl_2$	0.20	0.600	5.23 ± 0.12
	$NaCl+MgCl_2$	0.125	1.125	5.85 ± 0.13
MFC(B)	$CaCl_2$	0.075	0.225	10.97 ± 0.40
	$NaCl+CaCl_2$	0.025	1.025	10.56 ± 0.23
	$MgCl_2$	0.25	0.750	7.60 ± 0.40
	$NaCl+MgCl_2$	0.075	1.075	5.91 ± 0.28

Table 11: Comparison of divalent salts concentration in pure brines and in brines composed to mixture of salts leading to minimum IFT.

3.3 Effect of cation polarisability on the IFT of oil LVC(C) and MFC(B)

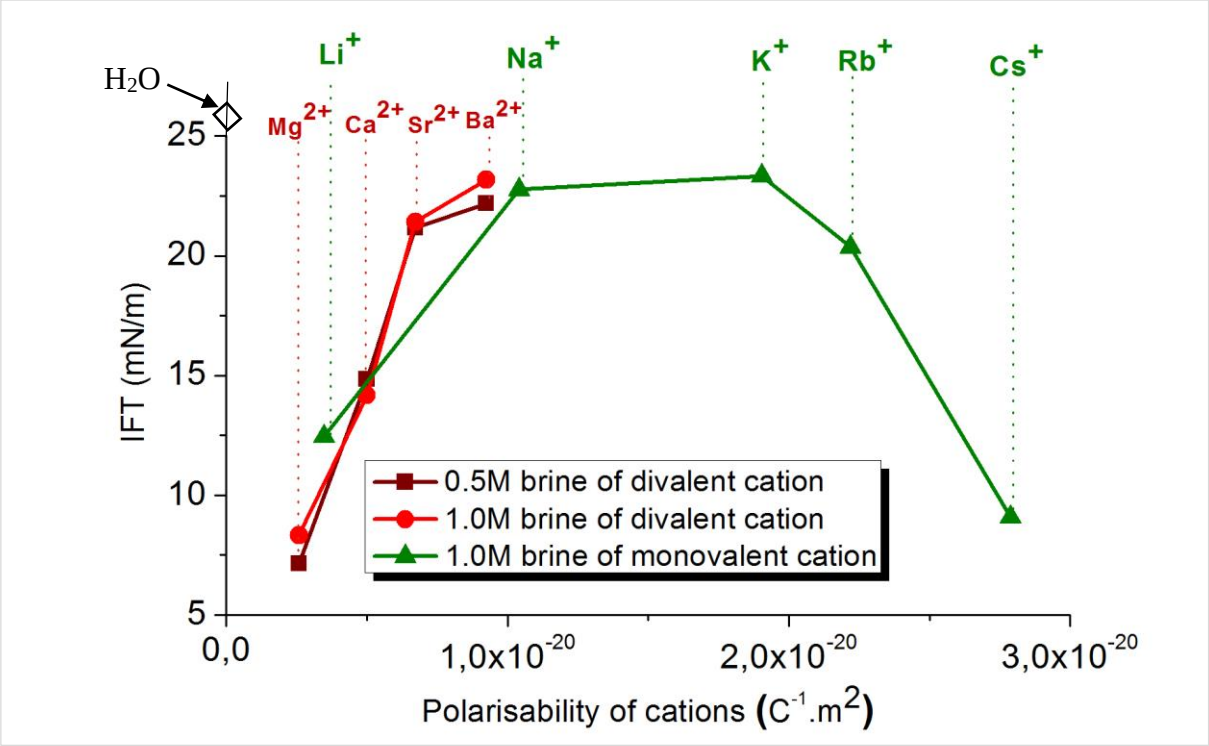

Figure 15: Interfacial tension of oil LVC(C) as a function of the polarisability of cations.

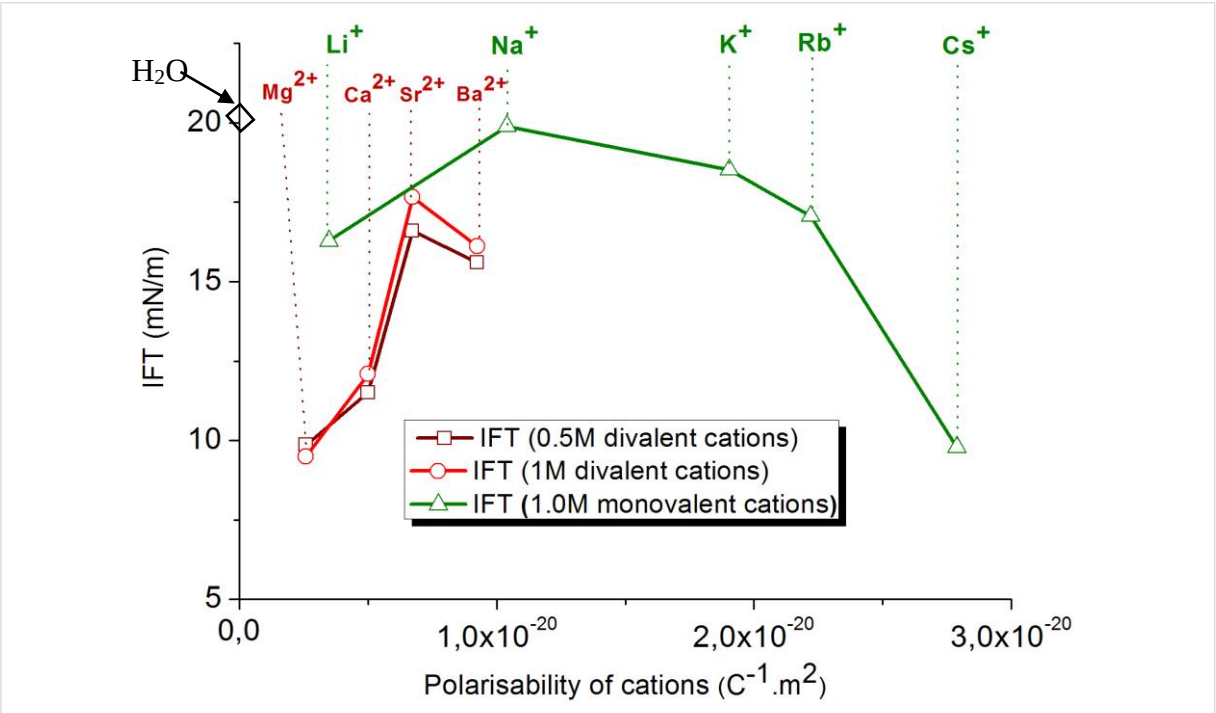

Figure 16: Interfacial tension of oil MFC(B) as a function of the polarisability of cations.

As for the model system, the effect of polarisability of cations on the IFT of the crude oils has been investigated by using brines of $MgCl_2$, $CaCl_2$, $SrCl_2$, $BaCl_2$, LiCl, NaCl, KCl, RbCl and CsCl (Figures 15 and 16). As far as the divalent salts are concerned, IFTs with salts of both 0.5M and 1M have been measured. In general, it can be observed that the IFTs at a concentration of 1.0M are slightly higher compared to those measured at 0.5M (with the MS, the IFTs at 0.5M and 1M were identical). However, for both oils and salt concentrations, the tendency observed with the divalent salts is an increase in IFT with increasing polarisability of the cations (or rather decreasing polarising capacity). For identical valencies, the cations getting larger, in addition to decreased electrostatic attraction only a limited amount are being to position at the interface.

As far as the effect of the monovalent cations on oil LVC(C) is concerned, up to K^+ very similar results as the MS has been observed i.e increasing polarisability is followed by increase in interfacial tension. The smallest and most polarising cations were most attracted to the oil interface. However, compared to the MS, a drastic reduction of the IFT of oil LVC(C) has been recorded in the presence of chaotropes Rb^+ and Cs^+. Their large size, high polarisability, low hydration cause them to move towards the interface and interact with surfactants other than carboxylic groups. Indeed in our MS interaction between these chaotropic ions and the kosmotropic COO^- group was favoured to a lesser extent (Figure 6 v/s Figures 15 and 16).

Concerning the effect of cations on oil MFC(B), the overall "bell-shape" of IFT as a function of cation polarisability observed with oil LVC(C) is conserved. Moreover, apart from $Mg^{2+}$and Li^+, the IFT recorded with the other cations are lower for MFC(B) compared to LVC(C). Globally, these results are in agreement with the higher amount of surface active molecules present in MFC(B). Regarding Mg^{2+} and Li^+, due their specificity towards the smaller surfactants (resins), it appears that more asphaltenes are present at the surface of oil MFC(B). This argument can also be backed-up by a lower IFT of MFC(B) (11.51 ± 0.34) compared to LVC(C) (14.83 ± 0.32) in the presence of Ca^{2+}.

3.4 Effect of anion polarisability on the IFT of oil LVC(C) and MFC(B)

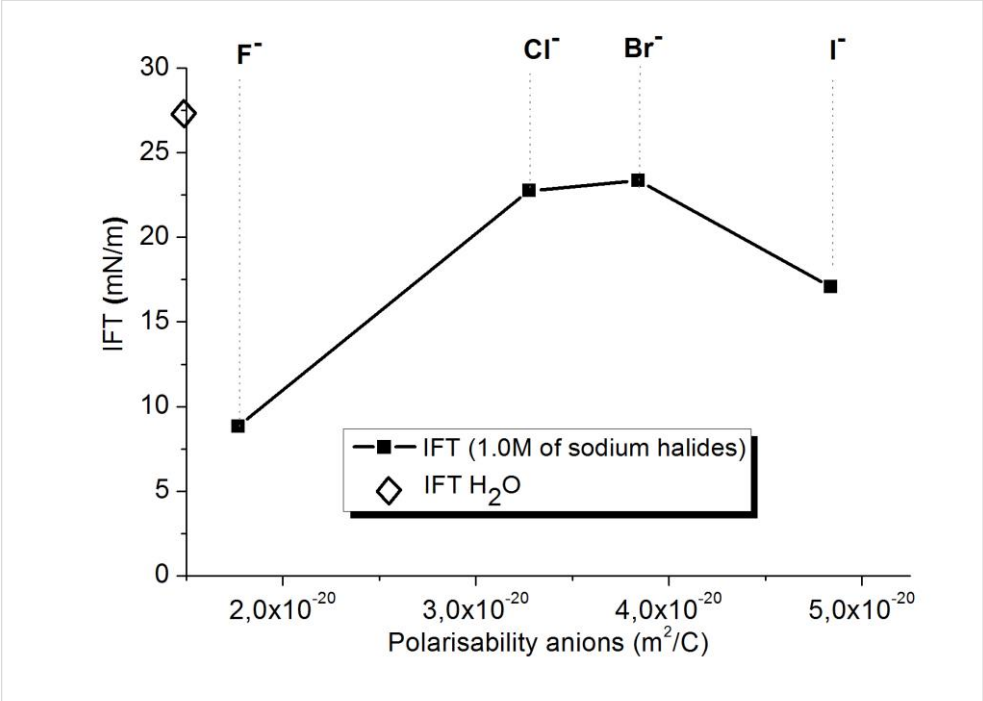

Figure 17: Interfacial tension of oil LVC(C) as a function of the polarisability of anions of sodium halides.

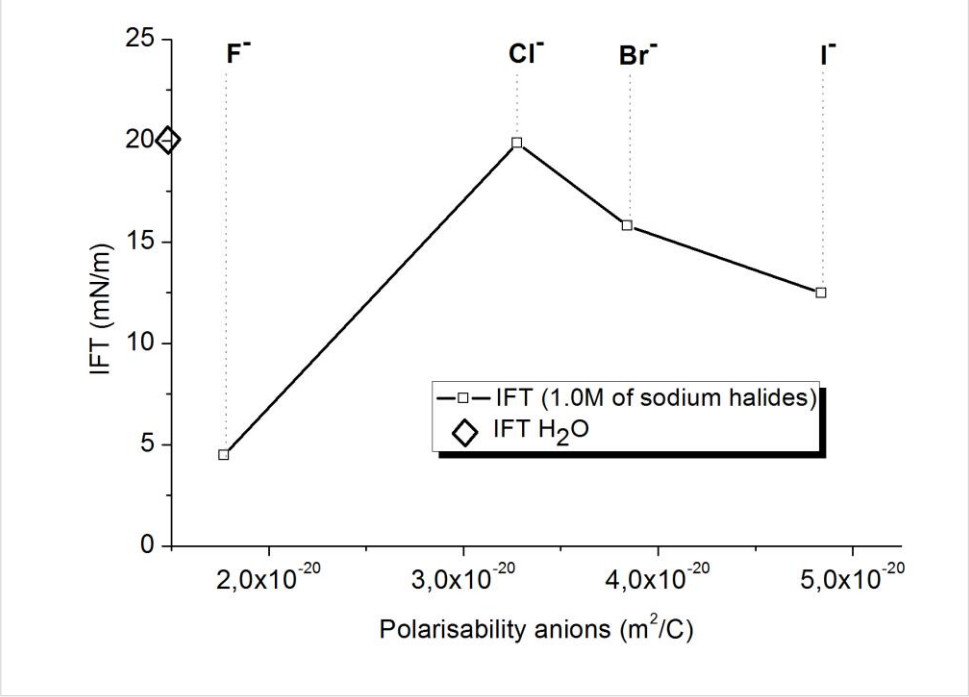

Figure 18: Interfacial tension of oil MFC(B) as a function of the polarisability of anions of sodium halides.

Having investigated the effect of the nature of cation on the crude oils, the effect of anions have been investigated in a similar way as with the MS. The results of the variation of IFT with

brines of sodium halides are shown by Figures 17 and 18 for oils LVC(C) and MFC(B) respectively.

The trends observed with the oils are identical to those observed with pure dodecane and the MS. Again, IFT with the different anions are lower for MFC(B) compared to LVC(C). It is now clear and understandable that ions of high polarisability decrease IFT of both pure and crude oils. Moreover, the specific behaviour of small, low polarisability of F^- observed with the MS is confirmed with the two crude oils.

Summary and conclusion on the IFT of MS and the crude oil

From the different studies, it has been observed that salt concentration plays an important role on the IFT of the three systems. For instance, IFT of each system was minimum at a given salt concentration, termed as the "optimum salinity".

Secondly, the nature of the ions composing the salts play a key aspect in IFT reduction. The small kosmotropic cations (Mg^{2+}, Li^+ and Ca^{2+}) revealed very low IFTs with the three systems under investigation. For instance with the MS, electrostatic attraction leading to ion-paring between the cations and COO^- was argued to account for the lowering of oil/water interfacial tension [23], [24]. Subtle differences between these ions were then attributed to the respective sizes and hardness of the different moieties. As far as the crude oils are concerned, very similar results were obtained with these cations (Mg^{2+}, Li^+ and Ca^{2+}). As such, we know approximately the type and amount of surfactants in the organic phases but all of them being present simultaneously, the observed trends have been explained with the aid of the studies of Lashkarbolooki [9]. For instance, the specificities of smaller cations like Mg^{2+} towards oxygen of resins and larger cations like Ca^{2+} towards the asphaltenes have been attributed to the lowering of IFT of the crude oils. Moreover, it is to be noted that in addition to resins and asphaltenes, the crude oils possess other polar acidic and basic molecules.

With the three systems, salts of monovalent ions like Na^+ and K^+ have had only slight influence on the IFT of the systems. However, for larger, more polarisable and low hydrated cations like Rb^+ and Cs^+, they moved towards the oil/water interface lowering IFT. Indeed, with the MS only a slight tendency had been observed due to low specificity of the cations with the COO^-. However, the presence of the larger surfactants in the crude oils promoted interactions with the latter cations.

As far as the effect of anions are concerned (in the order of decreasing polarisability), in line with literature studies [18], [27], large, highly polarisable and weakly hydrated chaotropic anion (I^-) lowered IFT of the three systems. Cl^- and Br^- of intermediate polarisability, had only limited impact on the IFT of the three studied organic systems. In the presence of F^-, despite being the least polarisable anion, drastic IFT reductions have been recorded. Indeed, following the studies of Collins and Fennell [23], [24], [28], they showed that small-small ions remain as ion pairs. We thus attributed the lowering of IFT to the Na^+-F^- entity which moved towards the oil/brine interface.

4. Emulsions of brines/crude oils

The surfactants present in oils partition at the interface and lower the IFT of the system; more the system interacts in a favourable way, the lower the IFT. As seen in the previous section, salt composition and concentration play a key role in the IFT of a system. Indeed, salting-in or salting-out of surfactants are promoted accordingly to the presence of salts. This section of the thesis aims at studying crude oil/brine emulsions at salt concentrations (of commonly used salts NaCl, $MgCl_2$ and $CaCl_2$) which led to minimum IFTs. Naturally, the minimum IFTs of oils LVC(C) and MFC(B) varying with the nature of the salts, a variation of the emulsions can be expected.

4.1 Proportion of organic phases and water leading to stable emulsions

Prior to all experiments, the crude oils have been mixed with water to determine the proportion of each phase needed. Indeed, the presence of surfactants in the oils should be able to give relatively stable emulsions with water, provided that they are present in sufficient amount.

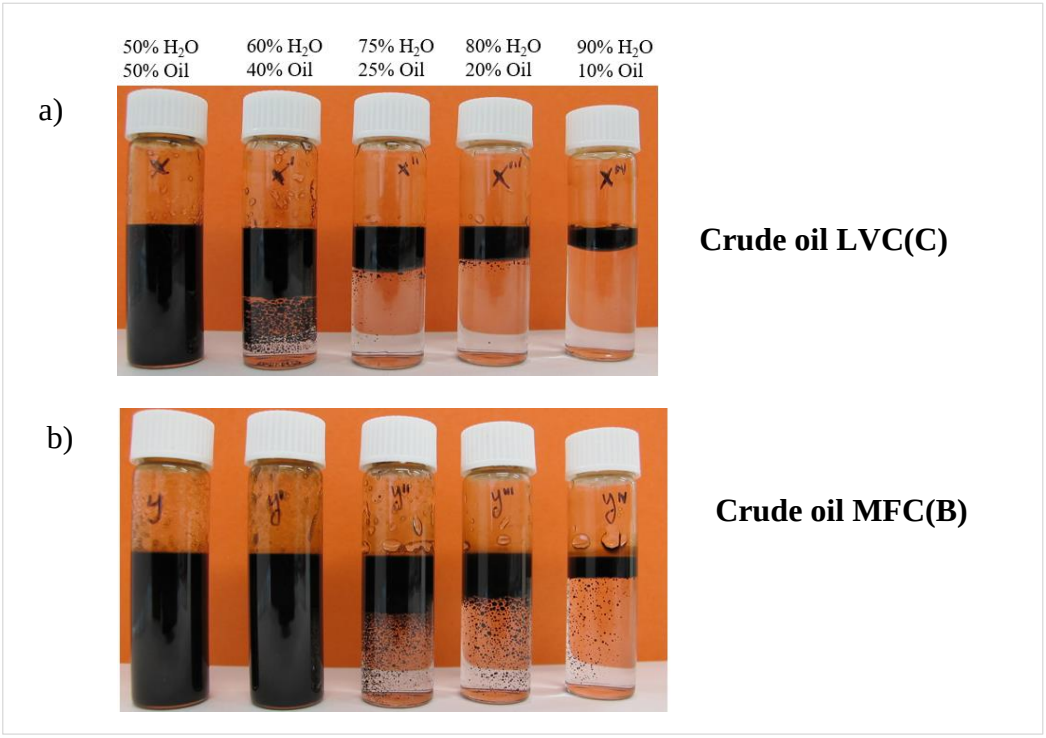

Figure 19: Emulsions resulting from different proportions of oils and water, 24 hours after mixing up of the 2 phases; a) Crude oil LVC(C); b) Crude oil MFC(B).

Figures 19 a) and b) respectively show the emulsions of oils LVC(C) and MFC(B) 24 hours after they were mixed up in a vortex during 30 seconds. It is to be noted that these emulsions had identical appearances during several weeks indicating their stability. As far as oil LVC(C) is concerned, the presence of 50% by volume of the oil was sufficient to give a macroscopically "miscible" appearance. For oil MFC(B), only 40% by volume was enough to give this stable "one-phase" aspect. These results are not surprising and are in agreement with the presence of greater amount of surfactants in oil MFC(B).

4.2 Proportion of organic phases and brines leading to stable emulsions

In a similar way to oil/water emulsions, the crude oils have been emulsified with brines at concentrations leading to minimum IFTs. Tables 12 and 13 respectively recapitulates the brines and their respective concentration leading to minimum IFT with the crude oils LVC(C) and MFC(B) which were determined in section 2.21

- **Oil LVC(C)**

Aqueous phase	Optimum salinity (M)	Corresponding IFT (mN/m)
H_2O	-	25.58 ± 0.05
NaCl	0.50	22.58 ± 0.35
$CaCl_2$	0.25	12.72 ± 0.14
$MgCl_2$	0.20	5.23 ± 0.12

Table 12: Brine composition and concentration leading to minimum IFT against oil LVC(C); as a matter of comparison IFT against water is also reported.

Figure 20 shows the different emulsions of oil LVC(C) and brines of NaCl, $CaCl_2$ and $MgCl_2$ into different proportions. For the purpose of comparison, oil/water emulsions have also been included. First of all it can be observed that in the presence of a 50% oil/50% water or brine, all the emulsions revealed a stable aspect. Indeed, with 50% by volume of oil, enough surfactant was present in order to give a stable emulsion (stable for months). On the other hand, decreasing the volume of the organic phase and increasing volumes of aqueous phase showed that the amount of surfactants was not in sufficient amount to promote emulsion stability, except with the 40% oil-60% brine of $MgCl_2$. Indeed, the presence of Mg^{2+} cations has been able to promote contact between the organic and water phase, while under similar conditions Na^+ and Ca^{2+} did not (Figure 21).

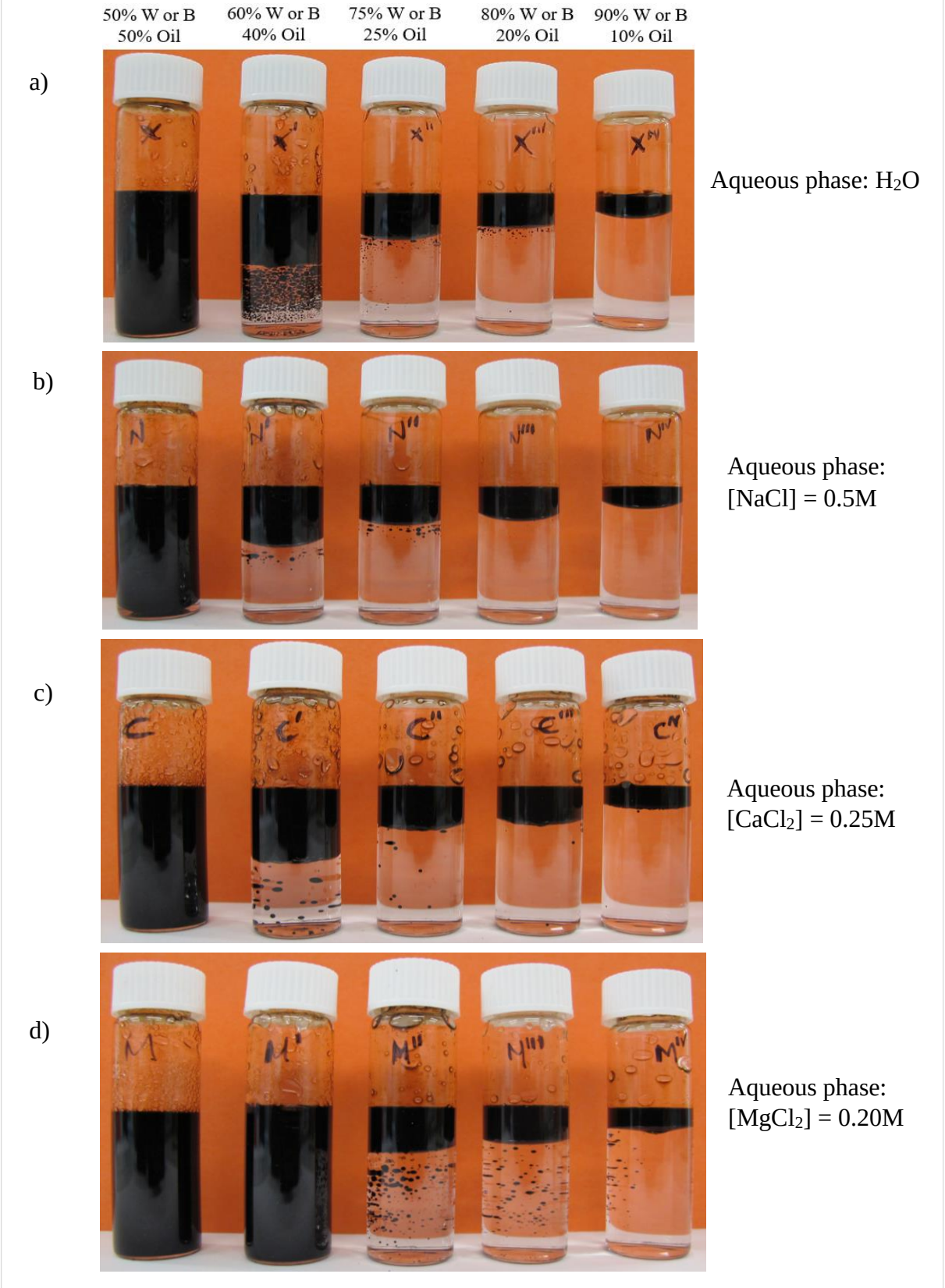

Figure 20: Emulsions of different proportions of oil LVC(C) and different brines, 24 hours after mixing up of the 2 phases; W and B respectively denoting water and brines; a) H_2O; b) NaCl; c) $CaCl_2$; and d) $MgCl_2$.

Macroscopically when comparing the effect of salts in a 40% oil/60% aqueous phase, it can be observed that more water has been resolved (oil and water separated into two distinct phases) in the presence of Na^+ compared to Ca^{2+}. While in the presence of Mg^{2+} stabilisation is observed.

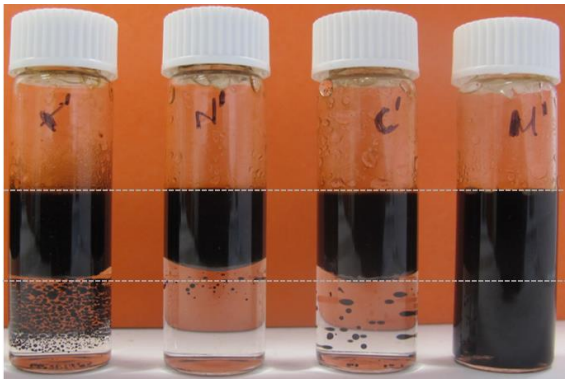

Figure 21: Comparison of emulsions made up of 40% crude oil LVC(C)/60% aqueous phase; from left to right the aqueous phases are: water (X'), NaCl (N'), $CaCl_2$ (C') and $MgCl_2$ (M') respectively.

- **Oil MFC(B)**

Aqueous phase	Optimum salinity (M)	Corresponding IFT (mN/m)
H_2O	-	20.23 ± 0.40
NaCl	0.25	18.40 ± 0.14
$CaCl_2$	0.075	10.97 ± 0.45
$MgCl_2$	0.25	7.60 ± 0.40

Table 13: Brines composition and concentration leading to minimum IFT against oil MFC(B); as a matter of comparison IFT against water is also reported.

The different mixtures of oil MFC(B) with the brines of NaCl, $CaCl_2$ and $MgCl_2$ are shown in Figure 22. Again, for the purpose of comparison, oil/water emulsions have also been included. In this particular case, a mixture of 40% oil/60% water which resulted in a stable emulsion has been modified by the presence of salts (Figure 23). For instance, NaCl and $CaCl_2$ destabilised the emulsion (to a lesser extent with $CaCl_2$), while in the presence of $MgCl_2$ the stability was maintained. As observed with oil LVC(C), it is worth noting that in the presence of 50% oil/50% aqueous phases, the emulsions were all stable.

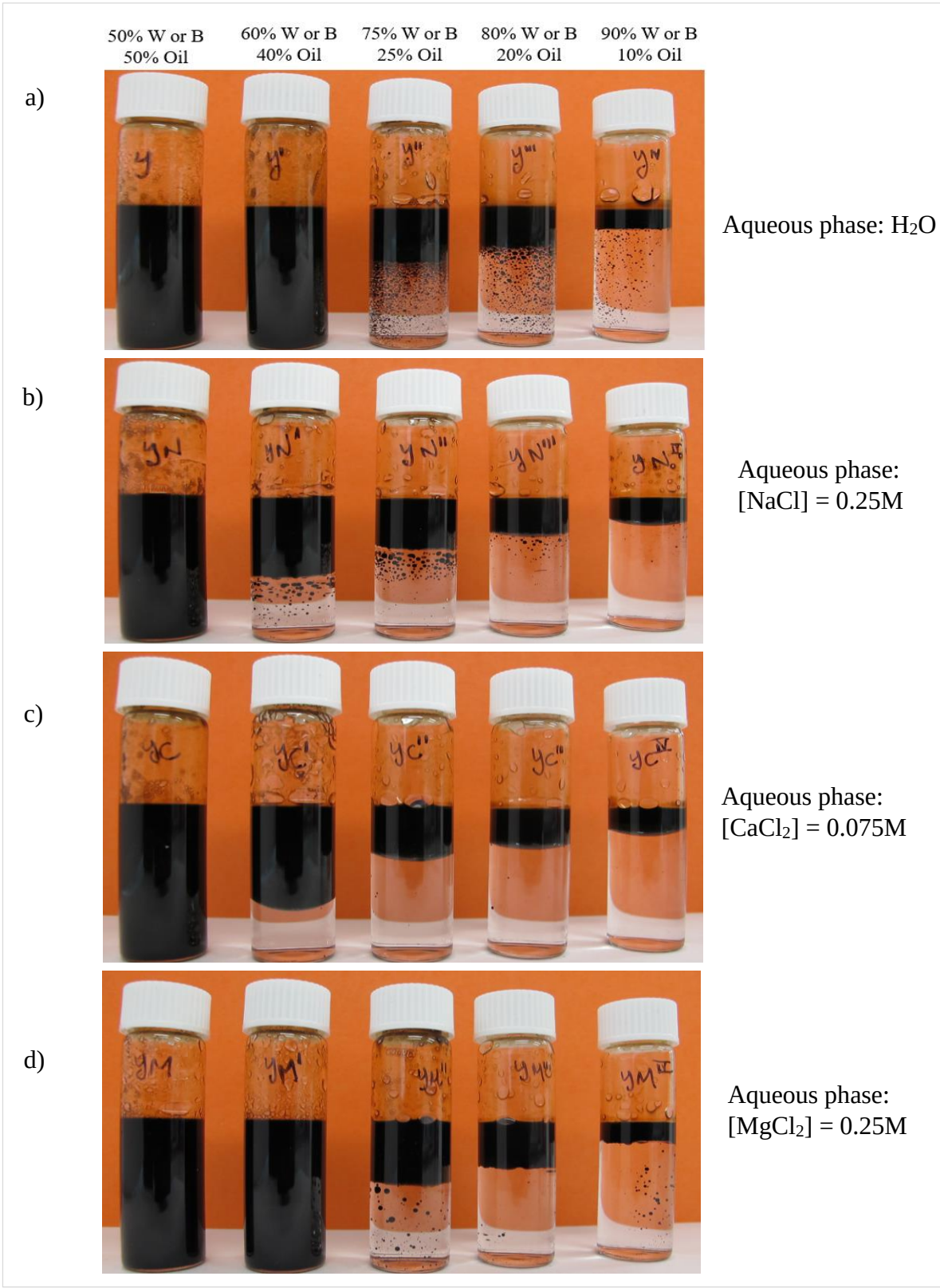

Figure 22: Emulsions of different proportion of oil MFC(B) and aqueous phases, 24 hours after mixing up of the 2 phases; W and B respectively denoting water and brines; a) H_2O; b) NaCl; c) $CaCl_2$; and d) $MgCl_2$.

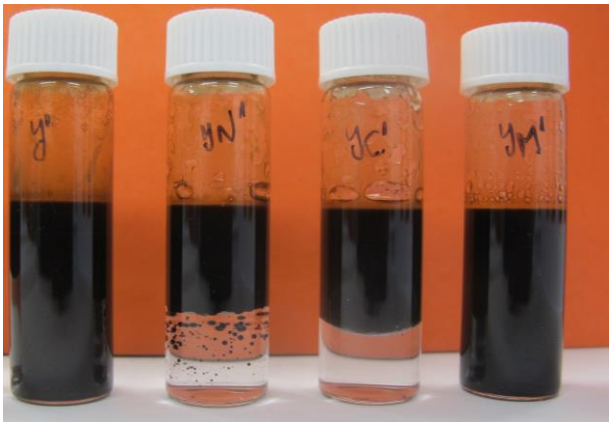

Figure 23: Comparison of emulsions with 40% crude oil MFC(B)/60% aqueous phase; from left to right the aqueous phases are: water (y'), NaCl (yN'), $CaCl_2$ (yC') and $MgCl_2$ (yM') respectively.

4.3 Stability of 50% oil / 50% aqueous phase emulsion

The differences in IFT and stability of emulsions of oils LVC(C) and MFC(B) can a priori be attributed to the presence of different amounts of surfactants and the specificity of salt species towards the different polar moieties. From the results in section 2.3.2., to be able to compare the respective contribution of cations on the stabilisation of the emulsions, it was thus interesting to analyse the mixtures resulting from 50% oil/50% aqueous phase (1-to-1 ratio). Indeed, it is only in this proportion that the emulsions were stable (irrespective of the aqueous phases). In addition to NaCl, $CaCl_2$ and $MgCl_2$, brines composed of mixture of NaCl and $CaCl_2$ and NaCl and $MgCl_2$ were also used to prepare a 1-to-1 emulsion with the oils. As with the latter individual salts, the concentration of the brines resulting from a mixture of two salts also corresponded to the optimum salinity i.e. resulting into the minimum IFT (Table 14). The drop size distribution of the different 50% oil/50% aqueous phases have then been measured. It is worth mentioning that the size measurement in each case has been performed with over 500 drops.

Brines	**Oil LVC(C)**		**Oil MFC(B)**	
	Volume to prepare brine (%)	Minimum IFT (mN/m)	Volume to prepare brine (%)	Minimum IFT (mN/m)
NaCl (1M) + $CaCl_2$ (0.5M)	NaCl = 92.5 $CaCl_2$ = 7.50	13.51	NaCl = 95.0 $CaCl_2$ = 5.0	10.56
NaCl (1M) + $MgCl_2$ (0.5M)	NaCl = 75.0 $MgCl_2$ = 25.0	5.5	NaCl = 85.0 $MgCl_2$ = 15.0	5.91

Table 14: Salt concentration and volume used to prepare brines composed of mixture of salts and their corresponding minimum IFTs; the brines have then been used to prepare 50% by volume of oil/50% by volume of brine emulsions

- **Oil LVC(C)**

As observed in Figure 24, the emulsions were all of W/O (water in oil type). Accordingly to Bancroft's rule the type of emulsion observed, can be attributed to surfactants of low HLBs and soluble in the continuous phase. Figure 25a) shows the droplet sizes in 1-to-1 emulsions of the oil with different aqueous phases (presence of NaCl, $CaCl_2$ and $MgCl_2$). It can be observed that in the presence of NaCl, the size distribution of the drops is very similar to that in the absence of salts. However in the presence of the divalent salts, the size distribution is shifted to the small

sizes, the number of small drops being a bit greater with $MgCl_2$ compared to $CaCl_2$. Figures 25 b) and c) show the comparison if size distribution of the dispersed phase in the presence of brines of pure divalent and mixture of monovalent and divalent salts. The results show that drops in brines of divalent salts and those in brines composed of mixture of salts are of comparable sizes (both when using $CaCl_2$ and $MgCl_2$).

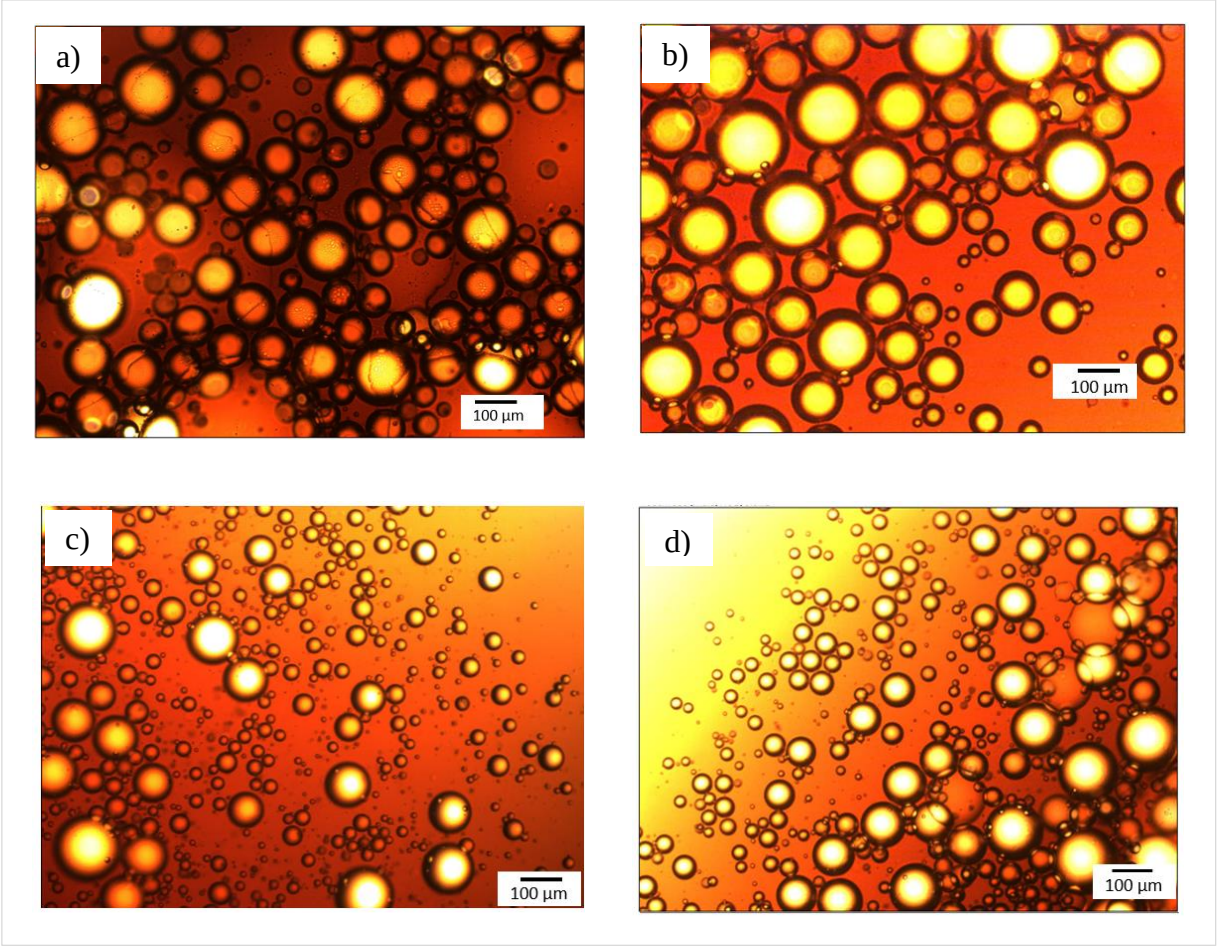

Figure 24: Emulsions of oil LVC(C): a) in water; b) in NaCl; c) in $CaCl_2$; and d) in $MgCl_2$.

a)

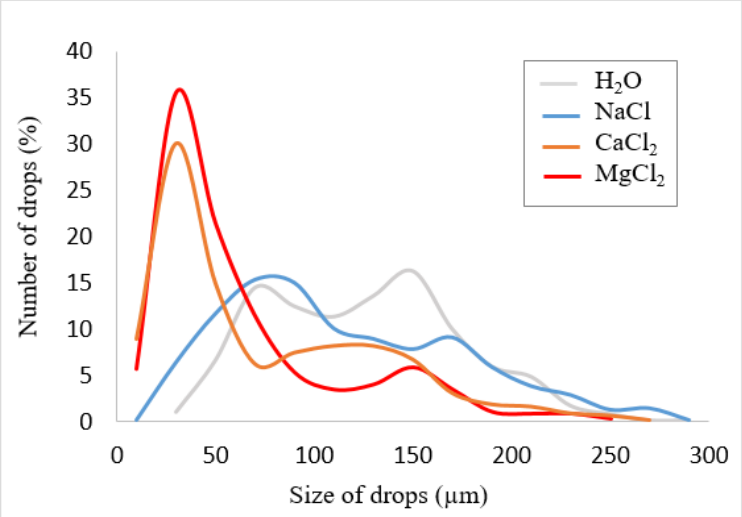

b)

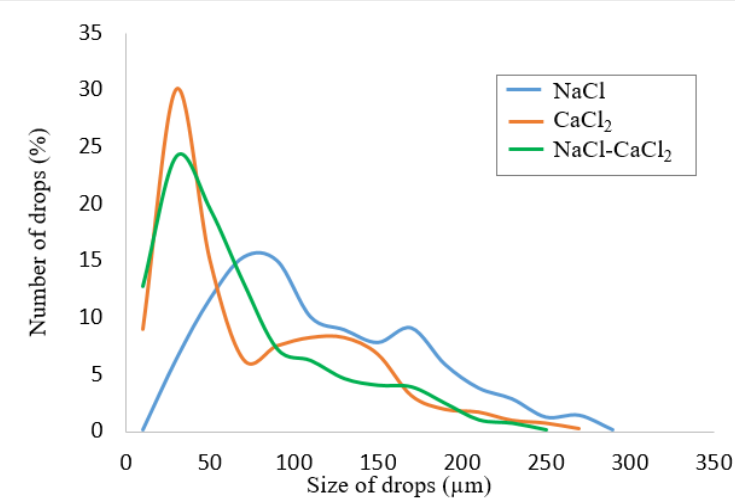

c)

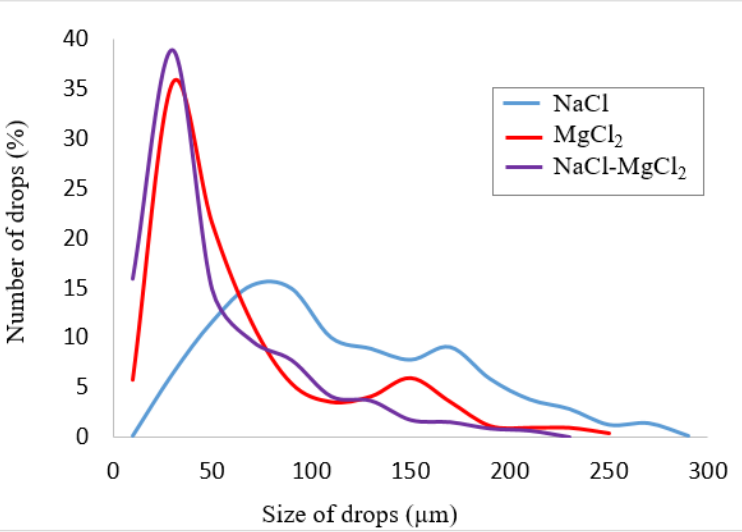

Figure 25: Size of drops of LVC(C)/aqueous phase emulsion: a) Size of H_2O drops in the presence of NaCl, $CaCl_2$ and $MgCl_2$; b) comparison in the presence of NaCl, $CaCl_2$ and mixture of NaCl-$CaCl_2$; b) comparison in the presence of NaCl, $MgCl_2$ and mixture of NaCl-$MgCl_2$.

Figure 26 shows the optical micrographs of the emulsions obtained with oil MFC(B) and the different aqueous phases. Again the emulsions of oil MFC(B) can be observed as water droplets dispersed in the organiv phase. Unlike oil LVC(C), in addition to dark precipitate-like structures, very small agglomerated drops have been observed in the emulsions of oil MFC(B). This aspect is probably linked to the asphaltene and resin content of MFC(B) which is about twice that of LVC(C). These structures have particularly been observed when the aqueous phase was pure water and consequently, size characterisation has been particularly been complex.

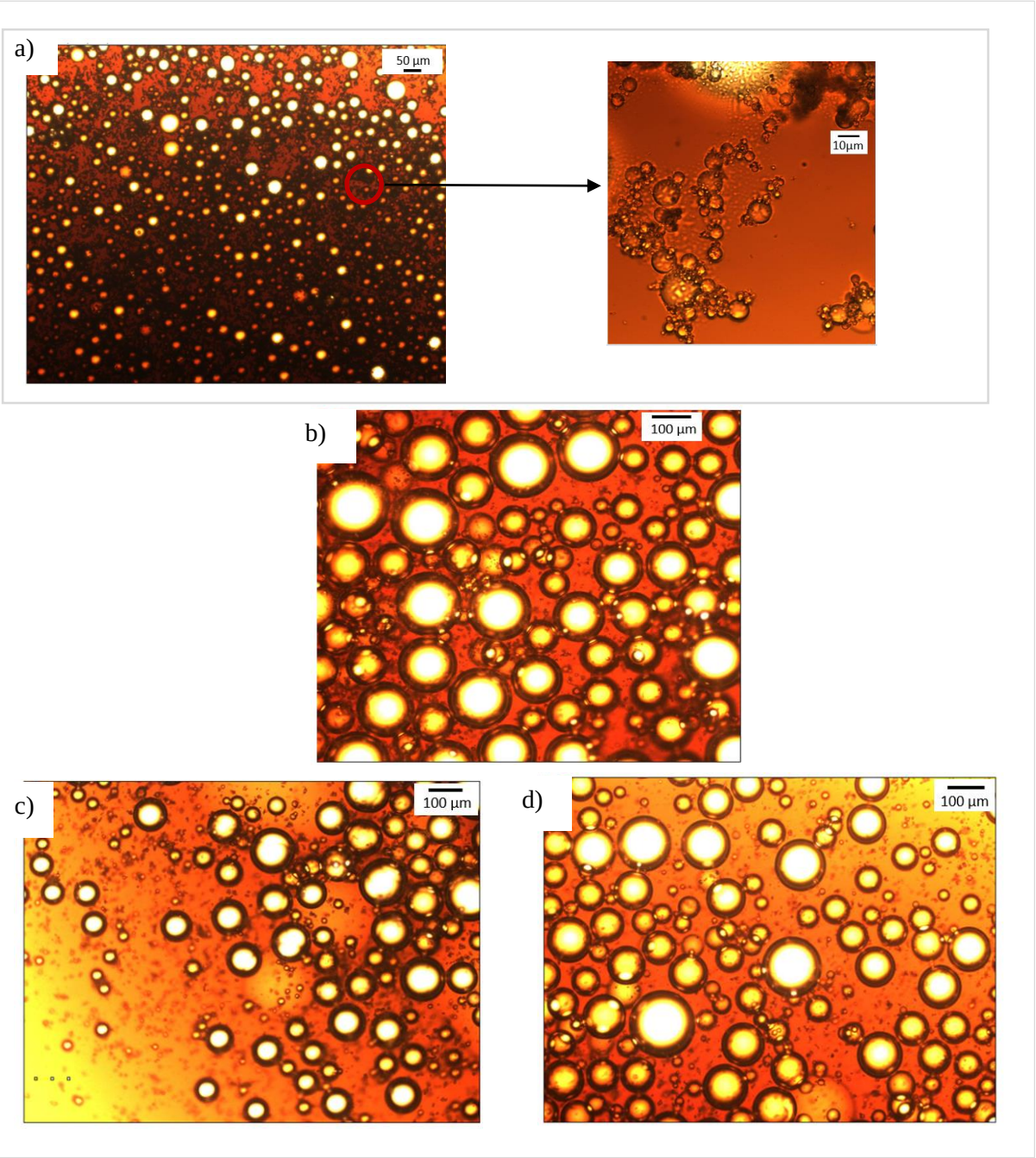

Figure 26: Emulsions of oil MFC(B): a) in water; b) in NaCl; c) in $CaCl_2$; and d) in $MgCl_2$.

a)

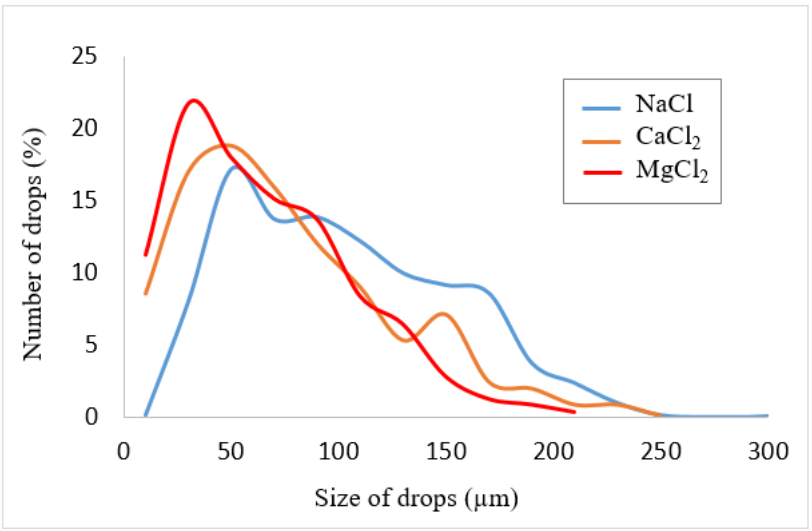

b)

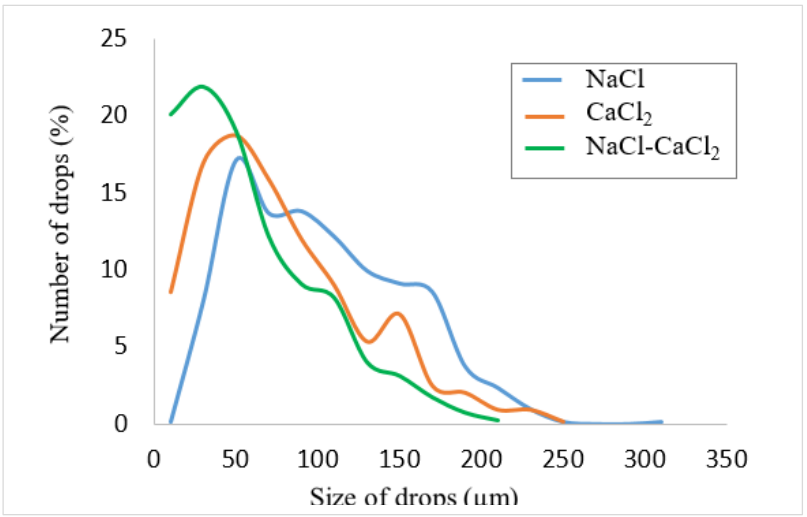

c)

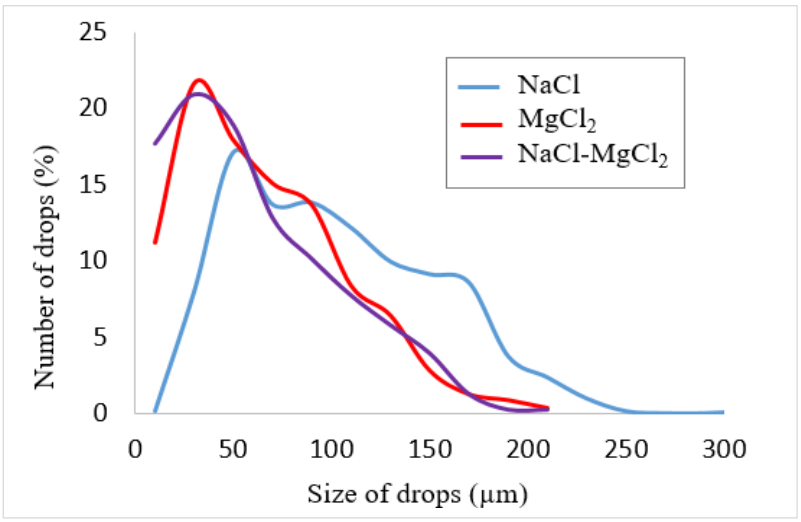

Figure 27: Size of drops of MFC(B)/aqueous phase emulsion: a) Size distribution of H_2O drops in the presence of NaCl, $CaCl_2$ and $MgCl_2$; b) comparison in the presence of NaCl, $CaCl_2$ and mixture of NaCl-$CaCl_2$; b) comparison in the presence of NaCl, $MgCl_2$ and mixture of NaCl-$MgCl_2$.

The size distributions (Figure 27) of the dispersed phase show very similar tendency to those observed with oil LVC(C) i.e. the droplets size distribution in the presence of the divalent cations are shifted to the small sizes compared to NaCl. Also, comparison of the distribution between brine of pure divalent salt and those composed of mixture of salts confirmed the observed tendency with oil LVC(C).

As far as the characterisation of the 50-50 emulsions of the two crude oils is concerned, the results are in agreement with the measured IFTs, i.e. NaCl on its own has only a marginal effect on the size distribution of the droplets, while in the presence of the divalent cations salting-in of the surfactants has been favoured (smaller size of the dispersed droplets). Indeed, a large number of small droplets are in agreement with an increase in the contact oil/aqueous phase surface (Figure 28 compares a large drop of water, which is split into smaller droplets and hence exhibiting larger surface contact in the presence of Mg^{2+} ions).

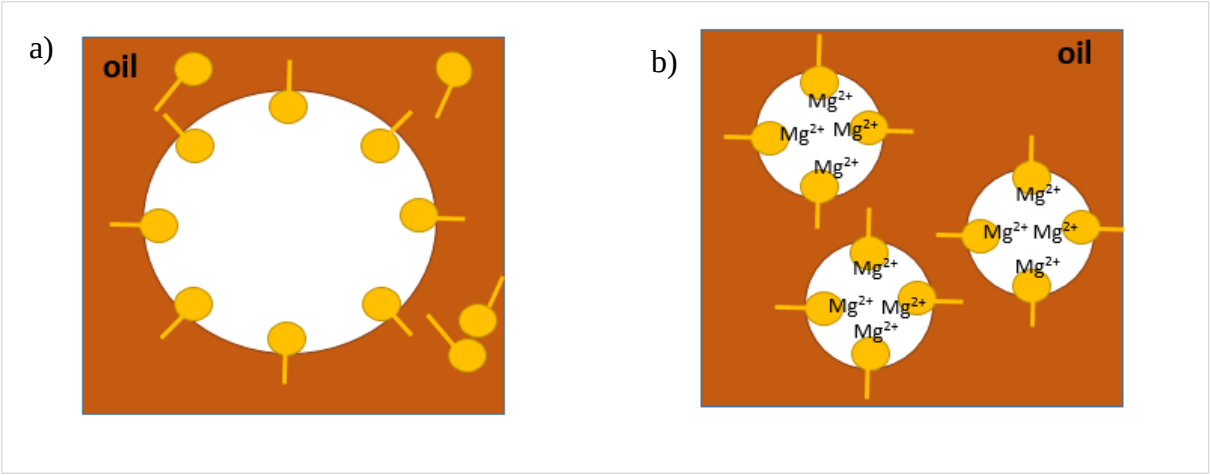

Figure 28: a) water drop in oil stabilised by surfactants; b) smaller drops of water in oil in the presence of Mg^{2+} ions.

Taking into consideration the drop size distribution of the dispersed water droplets into the different aqueous phases, we compared the number of surfactants exposed in each case. For instance, let us consider the surfactants at the interface of the droplets and model them by molecules possessing linear hydrophobic tails and polar head groups (the surface area covered by each head = $35A°^2$).

Table 15 shows the concentration of surfactants needed for W/O emulsion stabilisation under such an approximation of the surfactants. These results clearly reveal that in case of a maximum

of smallest water drops, the concentration of surfactants needed for emulsion stabilisation is $10x10^{-4}$ M for both oils.

Aqueous phase	**Surfactants in LVC(C) ($x10^{-4}$ M)**	**Surfactants in MFC(B) ($x10^{-4}$ M)**
H_2O	2.70	-
NaCl	3.40	3.70
$CaCl_2$	7.40	6.70
$NaCl+CaCl_2$	8.30	10.0
$MgCl_2$	7.30	7.80
$NaCl+MgCl_2$	10.0	9.40

Table 15: Concentration of surfactants needed for emulsion stabilisation with oils LVC(C) and MFC(B)

Oils LVC(C) and MFC(B) contain 8.2% by mass (≈$9x10^{-2}$ M) and 15.7% by mass (≈$18x10^{-2}$ M) of polar components respectively. The crude oil components seem to be in sufficient amount to provide enough surface active agents for emulsion stabilisation.

5. Conclusion

This chapter aimed at understanding crude oil/brine interactions via the measurements of interfacial tension and studies of the stability of emulsions. For this purpose a simplified model system (MS) composed of dodecane and oleic acid has been designed and the effect of brine compositions and concentrations has been studied both on the model system as well on two crude oils.

First of all, for a pure organic phase (dodecane), it has been observed that increasing salt concentration of NaCl and $MgCl_2$ caused its IFT to increase due to negative adsorption of ions at the oil/water interface. However, for the MS and the crude oils a reverse trend of IFT with increasing salt concentration was observed. Indeed, increasing salt concentration of NaCl, $CaCl_2$ and $MgCl_2$ were accompanied by a decrease of IFT to reach a minimum at an optimum salinity, due to electrostatic attraction and salting-in of surfactants at low salt concentration. As far as the nature of salt species is concerned, Na^+ had only a marginal effect on the IFT of the three systems while the divalent salts caused a marked reduction of the IFT (IFT $MgCl_2$ < $CaCl_2$ for the three systems). Further analysis of the effect of the nature of cations showed that small and highly polarising cations like Mg^{2+}, Li^+ and Ca^{2+} were attracted to the oil/water interface due to ion pairing with surfactants present in the organic phases. As the size of the cations was increased, IFT reduction became more and more hindered with Sr^{2+}, Ba^{2+}, Na^+, K^+. However, larger cations such as Rb^+ and Cs^+ have shown tendency to lowering of IFT with our MS and have had very marked IFT reduction with the crude oils. It appeared that large, highly polarisable, weakly hydrated and high cavitational energy cations are attracted to oil/water interface.

As far as the effect of anions are concerned, in the series of halogens F^- and I^- have decreased the IFT of pure dodecane, MS and the crude oils. Indeed, as observed with the highly polarising and highly polarisable cations, anions also have had similar tendency on the IFTs of the different systems.

After having studied the effect of ions on the IFT of oil/water interfacial tensions, confronting the crude oils with salt species (NaCl, $CaCl_2$, $MgCl_2$, NaCl+$CaCl_2$ and NaCl+$MgCl_2$) at optimum salt concentrations through emulsions have revealed the specificities of the ionic moieties. For instance, NaCl on its own have had only a marginal effect on the IFT of the crude oils. Emulsification in the presence of Na^+ have revealed dispersed droplets of water of sizes comparable to those in the absence of any ionic species (majority of drops of large size). However in the presence of the divalent cations, a large number of small drops have been

observed. Indeed, a large number of small drops promote the salting-in of surfactants and increase the oil/water contact surface. Moreover, it has been observed that in the presence of both NaCl and divalent salt, a synergistic effect took place, i.e. very identical drop size distribution has been observed with smaller concentration of the divalent salt.

6. Bibliography

[1] M. K. Sharma and D. O. Shah, “Use of Surfactants in Oil Recovery,” in *Developments in Petroleum Science*, vol. Volume 17, Part B, G. V. C. and T. F. Y. Erle C. Donaldson, Ed. Elsevier, 1989, pp. 255–315.

[2] D. Yang and Y. Gu, “Interfacial Interactions Between Crude Oil and CO2 Under Reservoir Conditions,” *Pet. Sci. Technol.*, vol. 23, no. 9–10, pp. 1099–1112, Sep. 2005.

[3] M. A. Dahami, W. D. Constant, and J. M. Wolcott, “Alcohol-assisted alkaline flooding for enhanced oil recovery,” *Fuel*, vol. 67, no. 9, pp. 1242–1248, Sep. 1988.

[4] Z. Zhao, C. Bi, W. Qiao, Z. Li, and L. Cheng, “Dynamic interfacial tension behavior of the novel surfactant solutions and Daqing crude oil,” *Colloids Surf. Physicochem. Eng. Asp.*, vol. 294, no. 1–3, pp. 191–202, Feb. 2007.

[5] A. Bera, A. Mandal, and B. B. Guha, “Synergistic Effect of Surfactant and Salt Mixture on Interfacial Tension Reduction between Crude Oil and Water in Enhanced Oil Recovery,” *J. Chem. Eng. Data*, vol. 59, no. 1, pp. 89–96, Jan. 2014.

[6] B. Kumar, “Effect of salinity on the interfacial tension of model and crude oil systems,” *Dr. Diss. Univ. Calg.*, 2012.

[7] A. RezaeiDoust, T. Puntervold, S. Strand, and T. Austad, “Smart Water as Wettability Modifier in Carbonate and Sandstone: A Discussion of Similarities/Differences in the Chemical Mechanisms,” *Energy Fuels*, vol. 23, no. 9, pp. 4479–4485, Sep. 2009.

[8] S. Standal, J. Haavik, A. M. Blokhus, and A. Skauge, “Effect of polar organic components on wettability as studied by adsorption and contact angles,” *J. Pet. Sci. Eng.*, vol. 24, no. 2–4, pp. 131–144, Dec. 1999.

[9] M. Lashkarbolooki, S. Ayatollahi, and M. Riazi, “Effect of Salinity, Resin, and Asphaltene on the Surface Properties of Acidic Crude Oil/Smart Water/Rock System,” *Energy Fuels*, vol. 28, no. 11, pp. 6820–6829, Nov. 2014.

[10] F. Moeini, A. Hemmati-Sarapardeh, M.-H. Ghazanfari, M. Masihi, and S. Ayatollahi, “Toward mechanistic understanding of heavy crude oil/brine interfacial tension: The roles of salinity, temperature and pressure,” *Fluid Phase Equilibria*, vol. 375, pp. 191–200, Aug. 2014.

[11] J. C. Seccombe, A. Lager, K. J. Webb, G. Jerauld, and E. Fueg, “Improving Wateflood Recovery: LoSalTM EOR Field Evaluation,” in *SPE-113480-MS*, SPE, 2008.

[12] A. Lager, K. Webb, C. Black, M. Singleton, and K. Sorbie, “Low Salinity Oil Recovery-An Experimental Investigation1,” *Petrophysics*, vol. 49, no. 1, 2008.

[13] B. Soraya, C. Malick, C. Philippe, H. J. Bertin, and G. Hamon, “Oil Recovery by Low-Salinity Brine Injection: Laboratory Results on Outcrop and Reservoir Cores,” in *SPE-124277-MS*, SPE, 2009.

[14] B.-Y. Cai, J.-T. Yang, and T.-M. Guo, “Interfacial Tension of Hydrocarbon + Water/Brine Systems under High Pressure,” *J. Chem. Eng. Data*, vol. 41, no. 3, pp. 493–496, Jan. 1996.

[15] E. Serrano-Saldaña, A. Domínguez-Ortiz, H. Pérez-Aguilar, I. Kornhauser-Strauss, and F. Rojas-González, “Wettability of solid/brine/n-dodecane systems: experimental study of the effects of ionic strength and surfactant concentration,” *Proc. Third Int. TRIPrinceton Workshop Charact. Porous Mater. Angstroms Millim.*, vol. 241, no. 1–3, pp. 343–349, Jul. 2004.

[16] A. Goebel and K. Lunkenheimer, “Interfacial Tension of the Water/n-Alkane Interface,” *Langmuir*, vol. 13, no. 2, pp. 369–372, Jan. 1997.

[17] S. Zeppieri, J. Rodríguez, and A. L. López de Ramos, “Interfacial Tension of Alkane + Water Systems,” *J. Chem. Eng. Data*, vol. 46, no. 5, pp. 1086–1088, Sep. 2001.

[18] R. Aveyard and S. M. Saleem, “Interfacial tensions at alkane-aqueous electrolyte interfaces,” *J. Chem. Soc. Faraday Trans. 1 Phys. Chem. Condens. Phases*, vol. 72, no. 0, pp. 1609–1617, 1976.

[19] W. Kunz, *Specific ion effects*. World Scientific, 2010.

[20] E. Lima, B. De Melo, L. Baptista, and M. Paredes, “Specific ion effects on the interfacial tension of water/hydrocarbon systems,” *Braz. J. Chem. Eng.*, vol. 30, no. 1, pp. 55–62, 2013.

[21] W. Kunz, *Specific ion effects*, vol. 325. World Scientific, 2010.

[22] E. Sedlák, L. Stagg, and P. Wittung-Stafshede, “Effect of Hofmeister ions on protein thermal stability: Roles of ion hydration and peptide groups?,” *Arch. Biochem. Biophys.*, vol. 479, no. 1, pp. 69–73, Nov. 2008.

[23] K. D. Collins, “Charge density-dependent strength of hydration and biological structure.,” *Biophys. J.*, vol. 72, no. 1, p. 65, 1997.

[24] K. D. Collins, “Ions from the Hofmeister series and osmolytes: effects on proteins in solution and in the crystallization process,” *Macromol. Cryst.*, vol. 34, no. 3, pp. 300–311, Nov. 2004.

[25] P. Atkins, “Physical Chemistry,” *Press Oxf. Univ.*, vol. Sixth edition, 1998.

[26] Z. Yang, “Hofmeister effects: an explanation for the impact of ionic liquids on biocatalysis,” *Ind. Biotechnol. Curr. Status Future Dev. Sustain. Hum. Soc.*, vol. 144, no. 1, pp. 12–22, Oct. 2009.

[27] A. P. dos Santos and Y. Levin, “Ions at the Water–oil Interface: Interfacial Tension of Electrolyte Solutions,” *Langmuir*, vol. 28, no. 2, pp. 1304–1308, Jan. 2012.

[28] C. J. Fennell, A. Bizjak, V. Vlachy, and K. A. Dill, “Ion Pairing in Molecular Simulations of Aqueous Alkali Halide Solutions,” *J. Phys. Chem. B*, vol. 113, no. 19, pp. 6782–6791, May 2009.

V: Triple phase oil/brine/clay interaction

Table of contents

List of Tables

List of Figures

Introduction

In this chapter we aimed at investigating triple phase oil/brine/clay interactions by two methods: (i) contact angle measurements and (ii) studies of the stability of oil/brine emulsions in the presence of clay particles.

Wettability of clay minerals: As seen in chapter 3, contact angles indicate the relative affinity of two fluids for a solid surface. The study of wettability measurements aimed at measuring contact angle of oil drops deposited on smooth mica surfaces in the presence of different aqueous phases. Indeed, in chapter three we tried to measure contact angles on clay films at oil/air/clay interface but the oils rapidly spread on the surfaces. Here, in the presence of an aqueous phase, the contact angles are driven by the balance of surface and interfacial tensions between the oil/clay film and the oil/aqueous phase respectively. It is known that the wettability of oil/brine/solid is affected by brine composition and pH [1]. Hence, we investigated the adhesion of crude oils on mica surface in the presence of brines composed of salts of monovalent cations (NaCl and KCl) and of divalent cations ($CaCl_2$ and $MgCl_2$).

Emulsion stability: Some studies have reported that oil recovery is improved by the formation of emulsions whereby oil is carried with the displacing aqueous phase [2], [3]. If on one hand the process of emulsification is most likely to take place through surfactant stabilisation (as seen in chapter four), on the other hand, the detachment of clay particles from the rock surfaces is also expected to contribute to stability via pickering emulsions. Indeed it has been shown that inorganic particle stabilised emulsions are more stable compared to emulsions stabilised by asphaltenes only [4]. Studies have also reported that the stability of particle stabilised emulsions are governed by the particle size and shape, concentration of the particles, wettability of the particles, pH and salt concentration of the aqueous phase [5]–[9]. In the second part of this chapter, we thus added different amounts of different clay particles into different aqueous phases and emulsification has then been carried out with the oils. We emphasised on the stability of 50% oil/50% aqueous phase emulsions in the presence of clays. It is worth mentioning that 50% oil/50% aqueous phase emulsions were already stable during several weeks in the presence of water, NaCl, $CaCl_2$ and $MgCl_2$.

1. Experiments and set-up for triple phase oil/brine/clay interaction

1.1 Contact angle measurements

By the means of contact angle measurements, triple phase oil/brine/clay interactions have been determined. For this purpose, mica sheets from Metafix have been used. Indeed freshly cleaved muscovite mica surfaces are crystalline, smooth and possess a similar structure as illite which is commonly encountered in sandstone reservoirs [10].

The mica was thus first cleaved and its surface exchanged with Na^+, K^+, Ca^{2+}, and Mg^{2+} by using NaCl (1M), KCl (1M), $CaCl_2$ (0.5M) and $MgCl_2$ (0.5M) respectively according to the procedure described in Figure 1.

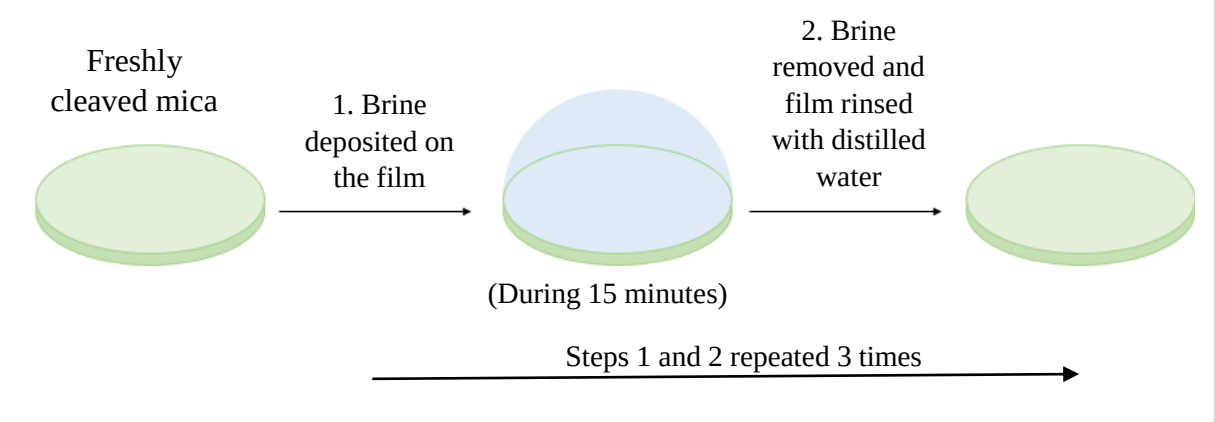

Figure 1: Procedure for exchanging mica films.

Contact angles of LVC(C) and MFC(B) on the mica sheets exchanged with Na^+, K^+, Ca^{2+} and Mg^{2+} have been measured in water and in the following brines:

- Mica-Na^+ in 1M NaCl
- Mica-K^+ in 1M KCl
- Mica-Mg^{2+} in 0.5M $MgCl_2$
- Mica-Ca^{2+} in 0.5M $CaCl_2$

Contact angles have then been measured by depositing 5µL of oils on the mica surfaces as shown in Figure 2.

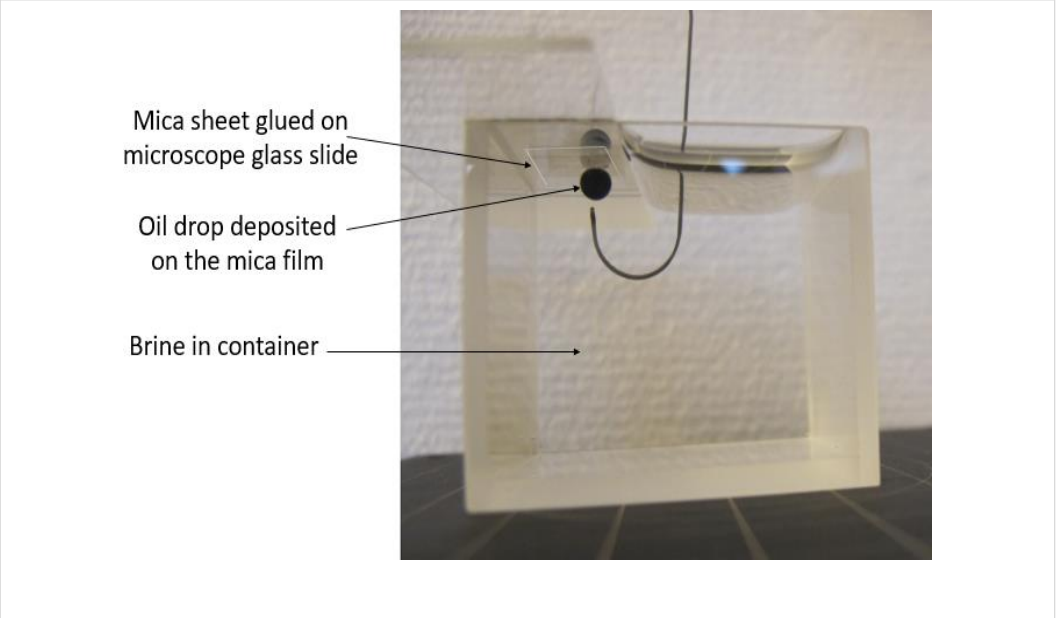

Figure 2: Set-up used for contact angle measurements.

1.2 Crude oil/aqueous phase emulsion in the presence of clays

From the previous studies of the stability of emulsion of crude oils in the presence of brines (chapter 4, section 2.2), the results showed that Mg^{2+} ions promoted stabilisation to the greatest extent (both of oils LVC(C) and MFC(B)). For this reason, the brine of $MgCl_2$ at concentrations leading to the minimum IFTs with the two oils have been chosen to investigate the effect of the amount of clay minerals on the emulsions. Once the amount of clay minerals investigated, the type of clay has been varied to investigate the effect of its nature on the stability of oil/brine emulsions. For this purpose, brines of NaCl, $CaCl_2$, $MgCl_2$, NaCl+$CaCl_2$ and NaCl+$MgCl_2$ at concentrations leading to the lowest IFT with the crude oils have been used.

1.2.1 Oil LVC(C)

1.2.1.1. Determination of the amount of clay needed to destabilise emulsion of LVC(C)

Different amounts of kaolinite particles (size <2µm) were first dispersed in brine of $MgCl_2$ (Table 1). The resulting suspensions were then mixed in a proportion of 50% by volume with 50% by volume of crude oil (corresponding to a 1 to 1 ratio).

Brine	Concentration of brine (M)	Clay mineral	Concentration of clay mineral (% by mass)
$MgCl_2$	0.20	kaolinite	1.000 0.500 0.250 0.040 0.030 0.020 0.010 0.005

Table 1: Brine and clay mineral used with oil LVC(C).

1.2.1.2. Influence of the type of clay mineral on emulsion stability

Tables 2a) and 2b) recapitulates the different brines and their corresponding concentration/ volume leading to the lowest IFT with oil LVC(C).

Brine	Conc (mol/L)
NaCl	0.50
$CaCl_2$	0.25
$MgCl_2$	0.20

2a)

Brine	Volume (%)
NaCl(1M)-$CaCl_2$(0.5M)	92.5 - 7.5
NaCl(1M)-$MgCl_2$(0.5M)	75 - 25

2b)

Table 2: a) Concentration and b) volumes of brines leading to minimum IFT with oil LVC(C).

Suspensions were then prepared by adding 0.04% by mass of the following clay minerals to the brines:

- Kaolinite: K4-Na^+ (hexagonal shape of size < 2µm)
- Illite: Imt2-Na^+ (irregular shape of size < 2µm)
- Nontronite: NAu1-Na^+, NAu1-K^+ and NAu1-Ca^{2+} (lathes of 200x700 nm)
- Wyoming montmorillonite: SWy-Na^+ (discs of 250 nm).

As such these clays provide a wide scan of minerals in order to investigate the effect of charged and uncharged clay minerals, non-swelling and swelling clay minerals, and the effect of exchangeable ions.

1.2.2 Oil MFC(B)

1.2.2.1. Determination of the amount of clay needed to destabilise emulsion of MFC(B)

As with oil LVC(C), different amounts of kaolinite particles (size <2µm) were first dispersed in brine of $MgCl_2$ (Table 3). The resulting suspensions were then mixed in a proportion of 50% by volume with 50% by volume of crude oil (1-to-1 ratio). As a matter of comparison, similar experiments have been performed with illite particles (size fraction <2µm) possessing permanent surface charges compared to kaolinite. As an illustration, illite suspensions with oil before mixing is shown by Figure 2.

Brine	**Concentration of brine (M)**	**Clay mineral**	**Concentration of clay mineral (% by mass)**
$MgCl_2$	0.25	Kaolinite	2.00
			1.00
		Illite	0.75
			0.50
			0.25
			0.10

Table 3: Brine and clay minerals used with oil MFC(B).

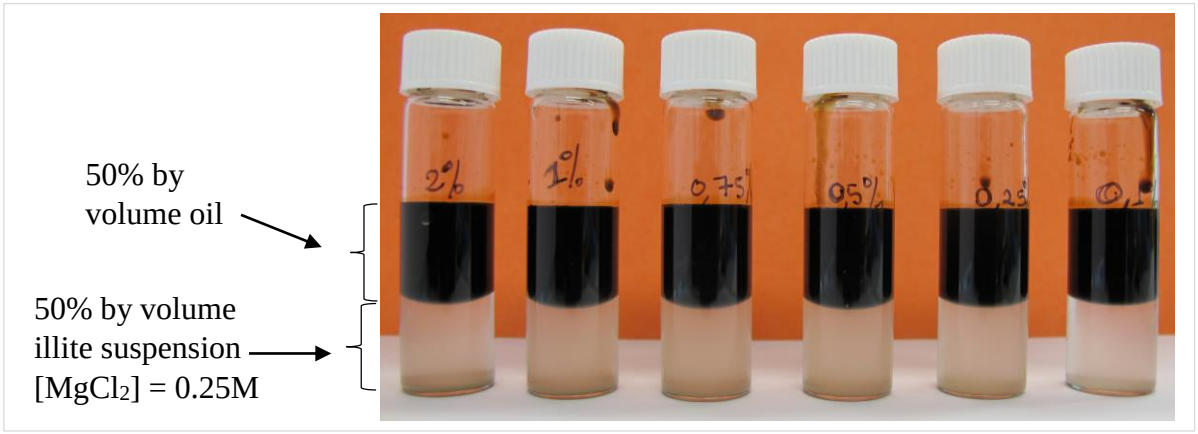

Figure 3: Different amounts of illite particles in brine of $MgCl_2$ used for emulsion with oil MFC(B).

1.2.2.2. Influence of the type of clay mineral on emulsion stabilisation/destabilisation

Tables 4a) and 4b) recapitulates the different brines and their corresponding concentration leading to the lowest IFT with oil MFC(B).

Brine	**Conc (mol/L)**
NaCl	0.250
$CaCl_2$	0.075
$MgCl_2$	0.250

4a):

Brine	**Volume (%)**
NaCl(1M)-$CaCl_2$(0.5M)	95 - 5
NaCl(1M)-$MgCl_2$(0.5M)	15 - 85

4b)

Table 4: a) Concentration and b) volumes of brines leading to minimum IFT with oil MFC(B).

Suspensions were then prepared by adding 1% by mass of the following clay minerals to the brines:

- Illite: Imt2-Na^+
- Kaolinite: K4-Na^+
- Wyoming montmorillonite: SWy-Na^+

2. Wettability of mica sheet

The oil wettability of mica sheets exchanged with Na^+, K^+, Ca^{2+} and Mg^{2+} immersed in water and brines have been determined with both oils LVC(C) and MFC(B). Indeed, under such conditions the contact angles are governed the equilibrium of interfacial tensions (γ) at the solid/aqueous phases, solid/organic phases and organic/aqueous phases.

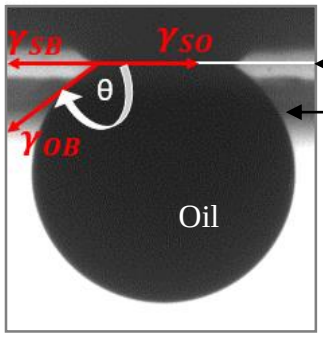

Mica surface

Brine

γ_{SW}: Interfacial tension at solid/water interface;

γ_{SO}: Interfacial tension at solid/oil interface;

γ_{OW}: Interfacial tension at oil/water interface

Figure 4: Contact angle of an oil drop deposited on mica surface in the presence of water.

2.1 Contact angle of oil LVC(C)

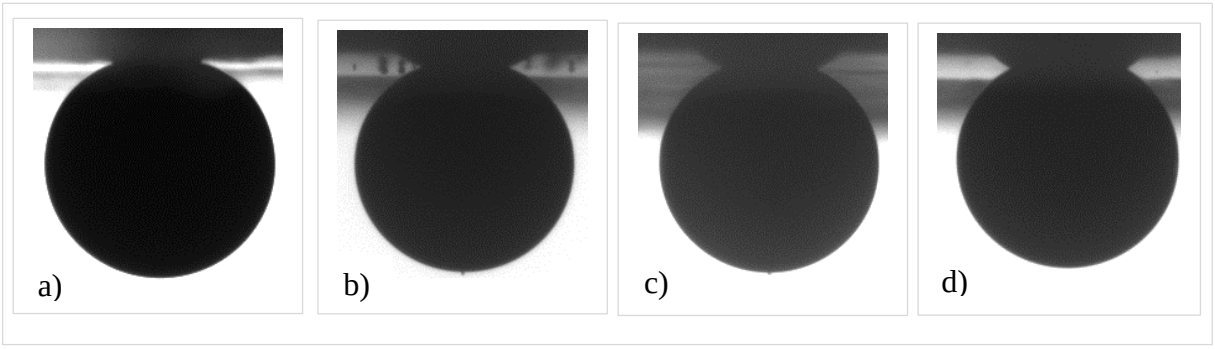

Figure 5: Drops of LVC(C) in water, on mica sheets exchanged with: a) Na^+; b) K^+; c) Ca^{2+}; d) Mg^{2+}.

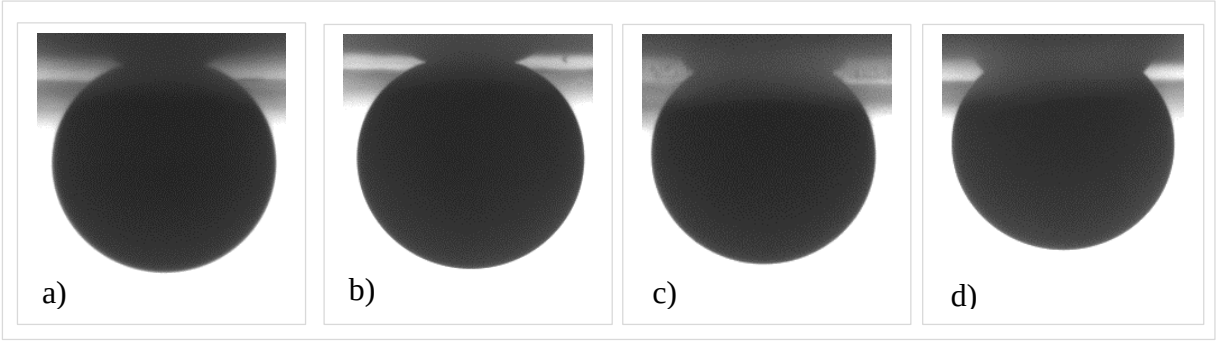

Figure 6: Drops of LVC(C) in brine on a): mica-Na^+ in NaCl; b) mica-K^+ in KCl; c) mica-Ca^{2+} in $CaCl_2$; d) mica-Mg^{2+} in $MgCl_2$.

Figures 5 and 6 show oil drops in equilibrium on mica surfaces in water and bine respectively. At first sight it can be observed that there is an evolution of the contact surface between the drop and the mica with respect to the presence of the different exchangeable ions and with the different brines. For instance, in water, the contact surface is visibly more important in the presence of the divalent cations than the monovalent cations. Very similar observations can be made in the presence of brines composed of divalent cations. As a matter of comparison the contact angles on the different systems are reported in Table 5.

Mica	**Contact angle of oil LVC(C) in H_2O (°)**	**Contact angle of oil LVC(C) in brine**	
		Brine	**Contact angle (°)**
• Mica-Na^+	160	NaCl	160
• Mica-K^+	158	KCl	163
• Mica-Ca^{2+}	150	$CaCl_2$	140
• Mica-Mg^{2+}	140	$MgCl_2$	133

Table 5: contact angles (± 3-5°)) of LVC(C) on mica exchanged with different cations, the whole system in equilibrium in water and brines.

Comparison of contact angles on the different mica surfaces in water, show smaller contact angles in the presence of the divalent cations, i.e. the oils drops are more adsorbed in the presence of ions like Ca^{2+} and Mg^{2+}. When comparing the contact angles in brines, firstly the results show similar tendency of evolution on the different mica surfaces. Secondly, in the presence of brines of divalent cations, a decrease of the contact angles compared to water has been recorded.

It is then worth comparing the solid/oil surface tension in water (γ_{SO}) and in the presence of brines (γ'_{SO}).

In water: $\gamma_{SW} = \gamma_{SO} + \gamma_{OW} \cos\theta$ Equation 1

In brine: $\gamma_{SB} = \gamma'_{SO} + \gamma_{OB} \cos\theta'$ Equation 2

Comparing the adsorption of the oils in the different phases:

$$(\gamma_{SB} - \gamma_{SW}) = (\gamma'_{SO} - \gamma_{SO}) + (\gamma_{OB} \cos\theta' - \gamma_{OW} \cos\theta) \quad \text{Equation 3}$$

From chapter 3, section 2.1.1, the results on nontronite and Wyoming montmorilonite samples showed no net differences between the contact angles of water and brines.

Contact angles on Nontronite films, NAu1	**Contact angles on Wyoming montmorillonite films, SWy**
• On NAu1-Na^+, $\theta_{H_2O} \approx \theta_{NaCl}$	• On SWy-Na^+, $\theta_{H_2O} \approx \theta_{NaCl}$
• On NAu1-K^+, $\theta_{H_2O} \approx \theta_{KCl}$	• On SWy-K^+, $\theta_{H_2O} \approx \theta_{KCl}$
• On NAu1-Ca^{2+}, $\theta_{H_2O} \approx \theta_{CaCl_2}$	• On SWy-Ca^{2+}, $\theta_{H_2O} \approx \theta_{CaCl_2}$

Table 6: Comparison of contact angle of water and brine on NAu1 and SWy.

Equation 3 is thus reduced to:

$$(\gamma'_{SO} - \gamma_{SO}) = (\gamma_{OW} \cos\theta - \gamma_{OB} \cos\theta') \qquad \text{Equation 4}$$

For the purpose of calculations, the different γ_{OW} and γ_{OB} are recapitulated in Table 7.

Liquids	**IFT (mN/m)**
• LVC(C)/H_2O	• 25.58
• LVC(C)/NaCl (1M)	• 22.76
• LVC(C)/KCl (1M)	• 23.33
• LVC(C)/$CaCl_2$ (0.5M)	• 14.83
• LVC(C)/$MgCl_2$ (0.5M)	• 7.13

Table 7: IFT of oil LVC(C) with different aqueous phases used during contact angle measurements.

The difference of surface tensions between mica surface and oil LVC(C) in the presence of the different brines and water ($\gamma'_{SO} - \gamma_{SO}$) are reported in Table 8. The results show that for the different exchangeable cations, there is an enhancement of adsorption of the components in the presence of brines compared to water ($\gamma'_{SO} < \gamma_{SO}$), the effect being more spectacular in the presence of the divalent cations.

Mica exchanged with different ions	$\gamma'_{SO} - \gamma_{SO}$ **(mN/m)**
• Mica-Na^+	- 2.65
• Mica-K^+	- 1.41
• Mica-Ca^{2+}	- 10.80
• Mica-Mg^{2+}	- 14.74

Table 8: Difference of mica/oil LVC(C) interfacial tension in water and in the presence of brine.

2.2 Contact angle of oil MFC(B)

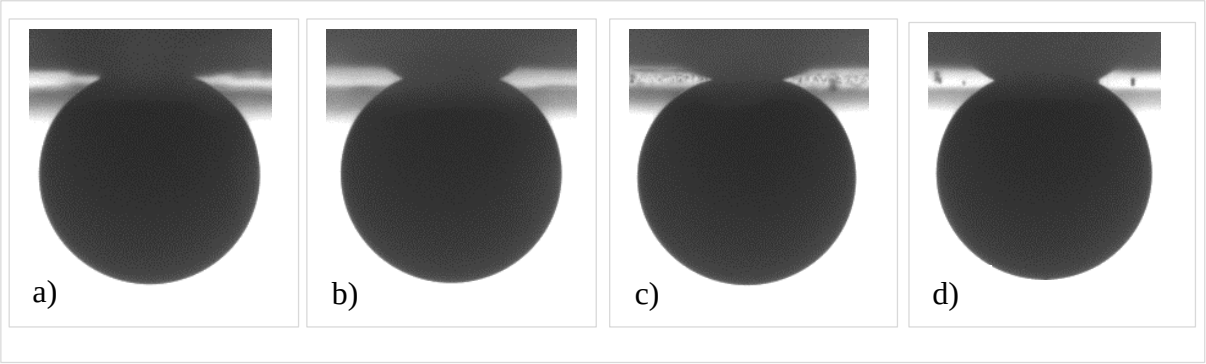

Figure 7: Drops of MFC(B) in water, on mica sheets exchanged with: a) Na^+; b) K^+; c) Ca^{2+}; d) Mg^{2+}.

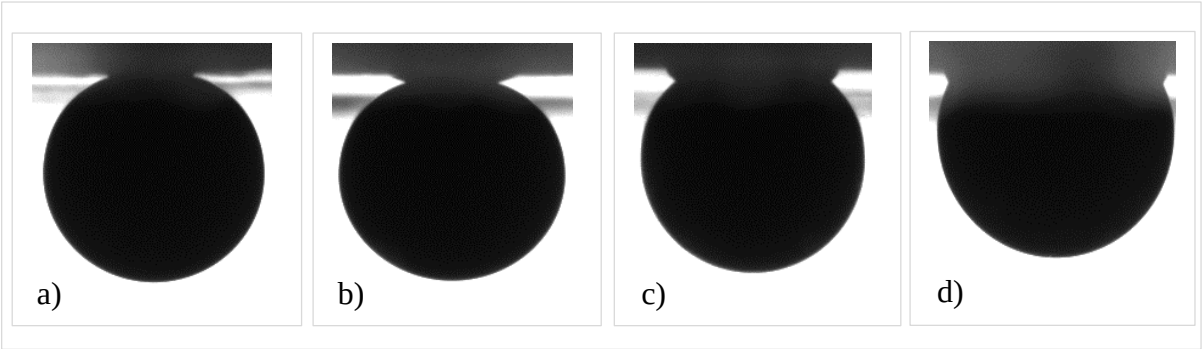

Figure 8: Drops of MFC(B) in brine on a): mica-Na^+ in NaCl; b) mica-K^+ in KCl; c) mica-Ca^{2+} in $CaCl_2$; d) mica-Mg^{2+} in $MgCl_2$.

As observed with oil LVC(C), the images of the drops on the different mica surfaces and in the presence of the different aqueous phases, show a net increase in solid/oil contact surface in the presence of the divalent cations (the phenomenon being enhanced in the presence of brines compared to water). The contact angles measured from these images are reported in Table 9.

Mica	Contact angle of oil MFC(B) in H_2O (°)	Contact angle of oil MFC(B) in brine	
		Brine	Contact angle (°)
• Mica-Na^+	160	NaCl	154
• Mica-K^+	167	KCl	157
• Mica-Ca^{2+}	154	$CaCl_2$	138
• Mica-Mg^{2+}	150	$MgCl_2$	112

Table 9: contact angles (± 5°) of MFC(B) on mica exchanged with different cations, the whole system in equilibrium in water and brines.

Tables 10 and 11 recapitulate the IFT of oil MFC(B) with different phases and the difference of solid/oil interfacial tension between water and brines respectively. As with oil LVC(C), an enhancement of crude oil components on the surface has been recorded in the presence of the divalent cations ($\gamma'_{SO} < \gamma_{SO}$).

Liquids	IFT (mN/m)
• MFC(B)/H_2O	• 25.58
• MFC(B)/NaCl (1M)	• 22.76
• MFC(B)/KCl (1M)	• 23.33
• MFC(B)/$CaCl_2$ (0.5M)	• 14.83
• MFC(B)/$MgCl_2$ (0.5M)	• 7.13

Table 10: IFT of oil MFC(B) with different aqueous phases used during contact angle measurements.

Mica exchanged with different ions	$\gamma'_{SO} - \gamma_{SO}$ (mN/m)
• Mica-Na^+	- 1.13
• Mica-K^+	- 2.66
• Mica-Ca^{2+}	- 9.63
• Mica-Mg^{2+}	- 13.83

Table 11: Difference of mica/oil MFC(B) interfacial tension in water and in the presence of brine.

2.3 Summary and interpretation of contact angles on mica surfaces

From the above experiments the following observations could be made:

- In water: a low effect of monovalent cations compared to the divalent cations has been recorded on the contact angle of oil drops on the mica surfaces;
- In brines: similar tendency as in water has been observed, i.e. in the presence of divalent cations more marked reduction of contact angles has been recorded. In a general way, the contact angles recorded on a given exchanged sample were lower in the presence of brine compared to water.

From these results we calculated the differences between oil/solid interfacial tension in water and brine. The results revealed $\gamma'_{SO} < \gamma_{SO}$, indicating that the adsorption of oil components was

promoted in the presence of brines (at least at the concentrations at which our experiments have been carried out). It is also worth mentioning that the phenomenon of adsorption has been more marked in the presence of the divalent cations compared to the monovalent cations under investigation.

Correlating these different results to those obtained in chapter 4 (regarding IFT measurements and analysis of drop size in emulsions), it follows that cations promoting salting-in of surfactants also promote the adsorption of oil components onto the clay surface. For instance, in the presence of the divalent cations, more surfactants being present at the oil/brine interface, adsorption of oil on the clay mineral surface has been promoted and thus reduced contact angle. These results are a priori in agreement with the mechanism of oil adsorption via cation bridges (polyvalent cations being more efficient than monovalent cations) postulated by Arnason [11].

3 Influence of clay minerals on emulsion of oil LVC(C)

3.1 Influence of the amount of kaolinite on the stability of emulsion of LVC(C) - $MgCl_2$

Figure 10 shows the emulsions of LVC(C) with brine of $MgCl_2$ but containing different amounts of kaolinite particles. It is worth mentioning that under similar conditions (a 50% oil/50% brine) but in the absence of clay particles, the emulsion showed kinetic stability during several weeks. The concentration of $MgCl_2$ used corresponds to the optimum salinity (leading to the minimum IFT of the oil with the aqueous phase). Here, in the presence of kaolinite particles, the stability of the emulsions are modified. In the presence of sufficient amount of clay minerals, the emulsions are destabilised in almost the two distinct phases. As the amount of clay particles is decreased, the emulsions are again stabilised.

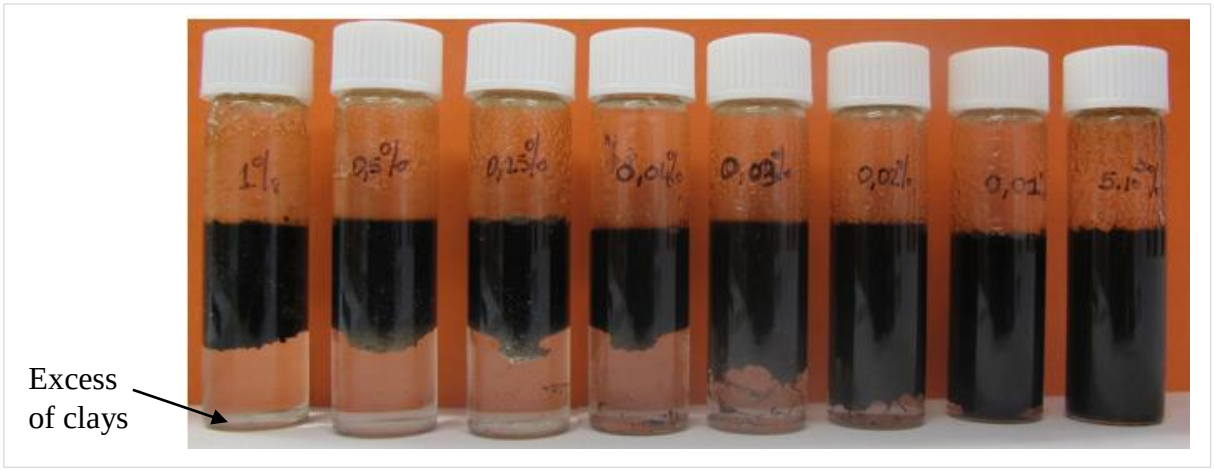

Figure 9: Emulsions of LVC(C) with brines of $MgCl_2$ containing different amounts kaolinite particles (from left to right: 1, 0.5, 0.25, 0.04, 0.03, 0.02, 0.01 and 0.005% by mass).

Let's consider a sample where the clay minerals are present in large excess, for e.g. the sample containing 0.5% of clays (Figure 10). In addition to the separation of the organic and aqueous phase, the excess of clay minerals can be observed at the bottom of the bottles. The upper phase viewed under the optical microscope by using polarised light show clay particles in suspension into the organic phase. A priori these experiments indicate that the surfactants which were previously available to stabilise oil/aqueous phase emulsion have been adsorbed on the clay particles. At the oil/brine interface, a "jelly-like" phase with clay particles suspended can clearly be identified. This intermediate phase can also be properly distinguished in the presence of 0.25% of clays.

As the amount of clay is decreased, for instance the 0.03% sample, only part of the available surfactants are “consumed” by the minerals and hence the rest remain available for oil/brine stabilisation. This phenomenon is even for marked (sample 0.005% of clay minerals) where the amount of clay is negligible so that a stable emulsion has been revealed.

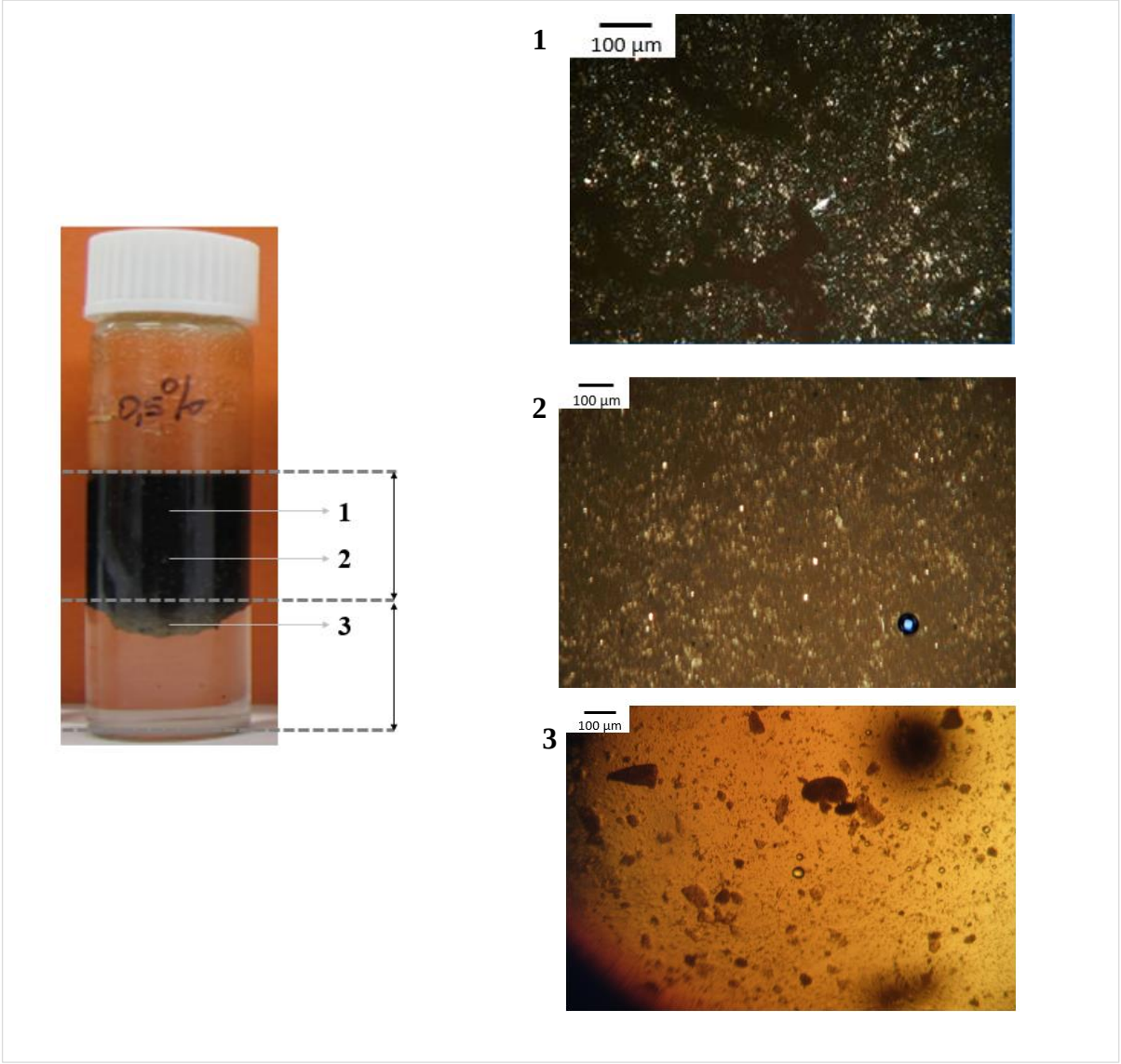

Figure 10: Analysis of oil LVC(C)/$MgCl_2$/0.5% by mass of Kaolinite; 1, 2 and 3 correspond to the different parts of the mixture.

3.2 Influence of different clay minerals on emulsions of oil LVC(C) with different brines

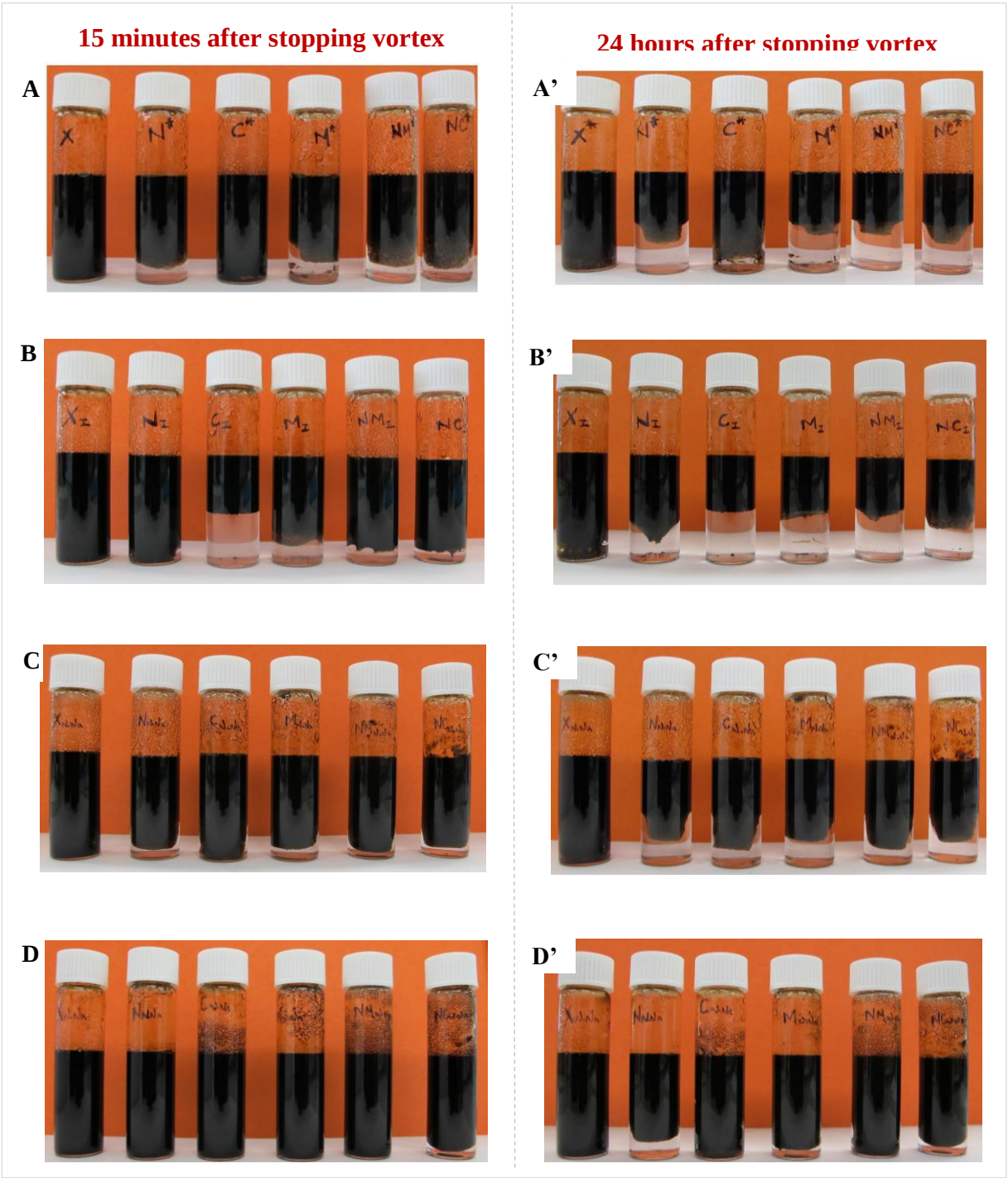

Figure 11: **A** and **A'**: 0.04% k4-Na^+; **B** and **B'**: 0.04% Imt2-Na^+; **C** and **C'**: 0.04% Nau1-Na^+; **D** and **D'**: 0.04% Swy-Na^+. (A, B, C and D): 15 minutes after vortex; (A', B', C' and D'): 24 hours after vortex. In each series from left to right, capital letters X, N, C, M, NM and NC respectively denoting water, NaCl, $CaCl_2$, $MgCl_2$, NaCl+$MgCl_2$ and NaCl+$CaCl_2$.

Having identified the effect of clay content on the stability of emulsions, we chose to investigate the effect of different brines by using 0.04% of different clays. From our previous experiments, the sample of 0.04% by mass of kaolinite was sufficient to observe a net destabilisation of emulsion.

Figure 11 shows the emulsions of oil LVC(C) with different brines and containing 0.04% by mass of sodium exchanged non-swelling clays (kaolinite and illite) and swelling clays (nontronite and montmorillonite). From these experiments, the following observations can be made:

(i) The presence of clays play a significant role and counter emulsion formation;

(ii) In the presence of equal clay content, a net difference of destabilisation in the presence of the non-swelling compared to the swelling clays can be observed (phase separation being more marked in the presence of non-swelling clays);

(iii) For these sodium exchanged clays, destabilisation occurs in the presence of brines compared to water. Indeed in the absence of salts, a W/O (Figure 12) emulsion can be observed with the clay particles being dispersed into the organic phase. In the presence of all salts at concentration leading to oil/brine minimum IFT, clay minerals have been able to counter emulsion formation to different extents and caused phase separation.

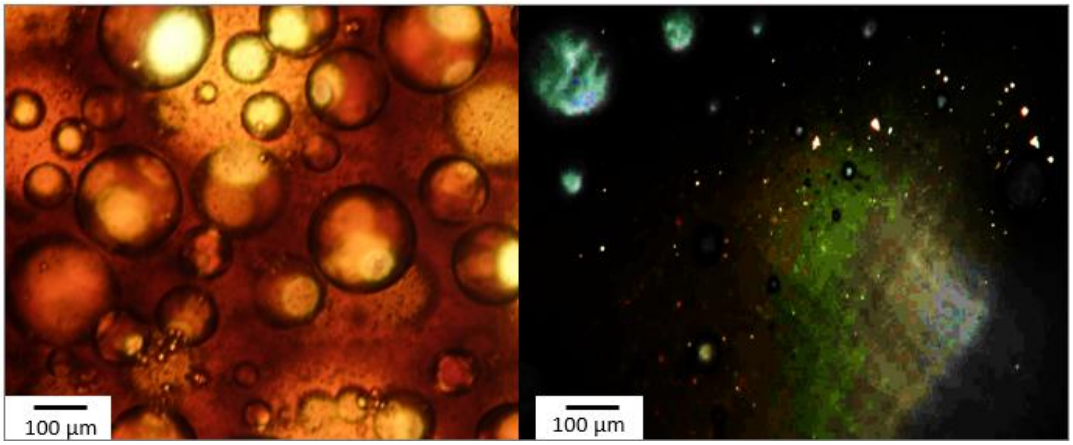

Figure 12: LVC(C)/water/kaolinite emulsion; left hand side image shows water drops dispersed into the organic phase; right hand side image (under polarised light) shows kaolinite particles dispersed in the organic phase.

(iv) As far as the effect of ions composing the brines are concerned, at this stage no net conclusion could be drawn.

Hence, regarding the effect of ions, we investigated the effect of the exchangeable ions (Na^+, K^+ and Ca^{2+}) at the surface of nontronite clays (Figure 13-sample at 24 hours). Again, as far as the different brines are concerned no net difference could be observed with the different clays. However, it is particularly interesting to observe the different samples in the presence of water. For instance, in the presence of NAu1-Ca^{2+}, the emulsion is destabilised to a greater extent compared to NAu1-K^+ and NAu1-Na^+. These results are in line with our observations in section 2, where adsorption of crude oil was promoted in the presence of the divalent cations. The effect of phase separation by NAu1-Ca^{2+} in water is even more visible by NAu1-Na^+ in $CaCl_2$ and NAu1-Na^+ in $MgCl_2$.

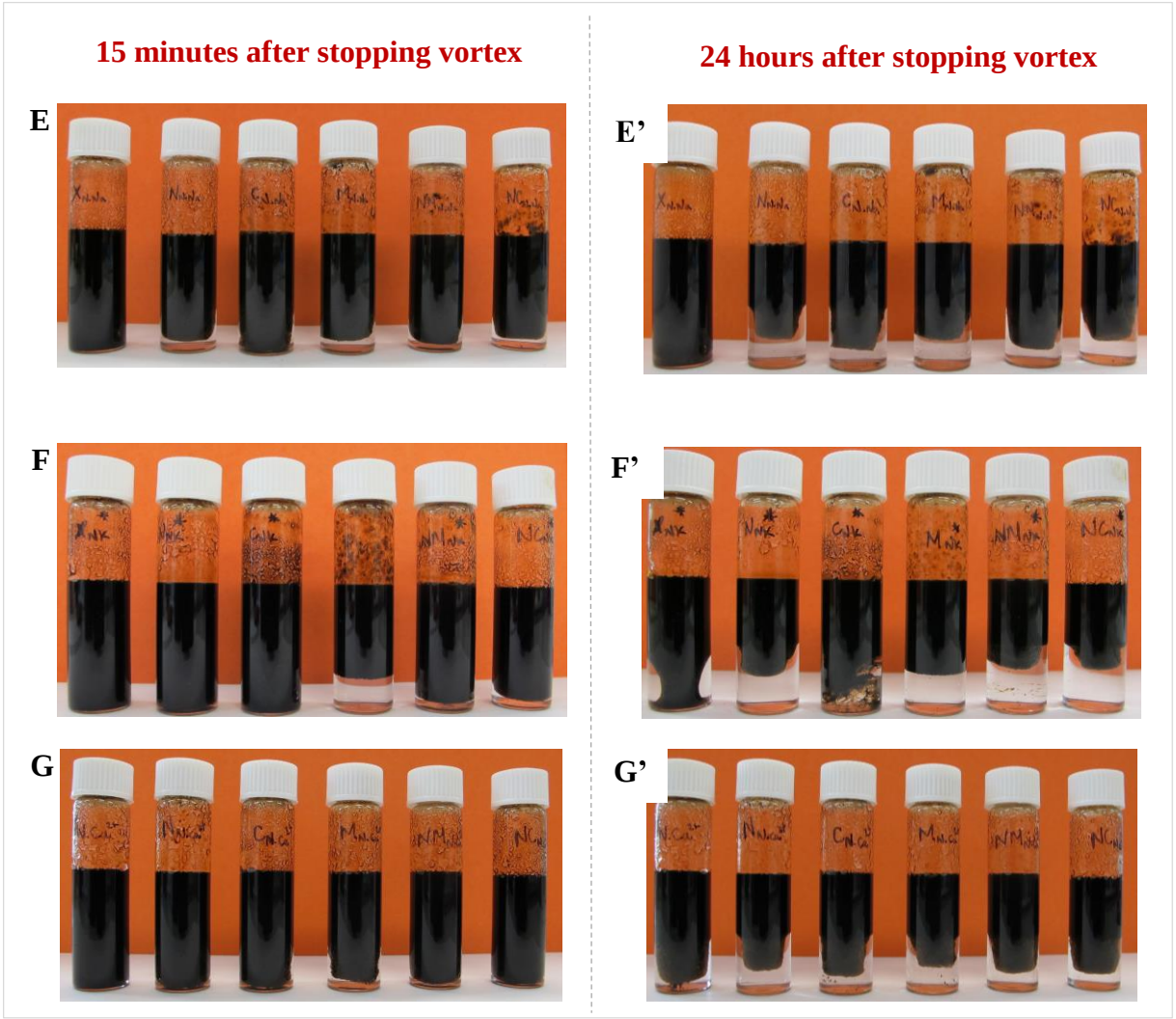

Figure 13: **E** and **E'**: NAu1-Na^+; **F** and **F'**: NAu1-K^+ and **G** and **G'**: Nau1-ca^{2+}. (E, F and G): 15 minutes after vortex; (E', F', and G'): 24 hours after vortex. In each series from left to right, capital letters X, N, C, M, NM and NC respectively denoting water, NaCl, $CaCl_2$, $MgCl_2$, NaCl+$MgCl_2$ and NaCl+$CaCl_2$.

4 Influence of clay minerals on emulsion of oil MFC(B)

4.1 Influence of kaolinite and illite content on the stability of emulsion of MFC(B)-$MgCl_2$

The effect of clay content on the stability of emulsion of oil MFC(B) has been investigated in a similar way to that of oil LCV(C). However, in addition to kaolinite mineral, we also investigated the effect of illite (Figure 14).

Figure 14: Emulsions of MFC(B) with brines of $MgCl_2$ containing different amounts kaolinite (A and A') and illite (B and B') particles; (A and B) and (A' and B') are images 24 hours and 3 months respectively after the different phases have been mixed up.

Figure 14 shows very similar results as those observed with different kaolinite content with oil LVC(C), i.e. with an excess of clay mineral, the emulsion is destabilised and with insufficient clay content, stabilisation of the emulsions are observed. However, it is to be noted that with identical clay content (for e.g. 1%, 0.5% and 0.25%) phase separation with oil MFC(B) is less marked compared to LVC(C) (Figure 9 versus Figure 14). These results are in agreement with the greater amount of polar components present in MFC(B).

Moreover, when comparing the effect of the two non-swelling but structurally neutral kaolinite and charged illite minerals, organic and aqueous phase separation is more marked in the presence of illite.

In the range of investigated clay content, the results show that 1% by mass of clays was taken as the optimum amount resulting in phase separation with both kaolinite and illite. Hence, this concentration of clay mineral was chosen to investigate the effect different clays and brines.

4.2 Influence of different clays on emulsions of oil MFC(B) with different brines

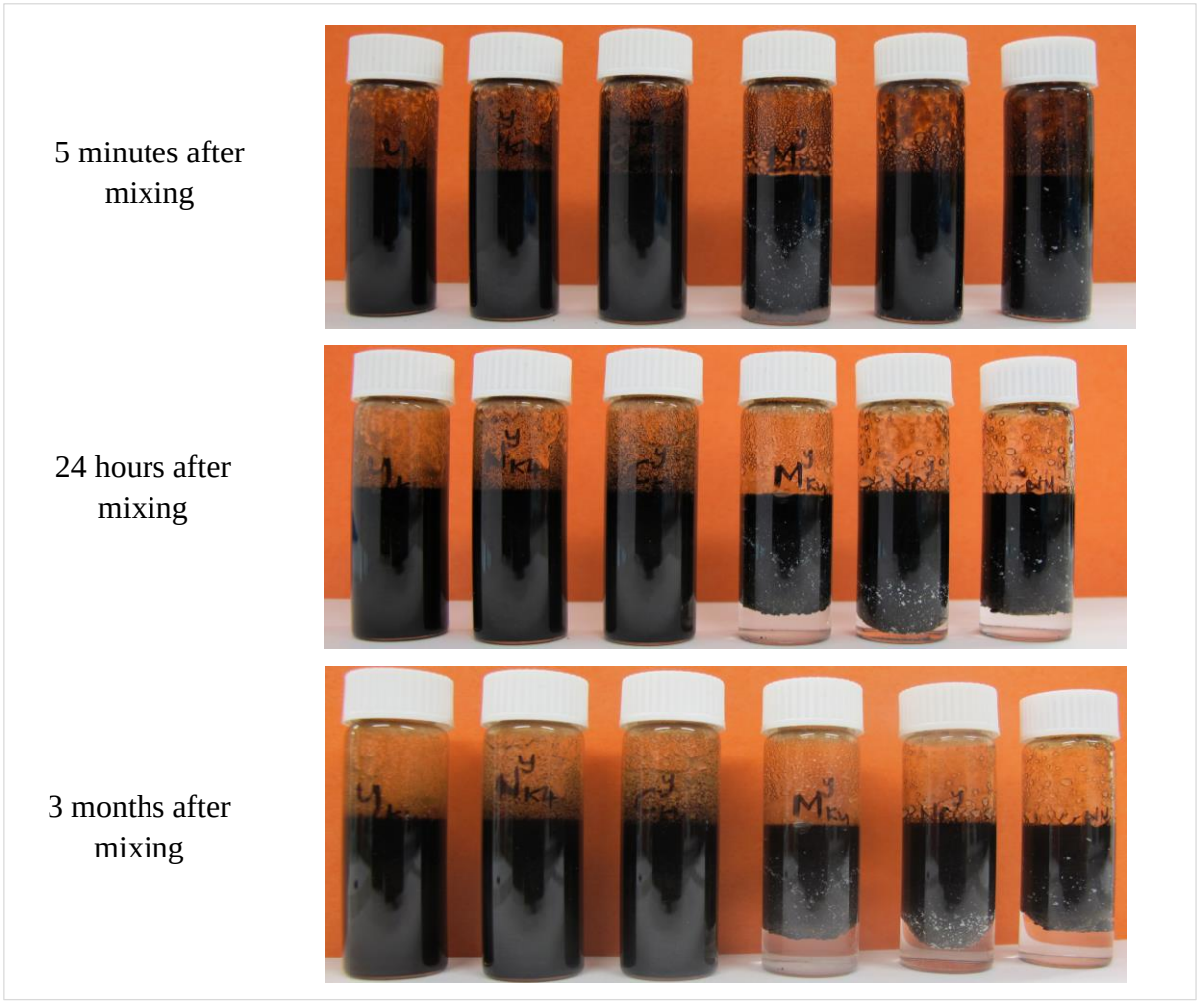

Figure 15: Emulsions of oil MFC(B) containing 1% of k4-Na^+ 5 minutes, 24 hours and 3 months after the different phases have been mixed up. In the series, from left to right capital letters X, N, C, M, NC and NM respectively denoting water, NaCl, $CaCl_2$, $MgCl_2$, NaCl+$CaCl_2$ and NaCl+$MgCl_2$.

Figures 15 and 16 show the oil MFC(B)/different brines/1% clays at different times after the three phases have been mixed up. As observed with oil LVC(C), a net difference between the non-swelling (K4 and Imt2) and the swelling (SWy) clays are recorded. Indeed, in the presence of equal clay content, the non-swelling clays have been able to counter emulsion formation to greater extent. However, in contrast to LVC(C) where in the presence of all brines a separation of phase was recorded, with MFC(B) brines of NaCl and $CaCl_2$ did not macroscopically influence the stability of emulsion. Indeed, following the previous results the effect of NaCl and $CaCl_2$ was not expected.

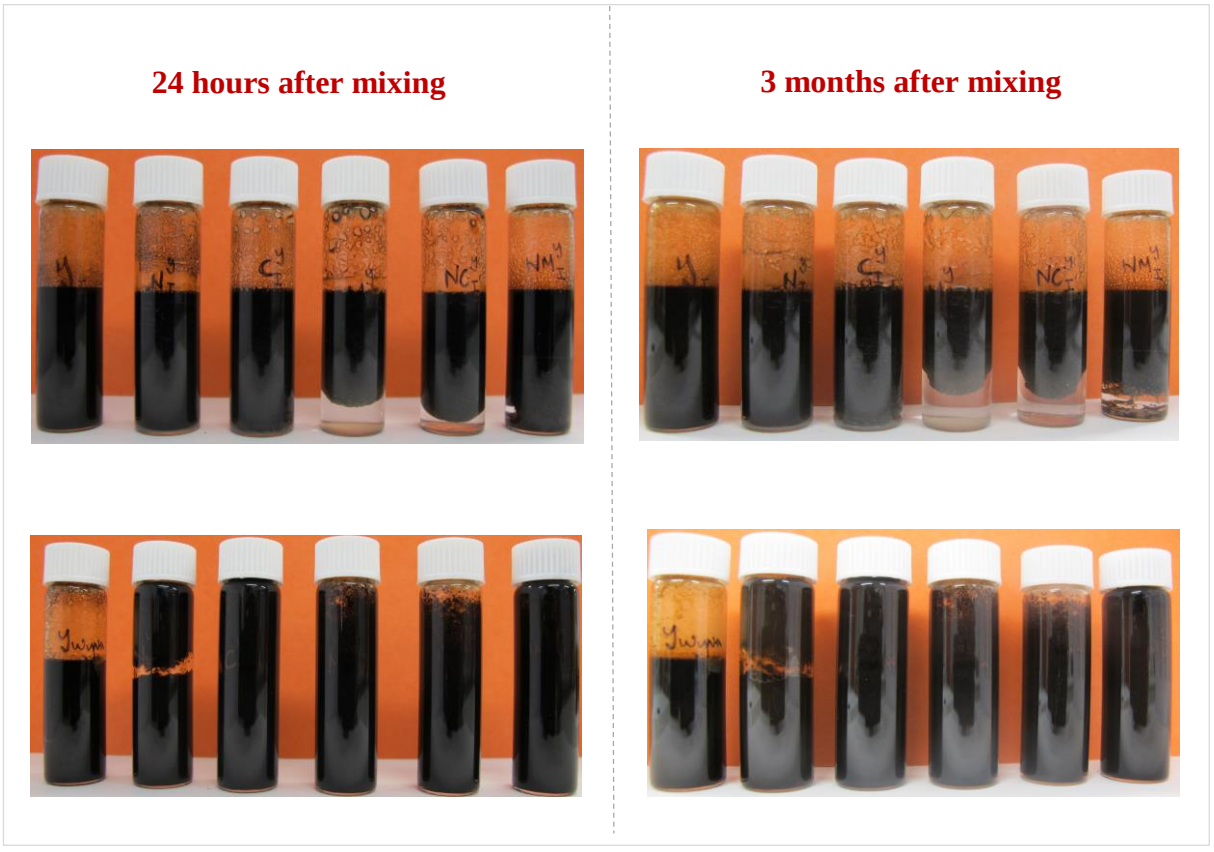

Figure 16: Emulsions of oil MFC(B) containing 1% of illite-Na^+ and SWy-Na^+ at different times after the three phases have been mixed up. In each series, from left to right capital letters X, N, C, M, NC and NM respectively denoting the aqueous phases water, NaCl, $CaCl_2$, $MgCl_2$, NaCl+$CaCl_2$ and NaCl+$MgCl_2$.

4.3 Summary and discussion

In this section with oil LVC(C) and MFC(B), we firstly investigated the effect of clay content by mixing together the three phases oil/$MgCl_2$/non-swelling clays. The concentrations of $MgCl_2$ which was used corresponded to the optimum salinities with the crude oils and non-swelling clay particles used were of sizes < 2µm in length. With LVC(C), the results showed that as long as an excess of kaolinite (with respect to the polar components of the crude oils) was present, the mixture predominantly separated into 2 distinct organic and aqueous phases. In addition, an intermediate "gelatinous aspect" small interfacial phase could be distinguished. Analysis of the organic phase showed dispersed clay particles into the oil. Tentative analysis of the intermediate phase under the optical microscope showed dense dark agglomerated zones. However at this stage no further characterisation has been made with respect to this intermediate phase. As the amount of clay minerals was gradually decreased, we observed that the oil/brine were gradually mixed up until a stable emulsion was observed in the presence of 0.005% kaolinite. These results could a priori be attributed to the adsorption of the oil surfactants onto the kaolinite particles so that they became completely hydrophobic and moved into the organic phase. Indeed in the presence of sufficient clay, all (or most) of the surfactants are adsorbed on the clay minerals so that they are no longer available for emulsion stabilisation. As clay content is decreased, only part of the surfactants being adsorbed on the minerals surface, the rest remain available for emulsion stabilisation.

With MFC(B), the content of kaolinite as well as that of illite has been investigated. Very similar results have been obtained with oil MFC(B), i.e. as clay content is decreased, phase separation became less apparent. However, at equal clay content (for example 1%, 0.5% and 0.25%) phase separation has been less marked with MFC(B) compared to LVC(C). This observation can a priori be attributed the presence of greater amount of polar components in MFC(B) compared to LCV(C) (15.7% and 8.2% respectively). Regarding the effect of the clay mineral, at identical content of kaolinite and illite, illite was more efficient in separating the phases. These results show the specificity of the surfactant molecules with respect to the mineral surfaces. Indeed, kaolinite expose two different basal surfaces (siloxane and hydroxyl) while illite possesses two identical siloxane surfaces. In addition, due to isomorphous substitution, the siloxane surfaces of illite possess a permanent charge. Besides the basal surfaces, clay minerals also possess lateral surfaces (edges aluminol and silanol charged positively and negatively at low and high pH respectively). Our results point towards a more specific

adsorption of the crude oil components on illite compared to kaolinite. However, further characterisations are needed to ascertain the localisation of adsorption on the clay minerals.

In line with the clay content and specificity of clay minerals, we investigated the effect of the nature of the aqueous phase as well as that of the clay minerals. For instance, with oil LVC(C), we observed that 0.04% by mass of kaolinite was sufficient to result in oil/aqueous phase separation. For oil MFC(B), in the range of investigated clay content, 1% by mass of clays was chosen as optimum. Hence with LVC(C), 0.04% by mass of illite, nontronite, montmorillonite and for MFC(B), 1% by mass of kaolinite, illite and montmorillonite were used in the presence of different aqueous phases (water, NaCl, $CaCl_2$, $MgCl_2$, NaCl+$CaCl_2$ and NaCl+$MgCl_2$). The different observations from these experiments are discussed below:

(i) In the presence of water, at short (15 minutes) and long times (≥ 24 hours) after the three phases have been mixed, both oils showed stable emulsions with all the different sodium exchanged clays (kaolinite, illite, nontronite, montmorillonite). Analysis of LVC(C)/water/kaolinite-Na^+ emulsion revealed a W/O emulsion with the minerals dispersed into the organic phase. These results show that not all the surfactants were adsorbed on the mineral surface so that some were still available for emulsion stabilisation. A priori, adsorption of surfactants engaged in the stabilisation of W/O emulsion are different from those adsorbed directly onto the mineral surface and require the presence of an ion to bridge on the kaolinite.

(ii) In water, when comparing NAu1-Na^+, NAu1-K^+ and NAu1-Ca^{2+}, we observed that some water was resolved from the emulsion in the presence of NAu1-Ca^{2+}. These results can be attributed to enhanced adsorption of crude oil components specifically in the presence of Ca^{2+} ions.

(iii) In the presence of the different salts, with all the clays separation of the organic and aqueous phases has been observed, the non-swelling clays showing more marked separation compared to the swelling clays. As such these results can be attributed to the reduced specific area available by the non-swelling clay minerals due to flocculation. Indeed the salt concentrations were greater than the critical coagulation concentration reported by Lagaly et al. for sodium montmorillonites [12].

5 Conclusion

In the first part of this chapter we investigated oil/brine/clay triple phase interaction by contact angle measurements. The clay mineral used for this purpose was smooth muscovite mica exchanged with Na^+, K^+, Ca^{2+} and Mg^{2+}. Oil drops in water on these surfaces revealed contact angles in the order of $Mg^{2+} < Ca^{2+} < Na^+ \sim K^+$. In brines, the contact angles decreased but followed similar trend, i.e. $Mg^{2+} < Ca^{2+} < Na^+ \sim K^+$. These results point towards the adsorption of crude oil components on the mica surface in the presence of ions, the effect being enhanced in the presence of the divalent ions.

In the second part of this chapter, we investigated the effect of clay minerals on the stability of the emulsions of the crude oils in the presence of different aqueous phases. The results showed that some crude oil components adsorb onto mineral surfaces directly while others needed an ion to bridge onto the clay. In the presence of brines at salinities leading to the minimum IFT, both the non-swelling and the swelling clays adsorb crude oil components. However, due to flocculation of the swelling clays at investigated salt concentrations, they had limited effect on the stability of emulsions.

6 Bibliography

[1] J. Buckley and N. Morrow, “An overview of crude oil adhesion phenomena,” *Phys. Chem. Colloids Interfaces Oil Prod.*, pp. 39–45, 1992.

[2] U. Türksoy and S. Bağci, “Improved oil recovery using alkaline solutions in limestone medium,” *J. Pet. Sci. Eng.*, vol. 26, no. 1–4, pp. 105–119, May 2000.

[3] R. C. Nelson, J. B. Lawson, D. R. Thigpen, and G. L. Stegemeier, “Cosurfactant-Enhanced Alkaline Flooding,” in *SPE-12672-MS*, SPE, 1984.

[4] D. M. Sztukowski and H. W. Yarranton, “Oilfield solids and water-in-oil emulsion stability,” *J. Colloid Interface Sci.*, vol. 285, no. 2, pp. 821–833, May 2005.

[5] A. Hannisdal, M.-H. Ese, P. V. Hemmingsen, and J. Sjöblom, “Particle-stabilized emulsions: Effect of heavy crude oil components pre-adsorbed onto stabilizing solids,” *Colloids Surf. Physicochem. Eng. Asp.*, vol. 276, no. 1–3, pp. 45–58, Mar. 2006.

[6] B. P. Binks and S. O. Lumsdon, “Pickering Emulsions Stabilized by Monodisperse Latex Particles: Effects of Particle Size,” *Langmuir*, vol. 17, no. 15, pp. 4540–4547, Jul. 2001.

[7] B. P. Binks and S. O. Lumsdon, “Catastrophic Phase Inversion of Water-in-Oil Emulsions Stabilized by Hydrophobic Silica,” *Langmuir*, vol. 16, no. 6, pp. 2539–2547, Mar. 2000.

[8] B. P. Binks and C. P. Whitby, “Silica Particle-Stabilized Emulsions of Silicone Oil and Water: Aspects of Emulsification,” *Langmuir*, vol. 20, no. 4, pp. 1130–1137, Feb. 2004.

[9] D. E. Tambe and M. M. Sharma, “Factors Controlling the Stability of Colloid-Stabilized Emulsions,” *J. Colloid Interface Sci.*, vol. 157, no. 1, pp. 244–253, Apr. 1993.

[10] L. Liu and J. S. Buckley, “Alteration of wetting of mica surfaces,” *J. Pet. Sci. Eng.*, vol. 24, no. 2–4, pp. 75–83, Dec. 1999.

[11] T. S. Arnarson and R. G. Keil, “Mechanisms of pore water organic matter adsorption to montmorillonite,” *Mar. Chem.*, vol. 71, no. 3–4, pp. 309–320, Aug. 2000.

[12] G. Lagaly and S. Ziesmer, “Colloid chemistry of clay minerals: the coagulation of montmorillonite dispersions,” *Adv. Colloid Interface Sci.*, vol. 100–102, pp. 105–128, Feb. 2003.

Summary and Conclusion

Summary and conclusion

The mechanisms underlying the technology of low salinity waterflooding (LSW) for enhanced oil recovery are still debated in the literature. Still, the growing demand for energy worldwide makes LSW a suitable technique for oil exploitation. In addition to the low cost involved in its implementation and operation, it has a reduced environmental impact due to minimal water pollution involved in the handling of chemicals during and after injection. In the aim of providing an insight into the benefits revealed by this technique, we firstly studied the wettability of clay minerals (chapter 3), followed by the study of oil/aqueous phase interactions (chapter 4) and finally, triple phase crude oil/brine/clay (COBR) interactions (chapter 5).

In chapter 3 we firstly studied solid/liquid interactions by investigating the wettability of clay minerals. For this purpose contact angle measurements (at the solid/liquid/vapour interface) have been made and the effect of exchangeable ions, surface roughness, particle size and relative humidity has been investigated for swelling clay minerals. For a given clay mineral of a given particle size, the results showed that water contact angles are essentially driven by the surface chemistry. As such, the nature of the exchangeable ion influenced the roughness of the clay films but finally it is the hydration energies which govern the contact angles (for instance, the surface roughness of K^+ exchanged film was lower than that of Ca^{2+} and yet, the contact angle on the K^+ film was higher than that of the Ca^{2+} film). However, we observed that for a clay mineral exchanged with a given cation, the contact angles were influenced by the size of the particles. Indeed, our results showed that films composed of particles of large sizes exhibited the largest contact angle while those composed of particles of small sizes exhibited the smallest contact angles. On the other hand, when comparing the contact angles at short times after drops were deposited, the different relative humidities (45%, 84% and 100%) showed no net influence on the contact angles. However, with time we observed a stabilisation of the contact angles (which reached a plateau) compared to those measured under ambient conditions. Working at high humidity can thus help us reach a stabilised contact angle by eliminating the phenomenon of evaporation. The different results in this section point towards an enhancement of water-wetness of clay mineral surfaces in the presence of cations which possess a very favourable hydration energy.

On the other hand, drops of crude oil deposited on the non-swelling as well as the swelling clays penetrated into the pores and spread on the surfaces. These results are an indication that

the clay minerals are far from being hydrophobic. However, it is worth mentioning that these experiments have been carried out to measure contact angles at the oil/solid/vapour interface under ambient conditions.

In chapter 4, we investigated oil/aqueous phase interactions: two crude oils and a model system (dodecane containing oleic acid) in the presence of different brines. Firstly, measurement of interfacial tension (IFT) of the three different organic phases showed that the IFT of all the systems dropped to a minimum at an optimum salinity and then either stayed constant or increased slightly beyond this point with increasing salt concentration. This result points towards an optimum salt concentration at which salting-in of surfactants present in the oils are favoured and result in the lowest IFT. Also, we investigated the effect of different cations and anions on the IFT of the three systems. In a general way, when the ions are classified according to their polarisability, our results show two types of behaviour: firstly, the highly polarising and highly polarisable ions and secondly, ions of intermediate polarisability. Indeed, small, hard and highly polarising cations (Mg^{2+}, Ca^{2+} and Li^{+}) and the small, soft and highly polarisable cations (Rb^{+} and Cs^{+}) result in very low IFTs. In the former case, we attributed these results to electrostatic attraction and ion-pairing, while in the latter case, in addition to electrostatic attraction, due to their large sizes, high polarisability, weak hydration and high cavitational energy, the cations were attracted to the oil/water interface. Intermediately polarisable cations such as Na^{+} and K^{+} only showed a marginal effect on the IFT of the organic phases. As far as the effect of anions are concerned, very similar results have been observed, i.e. low IFT with small and highly polarising F^{-} and with large and highly polarisable I^{-}. If the surfactant like behaviour of I^{-} ions are known, the behaviour of F^{-} ions show that it is the whole Na-F that moved towards the interface and lowered IFT.

In addition to IFT measurements for the study of liquid/liquid interactions, in the second part of the chapter we investigated the stability of emulsions of the crude oils with aqueous phases (water, NaCl, $CaCl_2$, $MgCl_2$, NaCl+$CaCl_2$ and NaCl+$MgCl_2$) at salinities leading to minimum IFTs for the brines. The results showed that all the aqueous phases resulted in stable W/O emulsions with the crude oils. In the presence of the ions, stability was decreased in the order of $MgCl_2 \approx$ NaCl+$MgCl_2$ > $CaCl_2 \approx$ NaCl+$CaCl_2$ > NaCl > Water. These results were obtained on the basis of drop size distribution analysis of the different emulsions. Again these results point towards the salting-in of surfactants in the presence of the smallest and highly polarising cations (the divalent cations in the studies series) and hence provide stability to emulsions.

In the 5th chapter, we investigated COBR interactions. In the first section, this has been achieved by contact angle measurements of crude oil drops on smooth mica surfaces with the whole system immersed in aqueous phases. In water, our results showed that crude oils were more adsorbed onto mica exchanged with the divalent salts, contact angles on mica-Mg^{2+} < mica-Ca^{2+} < mica-K^{+} ≈ mica-Na^{+}. When we preformed similar experiments in the presence of brines, our results showed smaller contact angles compared to water, however similar trend as in water was observed, i.e. an enhancement of adsorption of crude oil components in the presence of the divalent salts. Correlating these results to those obtained in the previous chapter, we can conclude that in the presence of salts favouring salting-in of surfactants, more crude oil components are available for adsorption onto mineral surfaces.

In the second part of chapter 5, we introduced different clay minerals in the presence of the crude oils and the different aqueous phases (for brines at salinities corresponding to the minimum IFTs with the crude oils). Firstly, we observed that clay concentration had an impact on the stability of crude oil/brine ($MgCl_2$) emulsions. In the presence of a threshold amount of clay minerals, a net separation of the oil/aqueous phase was observed. We attributed our observations to adsorption of surfactants onto the minerals surfaces (kaolinite and illite) and hence were no longer available for the stabilisation of emulsion. This result also show that in the presence of oil, brine and clay, adsorption of the surfactants on the clay minerals are energetically more favoured than their portioning at the oil/brine interface. When the amount of clay was decreased, as a result of more "free" surfactants, crude oil/brine emulsion stabilisation was observed again.

When clay minerals (sodium exchanged kaolinite, illite, nontronite and montmorillonite) at the threshold amount was added in water and then mixed with the crude oils, no separation of phase was observed. Compared to the results obtained above in the presence of brine of $MgCl_2$ instead of water, these results show that in absence of salts the surfactants were still available for emulsion stabilisation. Indeed, analysis of the LVC(C)/water/kaolinite emulsion revealed a W/O emulsion with kaolinite particles dispersed into the organic phase. These results further indicated that some surfactants were able to adsorb directly onto mineral surfaces while others needed an ion to act as a bridge (the surfactants engaged in stabilisation of emulsion).

Determination of the type of cation needed for surfactant adsorption onto the mineral surface was investigated by nontronite exchanged with Na^{+}, K^{+} and Ca^{2+}. The results showed that the

Ca^{2+} exchanged clay was more efficient in causing oil/water separation. Indeed due to adsorption of crude oil components onto mineral surfaces, less surfactants were available for emulsion stabilisation and hence oil/water phase separation was recorded. However, when we investigated the effect of brines (NaCl, $CaCl_2$, $MgCl_2$, NaCl+$CaCl_2$ and NaCl+$MgCl_2$), phase separation occurred at more or less similar extents. These results indicate that at concentrations leading to minimum IFT, all the cations were able to bridge surfactants on the mineral surfaces.

It is worth noting that the type of clay mineral played a significant role. With both of our crude oils in the presence of the different brines, the non-swelling clays were more efficient in causing phase separation compared to the swelling clays. Moreover, with oil MFC(B) we observed that illite was more efficient compared to kaolinite. The difference between the clays can be attributed to the reduced specific surface area available for adsorption due to flocculation of the swelling clays compared to the non-swelling clays. As far as the difference between kaolinite and illite are concerned, the difference are most probably linked to the surface charges and the specific surface area of the clay minerals. As far as the specific surface areas of the clay minerals are concerned, they are not available at present but are under measurements.

The necessary conditions reported for LSW to operate are (i) the presence of clays; (ii) the presence of polar components in oils; (iii) the presence of connate water; (iv) the presence of divalent cations in the connate water; and (v) a significant difference between the salinity of injected brine and in place water (injected brine concentration being much lower than that of the connate water). In order to investigate the effect of clay minerals, we used various clays in our studies. In the process of oil/brine phase separation, we observed that the non-swelling clay minerals have had a more pronounced effect compared to the swelling clays. However, we cannot completely discard the effect of the swelling clay minerals.

As far as the presence of polar components are concerned, indeed, they have been observed to act at different levels. First of all, they play a major role in IFT reduction. Indeed, in the absence of surfactants (pure dodecane), an increase of oil/brine IFT was recorded with increasing concentration of salts. This effect of IFT reduction is indeed a clue for the overcoming of capillary forces in pores of rocks. In conditions favouring emulsion formation, oil recovery could be increased by capillary desorption. Secondly, we observed that crude oil components are responsible for adsorption on the mineral surfaces. As such, our studies have pointed out towards the adsorption of some organic components directly onto the minerals while others needed the aid of ions. Accordingly to these observations, our work is partly in agreement with the theory of adsorption of surfactants via the aid of cation bridges (especially the divalent ions).

Prospects

During liquid-liquid interactions, we designed our model system by using dodecane and oleic acid. It appeared that a favoured interaction occurred between the hard carboxylate group and the small, hard and highly polarising cations. However, when brines composed of large, soft and polarisable cations were used, no net modification of IFT was recorded. We believe that as a complement to these results, another model system containing a surfactant with a soft polar headgroup, for example a sulfonate, should be designed. As such, this time we expect very little interaction of the surfactant head with the hard cations but a net reduction of IFT with the soft and polarisable cations.

In our study, crude oil/aqueous phase emulsions have been made by application of an external force. It is nevertheless interesting to investigate if the crude oils would spontaneously mix up with different aqueous phases if they are contacted. Indeed, during water injection into reservoirs the oils trapped into the confined pores are not subject to important mixing forces which could help in emulsion formation.

In the aim of detaching crude oil components from the rock surfaces, a better insight of their adsorption is required. For instance, we strongly believe that an isolation of the different polar components of crude oils and their adsorption on mineral surfaces need to be analysed thoroughly.

A modification of adsorption of crude oil components has been recorded in the presence of ions. For instance, at a threshold kaolinite content, stable water in oil emulsion has been observed in the absence of ions. However, the presence of Mg^{2+} ions in an identical mixture revealed separation of the organic and aqueous phase, with the clay minerals dispersed into the oil. It is clear that in the presence of ions the clay minerals are more oil wet. It is thus interesting to investigate if wettability alteration of the clay mineral could be achieved by progressively diluting the system.